Molecular genetic approaches for the determination of embryo viability

Katharina Eva Späth

St Cross College

Nuffield Department of Obstetrics and Gynaecology

University of Oxford



A thesis submitted for the degree of

Doctor of Philosophy

Hilary 2017

Dedicated to …

… my parents Erna & Georg

Liebe Mama, lieber Papa, ich widme euch meine Doktorarbeit zum Dank für Alles was ihr für mich getan habt. Es ist ein Glück euch als Eltern zu haben. Ich liebe euch ❤

… my siblings Max, Paula & Franz

Lieber Zwilling, liebe Kleinen, auch euch widme ich diese Arbeit. Danke, dass ich immer auf euch zählen kann. Ihr seid die besten Geschwister der Welt ❤

… my sister-in-law Theresa and my nieces Sophia & Luisa

Liebe Schwägerin, liebe Mäuse, ihr passt einfach perfekt zu uns. Deshalb widme ich auch euch diese Arbeit. Schön, dass es euch gibt ❤



Many thanks to …

… my DPhil supervisor

Thank you Dagan for your continuous guidance, support and trust***!***

… all Reprogenetics alumni

Thank you Elpida, Samer, Tishy, and all other former colleagues for all your help***!***

… my Oxford friends and fellow DPhil students

Thank you Dhruti & Maria for always being there for me. I love you guys***!***

… my friends back home

Thank you Pia & Ramona, and all other Berger Mädels, for your wonderful friendships***!***

… the NIHR Biomedical Research Centre

Many thanks for the stipend***!***



Table of contents

Abstract 5
Terminology lists 7
Abbreviations 7
Measurement units 10
Preface 11
CHAPTER 1: Introduction and study aims 14
1.1 Human preimplantation embryo development 15
1.2 Markers of embryo viability in assisted reproduction 19
1.2.1 Chromosome copy number 20
1.2.2 Mitochondrial DNA copy number 24
1.3 Preimplantation genetic testing 28
1.3.1 Preimplantation genetic screening 30
1.3.2 Preimplantation genetic diagnosis of mitochondrial DNA disease 34
1.4 Study aims 46
1.4.1 Development, validation and clinical application of a novel preimplantation genetic screening technique 46
1.4.2 Design, validation and clinical application of a protocol for preimplantation genetic diagnosis of mitochondrial DNA disease combined with comprehensive chromosome screening 47
CHAPTER 2: Materials and methods 48
2.1 Collection of biological material 50
2.1.1 Culture of untransformed cell lines 50
2.1.1.1 Sub-culture of cell lines 51
2.1.1.2 Cryopreservation and recovery of cells 53
2.1.2 Collection of buccal samples 54
2.1.3 Collection of peripheral blood 54
2.1.4 Culture of human embryos 55
2.2 Preparation of biological material 55
2.2.1 Cell isolation and preparation of embryo specimens 56
2.2.1.1 Cell isolation from cell culture 58
2.2.1.2 Buccal cell isolation from buccal swaps 58
2.2.1.3 Lymphocyte isolation from peripheral blood 58
2.2.1.4 Biopsy/Preparation of embryo specimens 59
2.2.2 Extraction of genomic DNA 60
2.2.2.1 DNA extraction from cell culture 60
2.2.2.2 DNA extraction from buccal swabs 61

2.2.2.3 DNA extraction from peripheral blood....62
2.3 DNA amplification protocols....62
2.3.1 Whole genome amplification....63
2.3.1.1 SurePlex DNA amplification....64
2.3.1.2 Multiple displacement amplification....66
2.3.2 Conventional polymerase chain reaction....67
2.3.2.1 Primer design....67
2.3.2.2 Conventional polymerase chain reaction protocol....69
2.3.3 Multiplex pre-amplification polymerase chain reaction....71
2.4 DNA quantification protocols....72
2.4.1 Fluorometric DNA quantification....73
2.4.2 Relative standard curve method....74
2.4.3 Bioanalyzer quantification....76
2.5 Chromosome screening protocols....79
2.5.1 Microarray comparative genomic hybridisation....79
2.5.2 Next-generation sequencing....83
2.5.3 Quantitative real-time polymerase chain reaction....88
2.5.3.1 StepOnePlus Real-Time PCR System protocol....90
2.5.3.2 QuantStudio 12K Real-Time PCR System protocol....91
2.6 Mitochondrial DNA mutation detection....91
2.6.1 Preparation of sequencing libraries....92
2.6.2 Preparation of template-positive Ion Sphere Particles....95
2.6.3 Sequencing of template-positive Ion Sphere Particles....98
2.6.4 Data analysis of sequencing output....99
CHAPTER 3: Development, validation and first clinical application of a rapid comprehensive chromosome screening technique utilising an array-based nano-scale quantitative DNA amplification technology....101
3.1 Introduction - **CHAPTER 3**....102
3.2 Materials and methods - **CHAPTER 3**....103
3.2.1 Ethics regarding the analysis of biological samples and embryo specimens....103
3.2.2 Study design, protocol validation and clinical implementation....105
3.2.3 Preparation of samples for protocol development and validation....108
3.2.4 IVF treatment, embryo culture and biopsy....108
3.2.5 Sample processing procedures....109
3.2.6 Data analysis....109
3.2.6.1 Statistical data analysis....109
3.2.6.2 Analysis of consistency of chromosome copy number results....110
3.3 Protocol development and validation - **CHAPTER 3**....111
3.3.1 Phase 1 - Feasibility of chromosome copy number analysis utilising quantitative real-time polymerase chain reaction....111

3.3.1.1 Protocol design Phase 1 111
3.3.1.2 Data analysis Phase 1 114
3.3.1.3 Results Phase 1 133
3.3.2 Phase 2 - Feasibility of OpenArray Technology for chromosome copy number analysis in genomic DNA samples 137
3.3.2.1 Protocol design Phase 2 137
3.3.2.2 Data analysis Phase 2 140
3.3.2.3 Results Phase 2 142
3.3.3 Phase 3 - Feasibility of OpenArray Technology for chromosome copy number analysis of cell samples 147
3.3.3.1 Protocol design Phase 3 147
3.3.3.2 Data analysis Phase 3 149
3.3.3.3 Results Phase 3 150
3.3.4 Phase 4 - Feasibility of OpenArray Technology for comprehensive chromosome copy number testing 162
3.3.4.1 Protocol design Phase 4 162
3.3.4.2 Data analysis Phase 4 164
3.3.4.3 Results Phase 4 166
3.3.5 Phase 5 - Feasibility of OpenArray Technology for comprehensive chromosome copy number testing using a modified array design 169
3.3.5.1 Protocol design Phase 5 169
3.3.5.2 Data analysis Phase 5 174
3.3.5.3 Results Phase 5 176
3.3.6 Phase 6 - Pre-clinical validation study 192
3.3.6.1 Protocol design Phase 6 192
3.3.6.2 Data analysis Phase 6 193
3.3.6.2 Results Phase 6 194
3.4 Clinical application of the developed protocol - **CHAPTER 3** 209
3.5 Discussion - **CHAPTER 3** 214
3.5.1 Development and validation of a robust quantitative real-time polymerase chain reaction protocol 215
3.5.2 Clinical application 219
3.5.3 Microdeletion detection 221
3.5.4 Mitochondrial DNA quantification 221
3.5.5 Advantages and limitations in comparison to currently available 24-chromosome screening techniques 224
3.5.6 Conclusion - **CHAPTER 3** 228
CHAPTER 4: Design, validation and first clinical application of a protocol for preimplantation genetic testing of mitochondrial DNA disease combined with comprehensive chromosome screening 229
4.1 Introduction - **CHAPTER 4** 230

4.2 Materials and methods - **CHAPTER 4** 233
4.2.1 Ethics regarding test development and clinical application 233
4.2.2 Patient details 235
4.2.3 Design of test development, validation and clinical application 238
4.2.4 Preparation of samples for test development and validation 239
4.2.5 IVF treatment, embryo culture and biopsy 240
4.2.6 Sample processing procedures 240
4.2.7 Comprehensive chromosome screening protocols 241
4.2.8 Statistical data analysis 241
4.3 Protocol development and validation - **CHAPTER 4** 242
4.3.1 Assessment of whole genome amplification protocols 242
4.3.2 Assessment of accuracy and sensitivity of the designed test 243
4.3.3 Assessment of patient and carrier samples 246
4.3.3.1 Patient A 246
4.3.3.2 Patient B 252
4.3.3.3 Patient C 256
4.3.3.4 Patient D 260
4.4 Clinical application of the developed protocol - **CHAPTER 4** 264
4.4.1 Case report Patient A 264
4.4.2 Case report Patient B 266
4.4.3 Case report Patient C 269
4.4.4 Case report Patient D 271
4.6 Discussion - **CHAPTER 4** 275
4.6.1 Protocol design and validation 276
4.6.2 Clinical cases 281
4.6.3 Conclusion - **CHAPTER 4** 286
CHAPTER 5: Concluding remarks 288
5.1 Evolution of preimplantation genetic testing 289
5.2 Assisted reproductive techniques to improve embryo selection 290
5.3 Assisted reproductive techniques to prevent mitochondrial DNA disease transmission 291
Bibliography 297
Appendices 327
Appendix A 328
Appendix B 372
Appendix C 385

Abstract

Thesis title: Molecular genetic approaches for the determination of embryo viability

Candidate name: Katharina Spath

College attended: St Cross

Department visited: Nuffield Department of Obstetrics and Gynaecology

Degree undertaken: Doctor of Philosophy

Term submitted: Hilary 2017

Since its first application in the 1990s, genetic testing of preimplantation embryos has undergone a major transformation and its utilisation continues to grow. While in preimplantation genetic screening, euploid embryos are identified and prioritised for uterine transfer, preimplantation genetic diagnosis identifies embryos free of genetic disease to avoid transmission of hereditary genetic disorders from parents to offspring.

This study aimed to deliver a novel preimplantation genetic screening protocol, which is capable of high accuracy aneuploidy detection utilising array-based, nano-scale quantitative real-time polymerase chain reaction. Furthermore, it focused on the development of a preimplantation genetic diagnosis protocol, which is capable of accurate detection of maternally inherited mitochondrial DNA mutations and which is fully compatible with comprehensive chromosome screening.

After extensive validation, the novel preimplantation genetic screening technique was successfully implemented clinically for testing of blastocyst-stage embryos and now offers a valuable option for couples undergoing *in vitro* fertilisation combined with preimplantation genetic screening. It is a unique method in that it is streamlined, rapid, versatile and less labour-intensive compared to other conventional methods for aneuploidy screening. Furthermore, it has the potential to become an in-house component of an *in vitro* fertilisation laboratory, thereby reducing the processing time and eliminating the need for embryo cryopreservation. This in turn will help reduce the cost of *in vitro* fertilisation cycles with preimplantation genetic screening.

In addition, a new preimplantation genetic diagnosis protocol for detection of mitochondrial DNA diseases in conjunction with comprehensive chromosome screening using a next-generation sequencing technology was developed and delivered. The new method was successfully applied in four *in vitro* fertilisation patients transmitting different mutations causing mitochondrial DNA disease. In one patient, the transfer of an unaffected embryo resulted in the birth of a healthy child.

In summary, two novel methods were successfully developed, validated and clinically implemented for preimplantation genetic screening and preimplantation genetic diagnosis of mitochondrial DNA diseases.

Terminology lists

Abbreviations

Abbreviations and acronyms used in the thesis are defined in the text when first used and summarised below.

ARMS	—>	amplification refractory mutation system
ART	—>	assisted reproductive treatment
ATP	—>	adenosine triphosphate
CCN	—>	chromosome copy number
CCS	—>	comprehensive chromosome screening
CGH	—>	comparative genomic hybridisation
CI	—>	confidence interval
Ct	—>	threshold cycle
DGR.1/DGR.2/DGR.3		target regions for DiGeorge microdeletion Syndrome testing
DNA	—>	deoxyribonucleic acid
DPBS	—>	dulbecco's phosphate-buffered saline
DTT	—>	dithiothreitol
EDTA	—>	ethylenediaminetetraacetic acid
FAM	—>	fluorescein amidite
FISH	—>	fluorescence in situ hybridisation
gDNA	—>	genomic DNA
ICM	—>	Inner cell mass
ICSI	—>	intracytoplasmic sperm injection
ID	—>	identification number

IQR	—>	interquartile range
ISPs	—>	Ion Sphere Particles
IVF	—>	*in vitro* fertilisation
LB	—>	lower border
LHON	—>	leber hereditary optic neuropathy
M.1/M.2/M.3	>	assays for mtDNA copy number testing
MBG	—>	minor groove binder
MDA	—>	multiple displacement amplification
MELAS	—>	mitochondrial encephalopathy, lactic acidosis, and stroke-like episodes Syndrome
MERRF	—>	myoclonic epilepsy associated with ragged-red fibers
MI	—>	first meiotic division
MIDD	—>	maternally inherited diabetes and deafness
MII	—>	second meiotic division
MILS	—>	maternally inherited Leigh Syndrome
mRNA	—>	messenger RNA
MRT	—>	mitochondrial replacement therapy
MST	—>	maternal spindle transfer
MT-ATP6	—>	mitochondrially encoded ATP synthase membrane subunit 6
MT-ND3	—>	mitochondrially encoded NADH:ubiquinone oxidoreductase core subunit 3
MT-TL1	—>	mitochondrially encoded tRNA-Leu (UUA/G) 1
mtDNA	—>	mitochondrial DNA
NaOH	—>	sodium hydroxide
NARP	—>	neuropathy, ataxia, and retinitis pigmentosa
nDNA	—>	nuclear DNA
NFQ	—>	nonfluorescent quencher

NGS	—>	next-generation sequencing
NIGMS	—>	National Institute of General Medical Sciences
NINDS	—>	National Institute of Neurological Disorders and Stroke
OMIM	—>	Online Mendelian Inheritance in Man
PCR	—>	polymerase chain reaction
PGD	—>	preimplantation genetic diagnosis
PGM	—>	Ion Personal Genome Machine
PGS	—>	preimplantation genetic screening
PGT	—>	preimplantation genetic testing
PND	—>	prenatal diagnosis
PNT	—>	pronuclear transfer
PVA	—>	polyvinyl alcohol
Q1	—>	first quartile
Q3	—>	third quartile
qPCR	—>	quantitative PCR
RFLP	—>	restriction fragment length polymorphism
RNA	—>	ribonucleic acid
rRNA	—>	ribosomal RNA
SD	—>	standard deviation
SEM	—>	standard error of the mean
SNP	—>	single-nucleotide polymorphism
TAMRA	—>	tetramethylrhodamine
TBE	—>	tris borate EDTA
Tm	—>	melting temperature
tRNA	—>	transfer RNA
TVC plugin	—>	Torrent Variant Caller plugin

UB —> upper border

WGA —> whole genome amplification

Measurement units

Abbreviations and symbols used to describe units of measurements are not explicitly defined in the thesis text but stated below.

°C —> degree Celsius

bp —> base pair

cm^2 —> square centimetre

V —> volt

w/v —> weight/volume

g —> gram
- pg —> picogram
- ng —> nanogram

M —> mole
- pM —> picomole
- µlM —> micromole
- nM —> nanomole
- mM —> millimole

b —> base
- kb —> kilobase
- mb —> megabase

l —> litre
- nl —> nanolitre
- µl —> microlitre
- ml —> millilitre

time —> s —> second
- min —> minute
- h —> hour

Preface

This thesis consists of five chapters. **CHAPTER 1** introduces the study and states the study's aims. **CHAPTER 2** details the materials and methods utilised in the study. **CHAPTERS 3** and **4** contain the study's results and include descriptions of the design and development as well as the validation and clinical application of two novel tests for the assessment of preimplantation embryos. Each of these results chapters is further divided into five sub-sections: (1) summary of the chapter's background; (2) summary of utilised methods; (3) description of test design, development and validation; (4) results obtained after clinical application; (5) discussion of the test and clinical results. **CHAPTER 5** summarises the study's outputs and discusses the developed tests and results in a broader context.

The study design, experimental work, data analyses and result interpretations presented in the thesis are original. I designed and performed the majority of the experimental laboratory work during the development and validation phases of both tests. Any laboratory experiments or other tasks required for development or validation purposes performed by collaborators or members of my laboratory team (Reprogenetics UK) are explicitly stated in the materials and methods sections of the results chapters (**CHAPTERS 3** and **4**). In brief, collection of biological material, including blood and buccal samples as well as embryo specimens was performed by trained personnel of collaborating clinics. Tubing of cells was performed by members of the Reprogenetics UK or Reprogenetics US teams. Processing of parts of donated research embryos utilised during the pre-clinical validation of the test described in **CHAPTER 3** was performed by members of the Reprogenetics US team. Furthermore, initial proof-of-concept

experiments performed during the development of the test described in **CHAPTER 3**, were set up at a supplier site (ThermoFisher).

I further designed all data analysis strategies and performed all computational and statistical data analyses utilised during the development and validation of both tests. This also includes the establishment of a functional data analysis algorithm (described in **CHAPTER 3**) which can be used for data analysis and result interpretation in a clinical setting. Of note, to decrease the analysis time, the algorithm was converted into a command line operated PERL script by a bioinformatician.

Following validation, both tests were implemented clinically and offered by Reprogenetics UK as part of their clinical services. I was responsible for the translation of both tests into clinical practice. This included training of laboratory members in carrying out the tests, analysing the data and interpreting the results. To comply with accreditation norms, I was also responsible for preparation of staff training manuals and competency assessment forms, standardised laboratory and analysis protocols as well as test result documentation and reporting documents. Once the tests were offered clinically, I and other trained members of the Reprogenetics UK team were responsible for the communication with clinics regarding enrolment of patients and reporting of test results as well as processing of clinical samples. Of note, the majority of the clinical cases described in **CHAPTER 3** and all of the clinical cases described in **CHAPTER 4** were performed by me. Data analyses and result interpretations were always either performed or overseen by me.

Embryo specimens from embryos generated by two US-based patients were pre-processed in the Reprogenetics US laboratory and aliquots of the samples shipped to

Reprogenetics UK for further analysis. All procedures involving samples from patients referred by UK-based clinics were performed at Reprogenetics UK.

Handling of patients, including counselling, referral, consenting and treatment as well as handling of embryos, including culture, biopsy and transfer was performed by collaborating clinics.

The generated clinical data described in **CHAPTER 3** was retrospectively compared to previously generated data using a different test. This test was also conducted at the Reprogenetics UK laboratory and was performed by me as well as other members of the team. The data was collected by the laboratory's scientific director.

CHAPTER 1: Introduction and study aims

This chapter introduces the background of the thesis. The chapter is divided into four main parts. In the first part, the processes regulating the different stages of human preimplantation embryo development are described. In the second part, predictors of embryo viability are discussed in the context of assisted reproductive treatment (ART), emphasizing on factors impacting on embryo competence and implantation potential, in particular numerical chromosome abnormalities and mitochondrial dysfunction. In the third part, various techniques used for the assessment of cells derived from *in vitro* fertilised embryos are reviewed, including methods for chromosome copy number (CCN) analysis as well as mitochondrial DNA (mtDNA) quantification and mutation testing. In the last section, the aims of the undertaken research, including the development and clinical application of two novel methods for chromosome and mtDNA copy number analysis as well as mtDNA mutation testing in embryo specimens, are outlined.

1.1 Human preimplantation embryo development

Human preimplantation embryo development is a complex and dynamic process wherein the fertilised oocyte is prepared for implantation in the endometrium, the inner lining of the uterus. The different stages of preimplantation development are tightly regulated by different cellular and molecular mechanisms as well as epigenetic and cytoplasmic changes (**Figure 1.1**).

Prior to implantation, the embryo undergoes a series of developmental changes (**Figure 1.1 A**). Fusion of a haploid oocyte and a haploid sperm cell results in the formation of a diploid single-cell zygote. The zygote then undergoes a total of four cleavage divisions which results in the formation of the 2-cell, 4-cell, 8-cell and 16-cell embryo. Approximately

four days following fertilization, the embryo's cells, the blastomeres, compact which results in the formation of the morula. Approximately one day later, the blastocyst-stage embryo is formed. It consists of an outer trophectoderm cell layer which surrounds a fluid filled cavity and a cluster of cells known as the inner cell mass (ICM). After implantation, the trophectoderm forms part of the placenta and the ICM gives rise to the fetus (reviewed by Niakan et al., 2012).

At the cellular level (**Figure 1.1 B**), oocyte fertilisation initiates the completion of female meiosis. Following an asymmetric cell division, the second polar body is extruded and the totipotent zygote is formed. The zygote then undergoes mitotic symmetric cell divisions to generate an increasing number of totipotent blastomeres. These then compact via an increase in cell adhesions which results in the formation of the morula consisting of tightly bound cells. At this stage, cell polarisation and segregation is initiated. This results in the differentiation of the cells into the trophectoderm and the ICM and in the cavitation and local distribution of the two cell lineages within the blastocyst-stage embryo (reviewed by Niakan et al., 2012).

A crucial process occurring during preimplantation development is the maternal-to-zygote genome transcription transition which is essential for embryo growth and development (**Figure 1.1 C**). The early cellular processes, such as cleavage divisions, are strongly dependent on the initial supply of maternal messenger RNA (mRNA) molecules and proteins. These components decrease during development and are gradually replaced by zygotic gene products that are generated from the 4- to 8-cell stage onwards following embryonic genome activation (Braude et al., 1988; Dobson et al., 2004).

A further crucial process of preimplantation development is the reprogramming of the nuclear genome through epigenetic changes, such as demethylation of parental DNA (**Figure 1.1 D**). During this process, epigenetic marks are removed from the nuclear DNA (nDNA). This is crucial in order to generate totipotent cells to ensure transition from a metabolism dependent on maternal components to a metabolism regulated by the embryo's own genome and to establish new epigenetic modifications necessary for cell lineage specifications (Okae et al., 2014; Smith et al., 2014; reviewed in Monk, 2015).

The described cellular changes and regulatory molecular mechanisms require energy in form of adenosine triphosphate (ATP), which are produced by the mitochondria present in embryonic cells. Biosynthesis of mitochondria is only initiated after blastulation. Hence, the embryo is dependent on energy generated by mitochondria of the mature oocyte. Because cleavage divisions result in a reduction of mitochondria per cell, the organelles undergo structural changes and cytoplasmic relocation to ensure sufficient energy supply (**Figure 1.1 E**). The changes in mitochondrial structure result in a higher energy output and the relocation of the organelles during cell cycles to sites of high energy demands ensures adequate energy supply for vital cellular processes (reviewed in Van Blerkom, 2004; reviewed in Chappel, 2013).

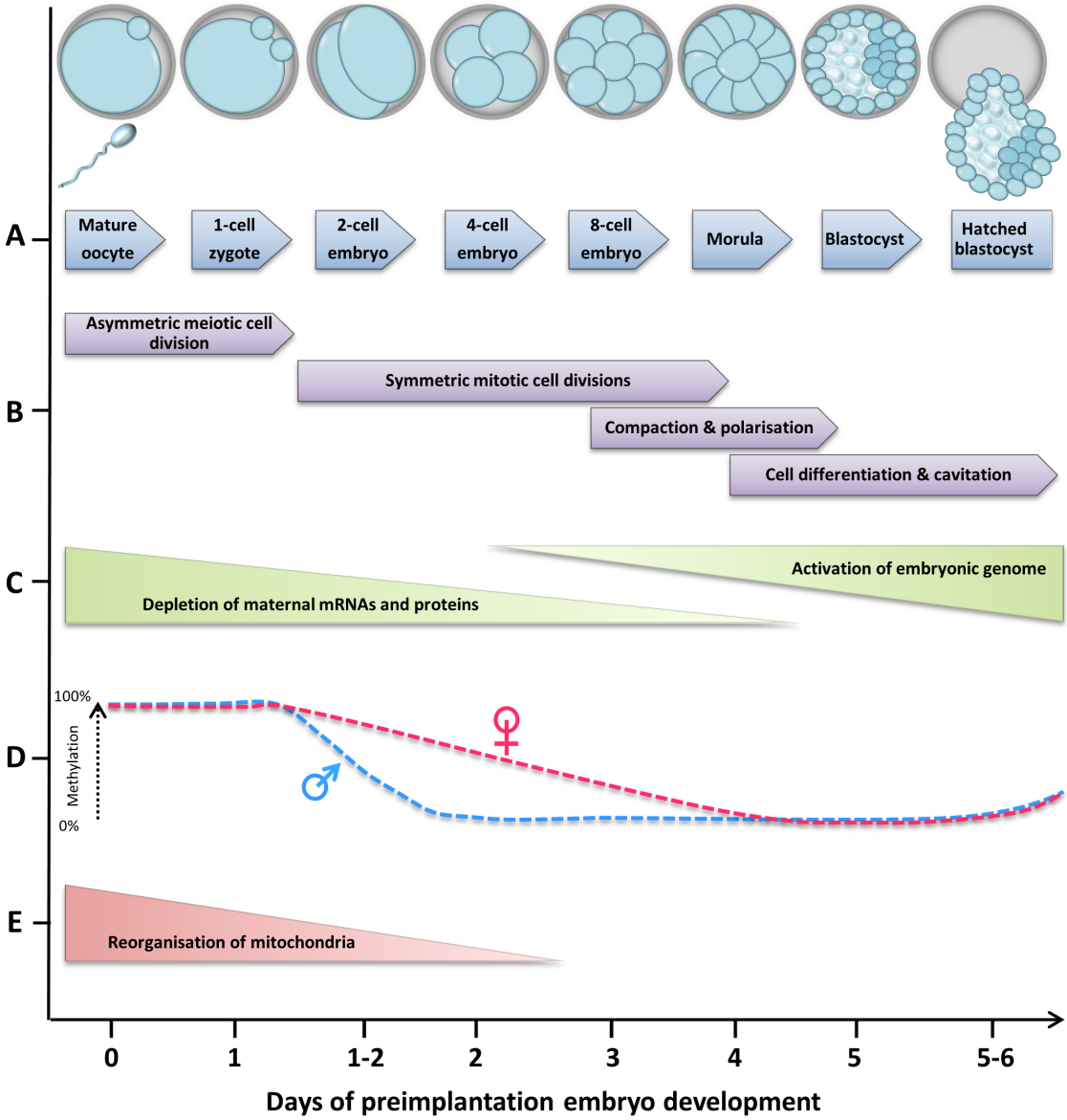


Figure 1.1: Human preimplantation embryo development. A: Phases of development. After fertilization, the zygote undergoes a series of cell divisions which results in the formation of the cleavage-stage embryo. At the 16-cell stage, the embryo compacts and forms the morula which consists of tightly bound blastomeres. This is followed by the generation of the blastocyst-stage embryo which consists of two different cell layers, the trophectoderm and the ICM, and a fluid filled cavity, the blastocoel. After hatching from the zona pellucida the blastocyst is ready to implant in the uterus. **B: Cellular processes.** Oocyte fertilisation leads to female meiosis completion and initiation of mitotic cell divisions. Cell compaction results in the formation of the morula. Cell polarisation is initiated which results in the differentiation of the embryonic cells into different cell lineages. **C: Embryonic genome activation.** Fertilisation results in the maternal-to-zygote genome transcription transition. While maternal mRNA and protein supplies gradually deplete, embryonic gene expression is initiated. **D: Epigenetic changes.** Embryonic genome activation requires reprogramming of the embryonic genome, whereby the maternal and paternal parts are actively and passively demethylated, respectively. *De novo* methylation is initiated prior to cell differentiation. **E: Reorganisation of mitochondria.** Following fertilisation, mitochondria undergo structural changes and are reorganised in embryonic cells to meet energy requirements.

1.2 Markers of embryo viability in assisted reproduction

Since the first baby was born as a result of *in vitro* fertilisation (IVF) in 1978, assisted reproductive techniques have improved significantly and are now responsible for approximately 3 % of all births in the UK (HFEA, 2018). However, despite major technological advances and decades of experience, it remains the case that about two thirds of all IVF cycles do not result in a live birth (Calhaz-Jorge et al., 2017).

One reason attributed to moderate IVF outcomes is poor embryo viability. In fact, the majority of embryos created through IVF is not capable of producing a viable pregnancy and most embryos transferred to the uterus fail to implant or miscarry shortly afterwards. In order to increase the chances of pregnancy, multiple embryos are often transferred. Although this practice improves the chances of positive IVF outcome it also increases the risk of multiple gestation and associated medical complications for the mother and her children (Pinborg, 2005).

In an attempt to increase pregnancy rates and to decrease multiple birth rates following IVF treatment, *in vitro* fertilised embryos are usually graded according to morphological criteria and those considered to display optimal characteristics are prioritised for uterine transfer (reviewed by Machtinger & Racowsky, 2013). Although morphological appearance and embryonic viability are correlated, embryo selection on this basis has only a limited capacity in improving IVF outcomes (Munné et al., 2007). It is therefore crucial to understand the mechanisms governing embryo development and the

causes underlying poor embryo viability in order to identify novel markers and to develop better tools which can aid in the selection of the best single embryo for transfer.

1.2.1 Chromosome copy number

To date, the best studied and most reliable predictor of embryo viability is the presence or absence of numerical chromosome abnormalities in embryonic cells. Aneuploidy, which describes the gain or loss of any of the 24 chromosomes, is extremely common during the early stages of embryonic development (Hassold & Hunt, 2001). If present in the majority of the cells, aneuploidy is likely to lead to early embryonic arrest, implantation failure and pregnancy loss (Lathi et al., 2008; Macklon et al., 2002; Magli et al., 2007; Morales et al., 2008; Munné et al., 1994).

Most aneuploidies in human embryos are *de novo* abnormalities and originate from chromosome segregation errors occurring during meiotic and/or mitotic cell divisions during gamete and preimplantation embryo development, respectively (Hassold & Hunt, 2001). Aneuploidies which are of meiotic origin are usually present in all embryonic cells. In contrast, aneuploidies which arise during mitotic cell divisions often occur in form of a 'mosaic' pattern resulting in embryos with different cell lines. Common mechanisms resulting in the generation of CCN errors during meiosis or mitosis are illustrated in **Figure 1.2** and **Figure 1.3**, respectively.

Meiosis, which consists of DNA replication and two consecutive cell division steps results in the formation of haploid gametes containing a single chromosome set. During the first meiotic division (MI) homologues chromosomes are separated following recombination and during the second meiotic division (MII) sister chromatids are

separated. As illustrated in **Figure 1.2**, aneuploidy can arise during both meiotic divisions, caused by non-disjunction of either homologues chromosomes (**Figure 1.2 B**) or of sister chromatids (**Figure 1.2 C**). Moreover, premature separation of sister chromatids prior to the completion of MI can result in the formation of aneuploid gametes (**Figure 1.2 D**). In addition, other less frequent mechanisms can cause generation of meiotic errors, including recombination failure and premature separation of homologous chromosomes during MI and premature separation of chromatids in MII (reviewed by Nagaoka et al., 2012). Different mechanisms can result in the generation of mitotic chromosome errors, of which non-disjunction of sister chromatids and anaphase lag are the most common (reviewed by Mantikou et al., 2012). Mosaic embryos can contain aneuploid cell lines only (**Figure 1.3 A**) or a mixture of aneuploid and euploid cell lines (**Figure 1.3 B**), which is largely dependent on the time the error(s) occurred.

Aneuploidy increases markedly with female age (reviewed by Nagaoka et al., 2012) but is not restricted to women of advanced maternal age. A high frequency of chromosomally abnormal embryos has been reported in younger women undergoing IVF treatment (Baart et al., 2006; Franasiak et al., 2014) and it is estimated that more than half of all embryos generated during IVF are chromosomally abnormal (Verlinsky et al., 2001). Importantly, the transfer of aneuploid embryos cannot be avoided via morphology-based embryo selection (Alfarawati et al., 2011; Capalbo et al., 2014; Fragouli et al., 2014). For this reason, testing of the presence of embryonic aneuploidy has been proposed as a strategy to aid in the selection of chromosomally normal embryos prior to uterine transfer (Munné et al., 1993a). Chromosome testing has been suggested to be of particular benefit to patients who suffer from recurrent miscarriage, recurrent IVF failure and patients of

advanced maternal age (reviewed by Wilton, 2002; Munné et al., 2005; Garrisi et al., 2009), as aneuploidy is likely to be more common in these patients. Chromosome testing has also been proposed as a strategy to improve selection for single embryo transfer in cases where multiple good-quality embryos are available to reduce multiple gestation risks (Yang et al., 2012; reviewed by Schoolcraft & Katz-Jaffe, 2013).

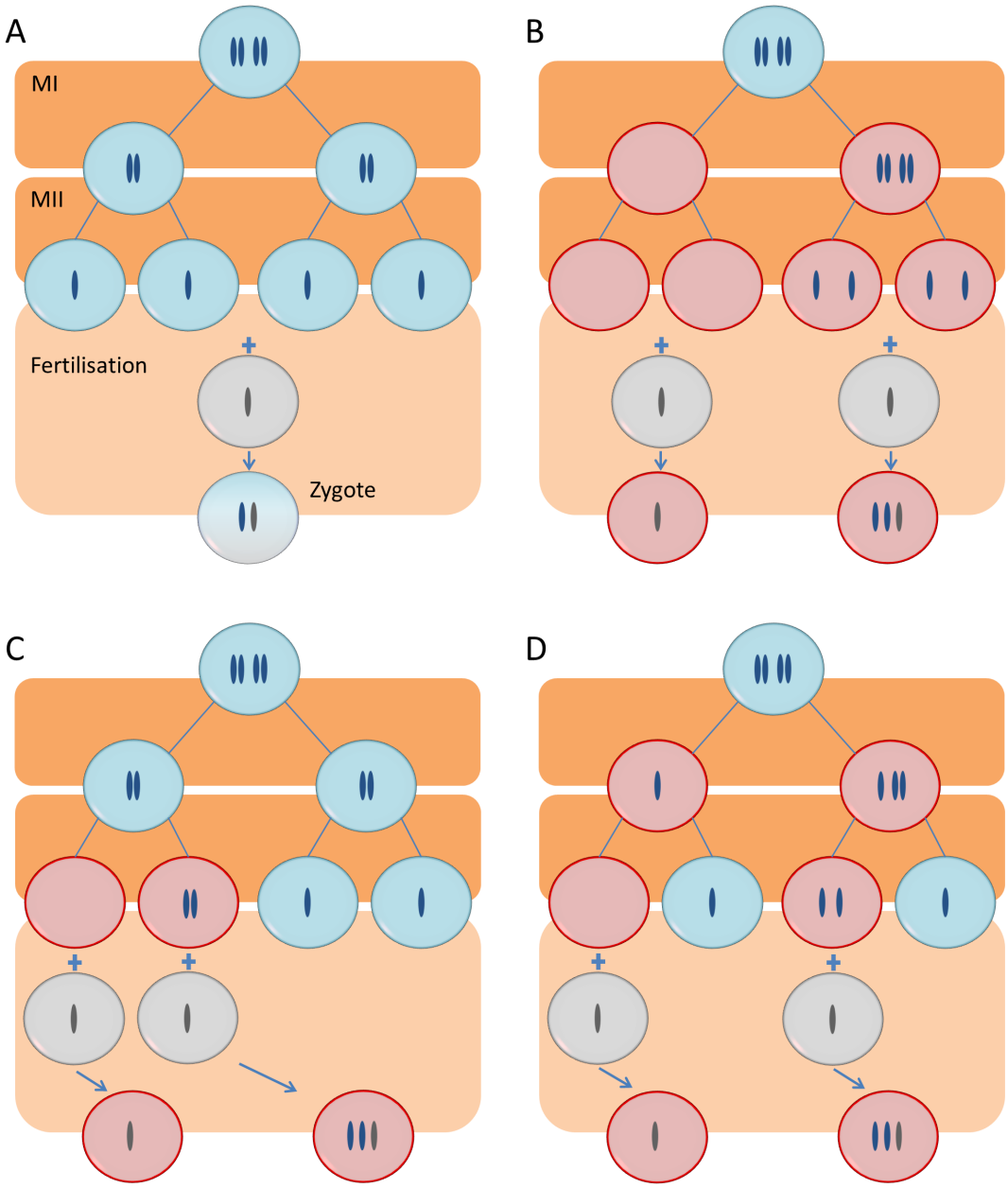


Figure 1.2: Schematic representation of common mechanisms resulting in aneuploidies of meiotic origin during gametogenesis. Cells coloured in blue or grey contain a normal CCN. Cells coloured in red are aneuploid. **A: Normal meiosis.** Diploid gametogonia (oogonia or spermatogonia) enter meiosis and undergo DNA doubling (not shown) resulting in the generation of diploid primary gametocytes (primary oocytes or primary spermatocytes). During MI, homologous chromosomes are separated resulting in the generation of haploid secondary gametocytes. During MII, sister chromatids are separated and haploid gametes (oocytes and spermatozoe) are formed. Fertilisation results in the generation of a zygote with a diploid chromosome content. **B: Non-disjunction during MI.** Failure of separation of homologues chromosomes results in the generation of chromosomally abnormal primary gametocytes and aneuploid zygotes. **C: Non-disjunction during MII:** Failure of sister chromatid separation results in the formation of aneuploid secondary gametocytes and zygotes. **D: Premature sister chromatid separation.** Separation of chromatids before MI completion can result in the generation of aneuploid primary gametocytes and zygotes.

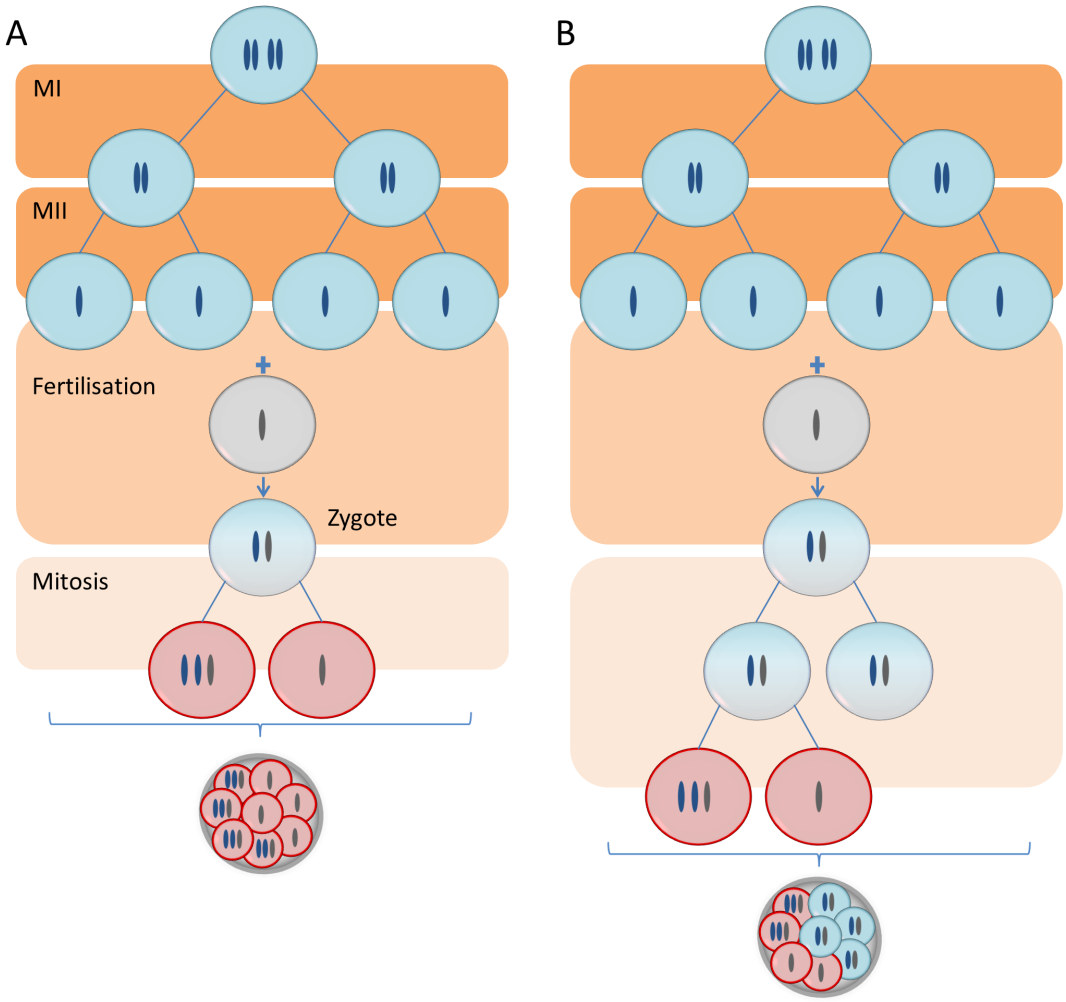


Figure 1.3: Schematic representation of the generation of mosaic mitotic aneuploidies during cleavage divisions. Cells coloured in blue or grey contain a normal CCN. Cells coloured in red are aneuploid. **A: Chromosome mal-segregation during the first mitotic division.** Chromosome segregation errors which occur during the first cleavage division result in the generation of fully mosaic aneuploid cleavage-stage embryos. **B: Chromosome mal-segregation during the second mitotic division.** Occurrence of chromosome segregation errors at the second or at a later cleavage division results in the generation of mosaic embryos with a mixture of euploid and at least two aneuploid cell lines.

1.2.2 Mitochondrial DNA copy number

Although embryonic aneuploidy is recognised as the major factor impacting on embryo viability, not all chromosomally normal embryos are capable of producing a viable pregnancy. In fact, approximately one third of all euploid embryos transferred to the uterus

fail to implant or fail to sustain implantation (Harton et al., 2013). It is clear that other factors, in addition to aneuploidy, impact on embryo viability.

During the past decade various other potential predictors of embryo viability have been explored, including morphokinetics of embryo development as well as the embryonic transcriptome, proteome and metabolome (reviewed by Aparicio-Ruiz et al., 2018; reviewed by Krisher et al., 2015; reviewed by Montag et al., 2013; reviewed by Uyar & Seli, 2014). However, investigation of these predictors has not yet led to the development of a reliable tool for routine embryo selection in the IVF laboratory.

More recently, researchers started to explore mitochondrial features as a potential biomarker of embryo viability and implantation potential. Mitochondria are organelles, which are present in the cytoplasm of most eukaryotic cells (**Figure 1.4**). Mitochondria contain their own genome, which is located in the mitochondrial matrix of the organelles. The mtDNA is a relatively small (approximately 16 kb in size), circular and double-stranded molecule containing 24 genes, which are involved in mtDNA translation [two ribosomal RNAs (rRNAs) and 22 transfer RNAs (tRNAs)] and 13 genes which encode sub-units of the respiratory chain (Anderson et al., 1981).

Mitochondria play an important role in different cellular mechanisms, including cell proliferation and cell differentiation, calcium homeostasis as well as lipid and iron sulphur cluster generation (reviewed by Khan et al., 2015). The most important function of mitochondria is the generation of cellular energy in form of ATP through oxidative phosphorylation (reviewed by Van der Giezen & Tovar, 2005).

Depending on cell type and energy demand, several hundreds of mitochondria can be present in a single cell (reviewed by Lightowlers et al., 1997). Importantly, of all cell types, mature oocytes carry the highest amount of mitochondria, up to 200,000 organelles, which are generated during oocyte maturation from a small starter pool present in the primordial germ cells (reviewed by Jansen & de Boer, 1998; reviewed by Shoubridge & Wai, 2007).

As biosynthesis of mitochondria is only initiated after implantation, successful completion of the different stages of preimplantation development is strongly dependent on energy generated by mitochondria coming from the ooplasm (reviewed by Chappel, 2013). As a consequence, mitochondrial dysfunction has a direct impact on embryo development and viability. For instance, mitochondrial malfunctioning is associated with ovarian insufficiency, meiotic spindle abnormalities and arrest, fertilisation failure, embryonic developmental arrest as well as poor embryo competence (Van Blerkom et al., 2000; reviewed by May-Panloup et al., 2007; Reynier et al., 2001; reviewed by Schatten et al., 2014; Yamanaka et al., 2011).

As mitochondria play a vital role in embryo development, mitochondrial function has been proposed as a clinical parameter for embryo selection, in addition to morphology and chromosome content. Several recent studies have investigated the relationship between mtDNA copy number and implantation potential in blastocyst-stage embryos. Research undertaken by Fragouli et al. (2015) and Diez-Juan et al. (2015) have shown a strong correlation between elevated mtDNA content and decreased implantation potential in blastocyst-stage embryos, suggesting that mtDNA copy number could serve as a potential biomarker for assessing viability of euploid embryos. Moreover, these findings

were confirmed in a recent blinded prospective non-selection study which demonstrated that euploid, good-quality embryos containing high amounts of mtDNA have a significantly reduced implantation potential (Fragouli et al., 2017b). Of note, two other recent studies failed to identify a correlation between implantation potential and mtDNA levels in euploid embryos (Treff et al., 2017; Victor et al., 2017). Hence, further studies are required to determine if measurement of embryonic mtDNA levels could be used in embryo selection.

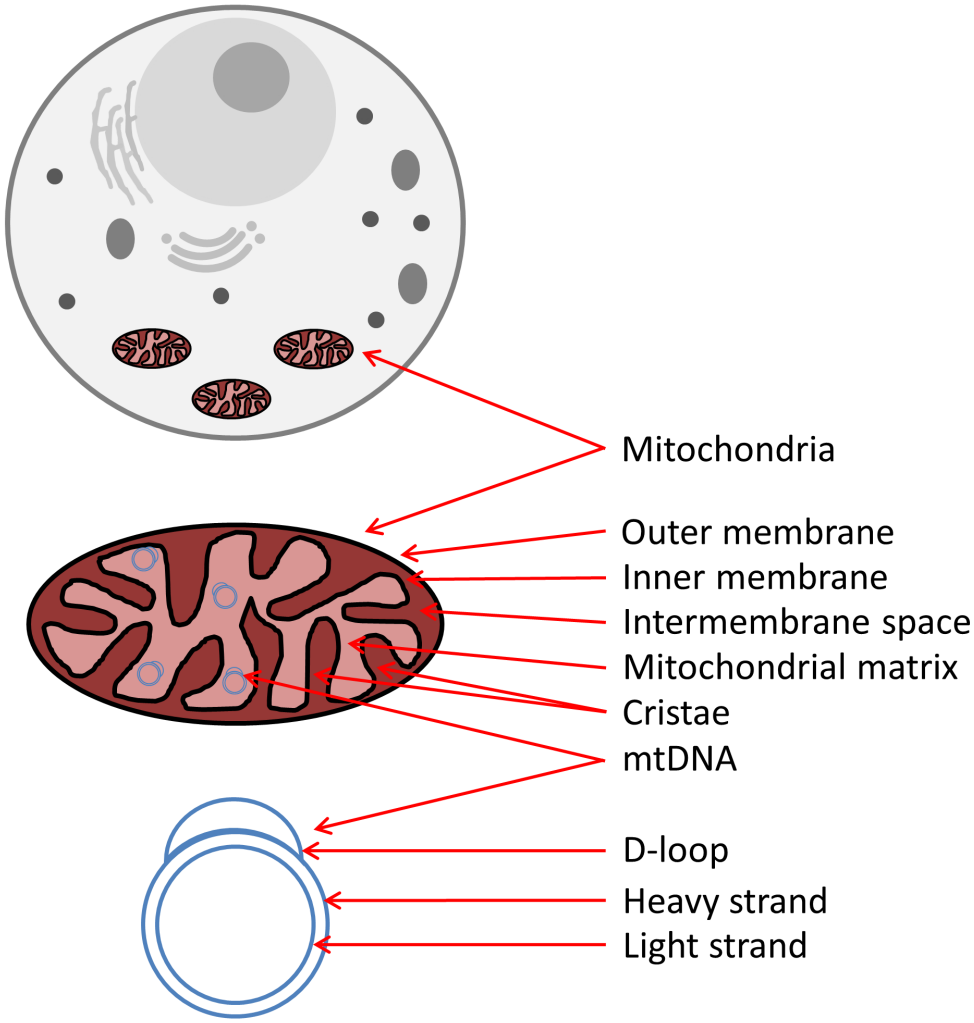


Figure 1.4: Schematic representation of mitochondrial structure and compartments. Mitochondria consist of two membranes, encompassing the intermembrane space. The inner membrane which is folded into cristae surrounds the mitochondrial matrix, which contains the mtDNA. The mtDNA molecule is circular and consists of an outer (heavy) and an inner (light) strand as well as a displacement loop (D-loop) for mtDNA replication and RNA transcription.

1.3 Preimplantation genetic testing

Preimplantation genetic testing (PGT) is an umbrella term describing procedures used for the genetic analysis of *in vitro* fertilised embryos prior to uterine transfer. Procedures involved in PGT can be divided into two main categories: (1) preimplantation genetic screening (PGS); (2) preimplantation genetic diagnosis (PGD). The term PGS is commonly used to describe cytogenetic techniques used for the analysis of numerical chromosome abnormalities in embryos of patients undergoing IVF treatment. In contrast, PGD mostly refers to the analysis of hereditary genetic disorders and is used to prevent disease transmission to the offspring (reviewed by Dahdouh et al., 2015c). In both cases, only embryos which are unlikely to carry chromosome abnormalities or genetic defects are selected and transferred to the uterus.

PGT can be performed at three different stages during preimplantation development (**Figure 1.5**): (1) at the time of fertilisation by removing the first and/or second polar body from the oocyte and/or the zygote; (2) at the cleavage-stage on day-3 post fertilisation by removing one or two blastomere(s); (3) at the blastocyst-stage on day-5 or day-6 post fertilisation by removing approximately five cells from the outer trophectoderm layer (reviewed by Harton et al., 2011).

Each of the techniques has its advantages and disadvantages. Polar body biopsy is considered to be the least invasive technique, since it does not reduce the embryo's total mass. If properly performed, it is unlikely that polar body biopsy will have a deleterious impact on embryo viability (reviewed in Verlinsky & Kuliev, 1996). However, testing is limited to the analysis of chromosome abnormalities arising during female meiosis and/or

genetic defects carried by the mother. Moreover, PGT in polar bodies is less cost-effective as compared to testing at later stages of development, because of the higher number of cells that need to be analysed, many of which may be associated with oocytes that fail to produce embryos suitable for transfer to the uterus.

In contrast to polar body testing, blastomere or trophectoderm biopsy allows additional detection of chromosome errors introduced by the sperm cell and those of post-zygotic origin as well as testing for paternal genetic defects. Cleavage-stage biopsy is considered by some to be more invasive than blastocyst-stage biopsy since the embryo consists of only approximately eight cells at the time of biopsy and at least one must be removed for analysis. In contrast, at the blastocyst-stage, the embryo is composed of approximately 200 cells and is therefore less likely to be adversely impacted by the removal of a small number of cells (Scott et al., 2013b). In addition, blastocyst-stage biopsy is likely to exhibit increased accuracy of PGD since a greater quantity of genetic material is available for analysis subsequently reducing the chances of allele dropout.

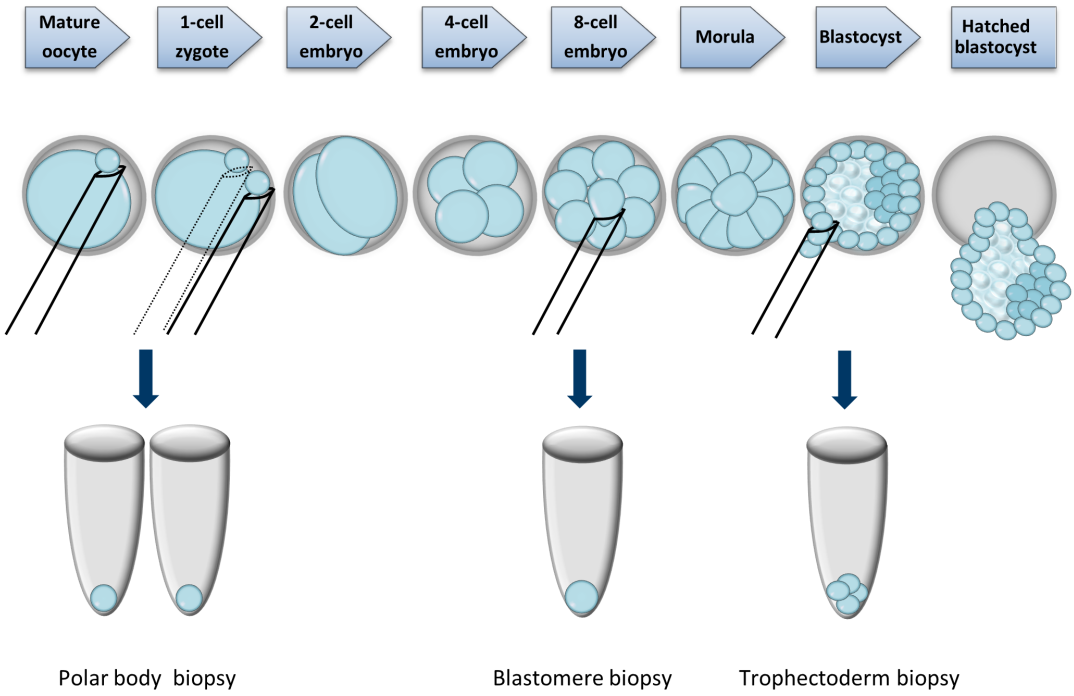


Figure 1.5: Embryo biopsy procedures. Embryonic material can be sampled at three different stages during embryo development, by removal of either one or both polar bodies, one or two blastomeres or several trophectoderm cells.

1.3.1 Preimplantation genetic screening

PGS was introduced into clinical practice in the mid-1990s. Ever since, efficiency of PGS in improving live birth rates has been a matter of debate. In theory, the transfer of a chromosomally normal embryo should enhance IVF outcomes. However, initial PGS approaches, utilising fluorescence *in situ* hybridisation (FISH) for the detection of aneuploidies in cleavage-stage embryos failed to deliver benefits to overall IVF outcomes in randomised clinical trials (Debrock et al., 2010; Hardarson et al., 2008; Jansen et al., 2008; Mastenbroek et al., 2007; Mastenbroek et al., 2011; Mersereau et al., 2008; Meyer et al., 2009; Schoolcraft et al., 2009).

The adverse results obtained from those trials may be explained by technical as well as biological limitations: (1) FISH is limited by the number of available probes and

hence the number of chromosomes that can be tested. At maximum, 12 chromosomes can be assessed simultaneously (Munné et al., 2010a), which means that aneuploidies not tested for are missed. Considering that aneuploidy can affect any of the 24 chromosomes (Fragouli et al., 2013), FISH represents a suboptimal PGS technique; (2) most of the FISH studies were performed on cleavage-stage embryos and involved the analysis of one or two cells. However, blastomere biopsy can be harmful to the embryo, particularly if two cells are biopsied (Cohen et al., 2007; reviewed in Munné et al., 2010b; Scott et al., 2013b; reviewed in De Vos & Van Steirteghem, 2001); (3) high levels of chromosomal mosaicism are frequent in cleavage-stage embryos, which means that the biopsied cell(s) may not be representative of the embryo remainder (Vanneste et al., 2009).

Taken together, incomplete cytogenetic evaluation of the chromosome complement, possible biopsy damage to the embryo as well as the possibility that the biopsied sample might not be representative of the entire embryo, represents a significant limitation of early FISH-based PGS studies. Moreover, a potential benefit of PGS on IVF outcomes is strongly dependent on the accuracy of the aneuploidy detection technique.

In the last 20 years, PGS approaches have undergone a steady stream of developments to overcome the previous limitations. A number of comprehensive chromosome screening (CCS) technologies have been developed and implemented in order to allow the analysis of all 24 chromosomes (**Figure 1.6**). These include comparative genomic hybridisation (CGH) techniques, initially metaphase CGH (Schoolcraft et al., 2010; Wells et al., 1999; Wilton et al., 2001) and later array CGH (Gutiérrez-Mateo et al., 2011), alongside with single-nucleotide polymorphism (SNP) arrays (Treff et al., 2010). Soon, the pool of available techniques was extended to include quantitative real-time PCR, also

referred to as real-time qPCR (Treff et al., 2012b) and most recently, next-generation sequencing (NGS) has entered the field of preimplantation testing (Fiorentino et al., 2014a; Fiorentino et al., 2014b; Wells et al., 2014; Yin et al., 2013).

The development of most of these CCS techniques was made possible as a result of whole genome amplification (WGA) techniques, which amplify the minute amount of DNA obtained from embryo biopsies to levels sufficient for downstream applications. As illustrated in **Figure 1.6 A**, the principle of CGH is that it relies on differentially fluorescently labelled DNAs from test and control samples which are then co-hybridised to metaphase chromosomes on a microscope slide (metaphase CGH) or to bacterial artificial chromosome clones immobilised on a microarray (array CGH). Fluorescent signals originating from both, test and control samples are then captured by scanning and signal intensities are converted into CCNs using specialised software (Gutiérrez-Mateo et al., 2011). In contrast, SNP arrays utilise polymorphic variant probes scattered across chromosomes. Labelled samples are co-hybridised to DNA probes bound to the glass surface of microscope slides. To assess CCNs, signal intensities are captured and allele frequencies of SNP probes are determined. Genotypic information of parental DNA can be used as references (reviewed by Harper and SenGupta, 2012).

In contrast to array-based techniques, real-time qPCR does not require WGA and instead uses a targeted amplification of genomic loci spread across the genome to enrich sample DNA content. This is followed by real-time qPCR where the amount of amplified DNA is quantified using fluorescently labelled probes and converted into copy number quantities (Treff et al., 2012b).

Finally, the most widely used NGS-based PGS protocols were developed and validated for the use of WGA products. After sequencing of sample DNA, the obtained sequences are aligned to a human reference genome. The mapped sequencing reads are then counted and the proportion derived from individual chromosomes is compared to an internal reference (Fiorentino et al., 2014a; Wells et al., 2014).

In addition to technological advancements, improvements in embryo culture and biopsy techniques have enabled culture of embryos up to the blastocyst-stage and testing of trophectoderm biopsy samples, rather than blastomeres (Kokkali et al., 2005; McArthur et al., 2005). Trophectoderm biopsy is thought to be less invasive as compared to cleavage-stage biopsy. Moreover an increased amount of cells obtained from a trophectoderm biopsy is likely to increase the capacity to detect errors caused by embryonic mosaicism. The clinical utilisation of these novel CCS methods was also enabled by the creation of cryopreservation tools and the development of improved freezing techniques such as vitrification (reviewed by Youssry et al., 2008). This means that there is sufficient time for genetic testing following trophectoderm biopsy.

Ever since the implementation of CCS, several observational studies (Forman et al., 2012; Greco et al., 2014; H.-L. Lee et al., 2015; Schoolcraft et al., 2010), as well as, randomized controlled clinical trials (Forman et al., 2013; Scott et al., 2013a; Yang et al., 2012) have been carried out in blastocyst-stage embryos to determine the success of these methods in improving IVF outcomes. The cumulative data obtained from all of these studies provides strong evidence in support of the hypothesis that PGS-based embryo selection can significantly improve IVF outcomes by increasing the chance of a viable pregnancy per embryo transfer. The data also supports the notion that miscarriage rates can be reduced

using PGS. Furthermore, benefits were observed in good prognosis patients in addition to those observed in poor prognosis patient categories.

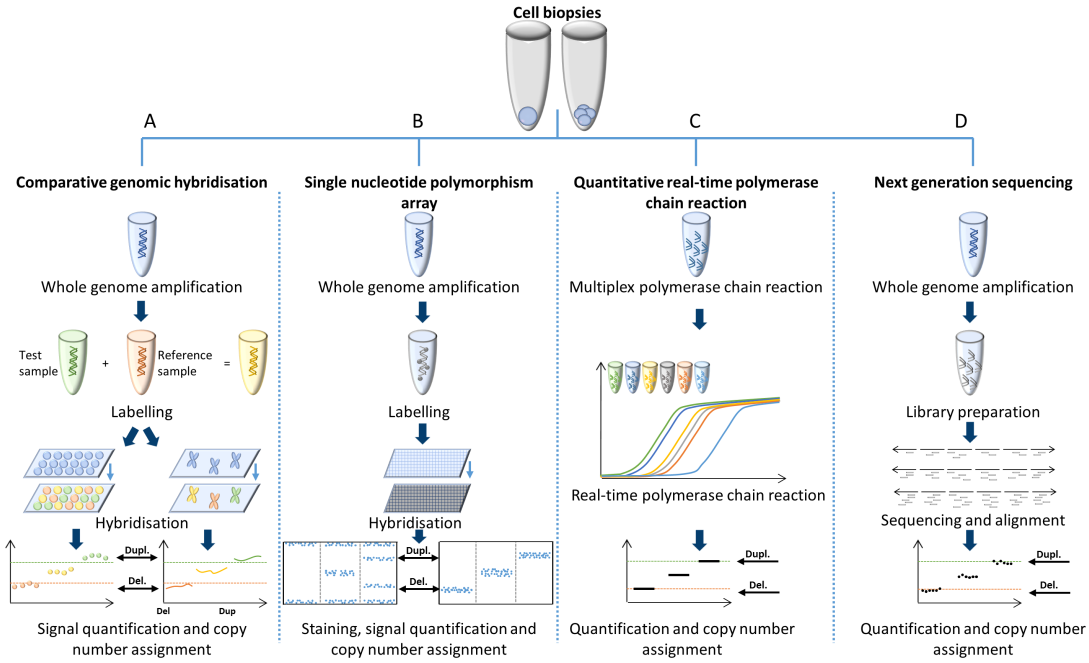


Figure 1.6: Illustration of methods used for CCS. Four different techniques have been utilised for CCS-based PGS. **A: CGH.** The technique is based on competitive *in situ* hybridisation of a test and reference sample. Following cell lysis and WGA the samples are differently labelled and co-hybridised to either artificial chromosome probes or to a metaphase spread of chromosomes. To determine changes in CCNs, fluorescent signals from test and reference samples are compared. **B: SNP array.** The technique is based on the detection and quantification of polymorphic variants. After cell lysis and WGA the sample DNA is biotin-labelled and hybridised to DNA probes. To assess CCNs, signal intensities and allele frequencies of SNP probes are measured. **C: Real-time qPCR.** Cell lysis is followed by pre-amplification of genomic regions scattered across the human genome. Each locus is then amplified separately during real-time qPCR. By measuring fluorescent signals coming from the probes that bind to the amplification products, quantities of each locus can be determined and converted into CCNs. **D: NGS.** Libraries, which are prepared from samples subjected to WGA, are sequenced. The resulting reads are aligned to the human genome and reads per bin counted. Changes in CCNs are determined by comparing the number of obtained reads to an internal control.

1.3.2 Preimplantation genetic diagnosis of mitochondrial DNA disease

Unlike PGS, which aims at increasing IVF outcomes by selecting euploid embryos for transfer, PGD aims to prevent the transmission of inherited diseases or genetic

abnormalities to the offspring by selecting embryos for transfer, which are unlikely to be affected by the tested genetic abnormality.

The main indications for PGD are recessive and dominant autosomal or X-linked single-gene disorders (e.g. Beta-thalassemia, Huntington's disease or Fragile-X Syndrome), chromosome disorders (e.g. Robertsonian or reciprocal translocations) as well as some forms of hereditary cancers, such as breast cancer caused by mutations in breast cancer type 1 and type 2 susceptibility protein genes (reviewed by Dahdouh et al., 2015c).

PGD was applied clinically for the first time in 1989 in couples at risk of transmitting X-linked disorders to their children (Handyside et al., 1990). At the time, PCR was used to determine the sex of the embryos prior to transfer by amplifying a segment of the Y chromosome. Since then, PGD strategies have considerably evolved. FISH was soon introduced for the purpose of embryo sexing in X-linked diseases (Munné et al., 1993b; Griffin et al., 1994) as well as the analysis of inherited structural chromosome abnormalities (Munné, 2001). These are now commonly tested using array CGH (Colls et al., 2012; Fiorentino et al., 2011) or SNP array technologies (Tan et al., 2013; Treff et al., 2011) and most recently using NGS-based testing (W. Zhang et al., 2016).

The analysis of monogenetic disorders was further improved by the introduction of PCR techniques, such as multiplex PCR combined with different downstream applications, such as minisequencing (Fiorentino et al., 2006) and most recently by the implementation of karyomapping, which utilises SNP arrays (Handyside et al., 2010).

Unlike PGD of monogenic or chromosome disorders where the presence or absence of specific mutations or chromosomal fragments is tested, PGD of mitochondrial

disease caused by mtDNA mutations aims to quantify the proportion of mutant and wild-type mtDNA molecules present in preimplantation embryos.

Mitochondrial and nuclear genetics are different in several aspects: (1) inheritance of mtDNA differs from the classic Mendelian inheritance. After fertilisation, all sperm-derived mtDNA molecules are actively destroyed (Pyle et al., 2015). As a result, the mtDNA is solely inherited from the mother (Giles et al., 1980), unlike the nDNA which is inherited from both parents; (2) the mtDNA is a multi-copy genome and depending on cell type and energy demand, between 100 to 10,000 copies can be present in a single somatic cell and more than 100,000 copies in a mature oocyte (reviewed in Cummins, 1998). In contrast, the nDNA is present in form of a single diploid copy in each cell; (3) the mtDNA is particularly prone to mutations and has a significantly higher mutation rate compared to its nuclear counterpart (Brown et al., 1979). Although, mtDNA is organised in DNA-protein structures, it lacks protective histone complexes, making it more susceptible to oxidative DNA damage (reviewed in Greaves et al., 2012). Furthermore, mtDNA replicates independently to the cell cycle and at a much higher rate than nDNA, which increases the possibility of replication errors. Finally, mtDNA repair mechanisms are less efficient as compared to the nDNA repair machinery (reviewed by Pinto & Moraes, 2015).

The term 'mitochondrial disease' comprises a heterogeneous collection of disorders which can differ in severity and disease onset and can affect different organs and tissues or groups of organs (reviewed by Wallace et al., 1999). Mitochondrial diseases are commonly characterised by a reduction in cellular energy production, which particularly affects organs high in energy demand such as the brain, liver or heart (reviewed by Greaves et al., 2012) leading to developmental delay, metabolic disorders and cardiovascular

diseases, amongst others (reviewed by Wallace et al., 1999). Although mitochondria contain their own genome, biological function is strongly dependent on nuclear-encoded proteins and regulated by both, the nuclear as well as the mitochondrial genome (Calvo et al., 2016). Consequently, mitochondrial diseases can be caused by genetic defects occurring in either of the genomes.

It is estimated that approximately 1:5,000 individuals develop a mitochondrial disease (Darin et al., 2001; Gorman et al., 2015; Skladal et al., 2003) and in about half of the cases, the disease is caused by a mutation or deletion present in the mtDNA (Gorman et al., 2015; Schaefer et al., 2008). Importantly, the carrier rate is much higher and it is estimated that about 1:200 individuals carry a potentially pathogenic mtDNA mutation (Chinnery et al., 2000; Elliott et al., 2008; Manwaring et al., 2007).

Since mtDNA is a multi-copy genome, mutated mtDNA copies and those carrying no mutation (wild-type) usually coexist in a single cell, which is known as heteroplasmy. A situation where only mutated or only wild-type mtDNA molecules are present is known as homoplasmy. Although mutations occur frequently in the mitochondrial genome, the impact on cell function is mostly insignificant, due to low levels of heteroplasmy. Only if a critical threshold of mutated mtDNA copies is exceeded, clinical symptoms manifest (Howell, 1983; Jeppesen et al., 2006; reviewed by Stewart & Chinnery, 2015). As a result, most carriers of a mtDNA mutation have no symptoms and are therefore unlikely to develop a mtDNA disease. In most mtDNA disorders, heteroplasmy levels are an indicator of disease severity which can range from asymptomatic to mild and severe (Black, Morten, Laborde & Poulton, 1996; White et al., 1999a). Sometimes, however, mtDNA mutations

only weakly correlate with the phenotype (Chinnery et al., 1997; Poulton et al., 2010; Thorburn & Dahl, 2001).

The difference in the proportions of mutant and wild-type mtDNA copies is believed to be caused by the mitochondrial genetic bottleneck occurring in the female germ line (reviewed by Carling et al., 2011). Female germ cell development is characterised by a drastic reduction in mtDNA molecules which can lead to a marked variability in heteroplasmy levels in oocytes of the same individual. Little is known about the exact mechanism, although three different mechanisms causing the genetic drift have been proposed: (1) unequal segregation of mtDNA variants between daughter cells, which is shown in **Figure 1.7** (Cree et al., 2008); (2) unequal segregation of nucleoids (mtDNA-protein complexes) containing identical mtDNA molecules, which is shown in **Figure 1.8** (Cao et al., 2007; reviewed by Carling et al., 2011); (3) preferential replication of mtDNA variants, which is sown in **Figure 1.9** (Wai et al., 2008).

Due to varying levels of heteroplasmy between individual oocytes of a mtDNA mutation carrier, mutation levels can differ markedly in the offspring. As a consequence, asymptomatic carriers are at risk of giving birth to children who are clinically affected. Vice versa, females who carry somatic mtDNA mutation can have mutation-free oocytes or oocytes with low heteroplasmy levels resulting in healthy children (Blok et al., 1997; Brown et al., 2001).

Currently no cure for mtDNA disease is available and treatment is limited to the management of symptoms (reviewed by Suomalainen, 2011). However, in order to minimise the risk of disease transmission to the offspring or to future generations, PGD can be performed in couples at risk of transmitting a mtDNA disease. Few reports on PGD of

mtDNA disease have been published, most of which focused on identifying the best developmental stage for biopsy and genetic analysis.

The feasibility of PGD of mtDNA disorders was for the first time demonstrated by Briggs et al. (2000) who demonstrated presence of mtDNA sequences in the first polar bodies of unfertilised human oocytes, concluding that testing at the earliest stage of embryonic development may be a suitable option for PGD. Shortly after, Dean et al. (2003) demonstrated that heteroplasmy levels measured in first polar bodies confirm those present in the oocyte using a heteroplasmic mouse model. Similarly, good agreement in heteroplasmy rates between second polar bodies and corresponding zygotes were observed in another murine model (Sato et al., 2005). In contrast, a recent study found that only modest correlations between first and second polar bodies and corresponding oocytes and zygotes were present in mice (Neupane et al., 2014b). Conflicting results on the utility of polar body biopsy for PGD of mtDNA disease has also been reported in several studies performed in humans. In a relatively larger study, which included 51 first polar bodies and their counterparts (oocytes, blastomeres and/or entire cleavage-stage embryos) derived from patients with various mtDNA mutations, little agreement was reported (Gigarel et al., 2011). This finding was supported by two additional studies, both of which did not find agreement between second polar bodies and corresponding first polar bodies and oocytes/blastomeres (Vandewoestyne et al., 2011; Vandewoestyne et al., 2012).

Alternative to the assessment of polar bodies, genetic analysis can be performed in blastomeres of cleavage-stage embryos. However, all studies performed to date reported presence of mosaicism between individual sister blastomeres, ranging from 0 - 24 % in variability (Steffann et al., 2006; Tajima et al., 2007; Monnot et al., 2011; Treff

et al., 2012a; Vandewoestyne et al., 2012). Due to the differences in heteroplasmy levels observed between individual blastomeres of the same embryo, two cells are often removed for PGD of mtDNA disease to increase accuracy of the test. However, biopsy of two blastomeres from cleavage-stage embryos is associated with decreased embryo viability (De Vos et al., 2009). Therefore, recent studies have focused on the assessment of trophectoderm biopsies obtained from blastocyst-stage embryos, which is known to be less invasive compared to cleavage-stage biopsy (Scott et al., 2013b). Moreover, since multiple cells are retrieved, testing of mutation load in blastocyst-stage biopsies should increase accuracy of predicting mutation load in the embryo. To date, two studies have been undertaken, assessing variability in heteroplasmy levels at the blastocyst-stage. Treff et al., (2012a) reported consistent distribution of mutant mtDNA copies between multiple trophectoderm biopsies of same blastocysts. Most importantly, trophectoderm mutant load resembled those found in the ICM. This finding was supported by a recent study by Heindryckx et al., (2014), where concordant heteroplasmy levels between individual trophectoderm biopsies of same blastocysts were found. Moreover, the authors also reported that mutation loads present in small cytoplasmic fragments resembled those detected in the trophectoderm.

To date, two different techniques for PGD of mtDNA disease have been applied clinically which have resulted in the birth of eleven children (reviewed in Greenfield et al., 2017). These include analysis based on either restriction fragment length polymorphism (RFLP) or amplification refractory mutation system (ARMS). In both techniques, the biopsied cell(s) are lysed and the DNA is isolated. This is followed by PCR, wherein the locus containing the mutation of interest is amplified (**Figure 1.10**).

The RFLP technique utilises restriction enzymes that target either the wild-type or mutant allele. Following enzymatic digestion of the amplification product the resulting DNA fragments are assessed. This can be done via visualisation of the separated fragments after either agarose gel electrophoreses or capillary electrophoresis (**Figure 1.10 A**). Of note, in clinical PGD cases the latter visualisation tool is used, as it allows the calculation of heteroplasmy levels in addition to the detection of presence or absence of the mutation (Heindryckx et al., 2014; Monnot et al., 2011; Sallevelt et al., 2013; Steffann et al., 2006; Thorburn et al., 2009). Of note, the accuracy of this technique has been questioned as it is associated with frequent technical errors, such as incomplete digestion or heteroduplex formation, resulting in mtDNA mutation quantification errors (Monnot et al., 2011).

As illustrated in **Figure 1.10 B**, the ARMS technique for PGD of mtDNA disease utilises real-time qPCR using two differentially labelled probes, of which one binds to the mutant and the other to the wild-type allele. Presence or absence of the wild-type and/or mutant allele as well as heteroplasmy levels are assessed by measuring signal quantities of the bound probes (Singh et al., 2006; Treff et al., 2012a). Of note, mtDNA mutant levels of one child conceived after application of ARMS was significantly higher after birth as compared to the level predicted at the time of PGD (Mitalipov et al., 2014).

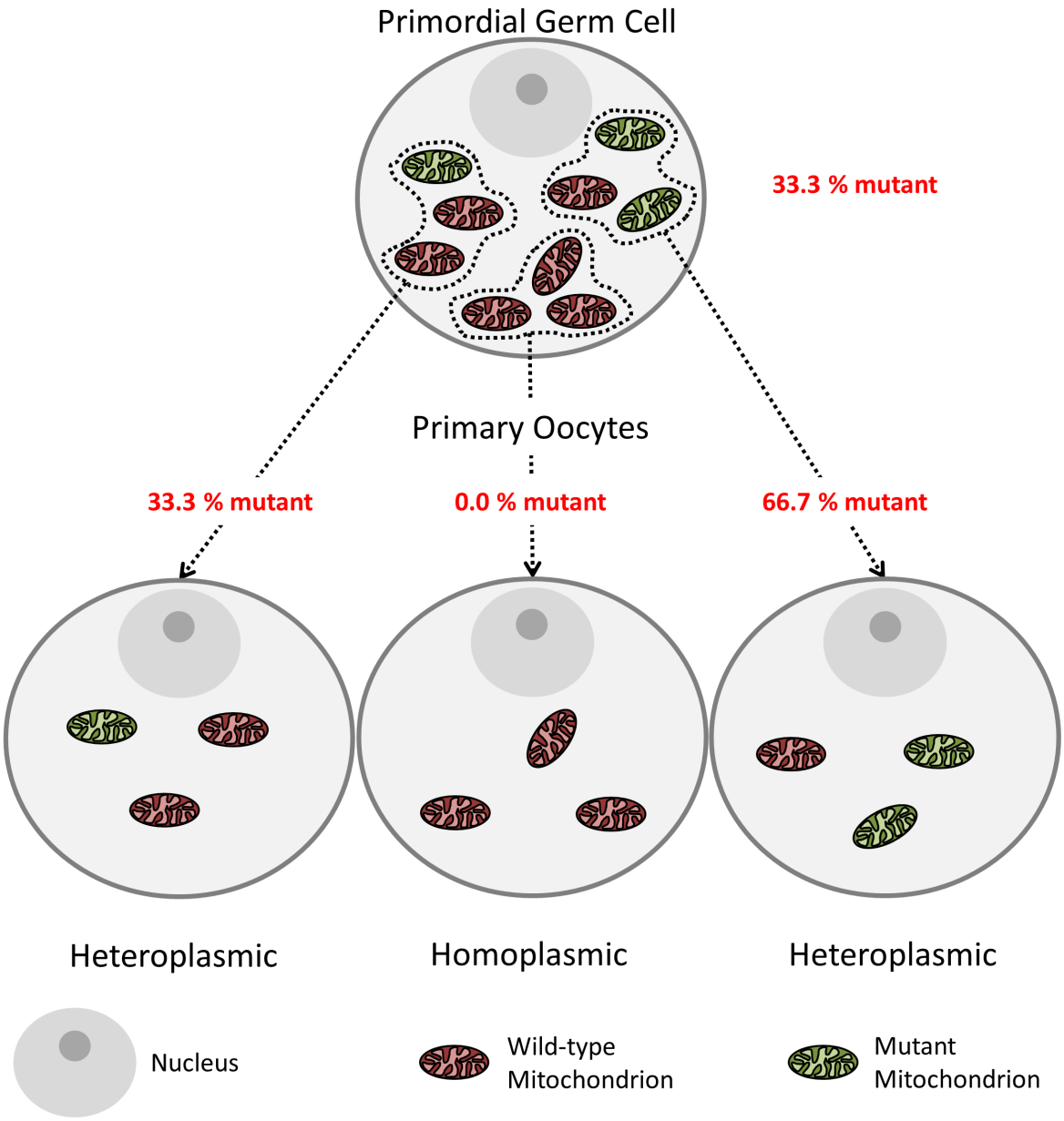


Figure 1.7: Unequal segregation of mtDNA variants. The proposed mechanism suggests that the marked reduction in mtDNA molecules occurring during female germ line development is leading to an unequal parting of mutated and wild-type mtDNA molecules resulting in the generation of oocytes carrying identical mtDNA genotypes (homoplasmic for either mutant or wild-type molecules) or in heteroplasmic oocytes containing a mix of wild-type and mutant mtDNA copies.

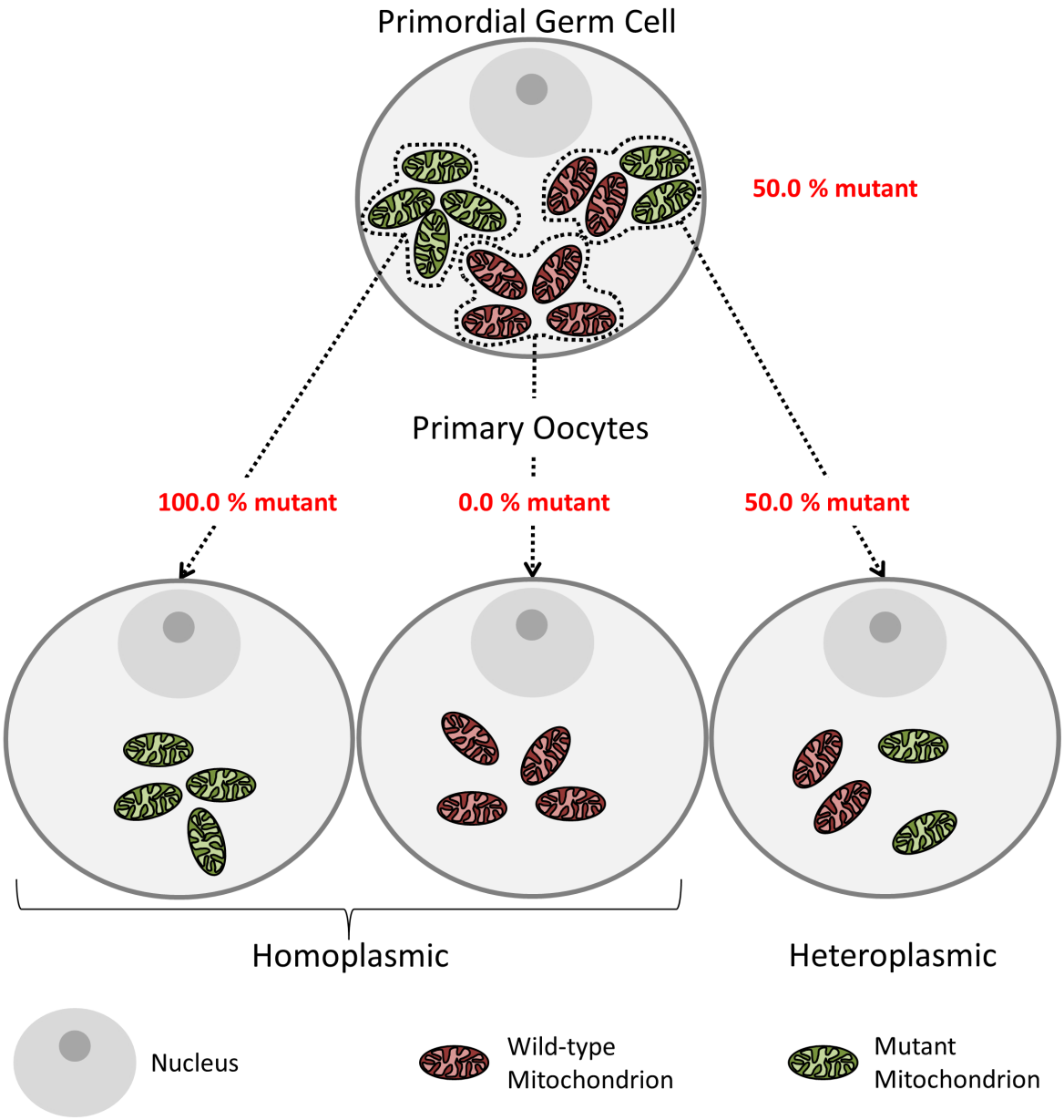


Figure 1.8: Unequal segregation of nucleoids with identical mtDNA molecules. The proposed mechanism suggests that identical mtDNA molecules form clusters (nucleoids) which segregate together to daughter cells. This causes an unequal parting of mutated and wild-type mtDNA molecules and results in the generation of homoplasmic or heteroplasmic oocytes.

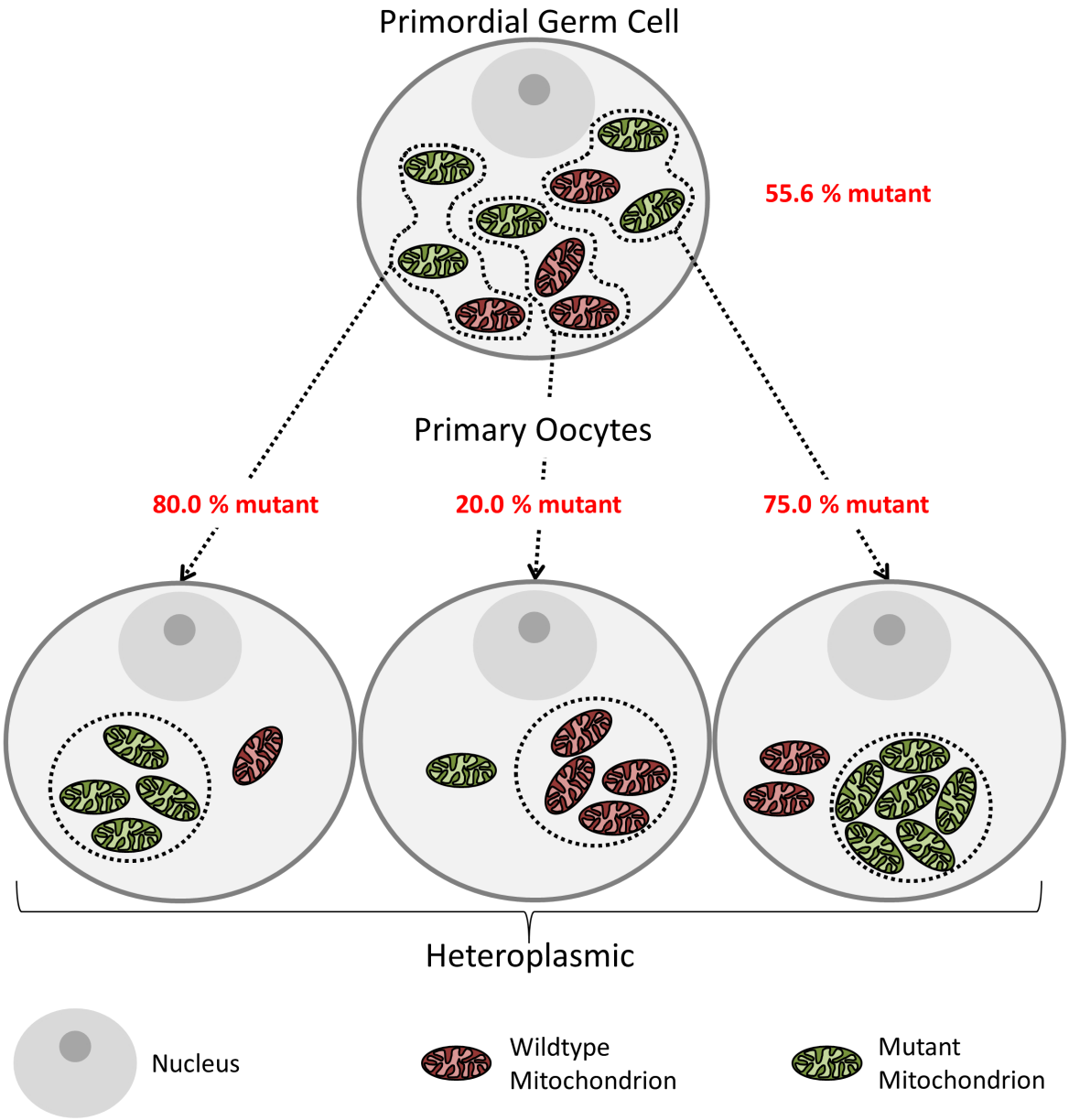


Figure 1.9: Preferential replication of mtDNA variants. The proposed mechanism describes an unequal amplification of sub-groups of mtDNA variants during oocyte maturation. Like other proposed mechanisms, it can lead to the generation of homoplasmic or heteroplasmic oocytes.

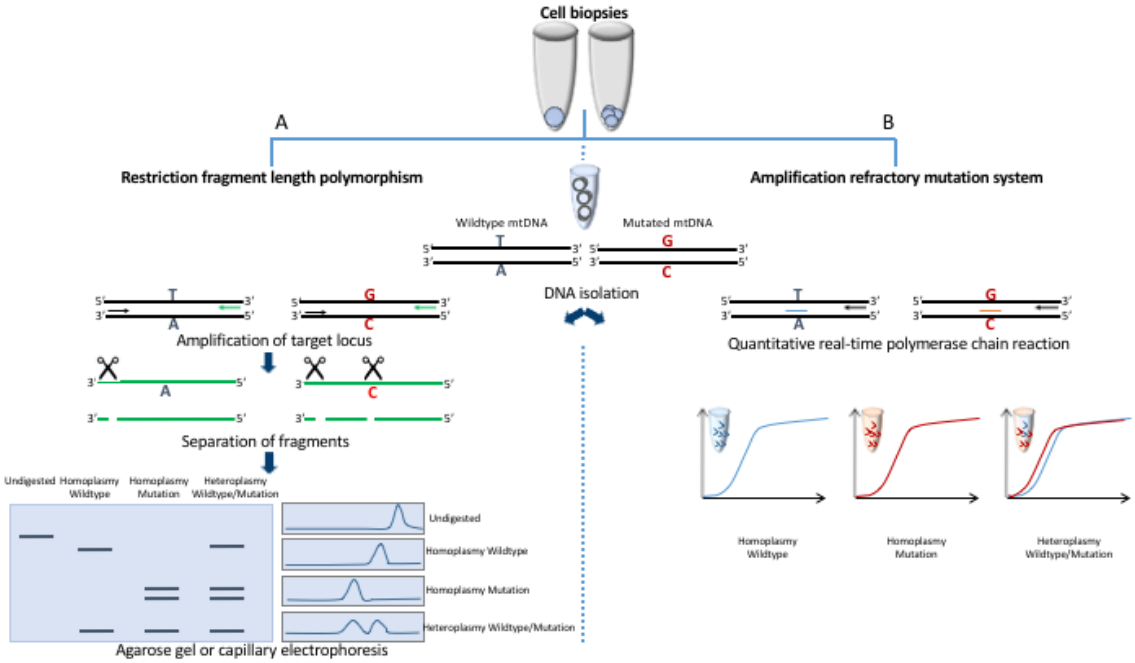


Figure 1.10: Illustration of methods used for PGD of mtDNA disease. Two different PCR-based methods have been used for PGD of mtDNA disease. **A: RFLP.** Following amplification of the mutation site with labelled primers (forward and/or reverse) PCR products are enzymatically digested using restriction enzymes that bind to one of the alleles (mutant or wild-type). In some cases the enzyme also binds to an artificial restriction site in one of the primer sequences to check digestion efficiency (pictured). The resulting DNA fragments are separated via electrophoresis. In order to determine exact allele ratios, capillary electrophoresis is performed whereby levels of mutant and wild-type alleles are calculated according to the peak areas. **B: ARMS.** Amplification of the mutation site is performed via qPCR utilising TaqMan chemistry. Two different fluorescently-labelled probes are employed, of which one binds only to the mutant and the other only to the wild-type allele. By measuring the fluorescent signal emitted during PCR, quantities of each allele can be inferred and mutant and wild-type ratios calculated.

1.4 Study aims

The aim of the project was to develop, validate and apply two novel PGT methods: (1) PGS combined with mtDNA copy number analysis; (2) PGD of mtDNA disease combined with CCS.

1.4.1 Development, validation and clinical application of a novel preimplantation genetic screening technique

Most of the currently available PGS techniques have dramatically improved the quality of PGS testing, however they also come with significant drawbacks. Collectively, they all require extensive processing times, are labour-intensive and require complex analysis tools. In addition, with exception of the real-time qPCR approach by Treff et al., (2012b), the long processing of samples (from sample reception until result generation) means that embryos often need to be cryopreserved, adding to the overall cost of the IVF/PGS treatment, restricting patient access. Moreover, incorporation of simultaneous mtDNA quantification in current PGS techniques is difficult and often requires separate testing.

In order to overcome the outlined drawbacks associated with current PGS techniques, the first aim of the study was to design, develop, validate and clinically apply a novel technique for CCS in blastocyst-stage embryos that can be combined with mtDNA copy number analysis (described in **CHAPTER 3**).

1.4.2 Design, validation and clinical application of a protocol for preimplantation genetic diagnosis of mitochondrial DNA disease combined with comprehensive chromosome screening

To date, two techniques, based on RFLP and ARMS, have been developed for PGD of mtDNA disease. Although clinical application of these techniques resulted in the birth of eleven children, the accuracy and sensitivity in the analysis of mtDNA mutation levels has been questioned due to technical errors. Moreover current techniques do not allow incorporation of CCN screening.

To avoid the transfer of embryos affected by mtDNA mutations or aneuploidy, the second aim of the study was to design, validate and clinically apply a novel technique for accurate and sensitive detection of mtDNA mutation quantities combined with simultaneous analysis of numerical chromosome abnormalities (described in **CHAPTER 4**).

CHAPTER 2: Materials and methods

This chapter contains all materials used and methods performed during the course of the project. The chapter is organised in six different sections, describing sample collection and preparation procedures, DNA amplification and quantification protocols and further downstream applications, such as chromosome screening and mtDNA mutation detection (**Figure 2.1**). Each of the results chapters (**CHAPTER 3** and **CHAPTER 4**) contain additional materials and methods sections, which briefly summarise relevant methods and protocol deviations, if applicable. Furthermore, details on participating IVF clinics/patients, research ethics, consent of participating individuals, consent to treatment as well as information given to patients regarding clinical diagnostics is described separately in individual materials and methods sections of each of the results chapters.

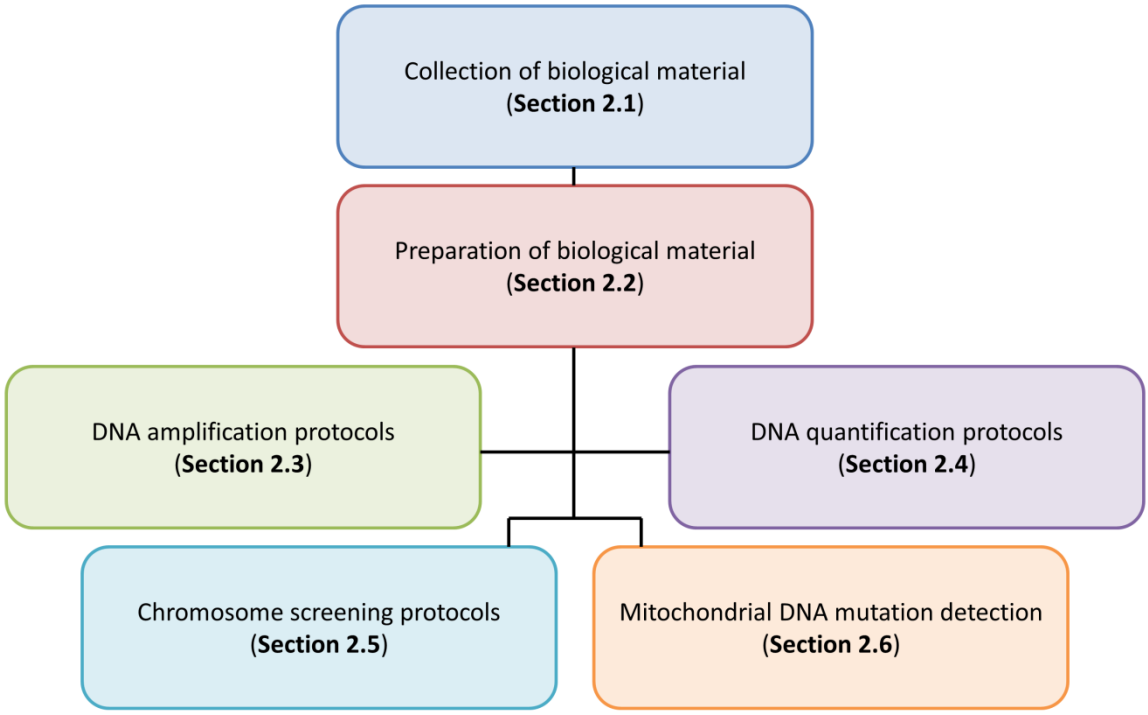


Figure 2.1: Structure of CHAPTER 2 - Materials and methods

2.1 Collection of biological material

Human biological samples used during the course of the project included cell line-derived cells, buccal cells, peripheral blood samples and embryo specimens. Collection and processing of human material derived from various sources (cell culture, buccal swabs, blood draw and embryo culture) is described in the following sub-sections (**Figure 2.2**).

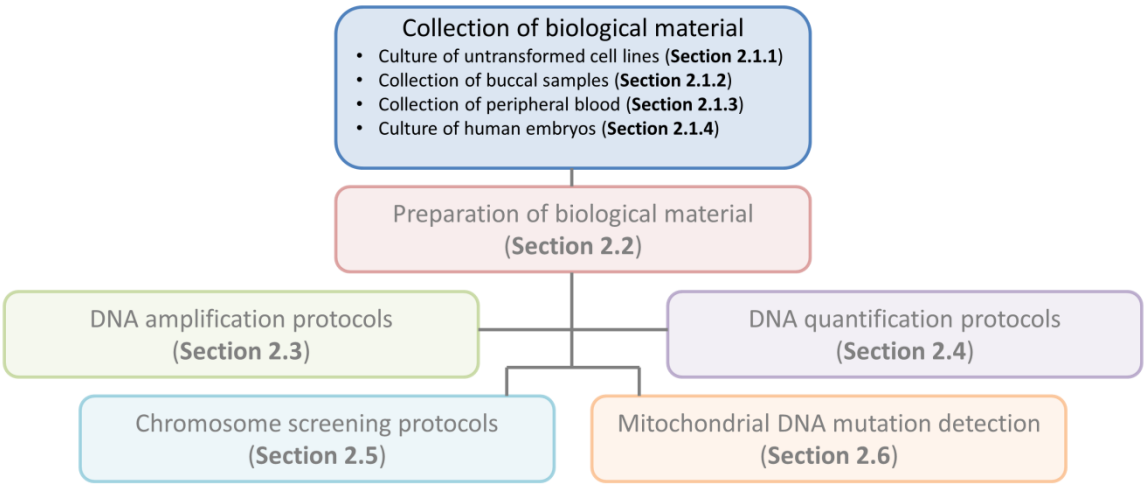


Figure 2.2: Sub-sections - Collection of biological material

2.1.1 Culture of untransformed cell lines

Established untransformed human cell lines were purchased from the Coriell Institute for Medical Research (Camden, New Jersey, US; https://catalog.coriell.org/) and obtained from two different cell repositories: NIGMS Human Genetic Cell Repository (National Institute of General Medical Sciences; https://catalog.coriell.org/1/NIGMS) and NINDS Repository (National Institute of Neurological Disorders and Stroke; https://catalog.coriell.org/1/NINDS). Cell lines included fibroblast culture, chorionic villus-derived cell culture and lymphoblast culture. Details on catalogue numbers,

repository and cell types as well as cell line characteristics are provided in **Table A.1** in **Appendix A**.

Adherent cell lines (fibroblast and chorionic villus-derived cells) and the lymphoblast cell line were shipped as monolayers or in suspension, respectively. Upon arrival, flasks were inspected for cell morphology, confluency and possible signs of biological contaminants. Cells were incubated overnight in shipping medium and depending on confluency either fed with culture medium or sub-cultured (**Section 2.1.1.1**) the next day. Sub-cultures were prepared for cell/DNA isolation (**Sections 2.2.1.1** and **2.2.2.1**). Surplus cells form sub-cultures were cryopreserved to create seed stocks and thawed when needed (**Section 2.1.1.2**).

All cell culture procedures were performed using aseptic techniques. Preparation of culture medium and cell handling was performed in a cell culture hood. The working area, all reagents and equipment were wiped with 70 % ethanol (Sigma-Aldrich) prior to use. Cell cultures and reagents were handled using sterile disposable equipment. All incubation steps took place in a humidified incubator at 37 °C, 5 % carbon dioxide, 5 % oxygen and 90 % nitrogen. Inspection of cells was performed using an inverted microscope. All reagents were pre-warmed at 37 °C in a water bath prior to use.

2.1.1.1 Sub-culture of cell lines

Sub-culture was performed in Chang Medium C (IrvineScientific), which was prepared according to the supplier's protocol. In brief, Chang Medium C Lyophilized Supplement was equilibrated to room temperature and dissolved in sterile distilled molecular grade water (GE Healthcare Life Sciences; 10 ml or 50 ml for total of 100 ml or

500 ml culture medium, respectively). The solution was transferred to the Chang Medium B Basal, followed by the addition of Glutamine (L-Glutamine 200 mM, Sigma-Aldrich; 1 ml or 10 ml for total of 100 ml or 500 ml culture medium, respectively) and antibiotics (Penicillin-Streptomycin Solution Stabilized, Sigma-Aldrich; 1 ml or 10 ml for total of 100 ml or 500 ml culture medium, respectively). DPBS (Dulbecco's Phosphate-Buffered Saline; ThermoFisher) was used to wash cells. For enzymatic dissociation of cells Trypsin-EDTA Solution 1X (Sigma-Aldrich) was used.

Sub-culture of adherent cell lines was performed in 25 cm^2 or 80 cm^2 cell culture treated flasks with filter caps. **Table 2.1** describes volumes of reagents used for different flask sizes. Shipping or culture medium was aspirated and cell monolayers were carefully washed with DPBS to remove remaining serum. Cells were then either fed with fresh culture medium or, if confluent transferred to a bigger culture flask or split. To allow cell dissociation from the flask surface, trypsin was added, followed by a brief incubation (5 - 10 min). Cell detachment was verified by visual and microscopical inspection. To inactivate trypsin, an equivalent amount of culture medium was added and the cell suspension transferred to a centrifuge tube. After centrifugation at 200 x g for 10 min, the supernatant was removed, the cell pellet was re-suspended in culture medium and the cell suspension transferred to a new flask. Cells were sub-cultured for 3 - 5 days until confluency was reached and prepared for cell/DNA isolation and/or frozen as outlined below.

Similar steps were followed for the sub-culture of cells grown in suspension. Cells were cultured in approximately 20 ml culture medium. For sub-culture, the cell suspension

was transferred to a conical tube, centrifuged at 200 x g for 10 min and the cell pellet re-suspended in fresh culture medium.

Table 2.1: Flask sizes and reagent volumes used for the sub-culture of adherent cell lines

Culture area (cm^2)	Reagent (ml)		
	DPBS	Trypsin	Culture medium
25	5.0	3.0	10.0
80	10.0	6.0	20.0

2.1.1.2 Cryopreservation and recovery of cells

Surplus cells from sub-cultures were cryopreserved for long-term storage in liquid nitrogen. Cells were initially processed as described in **Section 2.1.1.1**. The cell suspension was centrifuged at 200 x g for 10 min. The cell pellet was re-suspended in approximately 5 ml freezing medium (Recovery Cell Culture Freezing Medium, ThermoFisher) and the suspension aliquoted into cryogenic storage vials (~1 ml per vial). Prior to the transfer to a nitrogen tank, cryovials were placed at -80 °C for several days. To ensure slow freezing of cell suspensions, vials were kept in a small cardboard box containing cotton wool.

For sub-culture of frozen cells, a cryovial was placed into a 37 °C water bath for approximately 1 min. After defrosting, the cells were transferred to a conical tube and diluted in about 10 ml culture medium. After centrifugation at 200 x g for 10 min, the cell pellet was re-suspended in fresh medium for subsequent sub-culture.

2.1.2 Collection of buccal samples

Buccal samples were obtained from patients and family members undergoing IVF and PGD treatment for a mtDNA disorder and were used for the development of new patient-tailored PGD tests. Two different buccal collection swabs were used: Isohelix SK-2S Buccal Swabs (Cell Projects Ltd) or Catch-All Sample Collection Swabs (Epicentre). Buccal swab kits, along with detailed instructions on how to collect buccal samples were sent to the patients via post. After sample collection, swabs were sent back by first class post and further processed for cell/DNA recovery. For the purpose of cell rather than DNA isolation (**Sections 2.2.1.2** and **2.2.2.2**), the Isohelix Swabs were used and retrieval of buccal cells performed in-house, for subsequent cell isolation.

2.1.3 Collection of peripheral blood

Whole blood samples were obtained from patients and family members undergoing IVF and PGD treatment of mtDNA disorders. Approximately 5 ml of peripheral blood was collected by trained clinical personnel of clinics performing the IVF treatment. The samples were drawn into sterile purple cap blood collection tubes containing anticoagulants to stabilize and preserve blood samples. Samples were posted and refrigerated at 2 - 8 °C until further processing for cell and/or DNA isolation (**Sections 2.2.1.3** and **2.2.2.3**).

2.1.4 Culture of human embryos

Embryo specimens were derived from *in vitro* cultured embryos of patients undergoing ART. The purpose of ART, patient details as well as participating clinics are specified in materials and methods sections of relevant results chapters.

To generate embryos *in vitro*, patients underwent controlled ovarian stimulation followed by oocyte retrieval. Fertilisation was performed either via IVF or intracytoplasmic sperm injection (ICSI). For the purpose of PGD, ICSI was commonly performed to reduce the risk of possible contamination by cumulus cells or surplus sperm which may be attached to the zona pellucida. After fertilisation embryos were cultured until day-3 or day-5/6 post fertilisation, when biopsy/collection of embryo specimens was performed (**Section 2.2.1.4**).

2.2 Preparation of biological material

Downstream genetic analyses were performed on cell and/or genomic DNA (gDNA) samples. The following sub-sections describe the isolation of cells/embryo specimens and the extraction of gDNA from different biological materials (**Figure 2.3**).

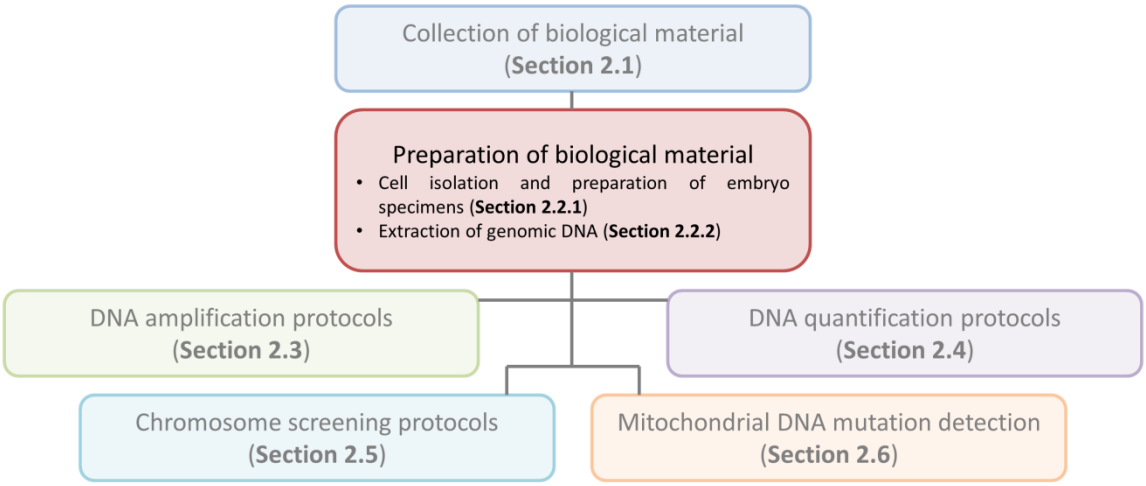


Figure 2.3: Sub-sections - Preparation of biological material

2.2.1 Cell isolation and preparation of embryo specimens

Samples containing single or few cells were prepared from cell culture, buccal swabs and peripheral blood samples and isolated in a clean room. This was performed by Dr Dagan Wells, Dr Jonas Sarasa, Dr Michalis Konstantinidis or Dr Araz Raberi. Preparation of all embryo specimens was performed in laboratories of participating IVF clinics by trained embryologists. To reduce the risk of extraneous DNA contamination, all cell samples as well as embryo specimens were successively washed in sterile 0.1 % (w/v) PVA (Polyvinyl alcohol, Sigma-Aldrich)/DPBS wash buffer. Sterile culture dishes (one dish per sample/embryo) containing several ~5 µl drops (cell wash drops) and ~10 µl drops (pipette wash drops) of wash buffer were prepared (**Figure 2.4**). To avoid sample contamination, pipettes were cleaned after initial cell pick up and in between cell washing steps by flushing with clean wash buffer.

For preparation of cell samples (cell lines, buccal cells and lymphocytes), approximately 10 µl of cell suspension (see **Sections 2.2.1.1**, **2.2.1.2** and **2.2.1.3**) was transferred to the first PVA/DPBS drop and mixed by pipetting. From this drop, few cells were transferred into the next drop, which was continued until the desired amount of cells was obtained (typically five and three cells or a single cell). Cell(s) were then washed in three new drops, placed in a sterile 0.2 ml microcentrifuge tube and spun down briefly to collect the cell(s) in the bottom of the tube.

For preparation of embryo specimens post biopsy (see **Section 2.2.1.4**), cell(s) were transferred to the first wash drop. To wash the cell(s), a few microliters of fresh wash buffer was expelled over the cell(s) causing them to be gently pushed into new, clean areas of the drop. The cell(s) were then transferred to a fresh drop of wash buffer and the procedure repeated. Ultimately, cells were processed through at least three distinct drops of wash buffer before finally being transferred to a sterile 0.2 ml microcentrifuge tube. In case embryo specimens were used for PGD of mtDNA disease, negative controls were generated consisting of approximately 2 µl of wash buffer from the last wash drop of each embryo biopsy. Microcentrifuge tubes were transferred to a tube rack and placed along with ice packs, which had been stored for at least 24 h at a temperature of -20 °C or lower, into a polystyrene box for same day or overnight delivery.

Isolated cell samples and embryo specimens were stored at -80 °C until further processing.

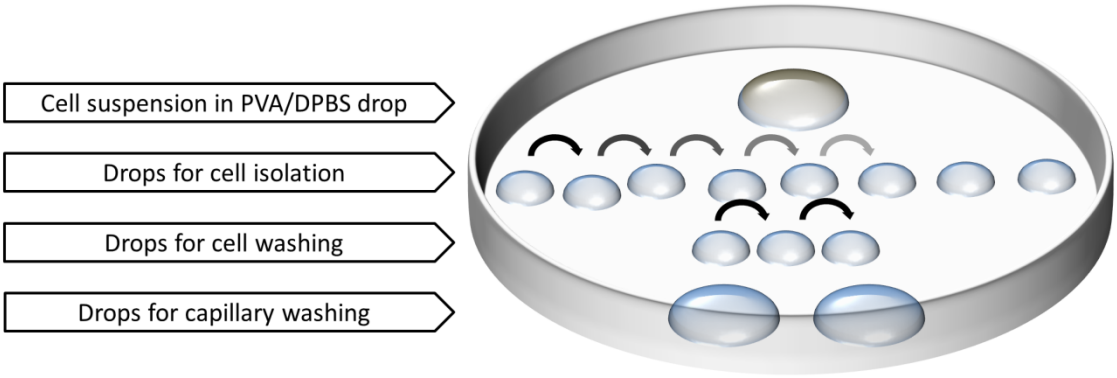


Figure 2.4: Preparation of a cell culture dish for cell isolation and washing

2.2.1.1 Cell isolation from cell culture

Prior to the isolation of cells, cultures were processed according to the steps described in **Section 2.1.1.1**. However, centrifugation took place at 100 x g for 10 min and instead of re-suspending the cell pellet in culture medium, cells were diluted in 0.5 - 1.0 ml DPBS and transferred to a sterile 1.5 ml microcentrifuge tube. Cell suspensions were stored at 2 - 8 °C and cell isolation performed on the same day (described above).

2.2.1.2 Buccal cell isolation from buccal swaps

After retrieval of buccal cells, swabs were placed into conical tubes, each containing approximately 2 ml DPBS. Swabs were rotated carefully in DPBS to release cells. The suspensions were kept at 2 - 8 °C and cells isolated as described above on the day of sample reception.

2.2.1.3 Lymphocyte isolation from peripheral blood

Ficoll-Paque Plus (GE Healthcare Life Sciences) was used to separate lymphocytes from blood plasma and other blood cell types and performed according to the

manufacturer's instructions (Ficoll-Paque PLUS, 71-7167-00 AG, 2007, GE Healthcare). In brief, 2 ml of fresh blood sample was diluted in 2 ml DPBS and mixed thoroughly. The entire mixture was then carefully layered in a sterile 15 ml conical tube onto 3 ml Ficoll-Paque Plus solution and centrifuged at 400 x g for 35 min until four different layers were visible (**Figure 2.5**). If layers were not clearly visible, a further centrifugation at 500 x g for 10 min was performed. Using a sterile Pasteur pipette, the upper plasma layer was carefully removed and discarded. Using a new pasteur pipette the lymphocyte layer was transferred to a sterile 1.5 ml microcentrifuge tube. Approximately three volumes of 0.1 % PBS/PVA were added prior to cell isolation to dilute the sample. The cell suspension was kept at 2 - 8 °C for same day cell isolation which was performed as described above.

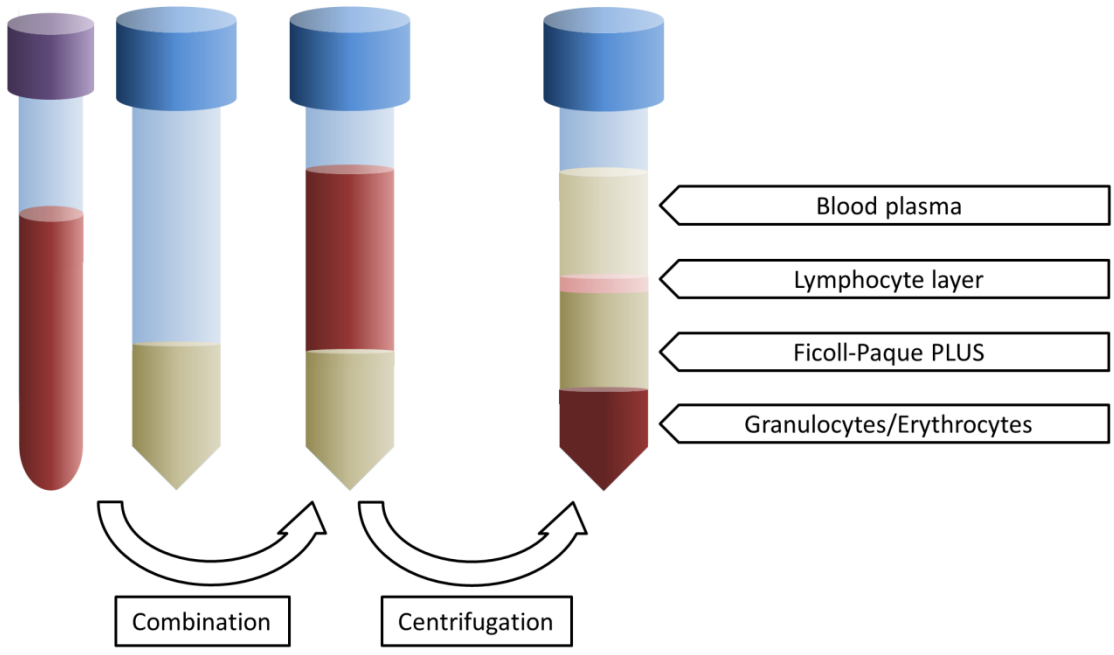


Figure 2.5: Graphical representation of lymphocyte retrieval from whole blood

2.2.1.4 Biopsy/Preparation of embryo specimens

Embryo samples used in the study included unfertilised and abnormally fertilised oocytes, entire embryos, disaggregated single sister blastomeres, cleavage- and

blastocyst-stage biopsies or remainder of embryos after biopsies. For the purpose of embryo biopsy, an opening of the zona pellucida was created with a laser, allowing the subsequent aspiration of cell(s) using a micromanipulation pipette. In case of cleavage-stage biopsy one or two blastomeres were retrieved on day-3 post fertilisation. At the blastocyst-stage several cells (typically three to ten) were removed from the outer trophectoderm layer on day-5 or day-6 post fertilisation. After cell aspiration/dissection, samples were washed and tubed (described above).

2.2.2 Extraction of genomic DNA

GDNA was extracted from cell cultured cells, buccal swabs and peripheral blood.

2.2.2.1 DNA extraction from cell culture

Preparation of cultured cells for gDNA extraction was performed as described in **Section 2.2.1.1**. However, after pelleting, cells were re-suspended in 200 µl DPBS. Cell suspensions were stored at 2 - 8 °C until further processing.

GDNA was extracted using the QIAamp DNA Mini Kit (Qiagen) and performed according to the manufacturer's instructions (QIAamp DNA Mini and Blood Mini Handbook, Third Edition, 04/2010, Qiagen). In brief, 20 µl of proteinase K, the entire cell suspension and 200 µl of Buffer AL were combined in a sterile 1.5 ml tube and mixed by vortexing for 15 s. The homogenous solution was placed in a water bath or heating block set to 56 °C for 10 min. After incubation, 200 µl of ethanol (Sigma-Aldrich) was added and mixed thoroughly. The mixture was then transferred to a 2 ml collection tube containing a QIAamp Mini spin column and centrifuged at 6,000 x g for 1 min. After placing the spin

column into a new 2 ml collection tube, 500 µl of Buffer AW1 was added, followed by a centrifugation at 6,000 x g for 1 min. After transfer of the column to a new collection tube and the addition of 500 µl Buffer AW2, the sample was centrifuged at full speed (~16,000 x g) for 3 min. To eliminate the possibility of buffer carryover, the column was placed into a new collection tube and centrifuged once more at full speed for 1 min. For elution of gDNA, 200 µl Buffer AE was added to the column, contained in a new sterile 1.5 ml tube, and incubated at room temperature for 5 min, followed by a centrifugation at 6,000 x g for 1 min. Extracted gDNA was stored at 2 - 8 °C.

2.2.2.2 DNA extraction from buccal swabs

GDNA extraction from Isohelix SK-2S Buccal Swabs was performed according to the manufacturer's instructions (Instructions for Isohelix DNA Isolation kit, 05/2015, Cell Projects Ltd) using the DNA Isolation kit DDK-50 (Cell Projects Ltd). To stabilise the DNA, 500 µl of LS solution and 20 µl of PK solution were added to the tube containing the buccal swab on the day of sample reception. The tube was placed in a water bath and incubated at 60 °C for 1 h. The entire cell suspension was transferred to a sterile 1.5 ml tube and combined with 400 µl CT solution. The tube was centrifuged at 12,000 x g for 7 min. After removal of the supernatant, the DNA pellet was re-suspended in 150 µl TE solution and incubated at room temperature for 5 min. Extracted gDNA was stored at 2 - 8 °C.

For gDNA extraction from the Catch-All Sample Collection Swab, the BuccalAmp DNA Extraction Kit (Epicentre) was used and all steps performed as recommended (Protocol for BuccalAmp DNA Extraction, Rev. A, 6/2006, Epicentre). In brief, the sample collection swab was placed into a tube containing pre-aliquoted QuickExtract Solution and

rotated five times to ensure sufficient buccal cell collection. The cell suspension was vortexed for 10 s and incubated in a water bath at 65 °C for 1 min. After vortexing for 15 s, the tube was transferred to a heating block and incubated at 98 °C for 2 min, followed by 15 s of vortexing. Isolated gDNA was stored at 2 - 8 °C.

2.2.2.3 DNA extraction from peripheral blood

For extraction of gDNA from peripheral blood samples, the same procedures as outlined in **Section 2.2.2.1** were followed using the QIAamp DNA Mini Kit (Qiagen) with 200 µl of whole blood. Extracted gDNA was stored at 2 - 8 °C.

2.3 DNA amplification protocols

Prior to various downstream applications, amplification of DNA derived from isolated cell samples, embryo specimens and gDNA was necessary (**Figure 2.6**). Depending on downstream applications, DNA was amplified either using WGA (**Section 2.3.1**), conventional PCR (**Section 2.3.2**) or multiplex pre-amplification PCR (**Section 2.3.3**).

All amplification reactions were performed in 0.2 ml microcentrifuge tubes and were prepared on a cold rack in a laminar flow hood located in a dedicated clean room to avoid exogenous cell/DNA contamination. All incubation steps were carried out in a thermal cycler. Amplification success after WGA and conventional PCR was assessed via agarose gel electrophoresis. The 1 % or 2 % agarose gels consisted of 1 g or 2 g UltraPure Agarose, respectively, dissolved in 100 ml 1X TBE (Tris Borate EDTA) Buffer (both ThermoScientific). Approximately 5 µl (per 100 ml TBE) of GelRed Nucleic Acid Stain

(Biotium) was used for DNA visualisation under UV light. Prior to gel loading, 3 - 5 µl of all amplified samples were diluted in 1 µl loading buffer (10X BlueJuice, ThermoFisher). A size standard (100 bp Low Scale DNA Ladder, ThermoFisher) was run along with all samples.

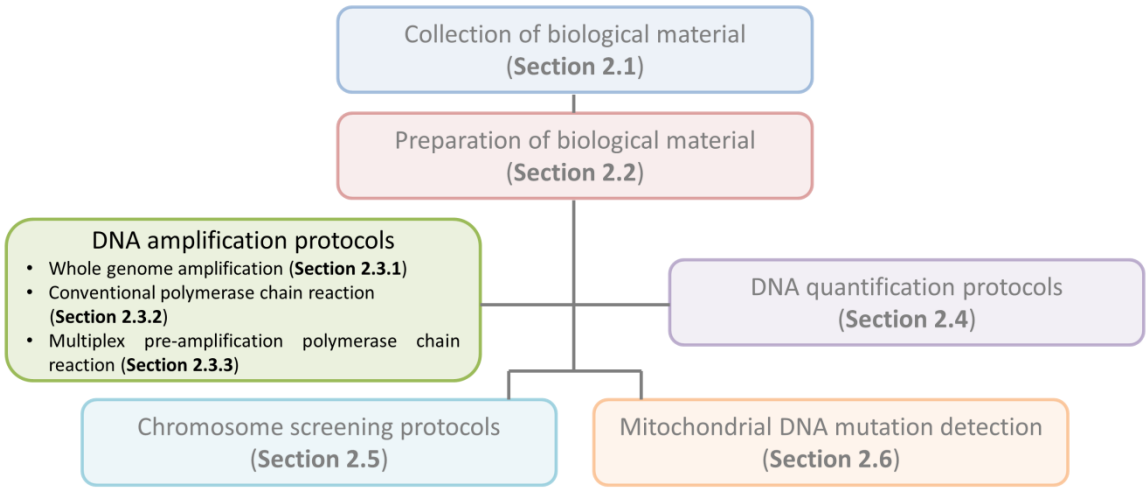


Figure 2.6: Sub-sections - DNA amplification protocols

2.3.1 Whole genome amplification

WGA technologies allow the amplification of the entire genome (nuclear and mitochondrial) and the generation of sufficient DNA for downstream applications from samples containing small amounts of DNA, such as samples consisting of few cells or embryo specimens. Two different WGA technologies were used during the project: (1) the SurePlex DNA Amplification System (Illumina); (2) the multiple displacement amplification (MDA) protocol (REPLI-g) by Qiagen. In both cases, cells were lysed followed by DNA amplification. In case of the SurePlex protocol, amplification was performed via PCR, while the MDA protocol is a non-PCR-based, isothermal amplification method. For evaluation of amplification products after WGA, samples were run on a 1 % agarose gel for

approximately 10 min at 200 V. A smear of DNA, composed of numerous fragments of varying sizes, was indicative of positive amplification (**Figure 2.7**).

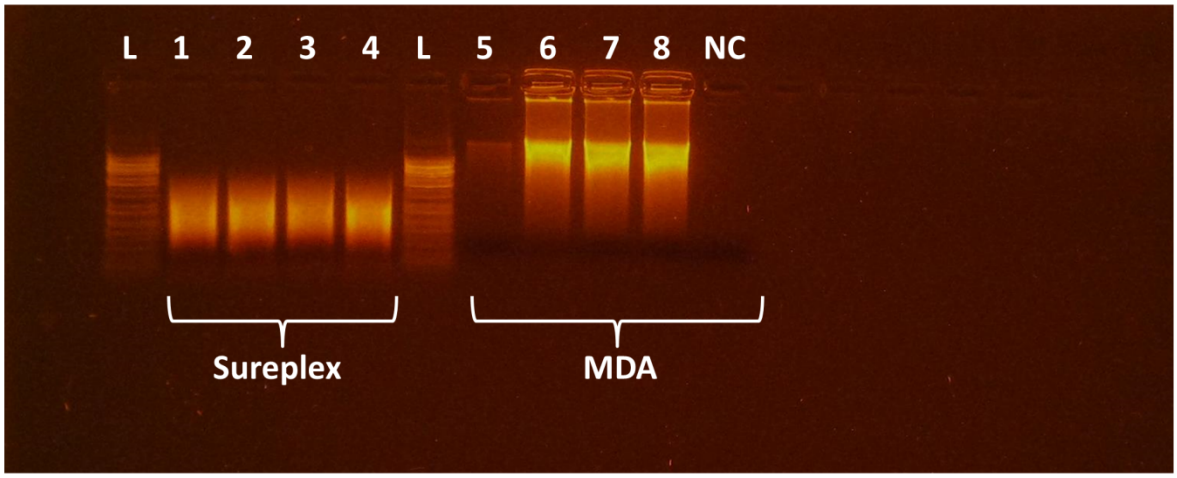


Figure 2.7: Gel image of WGA products. L = ladder. 1 - 8 = IDs of single lymphocyte samples. NC = negative control (water). Samples 1 - 4 were amplified with SurePlex and samples 5-8 and a NC using MDA. Sample 5 did not amplify.

2.3.1.1 SurePlex DNA amplification

All reaction components were supplied with the SurePlex DNA Amplification System kit (Illumina) and the protocol performed according to the manufacturer's recommendations (SurePlex Summary Protocol, 15053626 Rev. C, 11/2014, Illumina). In short, after a brief centrifugation, 3 µl of cell extraction buffer and 5 µl of extraction cocktail (**Table 2.2**) were added to the sample(s). A further brief centrifugation was followed by an incubation in a thermal cycler, programmed as described in **Table 2.3**. A volume of 5 µl pre-amp cocktail (**Table 2.4**) was added per sample followed by brief centrifugation and a second thermal cycler incubation (**Table 2.5**). Then, 60 µl of amplification cocktail (**Table 2.6**) was added per sample. Contents were mixed by flicking. Samples were briefly centrifuged and amplification performed according to the thermal cycler programme described in **Table 2.7**. Amplification products were stored at 2 - 8 °C.

Table 2.2: Extraction cocktail components (volume per sample)

Extraction cocktail reagents	Volume (µl)
Extraction enzyme dilution buffer	4.8
Cell extraction enzyme	0.2
Total	**5.0**

Table 2.3: Thermal cycler settings for cell lysis (heated lid: 110 °C)

Number of cycles	Cycle temperature (°C)	Incubation time (min)
1	75.0	10:00
1	95.0	04:00
1	4.0	hold

Table 2.4: Pre-amp cocktail components (volume per sample)

Pre-amp cocktail reagents	Volume (µl)
SurePlex pre-amp buffer	4.8
SurePlex pre-amp enzyme	0.2
Total	**5.0**

Table 2.5: Thermal cycler settings for pre-amplification (heated lid: 110 °C)

Number of cycles	Cycle temperature (°C)	Incubation time (min)
1	95.0	02:00
12	95.0	00:15
	15.0	00:50
	25.0	00:40
	35.0	00:30
	65.0	00:40
	75.0	00:40
1	4.0	hold

Table 2.6: Amplification cocktail components (volume per sample)

Amplification cocktail reagents	Volume (µl)
SurePlex amplification buffer	25.0
SurePlex amplification enzyme	0.8
Nuclease-free water	34.2
Total	**60.0**

Table 2.7: Thermal cycler settings for amplification (heated lid: 110 °C)

Number of cycles	Temperature (°C)	Time (min)
1	95.0	02:00
14	95.0	00:15
	65.0	01:00
	75.0	01:00
1	4.0	hold

2.3.1.2 Multiple displacement amplification

MDA was performed using the REPLI-g MIDI Kit (Qiagen). Reaction components are specified in the following tables. A modified version of the manufacturer's protocol (REPLI-g Mini/Midi Handbook, 1068896, 07/2011, Qiagen) was applied. In short, samples were briefly centrifuged. Per sample, a volume of 2.5 µl alkaline lysis buffer (**Table 2.8**) was added. After a brief centrifugation, samples were incubated in a thermal cycler, programmed as described in **Table 2.9**. A volume of 44 µl of amplification mix (**Table 2.10**) and 1 µl of Repli-g Midi DNA Polymerase were added to each sample followed by flicking, brief centrifugation and a second thermal cycler incubation (**Table 2.11**). Amplification products were stored at 2 - 8 °C.

Table 2.8: Alkaline lysis components (volume per sample)

Alkaline lysis buffer reagents	Supplier	Volume (µl)
Nuclease-free PCR grade water	Roche Diagnostics	0.75
DL-Dithiothreitol solution (DTT; 0.1 M)	Sigma	1.25
Sodium hydroxide solution (NaOH; 1.0 M)	Sigma	0.5
Total		**2.5**

Table 2.9: Thermal cycler settings for cell lysis (heated lid: 110 °C)

Number of cycles	Cycle temperature (°C)	Incubation time (min)
1	65.0	10:00
1	4.0	hold

Table 2.10: Amplification mix components (volume per sample)

Amplification mix reagents	Supplier	Volume (µl)
Nuclease-free PCR grade water	Roche Diagnostics	12.5
Tricine (0.4 M)	Sigma	2.5
Repli-g midi reaction buffer (1.0 M)	Qiagen	29
Total		**44**

Table 2.11: Thermal cycler settings for MDA amplification (heated lid: 110 °C)

Number of cycles	Cycle temperature (°C)	Incubation time (min)
1	30.0	120:00
1	65.0	05:00
1	4.0	hold

2.3.2 Conventional polymerase chain reaction

Conventional PCR was carried out for the amplification of specific DNA loci using primers (**Section 2.3.2.1**) designed as part of the development of PGD tests for the detection of mtDNA mutations. Conventional PCR was performed on cell samples, embryo specimens, gDNA and WGA products (**Section 2.3.2.2**).

2.3.2.1 Primer design

Genetic reports of patients and family members referred for PGD were used as a source of information for primer design (details on genetic disorder/mutation and primer sequences are described in the materials and methods section of **CHAPTER 5**). Specific primer pairs flanking mutation sites (single base changes) were designed to target the loci of interest. Initially, mtDNA, mRNA and protein sequences were retrieved from NCBI

(National Center for Biotechnology Information) and the affected nucleotides, as well as the corresponding amino acids identified. To verify that correct nucleotide positions were chosen, several codons surrounding the mutation sites were matched to the corresponding amino acids in the protein sequences. The identified DNA sequences were then used to design primers.

Five different, freely available online platforms were used for primer design: (1) **Primer3web** (http://bioinfo.ut.ee/primer3/); (2) **Oligo Calc: Oligonucleotide Properties Calculator** (http://biotools.nubic.northwestern.edu/OligoCalc.html); (3) **SNPCheck3** (http://snpcheck.net); (4) **Reverse Complement** (http://reverse-complement.com); (5) **Primer-BLAST** (http://www.ncbi.nlm.nih.gov/tools/primer-blast/).

Initially, the identified target DNA sequences, as well as flanking sequences, were pasted into Primer3web, which was used to pick primers resulting in approximately 100 bp product sizes. Care was taken to ensure that primers were chosen according to the following parameters: primer size: 18 - 24 bases (optimum: 20 bases); primer melting temperature (Tm): 58 - 64 °C (maximum difference between forward and reverse primers: 1 °C); primer GC content: 40 - 60 % (optimum: 50 %). Self-complementarity, potential hair pin formation and self-annealing sites of the identified primers were assessed using Oligo Calc. SNPCheck3 was used to verify that primer binding sites do not contain previously identified SNPs. To identify the reverse primer in the original DNA sequence, reverse complement software was used, which converts the primer sequence into its reverse counterpart. Finally, the Primer-BLAST tool was used to check specificity of the primers.

Primers were purchased at 100 µM concentration from Eurogentec and stored at - 20 °C.

2.3.2.2 Conventional polymerase chain reaction protocol

For all sample types, PCR reactions of 15 µl were performed. **Table 2.12** describes the protocol used for amplification of gDNA and WGA products. A master mix was prepared (14.5 µl per sample) and combined with 0.5 µl of the sample to be amplified.

In case PCR was performed on cell samples, a modified version of the protocol was applied. Cell samples were initially subjected to an alkaline lysis as described in **Section 2.3.1.2** (**Table 2.8**), followed by subsequent addition of 12.5 µl of master mix (**Table 2.13**). Negative controls consisting of PBS/PVA (for PGD) and/or nuclease-free water were set up and processed along with all other samples to assess possible sample contamination prior or during the amplification process. PCR cycling conditions are described in **Table 2.14**. The annealing temperature varied and was dependent on primer Tm. To optimise PCR amplifications for different primer sets and to determine optimal annealing temperature, an initial gradient PCR using gDNA was performed. For assessment of gradient PCR products as well as band sizes after conventional PCR a 2 % agarose gel was prepared and run at 100 V for approximately 45 min (**Figure 2.8**). Amplicons were stored at 2 - 8 °C.

Table 2.12: Components for PCR of gDNA and WGA products (volume per sample)

Amplification mix reagents	Supplier	Volume (µl)
Nuclease-free PCR grade water	Roche Diagnostics	12.49
HotMaster Taq DNA Buffer with Magnesium	5 Prime	1.5
Forward primer (100 µM)	Eurogentec	0.06
Reverse primer (100 µM)	Eurogentec	0.06
dNTP Mix (10 nM)	ThermoFisher	0.3
HotMaster Taq DNA Polymerase	5 Prime	0.09
Total		**14.5**

Table 2.13: Components for PCR of cell samples (volume per sample)

Amplification mix reagents	Supplier	Volume (µl)
Tricine (0.4 M)	Roche Diagnostics	2.5
Nuclease-free PCR grade water	Roche Diagnostics	7.99
HotMaster Taq DNA Buffer with Magnesium	5 Prime	1.5
Forward primer (100 µM)	Eurogentec	0.06
Reverse primer (100 µM)	Eurogentec	0.06
dNTP Mix (10nM)	ThermoFisher	0.3
HotMaster Taq DNA Polymerase	5 Prime	0.09
Total		**12.5**

Table 2.14: Thermal cycler settings for amplification (heated lid: 110 °C)

Number of cycles	Temperature (°C)	Time (min)
1	96.0	01:00
35	94.0	00:15
	53.0 - 65.0	00:15
	65.0	00:45
1	65.0	02:00
1	4.0	hold

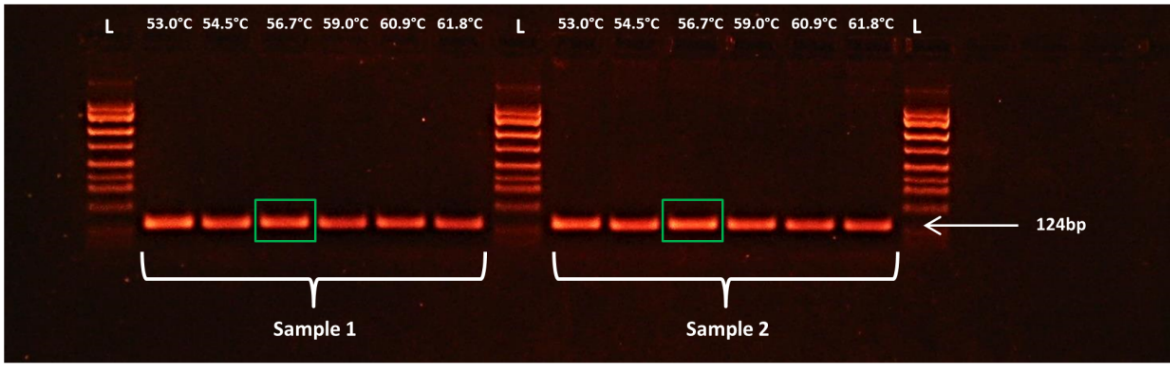


Figure 2.8: Gel image of gradient PCR. The image shows resulting bands after gradient PCR of a primer pair (forward primer: 60 °C Tm; reverse primer: 58 °C Tm) resulting in 124 bp product size. Two different gDNA samples were tested. Annealing temperatures ranged from 53.0 °C-61.8 °C. Only very little differences in band intensities between tested temperatures were observed and 56.7 °C was chosen as best annealing temperature (green box). L = ladder.

2.3.3 Multiplex pre-amplification polymerase chain reaction

Multiplex pre-amplification PCR was carried out for simultaneous pre-amplification of multiple nDNA and mtDNA loci using pre-designed TaqMan primers (ThermoFisher) to generate sufficient DNA templates for subsequent real-time qPCR. Specific details on primer characteristics and genomic location is discussed in the materials and methods section of **CHAPTER 4**. Multiplex pre-amplification was performed on cell samples and embryo specimens.

Initially, an alkaline lysis was performed (**Table 2.15**) and samples incubated according to **Table 2.9** in **Section 2.3.1.2**. For multiplex pre-amplification various PCR volumes were tested resulting in total reaction volumes of 50.0 µl, 22.75 µl and 14.25 µl (**Table 2.16**). PCR cycling conditions are described in **Table 2.17**. Amplicons were stored at -20 to -80 °C.

Table 2.15: Alkaline lysis components (volume per sample)

Alkaline lysis buffer reagents	Supplier	Volume (µl)
Nuclease-free PCR grade water	Roche Diagnostics	0.45
DTT (0.1 M)	Sigma	0.75
NaOH (1.0 M)	Sigma	0.3
Total		**1.5**

Table 2.16: Multiplex amplification mix components (volume per sample)

Amplification mix reagents	Supplier	Volume (µl)		
Nuclease-free PCR grade water	Roche Diagnostics	5.0	NA	NA
Tricine (0.4 M)	Sigma	5.0	2.5	1.5
TaqMan PreAmp Master Mix (2X)	ThermoFisher	25.0	12.5	7.5
Primer pool (0.2X)	ThermoFisher	12.5	6.25	3.75
Total		**47.5**	**21.25**	**12.75**

NA = not applicable.

Table 2.17: Thermal cycler settings for amplification (heated lid: 110 °C)

Number of cycles	Temperature (°C)	Time (min)
1	95.0	10:00
16	95.0	00:15
	60.0	04:00
1	99.0	10:00
1	4.0	hold

2.4 DNA quantification protocols

Prior to several downstream applications, measurement of sample DNA concentrations was required. Depending on the application, three different techniques were used (**Figure 2.9**). GDNA, WGA products and conventional PCR amplicons were quantified using a fluorometer (**Section 2.4.1**). Assessment of samples with very low amounts of DNA, such as sequencing libraries was performed using the relative standard

curve method (**Section 2.4.2**). If simultaneous analysis of DNA quantities and sizing of DNA fragments was required, assessment was performed using a bioanalyser (**Section 2.4.3**).

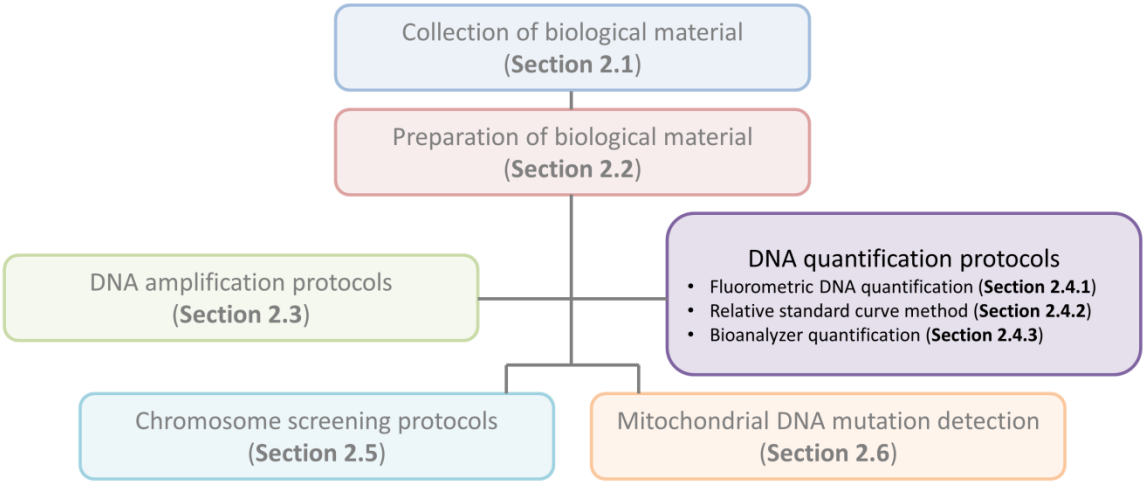


Figure 2.9: Sub-sections - DNA quantification protocols

2.4.1 Fluorometric DNA quantification

For fluorometric quantification, the Qubit dsDNA HS Assay Kit was used and samples analysed on a Qubit 2.0 Fluorometer (both ThermoFisher). The protocol was performed according to the supplier's instructions (Qubit 2.0 Fluorometer, MAN0003231, 10/2010, ThermoFisher). A working solution consisting of 199 µl dilution buffer and 1 µl of concentrated assay reagent was prepared for each sample and two standards. For measuring the concentration of standards, 190 µl working solution was combined with 10 µl of standard solution (supplied). To determine DNA concentration in test samples, 1 - 10 µl of sample was diluted in 190 - 199 µl working solution (total volume: 200 µl). Standards and samples were incubated at room temperature for 2 min, followed by quantification.

2.4.2 Relative standard curve method

The Ion Library Quantification Kit (ThermoFisher) was used to determine the concentration of sequencing libraries (see **Sections 2.6.1** and **2.6.2**). The manufacturer's protocol (Ion Library Quantitation Kit, 4468986 Rev. E, 2013, Life Technologies) was followed with slight variations, which are outlined below. The method enabled absolute quantification of DNA amounts in a given sample by comparison to known standards (derived from the *E. coli* DH10B Control Library, supplied). Reactions were performed on a StepOnePlus Real-Time PCR System (ThermoFisher). Initially, five standards with varying concentrations were prepared via serial 10-fold dilutions of the stock Control Library in nuclease-free water (**Table 2.18**). A 1:20,000 dilution of the sample(s) to be quantified was prepared (**Table 2.19**). A master mix was prepared (**Table 2.20**) and 7.5 µl combined with 2.5 µl of standard/diluted library sample or nuclease-free water, which served as a PCR negative control. Standards were run in triplicates and sample libraries in duplicates. For the PCR negative control a single reaction was prepared. Samples were processed in a 96-well plate according to **Table 2.21** in fast mode. Readings were taken automatically after completion of each of the 40 extension steps. **Figure 2.10** shows the PCR set-up in 96-well format, the amplification curves of the standards and libraries after real-time qPCR and the corresponding standard curve. The inbuilt StepOneSoftware (v2.2.2) was used for sample quantification.

Table 2.18: Serial dilutions of the E. coli DH10B Control Library

Standard	Control Library (µl)	Water (µl)	Fold dilution	Concentration (pM)
1	5.0	45.0	0.1	6.8
2	5.0 (standard 1)	45.0	0.01	0.68
3	5.0 (standard 2)	45.0	0.001	0.068
4	5.0 (standard 3)	45.0	0.0001	0.0068
5	5.0 (standard 4)	45.0	0.00001	0.00068

Table 2.19: Serial sample dilutions to create a 1:20,000 dilution

Dilution	Library (µl)	Water (µl)
1	1.0	19.0
2	1.0 (dilution 1)	99.0
3	5.0 (dilution 2)	45.0

Table 2.20: Components of the real-time qPCR master mix (volume per reaction)

Master mix reagents	Volume (µl)
Ion Library TaqMan qPCR Mix, 2X	5.0
Ion Library TaqMan Quantitation Assay, 20X	0.5
Nuclease-free water	2.0
Total	**7.5**

Table 2.21: Thermal cycler settings for amplification (heated lid: 100 °C)

Number of cycles	Temperature (C)	Time (min)
1	50.0	02:00
1	95.0	00:20
40	95.0	00:01
	60.0	00:20

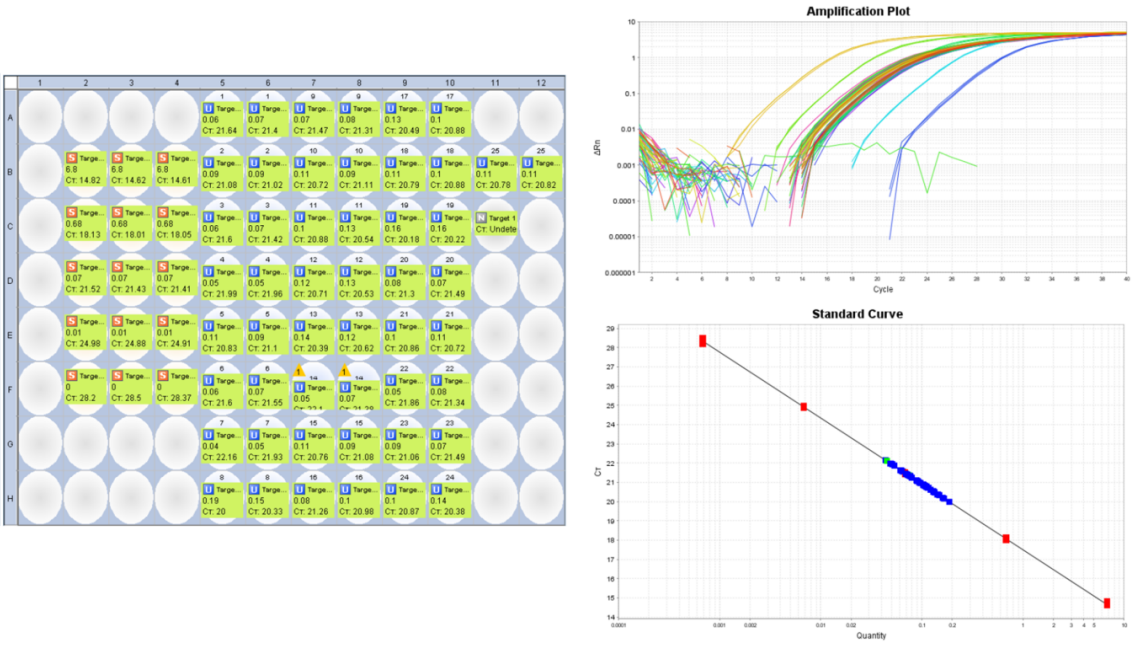


Figure 2.10: Real-time qPCR set-up with amplification plot and standard curve

2.4.3 Bioanalyzer quantification

To simultaneously determine DNA quantities and fragment sizes, the High Sensitivity DNA kit was used and samples processed on a 2100 Bioanalyzer instrument (both Agilent Technologies). The procedure is based on electrophoretic separation of low amounts of DNA fragments through microchannels embedded in a High Sensitivity DNA chip.

The procedure was performed according to the manufacturer's protocol (Agilent High Sensitivity DNA Kit Quick Start Guide, Rev. C, 08/2013, Agilent Technologies). In brief, a gel-dye mix was prepared by adding 15 µl of High sensitivity DNA dye concentrate to the tube containing the High sensitivity DNA gel matrix. The mixture was vortexed, briefly centrifuged and transferred to a column with a spin filter, followed by a centrifugation at 2240 g for 10 min. Chip priming and loading was performed in a chip priming station. A

volume of 9 µl of gel-dye mix was added to four dedicated wells of the chip. All remaining wells were filled with 5 µl marker solution. A volume of 1 µl of each of the samples to be analysed and of the DNA ladder was added to the sample (eleven in total) and ladder (one) wells. After vortexing at 2400 rpm for 1 min, the chip was placed in the bioanalyzer instrument and processed. Data was analysed using the 2100 Expert Software (Version: B.02.08.SI648(SR2), Agilent Technologies). The graphical bioanalyzer output is shown in **Figure 2.11**.

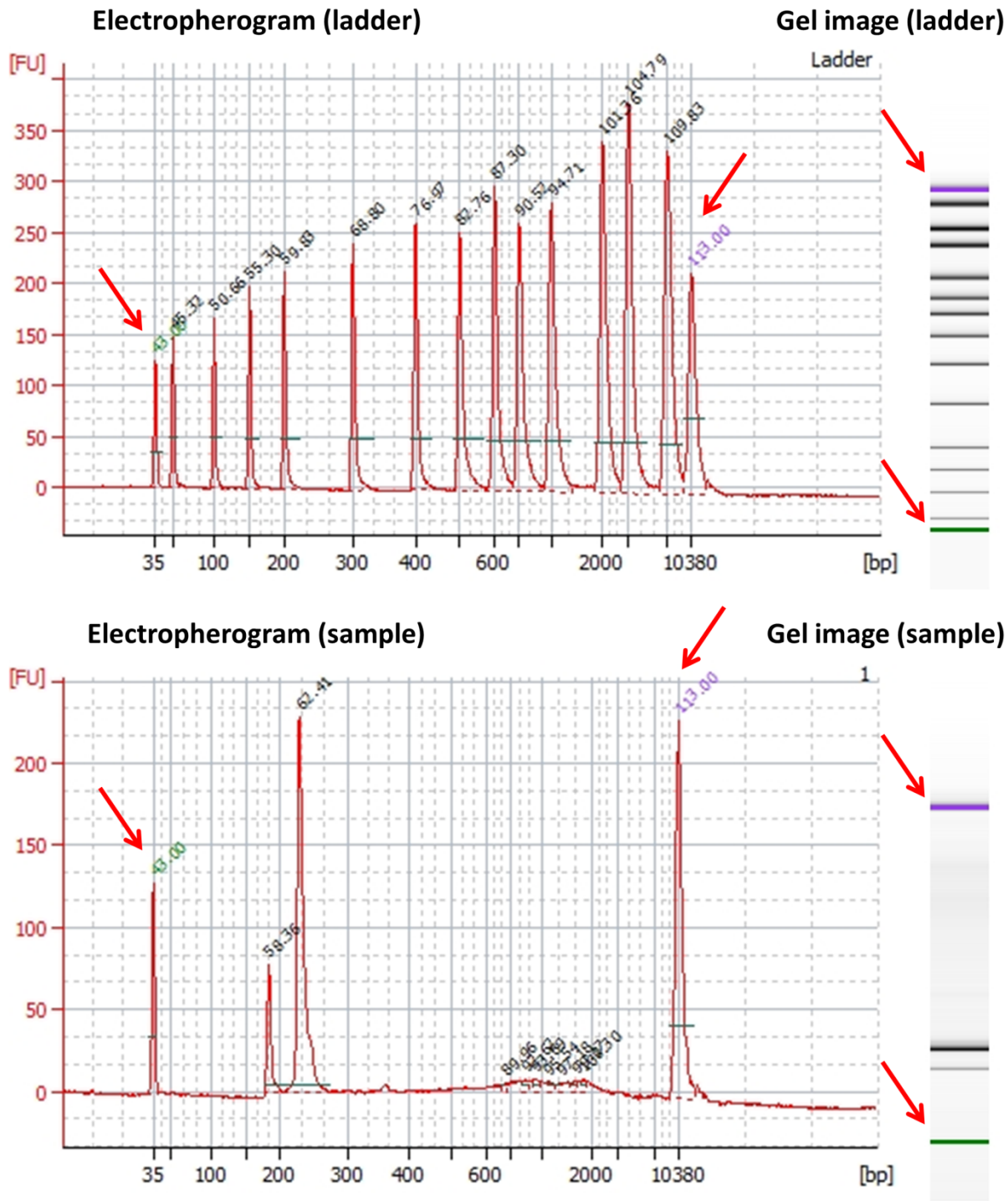


Figure 2.11: Graphical bioanalyzer output. The images show electropherograms and digital gel images of the ladder and one sample. Arrows indicate lower and upper marker (of known concentration). According to the ladder (shown in upper image) and markers, the size (in bp) and concentration (in pg/µl) of sample fragments can be determined.

2.5 Chromosome screening protocols

Three different techniques (**Figure 2.12**) were used to assess CCN in cell samples, embryo specimens, gDNA or WGA products: (1) array CGH; (2) NGS; (3) real-time qPCR. The first two techniques were performed using the 24sure and VeriSeq protocols from Illumina (**Sections 2.5.1** and **2.5.2**), which have been developed for the assessment of SurePlex products. Real-time qPCR (**Section 2.5.3**) was performed after initial multiplex pre-amplification of specific genomic loci (see **Section 2.3.3**).

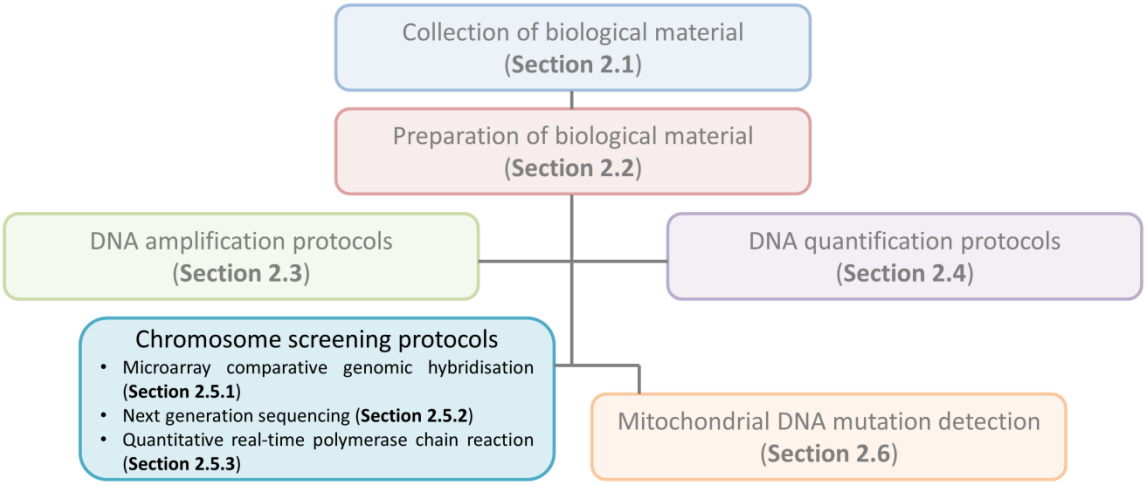


Figure 2.12: Sub-sections - Chromosome screening protocols

2.5.1 Microarray comparative genomic hybridisation

Array CGH is based on competitive fluorescence *in situ* hybridisation of test and reference samples to cloned DNA fragments of known genomic location. Samples and chromosomally normal references are labelled with two different fluorescent dyes and co-hybridised to bacterial artificial chromosome probes, which are immobilized on the microarray glass surface. Microarray slides are then scanned and signal intensities of the

resulting images converted into CCN calls by comparing to the references which were processed along with the samples.

The procedure was performed according to the supplier's protocol with slight deviations (24sure Single Channel Summary Protocol, August 2014, Illumina). Two kits were used: (1) the 24sure Microarray Pack (containing the Fluorescence Labeling System, COT Human DNA and 24sure Microarrays); (2) the SureRef Pack (containing SureRef Female and Male DNA).

For initial denaturation, 8 µl of sample (SurePlex product and SureRef Female and Male DNA) was combined with 5 µl of primer solution and incubated in a thermal cycler (**Table 2.22**). For labelling, two different master mixes containing either Cy3 dCTP or Cy5 dCTP were prepared (**Table 2.23**) and 12 µl added to the denatured samples followed by a further incubation in a thermal cycler for ~1.5 h (**Table 2.24**). After labelling, samples/references with contrasting dyes were combined in a 1.5 ml microcentrifuge tube and mixed with 25 µl COT Human DNA. To reduce volume, samples were placed into a pre-warmed centrifugal evaporator and centrifuged at 75 °C for approximately 20 min. Samples were then combined with 21 µl of pre-warmed DS Hybridisation Buffer, mixed thoroughly by flicking and vortexing and transferred to a heat block for 10 min of denaturation at 75 °C. A sample volume of 18 µl was loaded onto each slide hybridisation area and overlaid with a coverslip. Hybridisation took place overnight in a ClearHyb hybridisation system (SciGene) at 47 °C.

The next morning, coverslips were carefully removed and slides successively washed (**Table 2.25**) and dried via centrifugation at 170 x g for 3 min. For capturing of images, slides were scanned using a two channel laser scanner (InnoScan 700, Innopsys).

Hybridisation areas were identified using Mapix Software (Innopsys) and resulting images saved in TIFF format, for *in silico* data analysis, using the Bluefuse Multi Software (Ilumina).

The software compares DNA quantities of the test sample(s) to the reference samples and plots the ratios on a log2 scale. In case of a euploid sample, individual cloned DNA fragments derived from autosomes are associated with values around zero on the log scale. Chromosome losses and gains result in the values shifting away from zero to around -0.4 and +0.4, respectively. Since each sample is compared to both female and male references, the sex-mismatch with one of the references (reference of opposite sex) is indicated either by a blue or red line (mismatch to male or female reference, respectively).

Chromosome aneuploidy was analysed manually by visually inspecting sample profiles. Segmental losses or gains affecting only small parts of chromosomes were noted if they were clearly visible and at least 5 Mb in size. **Figure 2.13** illustrates the array CGH profiles of a euploid female (**A**) and male (**B**) sample. **Figure 2.14** shows profiles of a sample with a monsomy (**A**), a trisomy (**B**) and a segmental aneuploidy(**C**).

Table 2.22: Thermal cycler settings for denaturation (heated lid: 110 °C)

Number of cycles	Temperature (°C)	Time (min)
1	94.0	05:00
1	4.0	hold

Table 2.23: Labelling mix components (volume per sample)

Labelling mix reagents	Volume (µl)
Reaction buffer	5.0
dCTP-labelling mix	5.0
Cy3 dCTP or Cy5 dCTP	1.0
Klenow enzyme	1.0
Total	**12.0**

Table 2.24: Thermal cycler settings for labelling (heated lid: 110 °C)

Number of cycles	Temperature (°C)	Time (h)
1	37.0	1.5 - 24.0
1	4.0	hold

Table 2.25: Post hybridisation washes

Wash	Buffer	Temperature	Time (min)
1	2X SSC/0.05 % Tween 20	room temperature	10
2	1X SSC	room temperature	10
3	0.1X SSC	60 °C	5
4	0.1X SSC	room temperature	1

SSC (Saline-Sodium Citrate) and Tween 20 were supplied by Fisher BioReagents. Wash 3 was performed in a Hybex Microsample Incubator (SciGene).

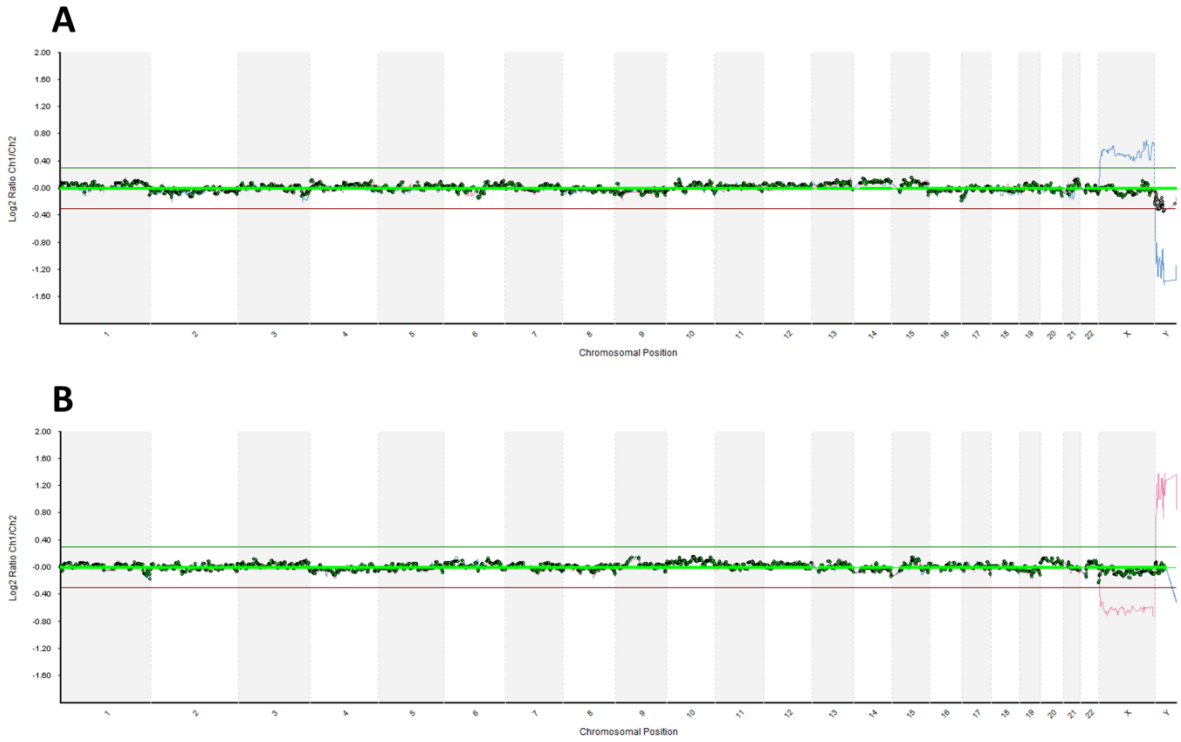


Figure 2.13: Array CGH profiles of euploid trophectoderm biopsies. A: 46,XX. **B:** 46,XY.

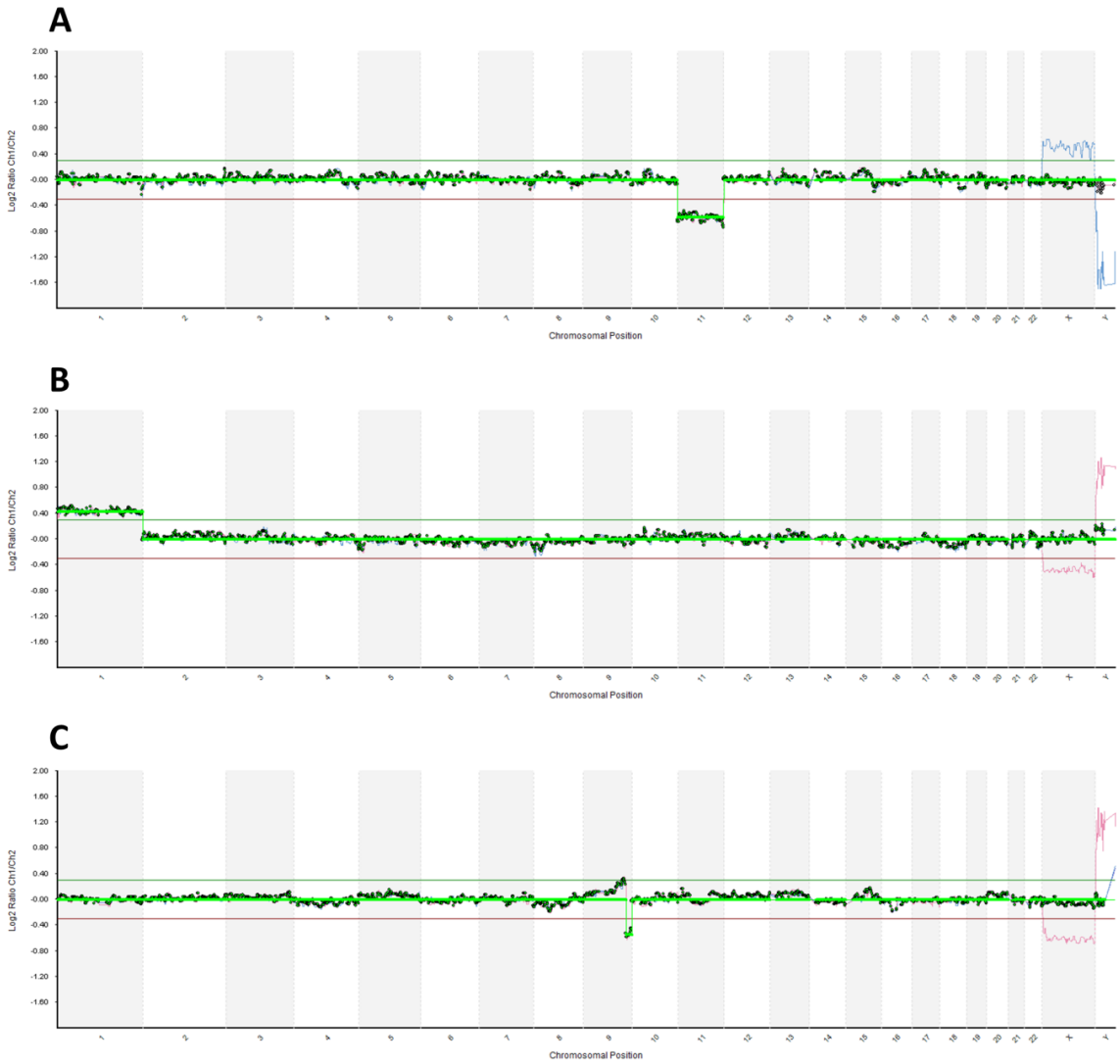


Figure 2.14: Array CGH profiles of aneuploid trophectoderm biopsies. A: 45,XX,-11. **B:** 47,XY,+1. **C:** 46,XY,-9q.

2.5.2 Next-generation sequencing

CCN analysis using NGS is based on the comparison of the relative number of sequencing reads obtained per given genomic region of the test sample(s) to the expected, previously computed number of sequencing reads of a reference.

The VeriSeq PGS Kit-MiSeq was used for preparation of sequencing libraries which were processed on a MiSeq Sequencing System (both Illumina). The protocol was

performed according to the supplier's recommendation (VeriSeq PGS Library Preparation Guide, February 2014, Illumina). At least 24 samples were processed and sequenced at the same time.

Initially, SurePlex products were quantified using the Qubit fluorometer (see **Section 2.4.1**) and diluted to 0.2 ng/µl. Then, a sample volume of 5 µl was combined and mixed with 10 µl Tagment DNA Buffer and 5 µl Amplicon Tagment Mix. After centrifugation at 280 x g for 1 min samples were placed in a thermal cycler, programmed as described in **Table 2.26**. Following incubation, samples were immediately neutralised by adding 5 µl of Neutralize Tagment Buffer. After homogenisation and centrifugation at 280 x g for 1 min, samples were placed at room temperature for 5 min.

For generation of sequencing libraries, 5 µl of Index 1 primer, 5 µl of Index 2 primer and 15 µl of Nextera PCR Master Mix were added to each sample. After a brief centrifugation and 1 min incubation, samples were transferred to a thermal cycler (**Table 2.27**). After amplification a PCR clean-up was performed. Samples were centrifuged at 280 x g for 1 min to collect condensation, combined with 45 µl AMPure XP beads (Beckman Coulter) and transferred to a microplate shaker (Illumina) set at 1,800 rpm for 2 min. After mixing, samples were incubated for 5 min at room temperature, followed by a brief centrifugation. To aggregate the magnetic beads prior to the clean-up washes, samples were placed on a magnetic stand for 2 min. The supernatant was carefully removed without disturbing the bead pellet and discarded. The beads were washed twice with 200 µl of freshly prepared 80 % ethanol (Sigma-Aldrich). Care was taken to completely remove any remaining ethanol after the second wash by placing samples on a heating block (set to 55 °C) for 5 min to allow beads to air-dry. Amplicons were re-suspended in

50 µl Resuspension Buffer by mixing on a shaker at 1,800 rpm for 2 min. After a brief centrifugation, samples were transferred back to a magnetic stand and incubated for 2 min. A volume of 45 µl of library-containing supernatant was transferred to new microcentrifuge tubes.

Next, the resulting libraries were normalised. Initially, Library Normalization Beads 1 (LNB1) and Additives 1 (LNA1) were mixed (ratio: 1 : 5.5). Then, a volume of 45 µl LNB1 / LNA1 mix was combined with 20 µl of PCR libraries and mixed thoroughly on a shaker (1,800 rpm, 30 min). After a short centrifugation, samples were placed on a magnetic stand for 2 min and the supernatant discarded. Beads were washed twice with 45 µl Library Normalization Wash 1 (LNW1) and mixed between each washing step on a shaker at 1,800 rpm for 5 min. Libraries were re-suspended in 30 µl of freshly prepared 0.1 N NaOH. After shaking at 1,800 rpm for 5 min and a brief centrifugation at 280 x g for 1 min samples were placed on the magnetic stand for 2 min. A volume of 25 µl of library-containing supernatant was removed and combined with 25 µl of Library Normalization Storage Buffer 1.

Prior to sequencing, equal volumes of normalised libraries were pooled and 15 µl of library pool combined with 85 µl Hybridization Buffer (HT1). The mixture was placed in a thermal cycler and incubated according to the programme described in **Table 2.28.** After denaturation, the entire mixture was combined with 600 µl cold HT1 and stored on wet ice until sequencing was performed.

Libraries were sequenced as described in the 'MiSeq System User Guide' (Part # 15027617, Illumina).

The sequencing output was analysed using Bluefuse Multi Software (Ilumina) which creates CCN profiles for each sample. All profiles were analysed manually and visually inspected. Monosomies and trisomies were plotted around copy numbers of 1 and 3, respectively. Segmental losses or gains affecting only small parts of chromosomes were called if they were clearly visible and at least 5 Mb in size. Mosaic chromosome gains and losses were called if copy numbers were lower than 1.8 or higher than 2.2, but did not reach the thresholds usually considered for calling non-mosaic aneuploidy. **Figures 2.15 A** and **B** illustrate the NGS profiles of a euploid female and male sample, respectively. **Figure 2.15 C** and **D** show profiles of samples with a whole chromosome monosomy and trisomy, respectively. **Figure 2.15 E** illustrates a segmental aneuploidy and **Figure 2.15 F** a mosaic loss.

Table 2.26: Thermal cycler settings for tagmentation (heated lid: 110 °C)

Number of cycles	Temperature (°C)	Time (min)
1	55.0	05:00
1	10.0	hold

Table 2.27: Thermal cycler settings for amplification of SurePlex products (heated lid: 110 °C)

Number of cycles	Temperature (°C)	Time (min)
1	72.0	03:00
1	95.0	00:30
12	95.0	00:10
	55.0	00:30
	72.0	00:30
1	72.0	05:00
1	4.0	hold

Table 2.28: Thermal cycler settings for library denaturation (heated lid: 110 °C)

Number of cycles	Cycle temperature (°C)	Incubation time (min)
1	96.0	03:00
1	4.0	05:00
1	4.0	hold

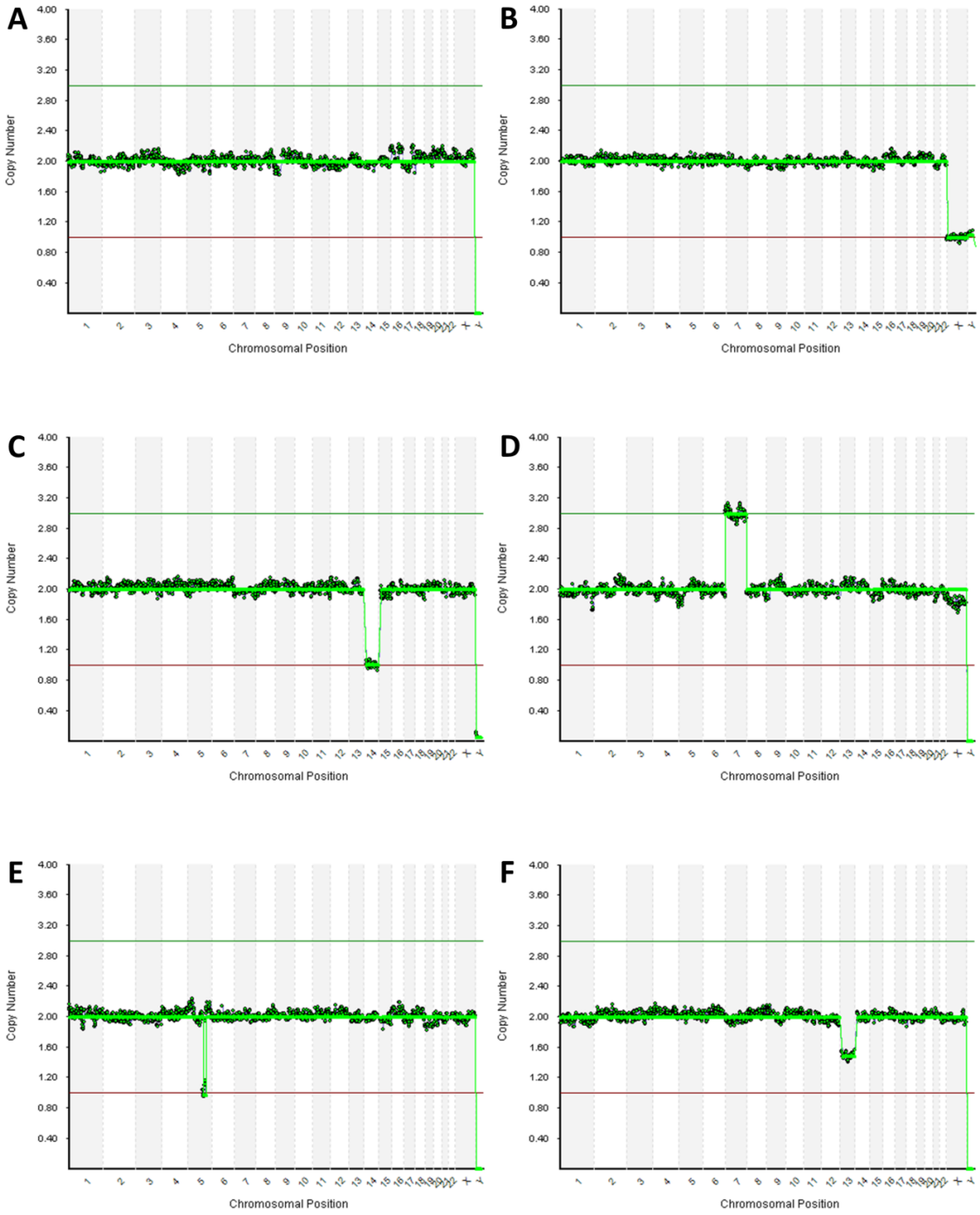


Figure 2.15: NGS profiles of trophectoderm biopsies. A: 46,XX. **B:** 46,XY. **C:** 45,XX,-14. **D:** 47,XX,+7. **E:** 46,XX,-5q. **F:** 45,XX,-13 (mosaic).

2.5.3 Quantitative real-time polymerase chain reaction

Real-time qPCR is based on the measurement of fluorescence signal intensities obtained during the amplification of specific genomic loci, which are then converted into relative DNA quantities. The technique was mainly used to test CCN in samples which were previously subjected to multiplex pre-amplification (see **Section 2.3.3**) but also applied to gDNA and SurePlex products. The method was further used to assess relative mtDNA copy numbers and the presence or absence of the DiGeorge microdeletion Syndrome. Real-time qPCR reactions were performed on a StepOnePlus (**Section 2.5.3.1**) or QuantStudio 12K (**Section 2.5.3.2**) Real-Time PCR System using TaqMan primers and probes. The principle of real-time qPCR using TaqMan chemistry is visualised in **Figure 2.16**. Details on primers and probes as well as data analyses are presented in **CHAPTER 3**.

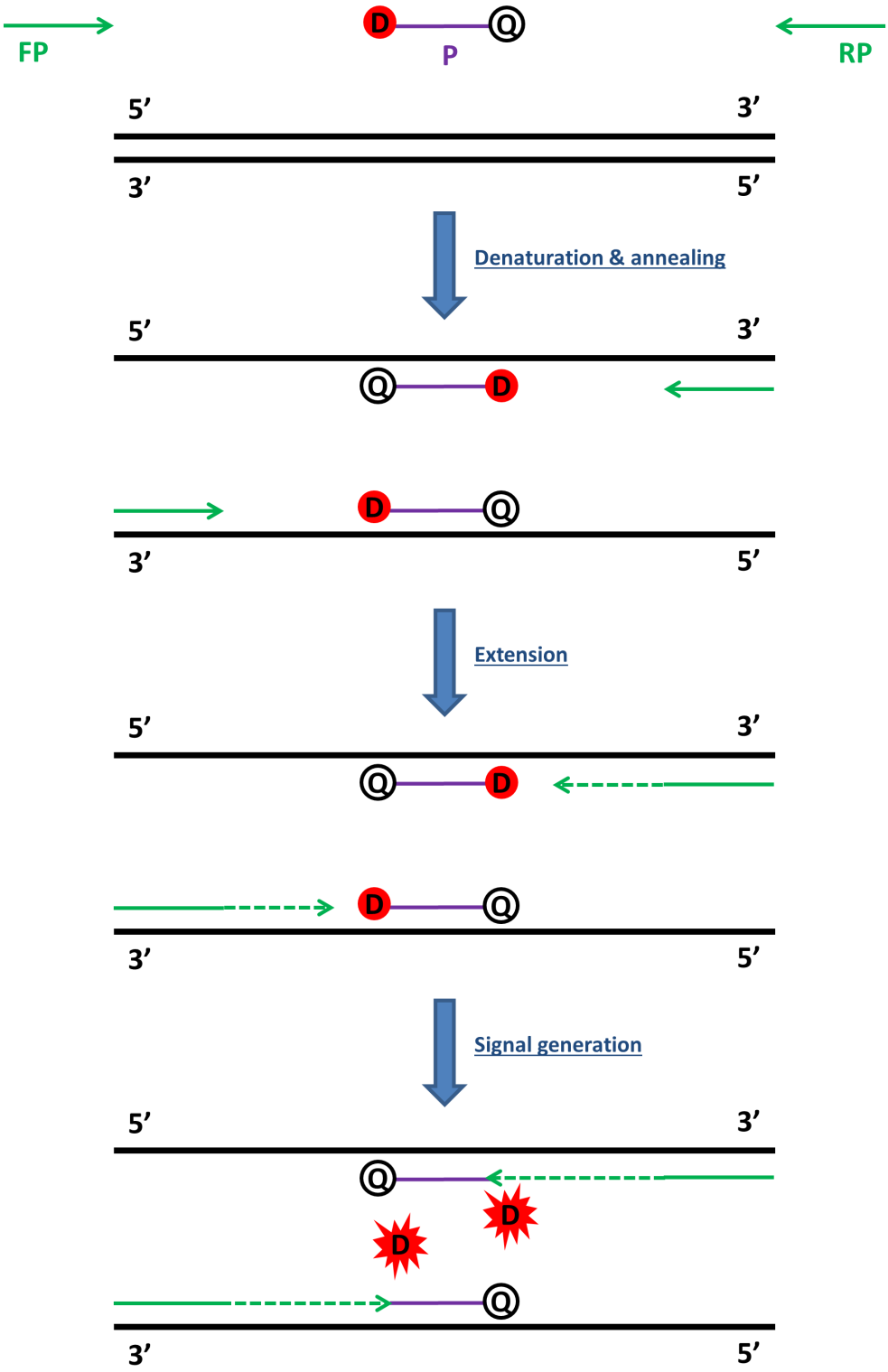


Figure 2.16: Principle of TaqMan-based real-time qPCR. Primers and the probe anneal to their complementary sequence. The probe has a fluorescence dye and a quencher dye attached. Due to the close proximity of both dyes no fluorescence is emitted. During primer extension, the probe is cleaved by the 5’ - 3’ exonuclease activity of the DNA polymerase, leading to dissociation of the dyes and in emission of fluorescence. FP = forward primer. RP = reverse primer. P = probe. D = fluorescence dye. Q = quencher dye.

2.5.3.1 StepOnePlus Real-Time PCR System protocol

Tables 2.29 and **2.30** describe the reaction mix and thermal cycler programme for real-time qPCR reactions performed on a StepOnePlus cycler. Each genomic locus was amplified in triplicate [reporter: FAM (fluorescein amidite); quencher: NFQ (nonfluorescent quencher)-MBG (minor groove binder)] along with a reference assay (reporter: VIC, quencher: TAMRA). Additionally two distinct negative controls were set up, consisting of either the pre-amplification negative control or of nuclease-free water replacing the sample DNA. Samples were set up and processed in 96-well plates.

Data was analysed using the inbuilt StepOneSoftware (ThermoFisher, v2.2.2).

Table 2.29: Real-time qPCR components (volume per reaction)

Alkaline lysis buffer reagents	Supplier	Volume (µl)
Nuclease-free PCR grade water	Roche Diagnostics	2.0
TaqMan Genotyping Mix	ThermoFisher	5.0
TaqMan Reference Assay	ThermoFisher	0.5
TaqMan Copy Number Assay	ThermoFisher	0.5
Sample	NA	2.0
Total		**10.0**

NA = not applicable.

Table 2.30: Real-time qPCR thermal cycler settings (heated lid: 100 °C)

Number of cycles	Cycle temperature (°C)	Incubation time (min)
1	95.0	10:00
40	95.0	00:15
	60.0	01:00

2.5.3.2 QuantStudio 12K Real-Time PCR System protocol

Real-time qPCR reactions were performed on a QuantStudio 12K Flex Real-Time PCR System (ThermoFisher) using custom-made arrays which were pre-spotted with TaqMan primers and probes. The samples were loaded onto the array automatically using a robotic system (QuantStudio 12K Flex OpenArray AccuFill System, ThermoFisher).

Samples which have previously been subjected to multiplex pre-amplification or Sureplex products were initially diluted in nuclease-free water (ratio: 1:9 dilution) and then combined with TaqMan OpenArray Real-Time PCR Master Mix (ThermoFisher) at a ratio of 1:4 (sample : Master Mix). GDNA was combined with Master Mix without prior dilution. Mixtures were then transferred to a 384-well plate and loaded onto the arrays by the robotic system.

Data was analysed using the QuantStudio 12K Flex Software (ThermoFisher, v.1.2.2) and customized algorithms created during this project (detailed in **CHAPTER 3**).

2.6 Mitochondrial DNA mutation detection

This section describes the NGS-based protocol used for the assessment of mtDNA mutations (**Figure 2.17**). Procedures included the preparation of sequencing libraries (**Section 2.6.1**), preparation and sequencing of template-positive Ion Sphere Particles [(ISPs), **Sections 2.6.2** and **2.6.3**] and the data analysis of the sequencing output (**Section 2.6.4**).

The method was applied to isolated cell samples (buccal cells and lymphocytes as well as embryo specimens), WGA products (MDA and SurePlex) and gDNA.

Prior to the generation of sequencing libraries a conventional PCR protocol (see **Section 2.3.2.2**) was performed to enrich the mtDNA region of interest.

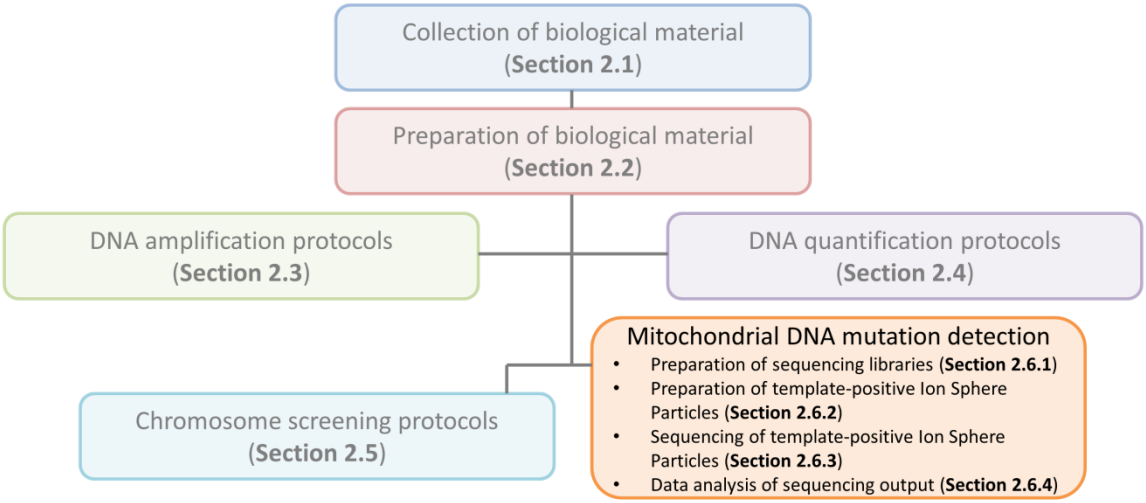


Figure 2.17: Sub-sections – Mitochondrial DNA mutation detection

2.6.1 Preparation of sequencing libraries

A modified version of the Ion Xpress Plus gDNA and Amplicon Library Preparation protocol (4471989 Rev. C, 3 Jan 2012, ThermoFisher) was utilised to create sequencing libraries. Reagents were supplied with the Ion Plus Fragment Library kit and the Ion Xpress Barcode Adaptors 1 - 16 and 17 - 32 Kits (both ThermoFisher). For purification of samples, Agencourt AMPure XP beads (Beckman Coulter) and freshly prepared 70 % ethanol (Sigma-Aldrich) was used. Prior to library preparation, sample DNA concentrations were quantified using the Qubit dsDNA HS Assay Kit (see **Section 2.4.1**).

Initially, PCR amplicons were subjected to an end-repair followed by a purification step. A volume of 21 µl of end-repair mixture (**Table 2.31**) was combined with 79 µl of sample, containing approximately 100 ng of DNA. The sample mixtures were then incubated at room temperature for about 20 min. To purify the samples, each mixture was combined with 180 µl of magnetic beads, thoroughly mixed and incubated for 5 min at room temperature. Samples were then placed on a magnetic rack for 3 min. Supernatant was removed and discarded and beads washed twice with 500 µl of ethanol. To allow evaporation of residual ethanol, samples were placed on a heat block set to 52 °C for approximately 5 min. To elute the DNA, 25 µl of Low TE was added to each sample and mixed thoroughly. The samples were placed on a magnetic rack for 1 min and the DNA-containing supernatant transferred to new microcentrifuge tubes.

Next, adapters and barcodes were ligated and a nick repair performed (**Table 2.32**). Sample mixtures were incubated in a thermal cycler programmed according to **Table 2.33**. To remove unbound adapter and barcode sequences a further purification step was performed using 180 µl of magnetic beads, followed by two ethanol washes (as described above). Samples were eluted in 25 µl of Low TE buffer.

To increase library quantities, an amplification step was performed. The entire volume of purified libraries was combined with 105 µl of amplification mix (**Table 2.34**) and amplification performed in a thermal cycler programmed as described in **Table 2.35**. Libraries were then purified once more as described previously. However, a volume of 195 µl of magnetic beads (instead of 180 µl) was used, followed by two ethanol washes. Libraries were eluted in 20 µl Low TE and stored at -80 °C until further processing.

Table 2.31: End-repair components (volume per sample)

Component	Volume (µl)
5X End Repair Buffer	20.0
End Repair Enzyme	1.0
Total	**21.0**

Table 2.32: Adapter/barcode ligation and nick repair components (volume per sample)

Component	Volume (µl)
10X Ligase Buffer	10.0
Ion P1 Adapter	2.0
Ion Xpress Barcode (1 - 32)	2.0
dNTP Mix	2.0
Nuclease-free Water	49.0
DNA Ligase	2.0
Nick Repair Polymerase	8.0
Sample	25.0
Total	**100.0**

Table 2.33: Thermal cycler settings for adapter/barcode ligation and nick repair (heated lid: 110 °C)

Number of cycles	Cycle temperature (°C)	Incubation time (min)
1	25.0	15:00
1	72.0	05:00
1	4.0	hold

Table 2.34: Library amplification components (volume per sample)

Component	Volume (µl)
Platinum PCR SuperMix High Fidelity	100.0
Library Amplification Primer Mix	2.0
Total	**102.0**

Table 2.35: Thermal cycler settings for library amplification (heated lid: 110 °C)

Number of cycles	Cycle temperature (°C)	Incubation time (min)
1	95.0	05:00
5	95.0	00:15
	58.0	00:15
	70.0	01:00
1	4.00	hold

2.6.2 Preparation of template-positive Ion Sphere Particles

Prior to library sequencing, ISPs, each containing clonally amplified sequences from a single library, were prepared. Template-positive ISPs were generated using the Ion PGM Template OT2 200 Kit and Ion PGM Enrichment Beads (both ThermoFisher). ISPs were prepared according to the Ion PGM Template OT2 200 Kit User Guide (Catalog Number: 4480974, Revision 5.0, ThermoFisher). Preparation of template-positive ISPs was performed using the Ion OneTouch 2 System (ThermoFisher), which consists of a thermal cycler (Ion OneTouch 2 Instrument) for clonal library amplification and of a robotic system (Ion OneTouch ES) for enrichment of template-positive ISPs.

Initially, sequencing libraries were quantified using the relative standard curve method (see **Section 2.4.2**). Additionally, a bioanalyzer analysis (see **Section 2.4.3**) was performed to verify library quantities and to ensure proper library preparation. Each library was then diluted in nuclease-free water to approximately 100 pM and equal sample volumes pooled.

To generate ISPs comprised of clonally amplified library sequences an emulsion PCR was performed. An amplification solution was prepared as described in **Table 2.36** and all reaction components combined and homogenised. Next, a volume of 100 µl of ISPs was added and the mixture vortexed and centrifuged at maximum speed for 5 s. The entire solution was then loaded into a reaction filter assembly (supplied), followed by the addition of 1500 µl of Reaction Oil. The assembly was then transferred to the dedicated thermal cycler and samples incubated overnight using the 'Ion PGM Template OT2 200 Kit' programme.

After PCR completion and collection of ISPs in two 1.5 ml recovery tubes, samples were spun down for 10 min. The supernatant was carefully removed and discarded. A volume of approximately 50 µl was left behind in each tube, ISPs re-suspended by pipetting up and down and contents of both tubes combined.

A volume of 2 µl was removed to assess if emulsion PCR was successful using the Ion Sphere Quality assay (ThermoFisher). The assay utilises two different probes labelled with AF 488 and AF 647 fluorochromes. The AF 488 probe binds to sequences attached to ISPs and the AF 647 to library-specific sequences. To determine the percentage of template-positive ISPs, quantities of both fluorochromes were measured using the 'Ion_pluginV310_AF' programme installed on a Qubit 2.0 Fluorometer (ThermoFisher).

A volume of 19 µl of Annealing Buffer and 1 µl of Ion Probes was added to the microcentrifuge tube containing 2 µl of previously collected ISPs and mixed. After a short centrifugation, the sample was incubated in a thermal cycler to anneal the probes (**Table 2.37**). Next, unbound probes were removed during three consecutive washing steps. During each step 200 µl of Quality Control Wash Buffer was added to the sample, followed

by a centrifugation at 15500 x g for 1.5 min. The supernatant was removed and discarded. After the last washing step, ISPs were re-suspended in approximately 200 µl Quality Control Wash Buffer and transferred to a Qubit assay tube. Additionally, a negative control was generated consisting of 200 µl Wash Buffer. The sample and negative control were then measured on the Qubit fluorometer. Ratios of both fluorochromes were calculated using the 'Qubit 2.0 Easy Calculatot Microsoft Excel Spreadsheet' (ThermoFisher). A ratio of 10 - 30 % of loaded beads was considered optimal for proceeding with the enrichment of template-positive ISPs.

To remove template-negative ISPs (ISPs that do not contain a library) an automated enrichment of template-positive ISPs was performed using magnetic streptavidin beads (Ion PGM Enrichment Beads, ThermoFisher). The entire volume of ISPs (about 100 µl) was transferred to the first well of an 8-well strip tube (supplied). Next, 13 µl of Dynabeads MyOne Streptavidin C1 Beads were transferred to a low-bind 1.5 ml microcentrifuge tube and placed on a magnetic rack for 2 min. The supernatant was removed and the beads re-suspended in 130 µl MyOne Beads Wash Solution. The entire mixture was then transferred to the second well of the 8-well strip tube. Wells 3, 4 and 5 were filled with 300 µl Ion OneTouch Wash Solution. Well 7 was loaded with 300 µl freshly prepared Melt-Off Solution (**Table 2.38**). After automated enrichment, template-positive ISPs were mixed with 10 µl Neutralization Solution and stored at 2 - 8 °C until further processing (maximum one day).

Table 2.36: Emulsion PCR components

Component	Volume (µl)
Nuclease-free Water	25.0
Ion PGM Template OT2 200 Reagent Mix	500.0
Ion PGM Template OT2 200 PCR Reagent B	300.0
Ion PGM Template OT2 200 Enzyme Mix	50.0
Library pool (100 pM)	25.0
Total	**900.0**

Table 2.37: Thermal cycler settings for annealing of probes (heated lid: 110 °C)

Number of cycles	Cycle temperature (°C)	Incubation time (min)
1	95.0	02:00
1	37.0	02:00

Table 2.38: Melt-Off solution components

Component	Volume (µl)
Tween Solution	280.0
NaOH (1M)	40.0
Total	**320.0**

Tween Solution was supplied. NaOH was purchased from Sigma-Aldrich.

2.6.3 Sequencing of template-positive Ion Sphere Particles

Library-containing ISPs were sequenced on the Ion Personal Genome Machine (PGM) System using Ion 314, Ion 316 or Ion 318 Chips and the Ion PGM Sequencing 200 Kit v2 (all ThermoFisher). Preparation of the PGM System prior to sequencing was performed according to the Ion PGM Sequencing 200 Kit v2 User Guide (Catalog Number 4482006, Revision 3.0, ThermoFisher).

Entire volumes of enriched, template-positive ISPs were used if sequencing was performed on a 316 or 318 Chip. In case ISPs were loaded on a 314 Chip half the volume

(about 100 µl) of ISPs was used. A volume of 5 µl of Control ISPs was added to the ISPs, mixed and centrifuged at 15500 x g for 2 min. The supernatant was carefully removed leaving behind 15 µl if sequencing was performed on 316 or 318 Chips or 3 µl if performed on a 314 Chip. ISPs were re-suspended in 27 µl (316/318 Chip) or 3 µl (314 Chip) of Sequencing Primer and incubated in a thermal cycler (**Table 2.39**). After incubation, 3 µl (316/318 Chip) or 1 µl (314 Chip) of Ion PGM Sequencing 200 v2 Polymerase was added. After 5 min incubation at room temperature, the entire mixture was loaded onto the chip and the sequencing run performed.

Table 2.39: Thermal cycler settings for annealing of sequencing primers (heated lid: 110 °C)

Number of cycles	Cycle temperature (°C)	Incubation time (min)
1	95.0	02:00
1	37.0	02:00

2.6.4 Data analysis of sequencing output

Initial processing of the sequencing data was performed on the Torrent Browser using the inbuilt Torrent Suit Software (ThermoFisher). The integrative Genomics Viewer (IGV, Version 2.3.32, Broad Institute) was used for preliminary data analysis of the sequencing output and to visualise the data.

For proper data analysis, the Torrent Variant Caller plugin (TVC plugin, v4.2.1.0, ThermoFisher) was used. The TVC plugin was specifically developed for the analysis of sequencing data generated on a PGM system and is used for the detection of genetic variants. To run the plugin, BED files (Targeted Region and HotSpot files) describing the mtDNA region of interest and the affected nucleotide were created and uploaded. Default

plugin settings were applied and the following configurations used: Chip Type: PGM, Library Type: AmpliSeq, Variant Frequency: Somatic, Parameter Settings: High Stringency. The plugin output included results on the allele call at the HotSpot region (variant nucleotide detected or not detected), the allele frequency (ratio between allele coverage and total coverage) as well as quality indicators (e.g. probability of incorrect call).

CHAPTER 3: Development, validation and first clinical application of a rapid comprehensive chromosome screening technique utilising an array-based nano-scale quantitative DNA amplification technology

This chapter describes the development and validation of a robust real-time qPCR protocol and the clinical application to blastocyst-stage embryos of patients undergoing IVF/PGS treatment. The chapter is divided into five sections. A brief introduction is followed by a materials and methods section which summarises the ethics, the study design and the applied methods. The third section states the different phases of protocol development and validation, including initial testing phases on cell line-derived samples, followed by a pre-clinical validation study using donated surplus embryos from clinical IVF cycles. The fourth section describes the results obtained after clinical implementation. Lastly, in the fifth section, developmental phases, clinical results as well as advantages and limitations of the novel method are discussed.

3.1 Introduction - **CHAPTER 3**

Most IVF patients require several treatment cycles to achieve a pregnancy which increases treatment costs for patients and public healthcare services and prolongs the time required to parenthood. The relative inefficiency of IVF is due, in part, to difficulties selecting the embryo with the greatest pregnancy potential for transfer. Traditional selection based on morphology is only weakly correlated with embryo viability and fails to reveal aneuploidy, one of the principal causes of implantation failure and miscarriage. For this reason, PGS has been proposed as a strategy for the identification of chromosomally normal embryos (Munné et al., 1993a).

Currently available CCS techniques, however, are laborious and typically require 24 hours or more for result generation. Given that some blastocysts are not ready for biopsy until late on day-5 or even day-6 post fertilisation, a 24-hour chromosome screening

test will often be incompatible with fresh embryo transfer, necessitating cryopreservation. Moreover, PGS remains relatively expensive restricting patient access.

For these reasons, the aim of this study was to develop, validate and clinically apply a novel, rapid and cost-effective CCS technique utilising a fully automated, array-based real-time qPCR methodology for testing of blastocyst-stage embryos.

In addition to the copy number analysis of all 24 chromosomes, the study further aimed to incorporate simultaneous quantification of mtDNA content, which could be used as an additional indicator of embryo viability. Moreover, feasibility of adding microdeletion syndrome testing was assessed.

3.2 Materials and methods - **CHAPTER 3**

3.2.1 Ethics regarding the analysis of biological samples and embryo specimens

For the initial development and validation of the real-time qPCR protocol, gDNA and cell samples were used. The samples were either prepared from peripheral blood obtained from members of the Reprogenetics UK team or derived from commercially available human cell lines.

Blood samples were collected by trained nurses at the Oxford Fertility clinic in compliance with the Reprogenetics UK donor consent form (FORM-USE OF OWN BLOOD_CONSENT-2).

All cell lines used during the course of the project were purchased from the Coriell Cell Repository (Camden, NJ, US). As stated by the American National Institute of Health Research, the use of commercially available established cell lines from the American Type Culture Collection or a similar repository is not considered human subjects research because cells are publicly available and all information on cell lines is also publicly available. Hence no ethical approval was required. Details on karyotype, culture type, repository type and Coriell catalogue IDs are provided in **Table A.1** in **Appendix A**.

Prior to clinical application, a pre-clinical study was performed and the technique applied to surplus embryos donated for research by patients who underwent IVF treatment at the Pacific Fertility Centre (California, USA). The use of donated embryos was approved by the Western Institutional Review Board (protocol number 20060680).

After extensive protocol validation the technique was offered by Reprogenetics UK as a clinical service for testing of blastocyst-stage embryos. The test was clinically applied to embryos derived from patients referred for PGS utilising the developed real-time qPCR protocol. All patients were referred for testing from a single UK clinic (Lister Fertility Clinic, London). The IVF centre had appropriate ethical and clinical approvals and relevant clinical treatment licenses in place. The clinic was advised to ensure that all patients were provided with counselling regarding PGS, prior to initiating treatment. Furthermore, to ensure that patients received appropriate counselling, informed consent was obtained in all cases, outlining treatment procedures as well as purpose, limitations, risks and benefits associated with PGS.

Data on IVF outcomes following PGS utilising the established real-time qPCR protocol was collected from March 2016 to December 2016 and then analysed

retrospectively. Results were compared to clinical array CGH data previously generated at Reprogenetics UK (from June 2010 to June 2016). Data on outcomes following PGS/IVF treatment is routinely collected as part of quality assurance at Reprogenetics UK by a third person (Dr Elpida Fragouli, Scientific Director) and was fully anonymised prior to the analysis. Advice on the correct path to take in terms of obtaining ethical approval for this type of analysis was obtained from the Clinical Trials and Research Governance (CTRG) of the University of Oxford prior to the data analysis. Since clinical data was collected previously and is therefore retrospective and anonymous, review from the Central University Research Ethics Committee (CURE) was not required.

3.2.2 Study design, protocol validation and clinical implementation

The development and validation of the real-time qPCR protocol was conducted in six phases. During the first phase of protocol development, feasibility of real-time qPCR as a tool for CCN analysis was assessed and tested on a traditional real-time qPCR instrument.

To enhance sensitivity, throughput and cost-effectiveness, the method was then transferred to a nano-scale array-based real-time qPCR system. As an initial proof-of-principle, an array for testing of just seven chromosomes was evaluated during Phase 2 and Phase 3 of protocol development.

During Phase 4 and Phase 5 a new real-time qPCR array, providing CCS, mtDNA quantification and detection of the DiGeorge microdeletion Syndrome was created and evaluated.

Following extensive validation using euploid and aneuploid gDNA and cell samples derived from karyotypically normal individuals as well as cell culture of aneuploid and euploid cell lines, a pre-clinical validation study was performed (Phase 6) and the established real-time qPCR method tested on trophectoderm biopsies derived from donated surplus blastocyst-stage embryos. To test accuracy of the method, real-time qPCR results were compared to results obtained from the corresponding embryos which were analysed via NGS-based CCS (described in **Section 2.5.2** in **CHAPTER 2**). Prior to NGS-based CCS, entire embryos were subjected to WGA using the Sureplex protocol (see **Section 2.3.1.1** in **CHAPTER 2**).

In addition to CCN analysis, mtDNA copy numbers were quantified in trophectoderm biopsies using the developed real-time qPCR protocol and results compared to relative quantities present in corresponding embryos. Content of mtDNA in entire embryos was assessed using a previously established mtDNA quantification method (Fragouli et al., 2015; Ravichandran et al., 2017). In brief, relative mtDNA quantities were determined in WGA products via real-time qPCR employing three TaqMan assays, amplifying two sequences present in the mitochondrial genome [referred to as '16s' targeting the mitochondrially encoded 16S ribosomal RNA gene (MT-RNR2) and 'MajArc' targeting the mitochondrially encoded NADH:ubiquinone oxidoreductase core subunit 4 (MT-ND4)] as well as one sequence present in repetitive Alu elements in the nDNA (referred to as 'Alu'). Alu served as a reference assay and was used for data normalisation. For sample processing, 1 µl of WGA product was diluted in 8 µl nuclease-free water and combined with 10 µl TaqMan Universal PCR Master Mix (ThermoFisher) and 1 µl of the 16s, MajArc or Alu assay. All reactions were performed in

triplicate according to the cycler conditions outlined in **Table 2.30** in **Section 2.5.3.1** in **CHAPTER 2**.

NGS-based CCS as well as quantification of mtDNA content in entire embryos used during the pre-clinical validation phase, was performed by members of the Reprogenetics US team in New Jersey.

Following the real-time qPCR protocol development and pre-clinical validation, the test was offered clinically to patients undergoing IVF/PGS treatment. Patients included in the study were referred for PGS due to previous pregnancy loss(es), previous IVF failure(s) as well as advanced maternal age. Embryos were biopsied on day-5 post fertilisation and samples shipped to Reprogenetics UK. Following sample receipt, trophectoderm cells were processed and analysed and results reported to the clinic in the evening of the day of biopsy. Embryo transfer took place early in the morning of day-6.

Real-time qPCR results obtained from IVF/PGS cycles were then compared to clinical outcomes of patients who underwent IVF/PGS using array CGH at the same clinic. The array CGH data included results of patients coming through for chromosome screening at the blastocyst-stage, combined with fresh embryo transfer, which took place in the afternoon of day-6. All patients were referred for array CGH testing due to a history of poor reproductive outcome (same indications as described above). Patients receiving PGS treatment due to a maternal or paternal chromosome rearrangement (such as reciprocal or Robertsonian translocations) were excluded from the study.

The utilised array-based real-time qPCR protocol further permitted mtDNA quantification in embryo biopsies and results are briefly discussed. Of note, only results on

CCN were reported to the clinic and the analysis of mtDNA content was not used for the purpose of embryo selection.

3.2.3 Preparation of samples for protocol development and validation

GDNA and cell samples used during Phases 1 - 5 of protocol development were either obtained from cell culture or from peripheral blood samples (see **Sections 2.1.1** and **2.1.3** in **CHAPTER 2**). Isolation of gDNA was performed as described in **Sections 2.2.2.1** and **2.2.2.3** in **CHAPTER 2**. Cell culture-derived cells and lymphocytes from peripheral blood samples were isolated as described in **Sections 2.2.1.1** and **2.2.1.3** in **CHAPTER 2**. All cell isolations were performed by Dr Dagan Wells.

Donated surplus blastocyst-stage embryos used during the pre-clinical validation phase had previously been cryopreserved on day-5 or day-6 post fertilisation. Following the thawing of embryos, trophectoderm biopsy was performed and biopsied cells as well as corresponding embryos tubed separately (see Section **2.2.1.4** in **CHAPTER 2**).

3.2.4 IVF treatment, embryo culture and biopsy

IVF treatment of patients referred for PGS utilising the established real-time qPCR protocol or array CGH, embryo culture and biopsy was performed as described in **Sections 2.1.4** and **2.2.1.4** in **CHAPTER 2** and took place in the referring IVF clinic.

WGA and cytogenetic testing utilising array CGH is described in **CHAPTER 2**, **Sections 2.3.1.1** and **2.5.1**.

3.2.5 Sample processing procedures

Procedures involved in the real-time qPCR set-up were performed as described in **CHAPTER 2**. In brief, all cell samples as well as embryo biopsies were subjected to cell lysis, followed by multiplex pre-amplification (described in **Section 2.3.3**). Real-time qPCR reactions were performed as outlined in **Section 2.5.3**. Initial array-based real-time qPCR experiments (Phases 2 - 4) were carried out at the ThermoFisher site in Paris. Pre-amplified samples were shipped on ice and processed by Dominique Dewolf (OpenArray Application Specialist, ThermoFisher). Subsequent analysis of the data was performed by me.

In addition to real-time qPCR, cell samples derived from some of the aneuploid cell lines, carrying structural chromosome abnormalities were subjected to WGA using the Sureplex protocol, followed by array CGH or NGS-based CCS to confirm previously established karyotypes. Procedures are described in **Sections 2.3.1.1**, **2.5.1** and **2.5.2** in **CHAPTER 2**.

3.2.6 Data analysis

3.2.6.1 Statistical data analysis

Statistical data analysis was conducted using GraphPad Prism v5.00 (GraphPad Software, La Jolla California, USA). Data was tested for normal distribution using the D'Agostino & Pearson omnibus normality test. For analysis of continuous variables [described as mean ± standard deviation (SD)] which followed a normal distribution the unpaired t test was performed. For variables which were not normally distributed the

Mann Whitney U test was performed. For comparison of categorical variables (described as frequencies) the Fisher's exact test was performed. Correlation analysis was carried out by calculating the Spearman's or Pearson rank correlation coefficient, depending on data distribution. All data analyses tests were performed two-tailed with a 95 % confidence interval (CI). A p-value < 0.05 was considered significant.

3.2.6.2 Analysis of consistency of chromosome copy number results

CCN results obtained from real-time qPCR experiments performed during the protocol development and validation phases were compared to the expected results. Results of gDNA and cell samples derived from cell lines were compared with previously established cell line karyotypes. Consistency of results obtained from embryo biopsies during the pre-clinical study was assessed by comparing to results obtained from the analysis of the embryo reminder using NGS-based CCS.

Sensitivity and specificity of real-time qPCR results were assessed on the basis of overall sample diagnosis (euploid or aneuploid samples) as well as on the basis of individual CCN calls (euploid or aneuploid chromosomes). Sensitivity was defined as the probability that real-time qPCR detects chromosome/sample aneuploidy (true-positive rate). Specificity was defined as the probability that real-time qPCR detects chromosome/sample euploidy (true-negative rate). Sensitivity and specificity was computed using the MEDCALC statistical software (https://www.medcalc.org/calc/diagnostic_test.php) and calculated as shown below using the following definitions and formulas:

True-positives: aneuploid chromosomes/samples identified as previously established

True-negatives: euploid chromosomes/samples identified as previously established

False-positives: wrongly identified aneuploid chromosomes/samples

False-negatives: wrongly identified euploid chromosomes/samples

Sensitivity: [True-positives / (True-positives + False-negatives)] x 100

Specificity: [True-negatives / (True-negatives + False-positives)] x 100

3.3 Protocol development and validation - **CHAPTER 3**

3.3.1 Phase 1 - Feasibility of chromosome copy number analysis utilising quantitative real-time polymerase chain reaction

3.3.1.1 Protocol design Phase 1

During the first phase of the protocol development, feasibility of comprehensive CCN analysis using real-time qPCR was assessed. A protocol targeting and amplifying a total of 96 distinct genomic regions distributed across all 24 chromosomes (four loci per chromosome) was designed (**Figure 3.1**).

For the amplification of all 96 genomic loci, TaqMan real-time qPCR assays were utilised. Assays, each consisting of a primer pair and a probe, were purchased from ThermoFisher which offers a wide range of partially pre-tested copy number variation assays spread across the entire genome (https://www.thermofisher.com/uk/en/home/life-science/pcr/real-time-pcr/real-time-pcr-assays/cnv-analysis-using-taqman.html).

Care was taken when selecting the 96 copy number assays to ensure that the chosen genomic loci were not located in regions with known copy number variation. Furthermore, assays located closest to the chromosome telomere region were selected to increase the possibility of detecting structural chromosome abnormalities, affecting only ends of chromosomes (e.g. partial gains or losses, unbalanced products of reciprocal translocations). For metacentric chromosomes two target sequences located on each chromosome arm were selected.

In addition to the 96 copy number assays, a control assay (TERT, located in the telomerase reverse transcriptase gene) was incorporated in the protocol which served as a reference assay in real-time qPCR experiments. In order to multiplex and process both assay types in a single reaction, the reference assay TERT utilised a different fluorescent probe as compared to the copy number assays (TAMRA probe labelled with VIC dye versus MGB probe labelled with FAM dye). This was important for data analysis to correct for possible pipetting errors, which may result in unequal amounts of input DNA between reactions and to further account for differing PCR efficiencies between different reactions or samples.

Assay IDs and genomic location of the selected copy number assays and the reference assay TERT are presented in **Table A.2** in **Appendix A**.

A total of 14 samples, each consisting of three cells were tested during Phase 1 of protocol development. Nine samples consisted of lymphocytes derived from a karyotypically normal female and male control individual (5 x 46,XX and 4 x 46,XY). The remaining samples consisted of fibroblasts derived from the cell culture of three different aneuploid cell lines (2 x 47,XY,+13; 1 x 47,XY,+18; 2 x 47,XY,+21).

Prior to real-time qPCR reactions, cells were lysed followed by a multiplex pre-amplification PCR to simultaneously amplify all 96 genomic regions and the reference assay in a single reaction. This was important to ensure sufficient amount of sample DNA for subsequent real-time qPCR reactions. Following multiplex pre-amplification, each of the 96 loci was then amplified separately during real-time qPCR, along with the reference assay TERT.

The protocol was tested on a traditional real-time qPCR cycler using 96-well plates. Since each of the 96 copy number assays was tested in triplicate (total of 288 reactions), to account for possible pipetting errors, three plates were processed per sample.

An algorithm transforming real-time qPCR data into CCN calls was developed using the samples processed during Phase 1 and calculations performed in Microsoft Excel.

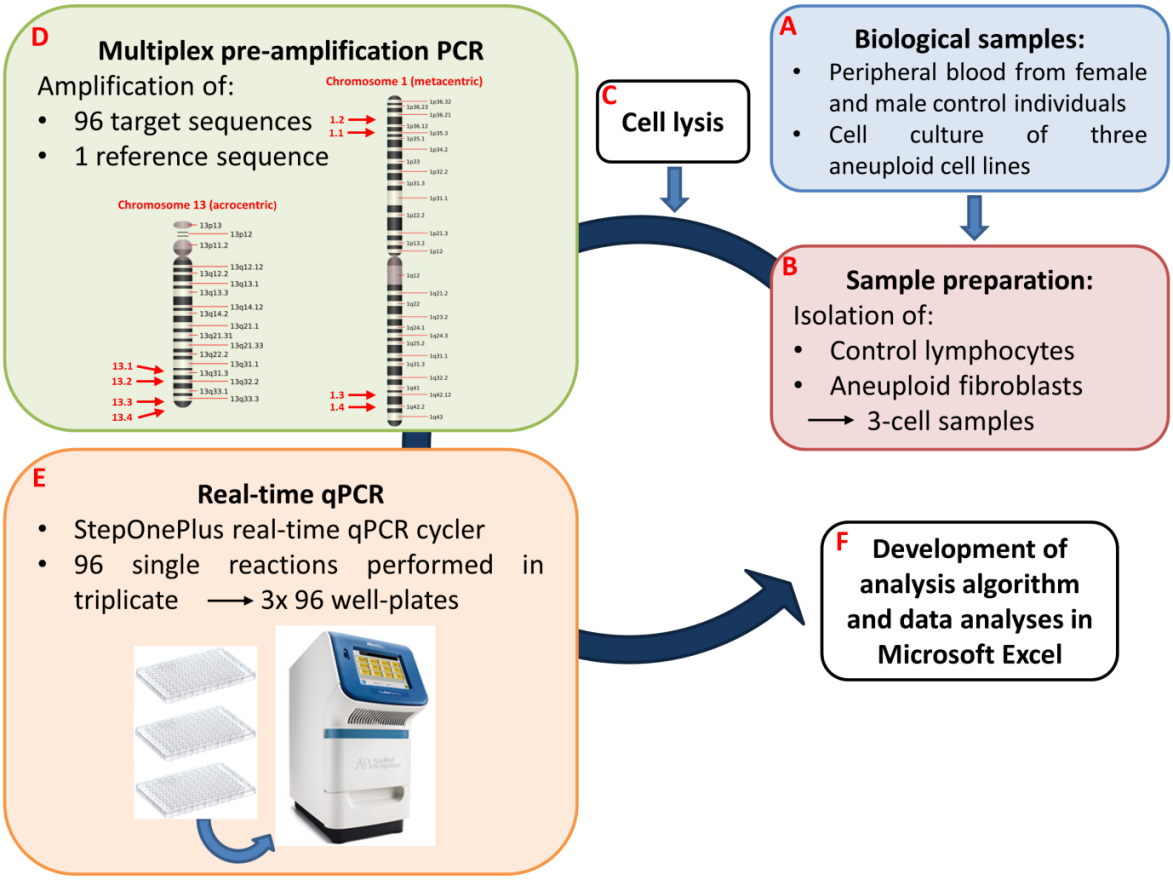


Figure 3.1: Flowchart describing Phase 1 of protocol development. **A/B:** Lymphocyte and fibroblast samples consisting of three cells were isolated from peripheral blood and fibroblast cell culture, respectively. **C:** Cell samples were subjected to cell lysis followed by (**D**) multiplex pre-amplification of 96 copy number assays and one reference assay. Copy number sequences were selected close to the telomere region and covered four loci on the q-arm of acrocentric chromosomes and two loci on p- and q-arms of metacentric chromosomes. **E:** After enrichment of gDNA sequences, each locus was amplified separately on a traditional real-time qPCR cycler. After measurement of fluorescence associated with the amplified products during real-time qPCR, (**F**) CCN was determined and calculations performed in Microsoft Excel. Chromosome images were obtained from Wikimedia Commons. Images of 96-well plates and real-time qPCR instrument were obtained from ThermoFisher.

3.3.1.2 Data analysis Phase 1

To calculate the CCN, an algorithm based on the delta delta threshold cycle (ΔΔCt) method (Livak & Schmittgen, 2001) was developed and tested on all samples processed during Phase 1 of protocol development. The nine samples derived from the female and

male control individuals further served as reference samples during algorithm development.

The developed analysis pipeline is based on the exponential amplification of initial input DNA during real-time qPCR. As shown in **Figure 3.2 A**, the increase in template DNA during amplification was monitored at each PCR cycle by measuring the accumulated amount of fluorescence dye coming from the cleaved probes. When the amplification curves of each reaction crossed a fixed threshold (0.1), a Ct value was assigned to each of the assays (referred to as Ct_{assay} or $Ct_{reference}$).

Since fluorescence signal intensities are directly proportional to the amount of generated DNA amplicons, relative DNA quantities were inferred by normalising the obtained Ct_{assay} values of each of the 96 copy number assays to the Ct values of the reference assay TERT ($Ct_{reference}$) which was co-amplified in the same reaction (**Figure 3.2 B**):

$$\mathbf{\Delta Ct_{assay} = Ct_{assay} - Ct_{reference}}$$

After assigning a ΔCt_{assay} value to each of the three replicates of each of the 96 copy number assays, a copy number assay-specific $\Delta Ct_{assay\,(mean)}$ was calculated by dividing the sum of the three ΔCt_{assay} values by three:

$$\mathbf{\Delta Ct_{assay\,(mean)} = (\Delta Ct_{assay\,(replicate\,1)} + \Delta Ct_{assay\,(replicate\,2)} + \Delta Ct_{assay\,(replicate\,3)}) / 3}$$

The resulting 96 copy number assay-specific $\Delta Ct_{assay\,(mean)}$ values were used to determine the fold change by considering the $\Delta Ct_{assay\,(mean)}$ values as the negative exponent of 2, which will be referred to as:

$2^{-\Delta Ctassay}$

The underlying idea of the analysis protocol is the assumption that the pattern of the $2^{-\Delta Ctassay}$ values of all four assays assessed per chromosome (e.g. copy number assays of chromosome 1: 1.1, 1.2, 1.3 and 1.4) was consistent between different samples. For example, **Figure 3.3** illustrates the $2^{-\Delta Ctassay}$ value pattern obtained from the four assays of chromosome 1 (**Figure 3.3 A**), chromosome 2 (**Figure 3.3 B**) and chromosome 21 (**Figure 3.3 C**) derived from three of the tested samples during Phase 1 (46,XX; 46,XY; 47,XY,+21).

Importantly, although $2^{-\Delta Ctassay}$ values of same assays differed in quantities between the three different samples (e.g. $2^{-\Delta Ctassay}$ values of assay 1.1 were 0.61, 0.56 and 0.49 in samples 46,XX, 46,XY and 47,XY,+21, respectively), the overall $2^{-\Delta Ctassay}$ pattern obtained for each chromosome showed close similarity between different samples. For example, in case of chromosome 1, $2^{-\Delta Ctassay}$ values were highest for assay 1.2 and lowest for assay 1.4 whereas assays 1.1 and 1.3 exhibited intermediate $2^{-\Delta Ctassay}$ values.

Of note, $2^{-\Delta Ctassay}$ values of the female sample were consistently higher compared to those of the normal male sample. $2^{-\Delta Ctassay}$ values derived from the trisomy 21 sample were the lowest for chromosomes 1 and 2, however, higher for chromosome 21.

$2^{-\Delta Ctassay}$ patterns of all 24 chromosomes were visually assessed ($2^{-\Delta Ctassay}$ patterns of chromosomes 3 - 20, 22, X and Y are shown in **Figure A.1** and **Figure A.2** in **Appendix A**). Importantly, a consistent pattern of $2^{-\Delta Ctassay}$ values between different samples was observed for all chromosomes. At the same time, a similar drop in $2^{-\Delta Ctassay}$ values was observed between the normal female and the normal male sample.

Furthermore, in most cases, $2^{-\Delta Ctassay}$ values of the 47,XY,+21 sample were lower compared to the female and male sample.

The chromosome-specific patterns further reflected a variation in assay amplification efficiencies and obtained $2^{-\Delta Ctassay}$ values indicated that some assays amplify at a higher rate than others during pre-amplification and/or real-time qPCR (e.g. samples with higher $2^{-\Delta Ctassay}$ values amplify better than those with lower $2^{-\Delta Ctassay}$ values).

Over- or under-amplification of certain assays, however, can have an impact on CCN assignment and may result in a false-positive or false-negative copy number call. For example, if a single copy number assay is poorly amplified, the entire chromosome might appear as being lost, while over-amplification may result in a false-positive chromosome gain.

It was possible that the observed variation in amplification efficiencies between different assays was caused, in part, by differences in amplicon length and amplicon GC content. For example, higher amplicon length may have lowered PCR efficiency of a specific assay, while a high GC content may have led to a higher amplification efficiency during real-time qPCR.

To test whether amplicon length and amplicon GC content impacted on assay-specific amplification efficiencies, relationships between both factors and $2^{-\Delta Ctassay}$ values were tested. Indeed, as shown in **Figure 3.4 A**, correlation analysis (taking into account all 96 copy number assays) revealed a negative correlation between the amplicon size and $2^{-\Delta Ctassay}$ values, which was significant ($r = -0.3242$, $p = 0.0025$). In

contrast, an increase in the amplicon GC content was positively correlated and also significant (r = 0.3428, p = 0.0016; **Figure 3.4 B**).

In order to ensure that each of the four chromosome-specific assays contribute equally to the overall CCN assignment a normalisation step was performed to correct for differences in amplification efficiencies between assays targeting the same chromosome. To do this, each $2^{-\Delta Ctassay}$ value was multiplied by an assay-specific multiplication factor. Multiplication factors were calculated from the $2^{-\Delta Ctassay}$ values obtained from the five female and four male control samples processed during Phase 1, which served as reference samples. Initially, the mean $2^{-\Delta Ctassay}$ value of each of the 96 copy number assays was calculated from all female and from all male samples (see **Figure 3.5 A** and **Figure 3.5 B**). Then, the average $2^{-\Delta Ctassay}$ values of female and male means were computed for each of the 96 copy number assays. To determine assay-specific multiplication factors, each of the four $2^{-\Delta Ctassay}$ values of a specific chromosome was then divided by the highest $2^{-\Delta Ctassay}$ value obtained for the chromosome (**Figure 3.5 C**).

After calculating the 96 assay-specific multiplication factors and after multiplying each assay by its specific multiplication factor, $2^{-\Delta Ctassay}$ values became more uniform, allowing the four assays of each individual chromosome to carry almost equal weight. This is shown in **Figure 3.6 A**, **B** and **C**, which illustrates patterns of $2^{-\Delta Ctassay}$ values after multiplication by assay-specific multiplication factors (same samples/chromosomes as shown in **Figure 3.3**).

Multiplication by copy number assay-specific multiplication factors further allowed reliable detection of possible outliers, namely assays which over- or under-amplified during multiplex pre-amplification and/or real-time qPCR. To identify and

alter possible outliers, a second normalisation step was performed which involved calculation of chromosome- and sample-specific threshold values [referred to as lower and upper borders (LB and UB)] and adjustment of $2^{-\Delta Ctassay}$ values falling below or above the borders.

To calculate LB and UB, the four $2^{-\Delta Ctassay}$ values of each chromosome were sorted in descending order. Then the first and third quartiles (Q1 and Q3) were calculated which in this case corresponded to the mean of the two lowest and the mean of the two highest $2^{-\Delta Ctassay}$ values, respectively. Next, the interquartile range (IQR) of the four assays of each individual chromosome was calculated by subtracting Q3 from Q1. Finally, LB and UB were determined using the following formulas:

LB = Q1 - (0.01 x IQR)

UB = Q3 + (0.01 x IQR)

Graphs on the right in **Figure 3.6** (**D**, **E** and **F**) illustrate examples of LB and UB for chromosomes 1, 2 and 21 in three different samples processed during Phase 1 (46,XX; 46,XY; 47,XY,+21; same samples as shown in **Figure 3.3**).

Any $2^{-\Delta Ctassay}$ values that fell below or above the chromosome- and sample-specific LB or UB were adjusted to match exactly LB and UB values, respectively. **Figure 3.7** illustrates the pattern of $2^{-\Delta Ctassay}$ values after outlier correction for chromosomes 1, 2 and 21 in three different samples (identical to those shown in previous figures).

The described two normalisation steps greatly reduced the variation in $2^{-\Delta Ctassay}$ values between assays of the same chromosome. This was reflected by a strong decrease in the SD between $2^{-\Delta Ctassay}$ values of the same chromosome. An example of the decreased SDs for chromosomes 1, 2 and 21 is shown in **Figure 3.8**, which illustrates gradually decreasing SDs following each normalisation step (mean SDs were calculated from the nine karyotypically normal male and female reference samples).

A decrease in the SDs observed after each normalisation step for the remaining chromosomes (3 - 20, 22, X and Y) is illustrated in **Figures A.3** and **A.4** in **Appendix A**.

After $2^{-\Delta Ctassay}$ normalisations, the sum of the four corrected $2^{-\Delta Ctassay}$ values was calculated for each chromosome to create a chromosome-specific $2^{-\Delta Ctchromosome}$ value:

$$\mathbf{2^{-\Delta Ctchromosome} = 2^{-\Delta Ctassay(1)} + 2^{-\Delta Ctassay(2)} + 2^{-\Delta Ctassay(3)} + 2^{-\Delta Ctassay(4)}}$$

Figure 3.9 illustrates $2^{-\Delta Ctchromosome}$ values obtained for chromosomes 1, 2 and 21 for three different samples (same samples as illustrated in previous images). $2^{-\Delta Ctchromosome}$ values varied between the samples and also varied between different chromosomes. Of note, $2^{-\Delta Ctchromosome}$ values of the female sample were consistently higher compared to those of the male sample. $2^{-\Delta Ctassay}$ values obtained from the trisomy 21 sample were the lowest for chromosomes 1 and 2, however higher for chromosome 21.

Importantly, a similar drop in $2^{-\Delta Ctchromosome}$ values was also observed between the female and the male sample in the remaining 21 chromosomes (shown in **Figures A.5** and **A.6** in **Appendix A**). Furthermore, in most cases $2^{-\Delta Ctchromosome}$ values coming from the trisomy 21 sample were lower as compared to the female and male sample values.

Given that the amplification patterns of the four assays of each chromosome were similar between different samples, even if amplification efficiencies differed, a specific value (in %) was assigned to each of the 24 chromosomes by assuming that the sum of each of the 24 $2^{-\Delta Ctchromosome}$ values is 100 %. This was done by dividing each of the 24 $2^{-\Delta Ctchromosome}$ values by the total amount of the 96 $2^{-\Delta Ctassay}$ values, multiplied by 100. **Figure 3.10** illustrates the values obtained for each chromosome in the three different samples shown in previous images (46,XX; 46,XY; 47,XY,+21).

Next, the exact copy number of each chromosome was determined by normalising to values obtained from the nine karyotypically normal female and male samples, which were used to create female and male reference data sets which consisted of the mean chromosome-specific values obtained from the five female and four male samples, respectively.

Calculation of CCN of autosomes using the example of chromosome 1 (Chr 1):

$$\mathbf{CCN_{Chr\ 1} = (\%_{Chr\ 1(test\ sample)} / \%_{Chr\ 1(female\ reference)}) + (\%_{Chr\ 1(test\ sample)} / \%_{Chr\ 1(male\ reference)})}$$

Calculation of copy number of chromosome X:

$$\mathbf{CCN_{Chr\ X} = (((\%_{Chr\ X(test\ sample)} / \%_{Chr\ X(female\ reference)}) \times 2) + (\%_{Chr\ X(test\ sample)} / \%_{Chr\ X(male\ reference)})) / 2}$$

Calculation of copy number of chromosome Y:

$$\mathbf{CCN_{Chr\ Y} = \%_{Chr\ Y(test\ sample)} / \%_{Chr\ Y(male\ reference)}}$$

Computed CCNs were plotted in a graph depicting copy numbers of all 24 chromosomes and analysed manually by visually inspecting the copy number profiles. Autosomal chromosomes with copy numbers ranging from 1.5 - 2.5 were called euploid

(CCN of two). Autosomal copy numbers above 2.5 were identified as trisomies (CCN of three). If values of chromosome X were in the range of 1.5 - 2.5, a copy number of two was assigned. If chromosome X values were below 1.5, a copy number of one was assigned.

Figure 3.11 illustrates CCN profiles of the three different samples prior to normalisation, after multiplication by an assay-specific multiplication factor and after outlier correction.

The normalisation of $2^{-\Delta Ctassay}$ values resulted in overall data smoothing and cleaner 24-CCN profiles. The reduced noise was also reflected by a decrease in the SD between all copy numbers of all 24 chromosomes for a given sample, as shown in **Figure 3.12**.

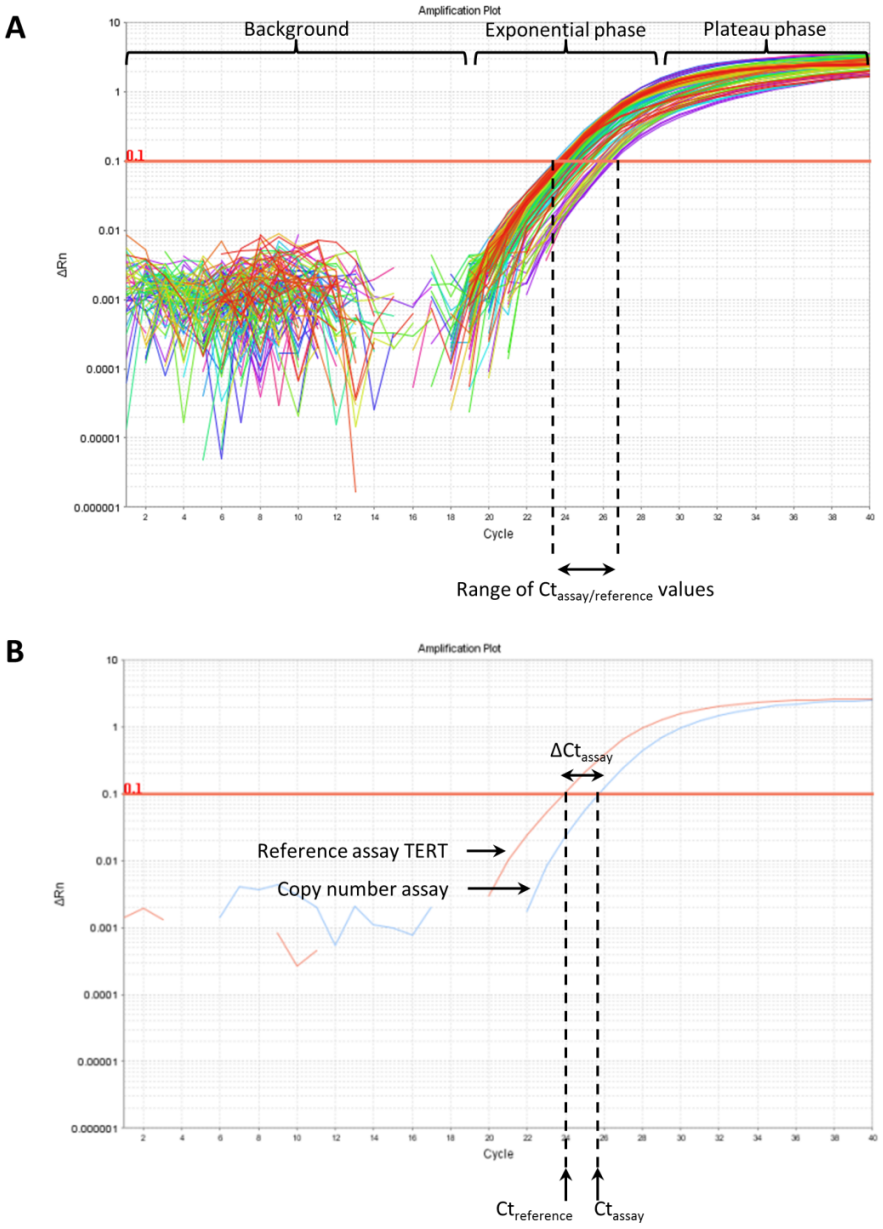


Figure 3.2: Real-time qPCR plots. A: Amplification plot obtained from 96 reactions performed in a 96-well plate. The x-axis shows PCR cycle numbers (total of 40). The y-axis represents fluorescent signal intensities measured during the amplification. Each coloured curve represents amplification of a single assay. The amplification curves can be divided into three different phases: (1) initial amplification phase - the signal intensities are yet too weak to be visualised and are overlaid by background signal; (2) exponential amplification phase - template DNA molecules double with each cycle; (3) plateau phase - depletion of PCR reagents leads to a flattening of the amplification curve. Individual Ct values (between dotted lines) were obtained during the exponential phase when the assigned threshold value (0.1; red line) intersected the amplification curves. **B: Amplification plot obtained from a single reaction.** The red and blue curves show amplification of the reference and one copy number assay, respectively. The range between the dotted lines represents the ΔCt_{assay} value.

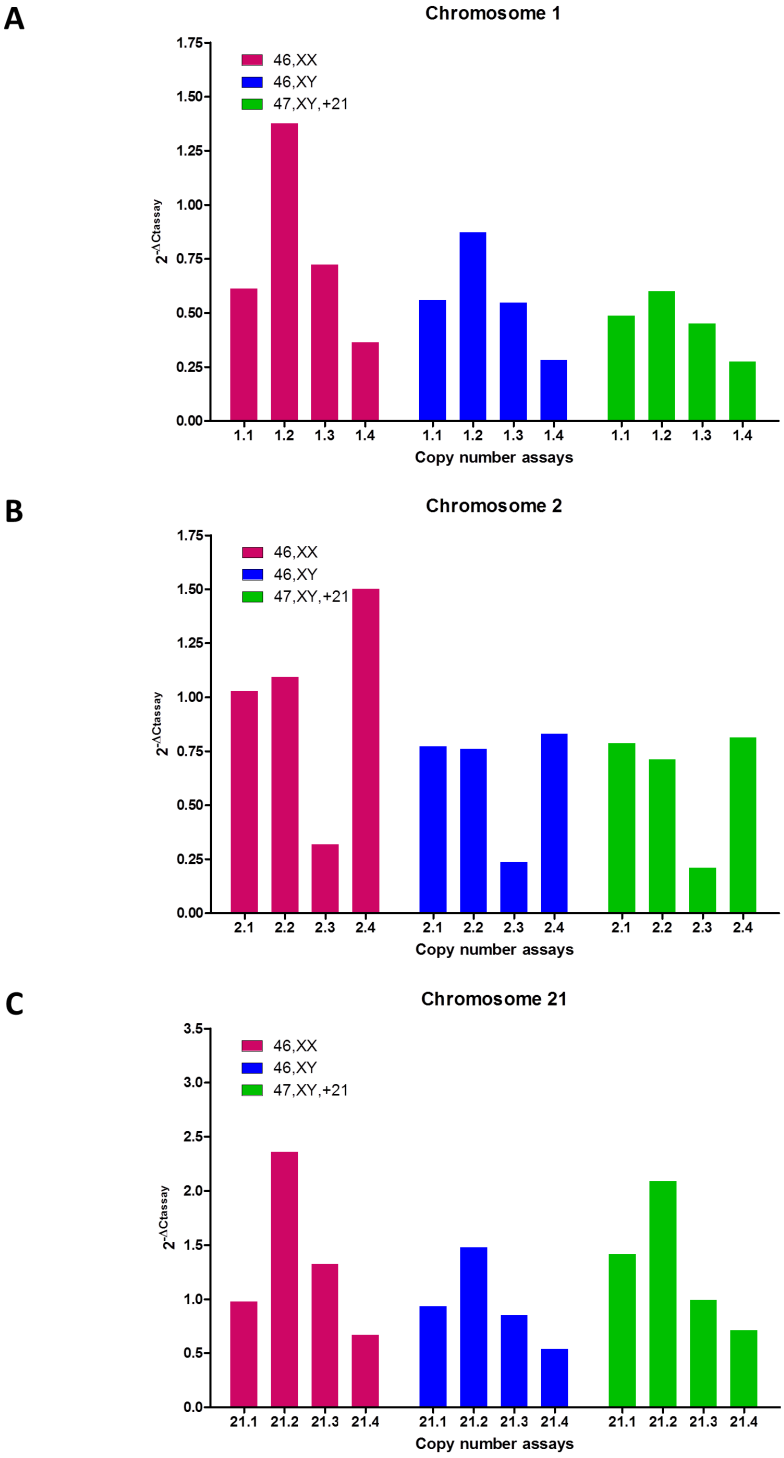


Figure 3.3: Pattern of $2^{-\Delta ctassay}$ values of chromosomes 1, 2 and 21 obtained from three different samples. Graphs **A**, **B** and **C** illustrate the pattern obtained from the four copy number assays of chromosomes 1, 2 and 21, respectively. Two of the three samples consisted of three lymphocytes derived from karyotypically normal female and male individuals (46,XX and 46,XY). The third sample consisted of three fibroblast cells derived from a male carrier of a trisomy 21 (47,XY,+21). The obtained $2^{-\Delta ctassay}$ values showed a chromosome-specific pattern which was consistent between different samples and independent of the sample type.

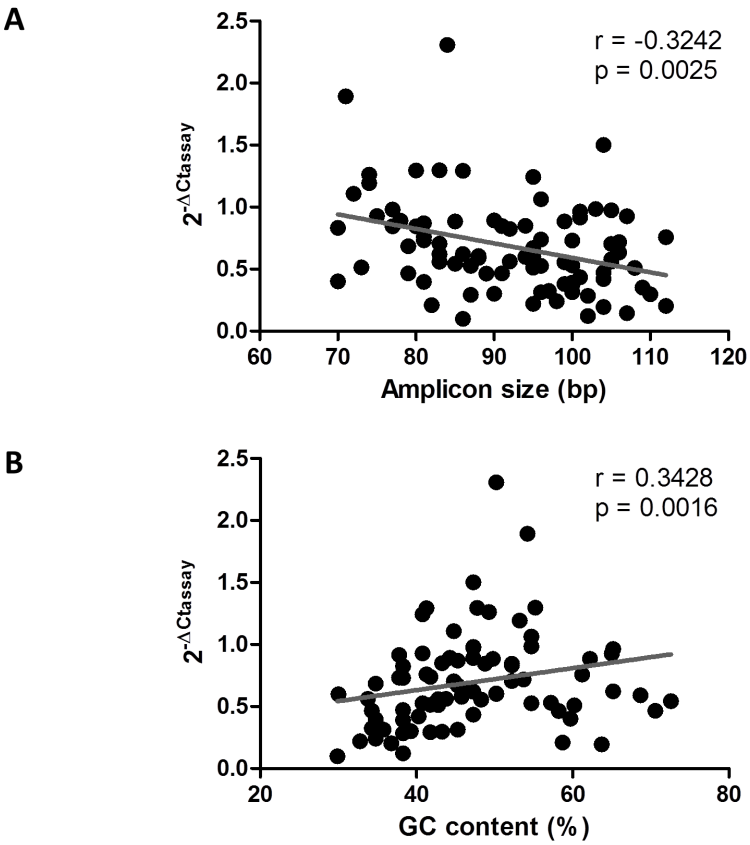


Figure 3.4: Correlation between $2^{-\Delta Ctassay}$ values and amplicon size and amplicon GC content. A: Relation of amplicon length and amplification efficiency ($2^{-\Delta Ctassay}$ values). B: Relationship between amplicon GC content and PCR efficiency. Each dot represents a single copy number assay. Linear regression lines are shown in grey. bp = base pairs. r = Spearman correlation. p = p-value. GC content was calculated using Genomics %G~C Content Calculator (Science Buddies; http://www.sciencebuddies.org/). Amplicon sequences were determined according to genomic coordinates provided by ThermoFisher ± 100 bp (~mean amplicon size).

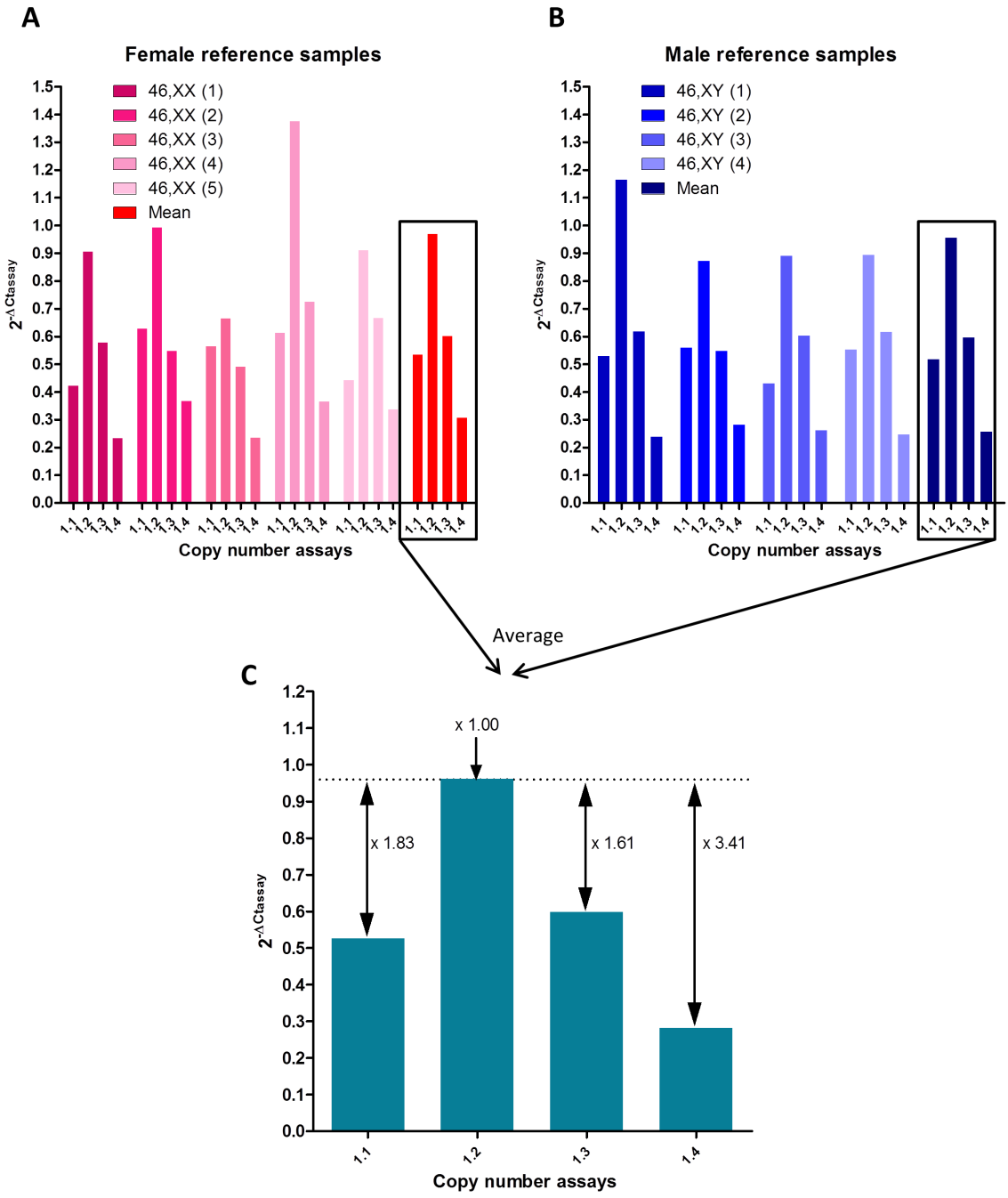


Figure 3.5: Calculation of multiplication factors using the example of chromosome 1. Graphs **A** and **B** illustrate $2^{-\Delta Ctassay}$ values of the female and male control samples processed during Phase 1, respectively. Graph **C** illustrates average $2^{-\Delta Ctassay}$ values of female and male mean $2^{-\Delta Ctassay}$ values. Each of the four copy number assays of chromosome 1 was divided by the assay with the highest $2^{-\Delta Ctassay}$ value (here: assay 1.2), which resulted in assay-specific multiplication factors of 1.83, 1.00, 1.61 and 3.41 for assays 1.1, 1.2, 1.3 and 1.4, respectively.

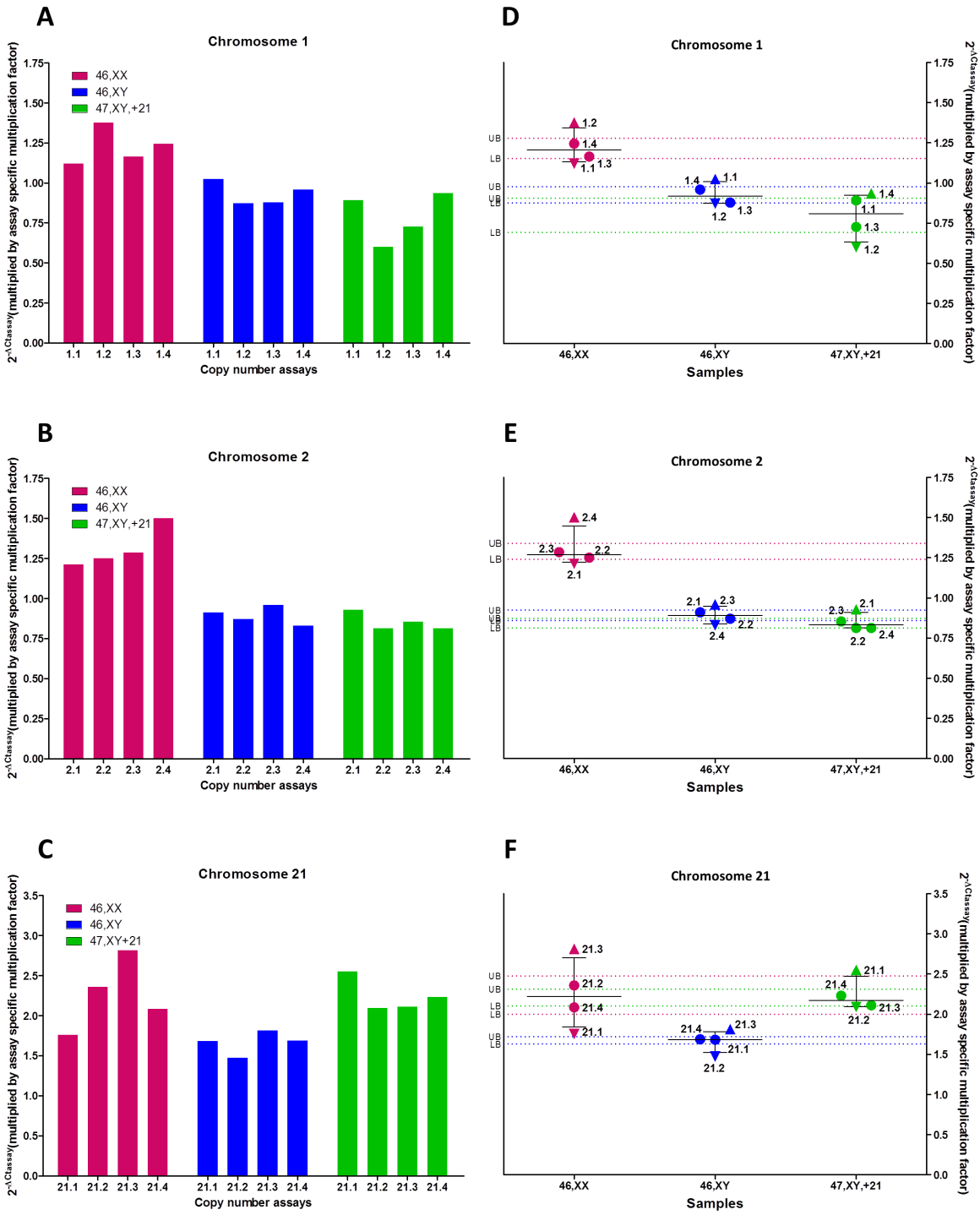


Figure 3.6: Pattern of $2^{-\Delta Ctassay}$ values after multiplication by assay-specific multiplication factors. Samples are identical to those depicted in **Figure 3.3**. Graphs on the left illustrate $2^{-\Delta Ctassay}$ values of chromosomes 1 (**A**), 2 (**B**) and 21 (**C**) after multiplication by assay-specific multiplication factors. Graphs on the right (**D**, **E** and **F**) show the normalised $2^{-\Delta Ctassay}$ values and their corresponding LB and UB; shown as dotted lines). Coloured round and triangular dots show $2^{-\Delta Ctassay}$ values that lie within and outside the borders, respectively.

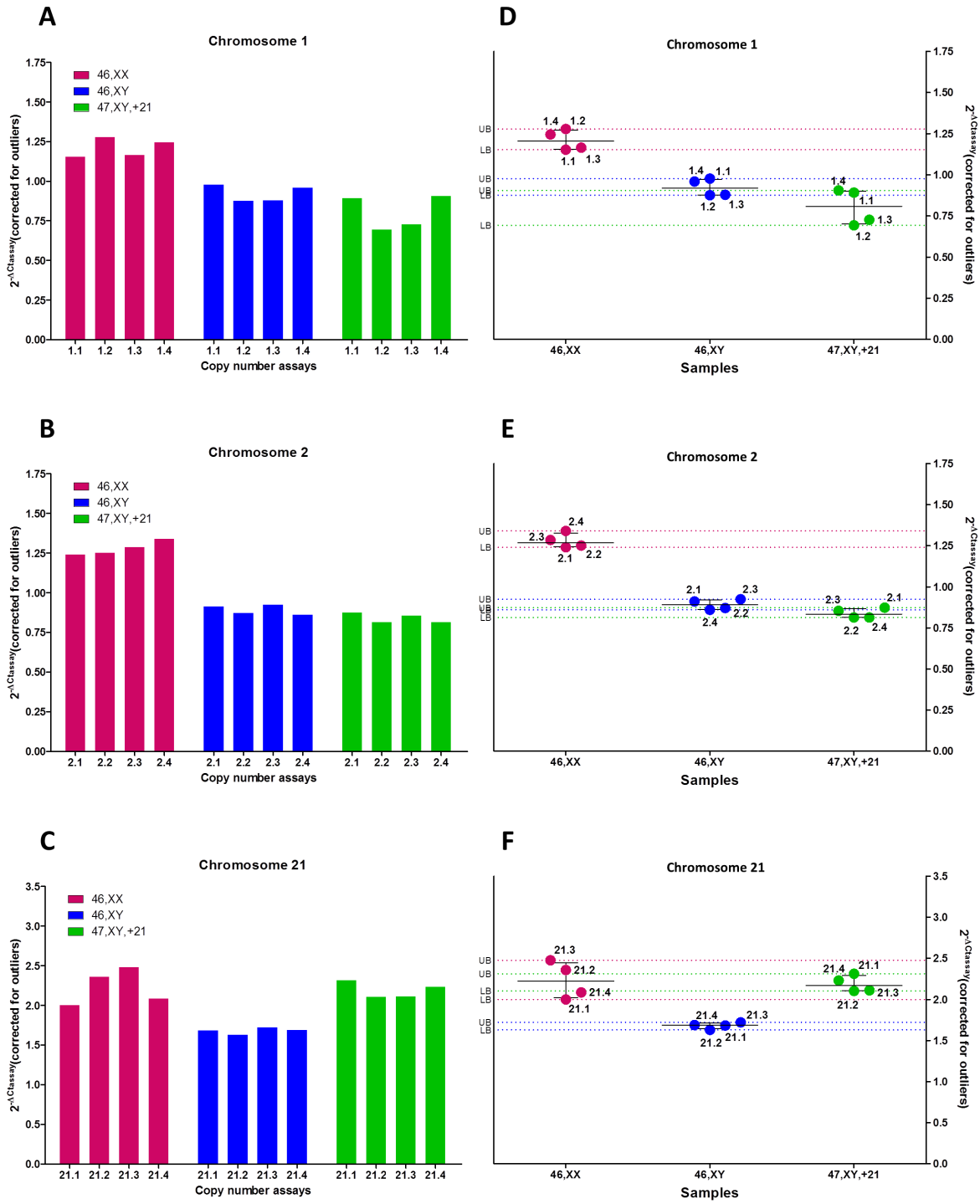


Figure 3.7: Pattern of $2^{-\Delta Ctassay}$ values after correction for outliers. Samples are identical to those depicted in **Figures 3.3** and **3.6**. Graphs on the left illustrate $2^{-\Delta Ctassay}$ values of chromosomes 1 (**A**), 2 (**B**) and 21 (**C**) after outlier correction. Graphs on the right (**D**, **E** and **F**) show the normalised $2^{-\Delta Ctassay}$ values (coloured round dots) after outlier correction, which now all lie within or on the corresponding LB and UB; shown as dotted lines.

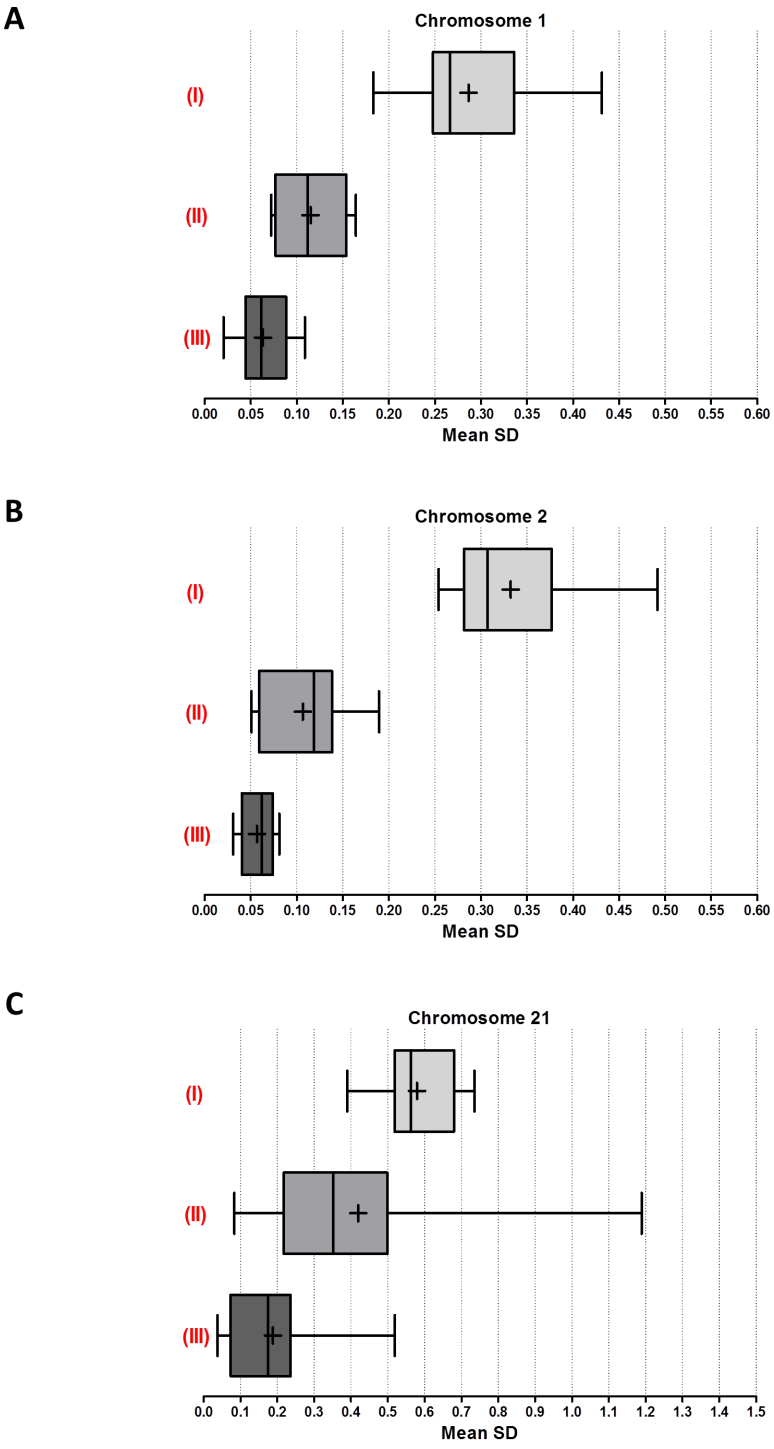


Figure 3.8: Box and whisker plots depicting the SD of $2^{-\Delta Ctassay}$ values before and after each of the normalisation steps. Graphs **A**, **B** and **C** illustrate mean SDs of $2^{-\Delta Ctassay}$ values for chromosomes 1, 2 and 21, respectively. Mean SDs were calculated from the nine control samples processed in Phase 1 (5 x 46,XX; 4 x 46,XY). Vertical lines in the middle of boxes depict median SDs. + signs indicate mean SDs. Error bars show smallest and largest SD values. **I:** Mean SDs prior to normalisation. **II:** Mean SDs after first normalisation (multiplication by assay-specific multiplication factor). **III:** Mean SDs after second normalisation (outlier correction).

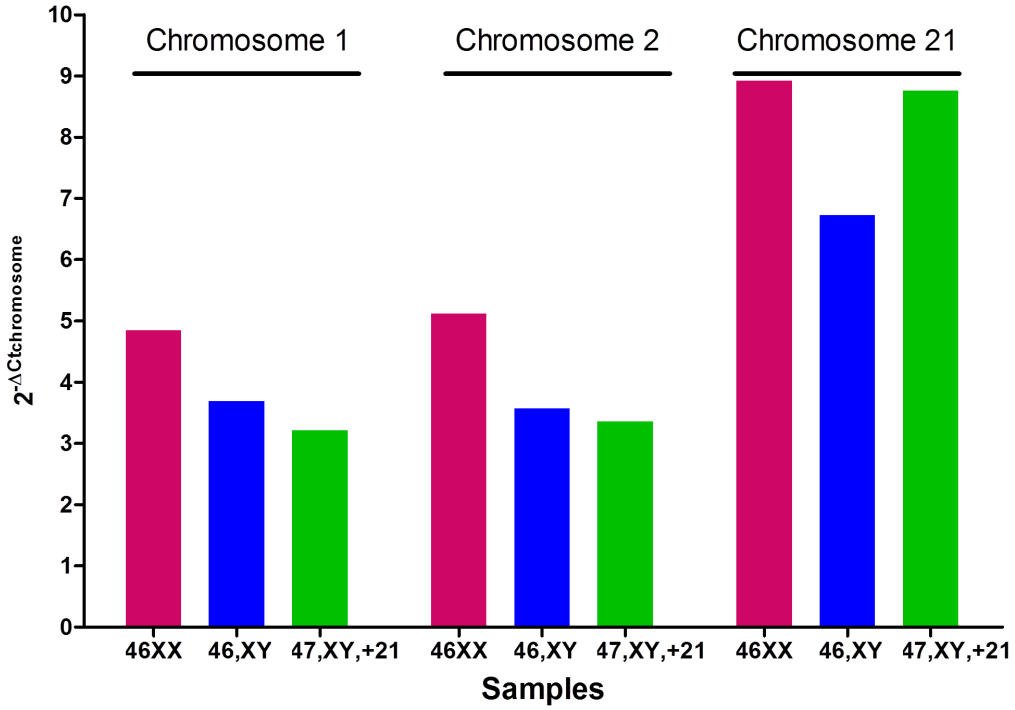


Figure 3.9: Chromosome-specific $2^{-\Delta Ctchromosome}$ values. The graph illustrates the sum of normalised $2^{-\Delta Ctassay}$ values ($2^{-\Delta Ctchromosome}$) for chromosomes 1, 2 and 21 obtained from three different samples. $2^{-\Delta Ctchromosome}$ values correspond to same samples as shown in previous images (**Figures 3.3**, **3.6** and **3.7**).

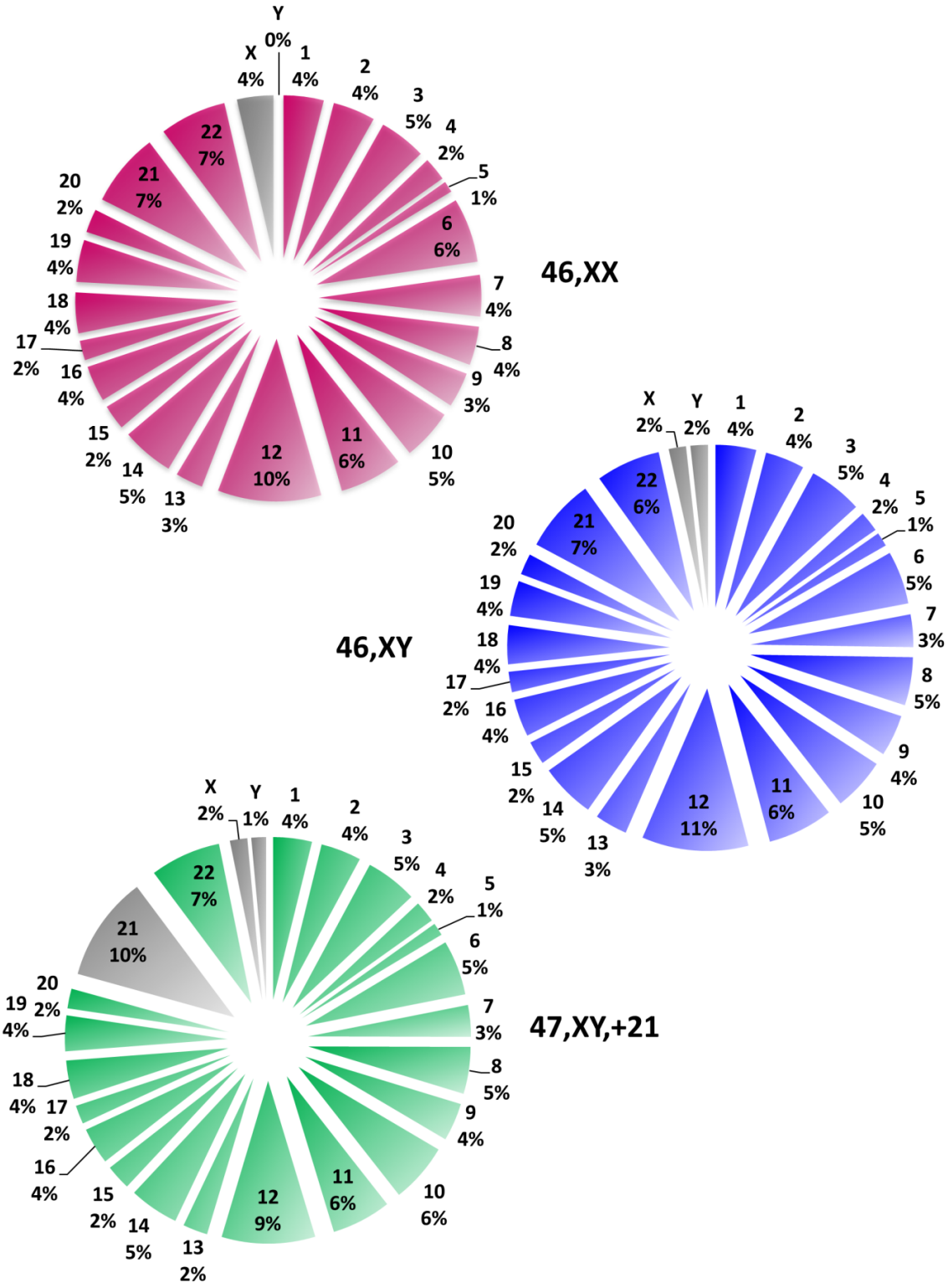


Figure 3.10: Values (in %) assigned to each of the 24 chromosomes of three different samples. Chromosome values correspond to same samples as shown in previous images (**Figures 3.3**, **3.6**, **3.7** and **3.9**). Aneuploid and sex chromosomes are shown in grey.

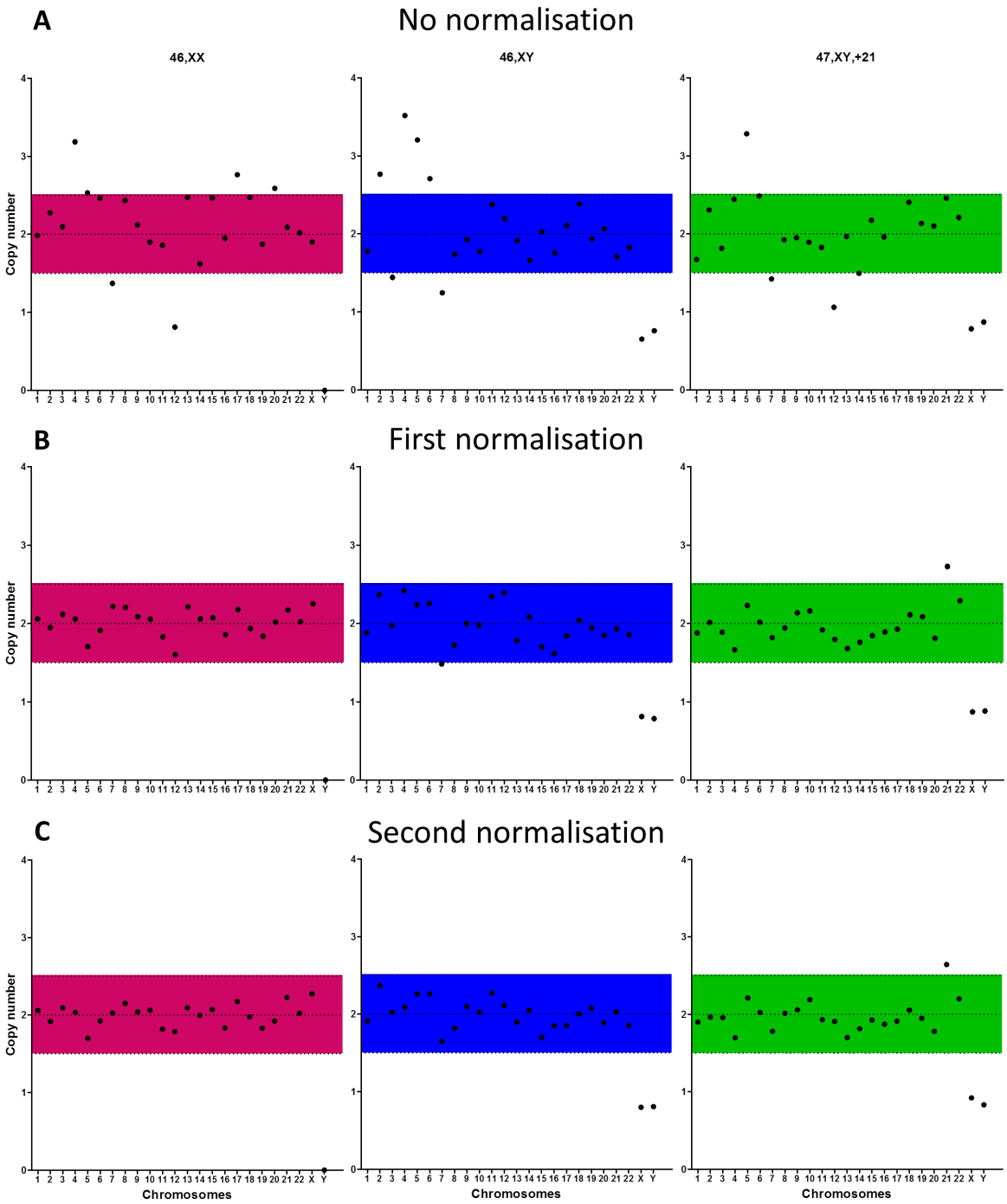


Figure 3.11: 24-CCN profiles before and after normalisation of three different samples. Copy number profiles illustrate results obtained from same samples as shown in previous images. **A: Copy number profiles without normalisation. B: Copy number profiles following multiplication of $2^{-\Delta Ctassay}$ values by assay-specific multiplication factors. C: Copy number profiles after correction of $2^{-\Delta Ctassay}$ outliers.**

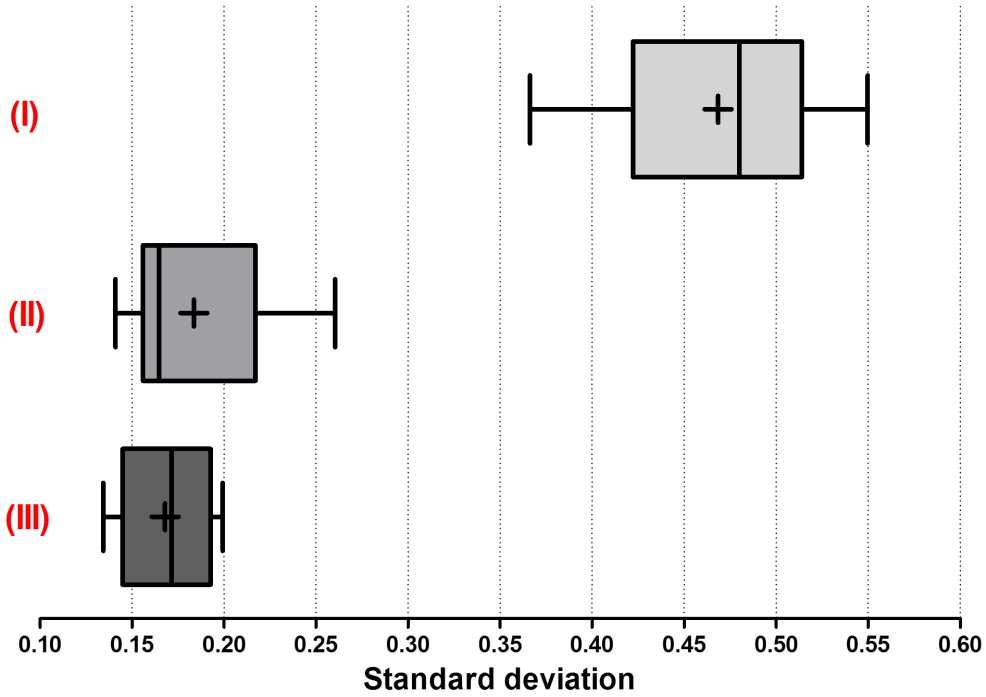


Figure 3.12: Box and whisker plots depicting the SD of CCNs before and after each of the normalisation steps. The graph illustrates mean SDs of copy numbers of chromosomes 1 - 22. Mean SDs were calculated from the computed CCNs (autosomes) of the nine control samples processed during Phase 1 (5 x 46,XX; 4 x 46,XY). Vertical lines in the middle of boxes depict median SDs. + signs indicate mean SDs. Error bars show smallest and largest SD value. **I:** Mean SDs prior to normalisation. **II:** Mean SDs after first normalisation (multiplication by assay-specific multiplication factor). **III:** Mean SDs after second normalisation (outlier correction).

3.3.1.3 Results Phase 1

During Phase 1 of the protocol development, a total of 14 samples, each consisting of three cells were processed and analysed. In addition to the nine euploid samples real-time qPCR was further performed on five fibroblast samples, derived from three different aneuploid cell lines (47,XY,+13; 47,XY,+18; 47,XY,+21). Real-time qPCR results were analysed using the developed algorithm described in **Section 3.3.1.2**. Results of all samples are presented in **Table 3.1**. **Figures 3.13** and **3.14** illustrate examples of real-time qPCR 24-CCN profiles obtained from samples of control individuals and aneuploid cell lines, respectively.

All tested samples amplified successfully. All euploid (samples 1 - 9) and aneuploid (samples 10 - 14) samples were correctly identified as chromosomally normal and abnormal, respectively. The gender was assigned correctly in all samples. Furthermore, a correct copy number was assigned to all autosomal chromosomes in all samples, resulting in a chromosome diagnosis accuracy of 100 % (336 / 336) and an overall sample diagnosis accuracy of 100 % (14 / 14). Therefore, sensitivity and specificity for CCN detection and overall diagnosis was 100 %. For calculations refer to **Table A.3** in **Appendix A**.

Table 3.1: Results obtained from three-cell samples derived from a female and male control individual and three different aneuploid cell lines

Samples	Karyotype		Agreement
	Expected	Real-time qPCR	
Lymphocyte samples from control individuals			
1	46,XX	46,XX	Yes
2		46,XX	Yes
3		46,XX	Yes
4		46,XX	Yes
5		46,XX	Yes
6	46,XY	46,XY	Yes
7		46,XY	Yes
8		46,XY	Yes
9		46,XY	Yes
Fibroblast samples form aneuploid cell lines			
10	47,XX,+13	47,XX,+13	Yes
11		47,XX,+13	Yes
12	47,XY,+18	47,XY,+18	Yes
13	47,XY,+21	47,XY,+21	Yes
14		47,XY,+21	Yes

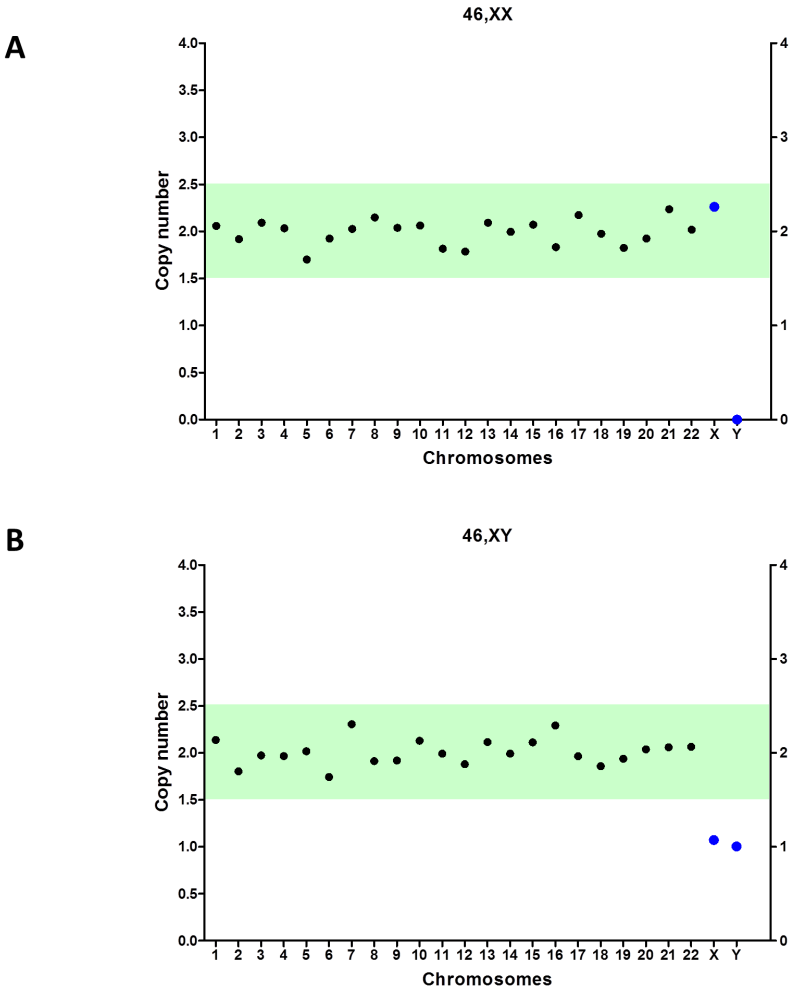


Figure 3.13: Examples of real-time qPCR 24-CCN profiles of karyotypically normal samples. Black and blue dots illustrate the copy number of autosomes and sex chromosomes, respectively. Areas shaded in green indicate CCN of two (ranging from copy number 1.5 - 2.5). Profile **A** shows the result obtained from cells of a female control individual and profile **B** from cells of a male control individual.

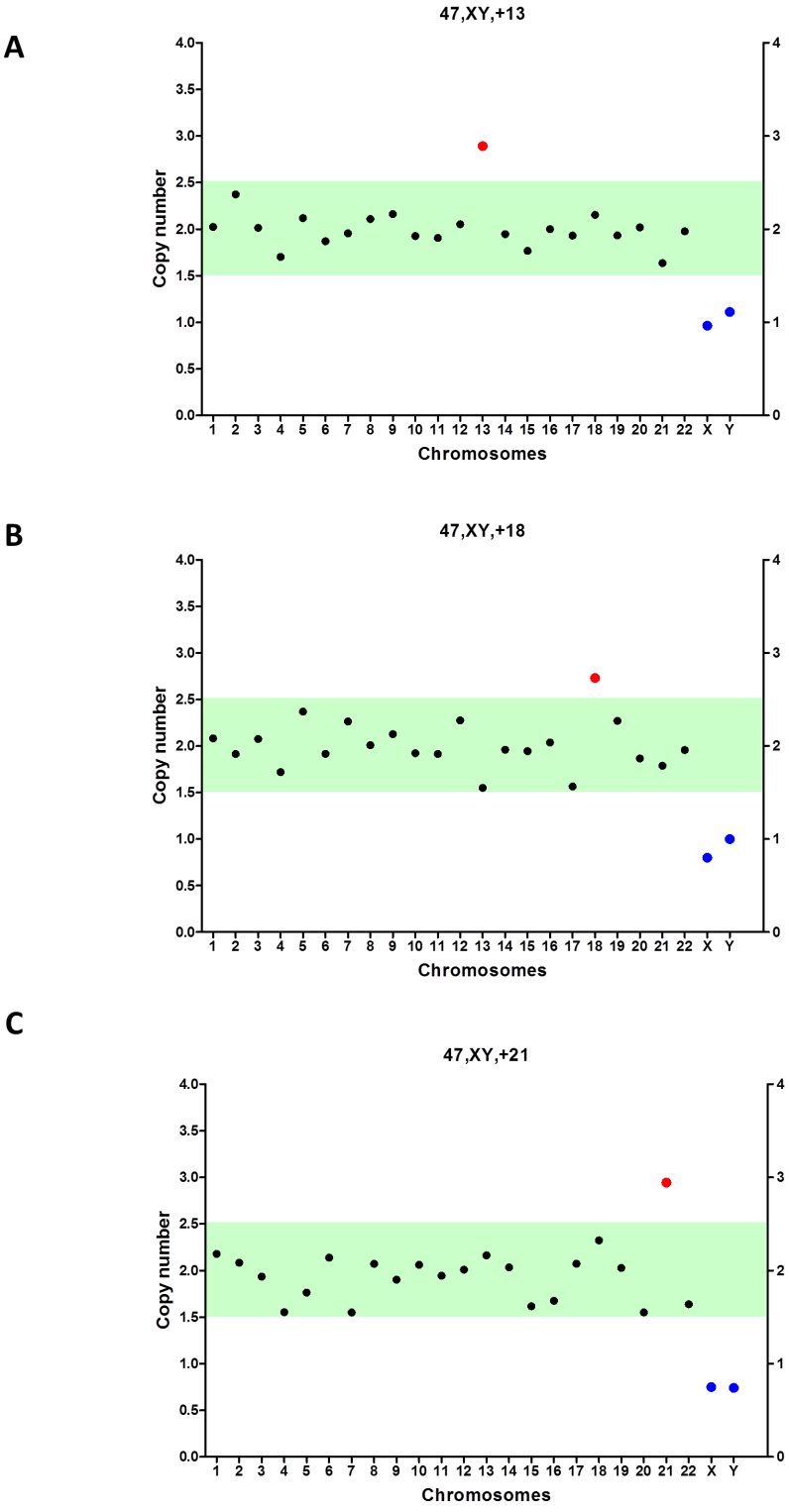


Figure 3.14: Examples of real-time qPCR 24-CCN profiles of aneuploid samples. Areas shaded in green indicate CCN of two (ranging from 1.5 - 2.5). Black dots illustrate autosomes with a copy number of two. Blue dots illustrate the copy number of the sex chromosomes. CCNs above the threshold of 2.5 indicated presence of a trisomy, which is illustrated by red dots. **A:** 47,XY,+13. **B:** 47,XY,+18. **C:** 47,XY,+21.

3.3.2 Phase 2 - Feasibility of OpenArray Technology for chromosome copy number analysis in genomic DNA samples

3.3.2.1 Protocol design Phase 2

Following the encouraging results obtained during Phase 1, the method was transferred to a nano-scale array-based real-time qPCR system (OpenArray Technology, ThermoFisher) to enhance sensitivity, throughput and cost-effectiveness.

The technology utilises small arrays (roughly the size of a microscope slide). Each array contains a total of 3072 through-holes (equal to 32 x 96-well plates) organised in 48 sub-arrays (64 through-holes per sub-array). Each through-hole represents the site of a single real-time qPCR reaction performed in a 33 nl reaction volume. The OpenArray Technology is fully automated and no mixing of sample DNA and primer/probe reagents is required as primers and probes are pre-spotted in the through-holes. Furthermore, loading of arrays with sample DNA is performed by a robotic system and no manual pipetting is required. The arrays were custom-made for this project and each through-hole pre-spotted by the supplier with a copy number primer/probe set.

The OpenArray Technology has mainly been developed for large gene expression and genotyping studies using either commercially available gene expression or genotyping Taqman assays. Copy number assays which were utilised during the course of this project have not been tested on the OpenArray platform by the supplier before.

Therefore, as an initial proof-of-principle, an array format for testing just 7 chromosomes (13, 16, 18, 21, 22, X and Y) was evaluated during Phase 2 of the study

(**Figure 3.15**) and chromosomes which are commonly present in an aneuploid form in miscarriages and those involved in CCN syndromes, such as Patau Syndrome, Edwards Syndrome, Down Syndrome, Klinefelter Syndome or Turner Syndrome, chosen.

Arrays utilised with the OpenArray technology can be ordered in different formats (https://www.thermofisher.com/uk/en/home/life-science/pcr/real-time-pcr/real-time-openarray/open-array-technology.html). During Phase 2 of protocol development, the 48 (sub-arrays) x 56 (data-points) design was chosen. This format allows simultaneous processing of 48 samples (one sample per sub-array) and the analysis of 56 different assays per sample (56 data-points per sub-array).

Although each sub-array contains 64 through-holes, only 56 trough-holes can be pre-spotted with a primer-probe set because remaining through-holes are utilised for quality assurance purposes and are used by the supplier during and after the manufacturing process.

Each through-hole can only be spotted with one primer-probe set targeting one individual genomic region. Therefore, the reference assay (TERT), which was used for data normalisation, was spotted in a separate through-hole. In contrast, during Phase 1, the reference assay was processed in same reactions as the copy number assays. Therefore, a second reference assay (RNase P, located in the ribonuclease P gene) was included in the array design in case TERT failed to amplify.

Since loading of the arrays is fully automated and performed by a robotic system, real-time qPCR reactions were not processed in triplicate, because of reduced risk of unequal loading or pipetting errors. Therefore, the remaining 54 through-holes were

spotted with 54 different copy number assays, targeting eight genomic regions located on chromosomes 13, 16, 18, 21, 22 and X and six regions located on chromosome Y. The chosen assays included the four assays tested during Phase 1 of protocol development. Additional assays were again selected on the basis of proximity to the chromosomes' telomere region while avoiding regions of known copy number variation. For metacentric chromosomes, additional assays were spread evenly between the p- and q-arm. Assay IDs and genomic location of the selected copy number assays and both reference assay are presented in **Table A.4** in **Appendix A**.

Since sensitivity and accuracy of the OpenArray methodology for copy number variation analysis was not known, the method was performed on gDNA samples, rather than cell samples. GDNA was extracted from peripheral blood of a female and male control individual as well as nine different aneuploid cell lines (48,XXY,+21; 47,XYY; 48,XY,+16,+21; 46,XX,+Xq; 47,XX,+22; 45,X0; 47,XY,+13; 47,XY,+18; 47,XY,+21). Each sample was processed twice, hence a total of 22 gDNA samples were processed during Phase 2 of protocol development. Furthermore, since gDNA was used for testing, no lysis and multiplex pre-amplification steps were included in the experimental set-up.

A modified version of the algorithm developed for real-time qPCR data analysis during Phase 1 was created to accommodate the new protocol design and all calculations performed in Microsoft Excel.

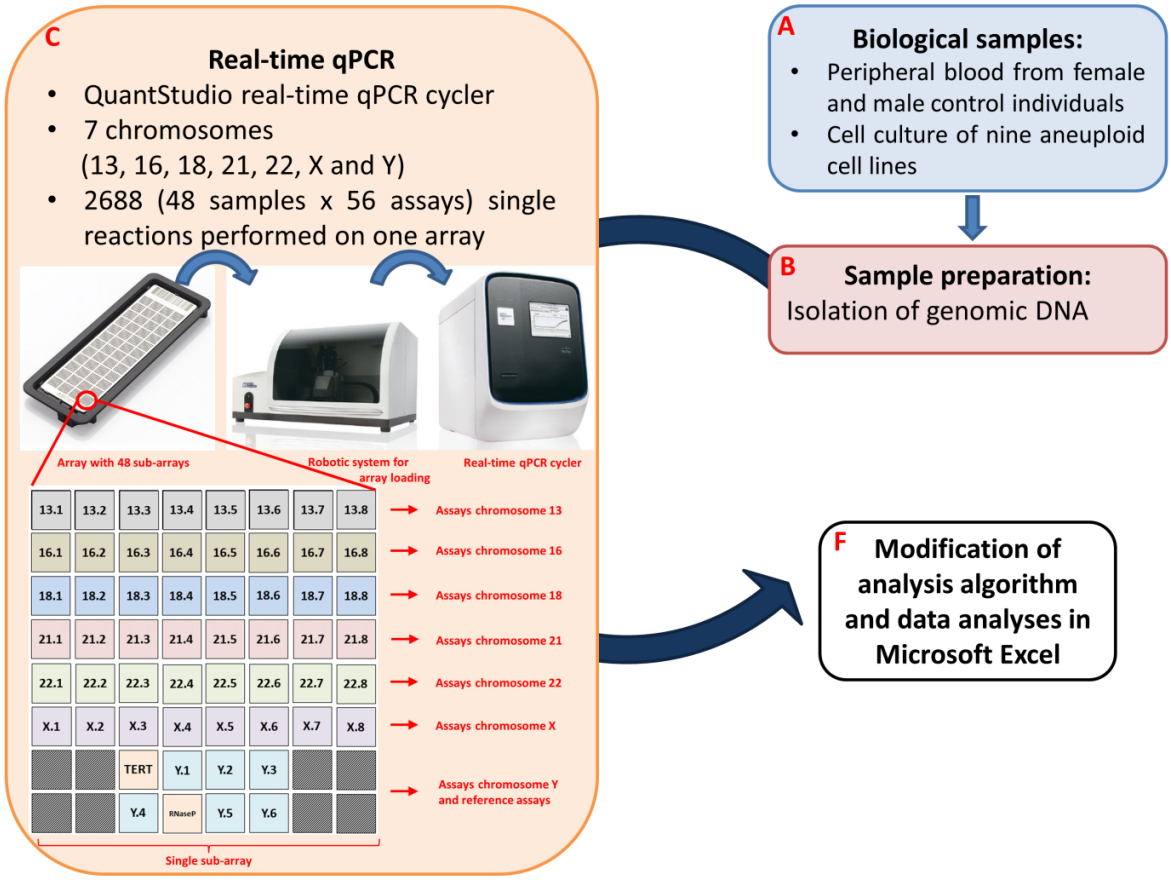


Figure 3.15: Flowchart describing Phase 2 of protocol development. A/B: GDNA was extracted from peripheral blood and cell culture. **C:** Arrays were pre-spotted with primer-probe sets covering a total of seven chromosomes. As illustrated above, each of the 48 sub-arrays contained eight copy number assays targeting chromosomes 13, 16, 18, 21, 22 and X as well as six assays targeting chromosome Y. Additionally, two reference assays (TERT and RNase P) were included. Sub-arrays shaded in grey were left empty. No cell lysis and multiplex pre-amplification was performed and gDNA samples were directly loaded on the arrays using a robotic system (QuantStudio 12K Flex OpenArray AccuFill System). Fluorescence associated with the amplified products was measured during real-time qPCR on the QuantStudio qPCR cycler, followed by (**F**) CCN calculation which was performed in Microsoft Excel. Array and instrument images were obtained from ThermoFisher.

3.3.2.2 Data analysis Phase 2

To calculate the CCN from data generated during Phase 2 a modified analysis protocol based on the algorithm developed during Phase 1 was generated.

Similarly to Phase 1, samples derived from control individuals (2 x 46,XX and 2 x 46,XY) were used to create a female and male reference data set.

Initially, Ct_{assay} values of each of the 54 copy number assays were normalised to the $Ct_{reference}$ value (TERT) to obtain the ΔCt_{assay} value. In contrast to Phase 1, the reference assay was not amplified in the same reaction and all 54 Ct_{assay} values were normalised to the same $Ct_{reference}$ value. Moreover, since copy number assays were not processed in triplicate reactions, no $\Delta Ct_{assay(mean)}$ values were calculated and the fold change of each ΔCt_{assay} value directly determined by considering the ΔCt_{assay} value as the negative exponent of 2 ($2^{-\Delta Ctassay}$).

Next, the same normalisation steps as described previously were performed to account for differences in amplification efficiencies between different assays and to identify and correct possible outliers. The multiplication factors used for the normalisation of each of the 54 $2^{-\Delta Ctassay}$ values were again calculated based on results obtained from all female and male control samples.

After multiplying each $2^{-\Delta Ctassay}$ value by its specific multiplication factor, LB and UB were calculated to determine chromosome- and sample-specific threshold values. $2^{-\Delta Ctassay}$ values were again sorted in descending order (per chromosome) and Q1 and Q3 calculated, which in this case corresponded to the mean of the four lowest and the mean of the four highest $2^{-\Delta Ctassay}$ values, respectively. For the calculation of quartiles of chromosome Y, the means of the three lowest and three highest $2^{-\Delta Ctassay}$ values were calculated. LB and UB were computed as previously described and $2^{-\Delta Ctassay}$ values falling above or below the borders adjusted.

Following data normalisation, the chromosome-specific $2^{-\Delta Ctchromosome}$ values were calculated by summing up the eight $2^{-\Delta Ctassay}$ values of each chromosome (six $2^{-\Delta Ctassay}$ values for chromosome Y).

Next, values (in %) were assigned to each of the seven chromosomes by dividing each of the seven $2^{-\Delta Ctchromosome}$ values by the total amount of the 54 $2^{-\Delta Ctassay}$ values, multiplied by 100. Calculation of the copy number of all autosomes and the sex chromosomes was identical as previously described. 7-CCN profiles were generated and analysed manually. Chromosomes falling on or below a copy number of 1.5 were identified as a single copy. Chromosomes with copy numbers equal to or above 2.5 were called trisomic.

3.3.2.3 Results Phase 2

Each of the eleven gDNA samples was tested twice. Two samples were derived from chromosomally normal individuals (female and male). All other gDNA samples were derived from the cell culture of nine different aneuploid cell lines (48,XXY,+21; 47,XYY; 48,XY,+16,+21; 46,XX,+Xq; 47,XX,+22; 45,X0; 47,XY,+13; 47,XY,+18; 47,XY,+21). Real-time qPCR results of all processed samples are presented in **Table 3.2**. Examples of real-time qPCR 7-CCN profiles are shown in **Figures 3.16** and **3.17**. Calculation of sensitivity and specificity is summarised in **Table A.5** in **Appendix A**.

Of all samples tested, 90.9 % (20 / 22) were diagnosed correctly as euploid or aneuploid. The four samples obtained from karyotypically normal individuals were correctly identified as being euploid. However, sample 10 and sample 12 were falsely identified as euploid and aneuploid, respectively, resulting in an overall diagnosis sensitivity of 94.12 % and specificity of 80.0 %. Among the 154 (22 x 7) chromosomes analysed, copy number was assigned correctly to 146 chromosomes (94.9 %). Of the expected 20 aneuploid chromosomes, 17 were correctly identified as being either lost or gained.

Three aneuploidies were missed (samples 6 and 10). Additionally, five chromosomes were wrongly identified as abnormal (samples 9, 12, 13 and 22), resulting in a sensitivity of 85.71 % and specificity of 96.24 %.

One of the tested cell lines (46,XX,+Xq) harboured a structural gain of chromosome X caused by an unbalanced chromosome rearrangement [46,XX,der(21)(21qter>21p11::Xq11>Xqter)mat]. The analysis algorithm however, was not designed to detect partial chromosome abnormalities since all copy number assays located on one specific chromosome were taken into account for overall CCN assignment.

Therefore, to get information on approximate breakpoints and on the number of genomic loci covering the structural gain of chromosome X, NGS (VeriSeq protocol, see **Section 2.5.2**) was performed on a cell sample derived from the 46,XX,+Xq cell line. As shown in **Figure A.7** in **Appendix A**, four of the eight genomic regions covering chromosome X were located on the extra chromosomal fragment. Hence, the extra copy of chromosome X detected in sample 11 was regarded as 'true-positive' when calculating test sensitivity and specificity because the analysis algorithm cannot discriminate between partial and whole chromosome abnormalities. Of note, chromosome X displayed a copy number of exactly 2.5 (**Figure 3.16 F**) and the trisomy was not as pronounced as compared to trisomies of other samples.

Table 3.2: Results obtained from gDNA samples derived from a female and male control individual and nine different aneuploid cell lines

Samples	Karyotype		Agreement
	Expected	Real-time qPCR	
Genomic DNA from control individuals			
1	46,XX	46,XX	Yes
2		46,XX	Yes
3	46,XY	46,XY	Yes
4		46,XY	Yes
Genomic DNA from aneuploid cell lines			
5	48,XXY,+21	48,XXY,+21	Yes
6		47,XXY	Partial
7	47,XYY	47,XYY	Yes
8		47,XYY	Yes
9	48,XY,+16,+21	47,XY,+16,-18,+21	Partial
10		46,XY	No
11	46,XX,+Xq	47,XXX	Yes[a]
12		47,XXYY,-22	No
13	47,XX,+22	46,XX,-21,+22	Partial
14		47,XX,+22	Yes
15	45,X0	45,X0	Yes
16		45,X0	Yes
17	47,XY,+13	47,XY,+13	Yes
18		47,XY,+13	Yes
19	47,XY,+18	47,XY,+18	Yes
20		47,XY,+18	Yes
21	47,XY,+21	47,XY,+21	Yes
22		48,XYY,+21	Partial

a = trisomy X was considered true-positive.

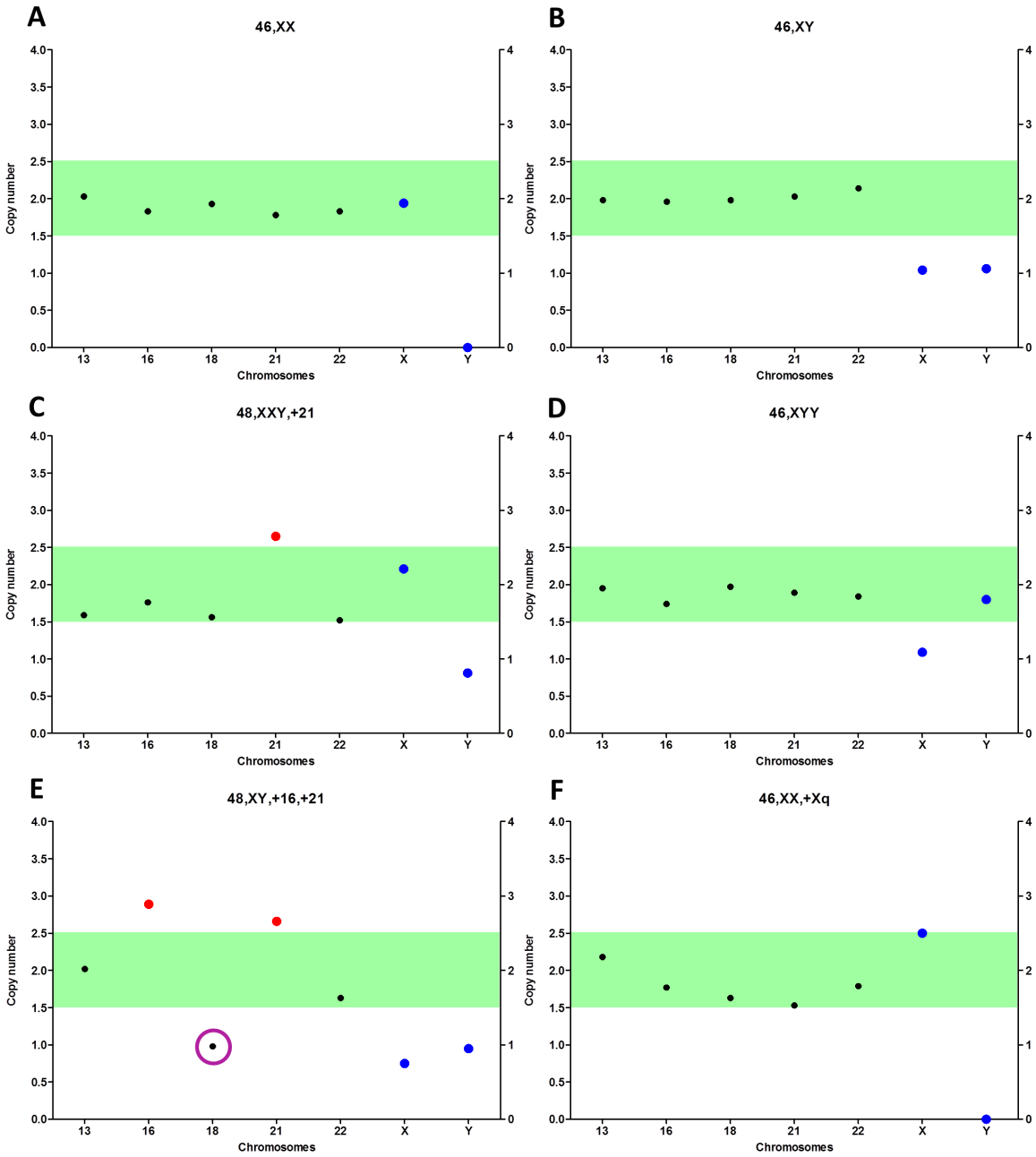


Figure 3.16: Examples of real-time qPCR 7-CCN profiles of euploid and aneuploid gDNA samples. Areas shaded in green indicate CCN of two (ranging from copy number 1.5 - 2.5). Black dots illustrate the copy number of the euploid autosomes. Blue dots illustrate the copy number of the sex chromosomes. Expected autosomal trisomies are illustrated by red dots. The purple circle indicates a chromosome which was falsely identified as aneuploid. Pictured cell line profiles: **A:** 46,XX; **B:** 46,XY; **C:** 48,XXY,+21; **D:** 47,XYY; **E:** 48,XY,+16,+21; **F:** 46,XX,+Xq.

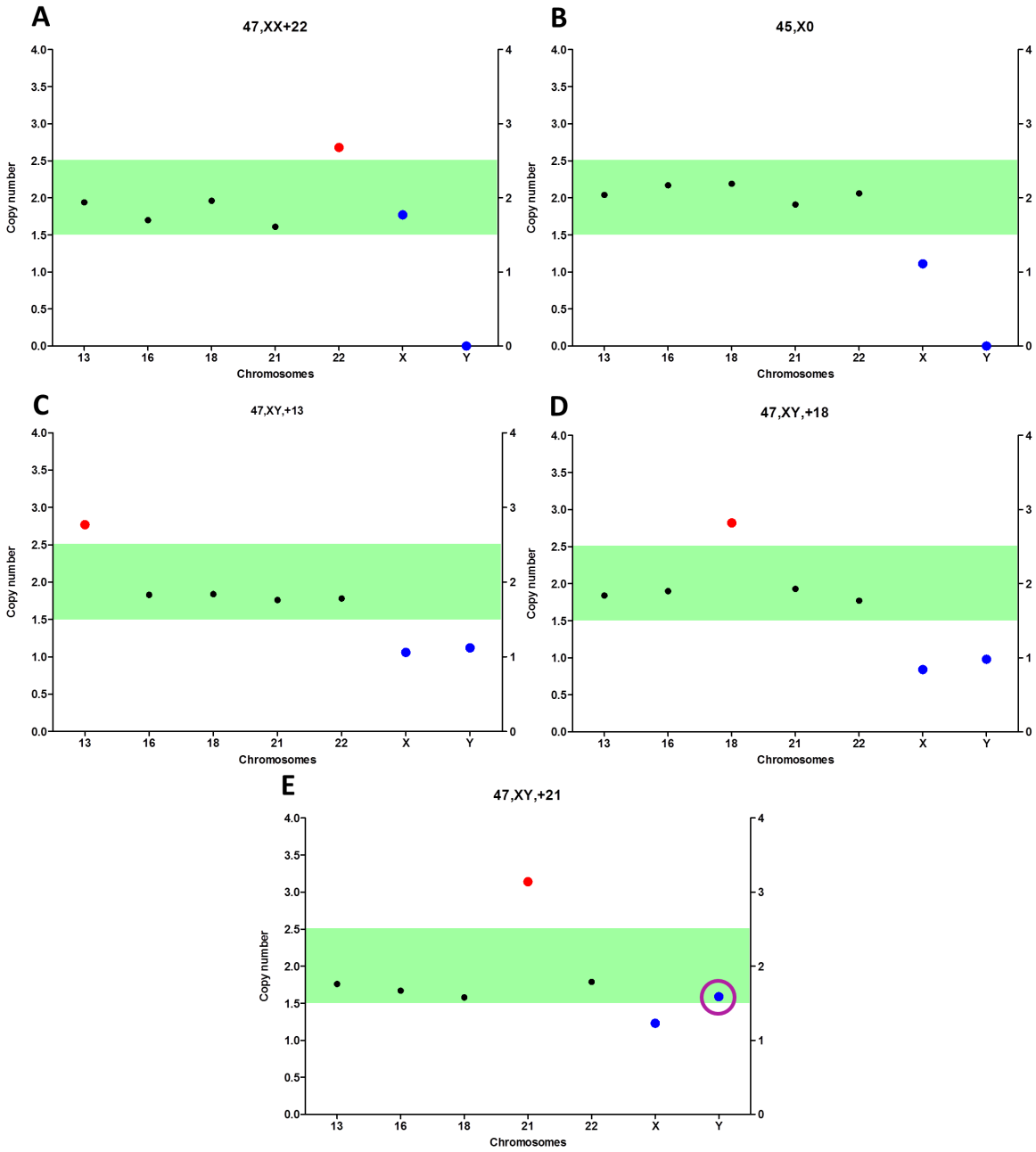


Figure 3.17: Examples of real-time qPCR 7-CCN profiles of aneuploid gDNA samples. Areas shaded in green indicate CCN of two (ranging from copy number 1.5 - 2.5). Black dots illustrate the copy number of the euploid autosomes. Blue dots illustrate the copy number of the sex chromosomes. Expected autosomal trisomies are illustrated by red dots. The purple circle indicates a chromosome which was falsely identified as aneuploid. Pictured cell line profiles: **A:** 47,XX,+22; **B:** 45,X0; **C:** 47,XY,+13; **D:** 47,XY,+18; **E:** 47,XY,+21.

3.3.3 Phase 3 - Feasibility of OpenArray Technology for chromosome copy number analysis of cell samples

3.3.3.1 Protocol design Phase 3

During Phase 3 of protocol development, the methodology was applied to samples consisting of cells, rather than gDNA. The same array design as outline above (Phase 2) was used. However, instead of loading the samples directly onto the arrays, a cell lysis and multiplex pre-amplification step was included to enrich the 56 loci in cell samples prior to real-time qPCR experiments (**Figure 3.18**).

During Phase 1 multiplex pre-amplification reactions were performed in approximately 50.0 µl reaction volumes, which was recommended by the supplier. Of note, pre-amplification volumes differed slightly between different samples and were dependent on the volume of wash buffer dispensed along with the isolated cells. The reagents used during the initial pre-amplification step are relatively expensive. Therefore, to reduce costs of the methodology, multiplex pre-amplification reactions consisting of two smaller reaction volumes (approximately 25 µl and 15 µl) were tested during Phase 3.

Initially, a total of 92 cell samples were processed following multiplex pre-amplification in two different reaction volumes (46 samples were amplified in ~25 µl and another 46 samples were amplified in ~15 µl). In order to mimic the number of cells present in a trophectoderm biopsy, processed cell samples consisted of either three or five cells. Similarly to Phase 2, cell samples were derived from peripheral blood of a female and male control individual as well as nine different aneuploid cell lines (48,XXY,+21; 47,XYY;

48,XY,+16,+21; 46,XX,+Xq; 47,XX,+22; 45,X0; 47,XY,+13; 47,XY,+18; 47,XY,+21). After obtaining results from samples consisting of three and five cells, the method was applied to a total of 46 single-cell samples. These cells were obtained from same sources as specified above.

The analysis algorithm developed during Phase 2 was used for the analysis of data obtained during Phase 3 of protocol development.

In order to ensure, that smaller multiplex pre-amplification volumes have no impact on CCN assignment, feasibility of the proposed reaction volumes was initially tested on three cell samples, each consisting of three cells isolated from the 47,XY,+18 cell line. Samples were processed on a traditional real-time qPCR cycler instead of the OpenArray platform. Hence, for data analysis of these three samples, a modified version of the algorithm developed during Phase 1 was applied.

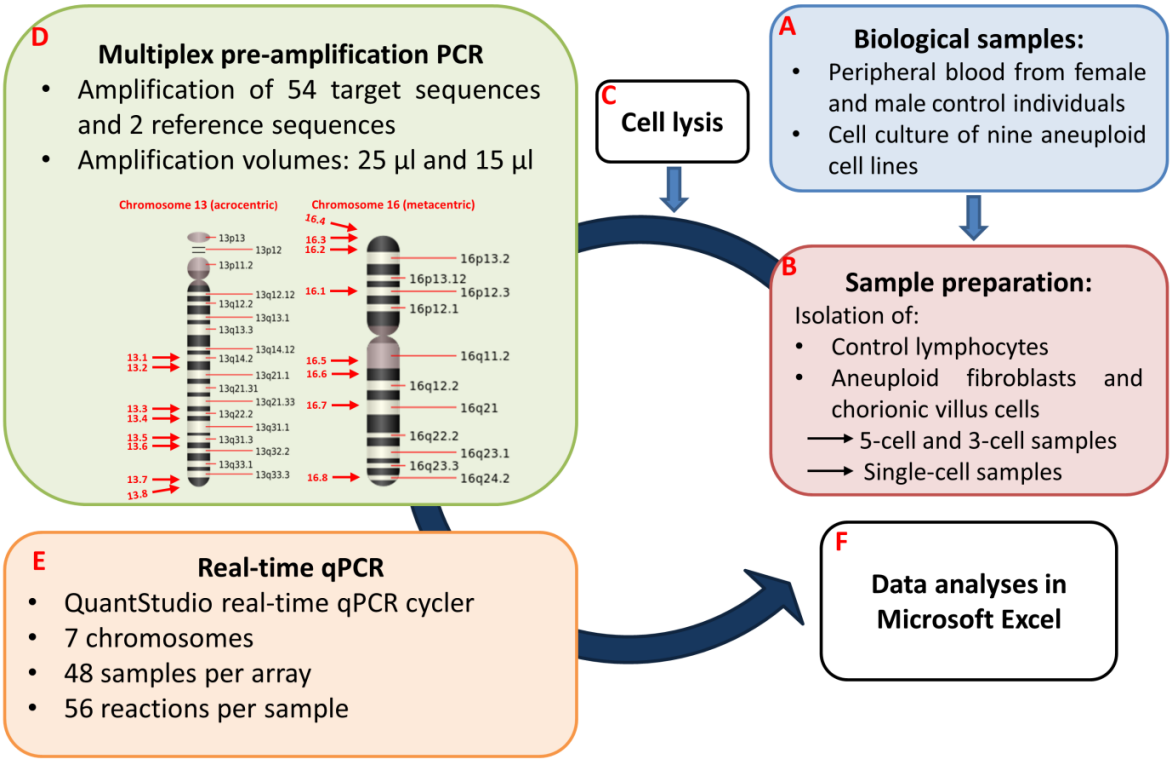


Figure 3.18: Flowchart describing Phase 3 of protocol development. A/B: Lymphocyte as well as fibroblast and chorionic villus-derived samples consisting of three and five as well as single cells were isolated from peripheral blood and cell culture, respectively. **C:** Cell samples were subjected to cell lysis followed by (**D**) multiplex pre-amplification of 54 copy number and two reference assays. Copy number and reference assays were identical to those selected during Phase 2. **E:** After enrichment of gDNA sequences, each of the loci was amplified separately during real-time qPCR on the OpenArray platform (as described in **Figure 3.15**). **F:** CCNs were calculated in Microsoft Excel using the analysis protocol developed during Phase 2. Chromosome images were obtained from Wikimedia Commons.

3.3.3.2 Data analysis Phase 3

For the analysis of the 138 cell samples processed on the OpenArray platform, the algorithm developed during Phase 2 was applied. Of note, to adjust the analysis protocol to the analysis of cell samples (rather than gDNA), real-time qPCR results obtained from karyotypically normal lymphocytes processed during Phase 3 were used to create female and male reference data sets.

For the analysis of the three cell samples (47,XY,+18) which were processed on a regular real-time qPCR instrument, the analysis protocol developed during Phase 1 was used and adjusted to the analysis of seven, instead of 24 chromosomes. Furthermore, karyotypically normal samples processed during Phase 1 served as references.

3.3.3.3 Results Phase 3

Prior to the processing of cell samples on the OpenArray real-time qPCR system, feasibility of smaller pre-amplification volumes was tested and three samples processed on a traditional real-time qPCR cycler. **Figure 3.19** illustrates the obtained results following amplification in different pre-amplification volumes (~50.0 µl, ~25 µl and ~15 µl). Because trisomy 18 was clearly visible in all three tested cell samples, multiplex pre-amplification of the 92 three- and five-cell samples was subsequently performed in the two lower reaction volumes (~25 µl and ~15 µl) prior to the OpenArray real-time qPCR experiments.

Cell samples processed on the OpenArray platform consisted of either three or five cells isolated from peripheral blood of karyotypically normal individuals and from cell culture of nine different aneuploid cell lines. Half of the 92 samples were pre-amplified in a ~25 µl reaction volume and the other half in a ~15 µl reaction volume prior to real-time qPCR experiments.

Real-time qPCR results of three- and five-cell samples which were pre-amplified in ~25 µl and ~15 µl reaction volume are presented in **Tables 3.3** and **3.4**, respectively. Examples of real-time qPCR 7-CCN profiles are presented in **Figures 3.20** and **3.21**, which illustrate a mix of CCN profiles of samples consisting of three or five cells following pre-amplification in different reaction volumes. Sensitivity and specificity of the method

following pre-amplification in ~25 µl and ~15 µl was calculated separately and is summarised in **Tables A.6** and **A.7** in **Appendix A**, respectively.

The gender was assigned correctly in all samples pre-amplified in a ~25 µl reaction volume. Moreover, 95.7 % (44 / 46) of the samples were correctly identified as euploid or aneuploid. However, two aneuploid cell samples (samples 35 and 37) derived from the 47,XY,+13 cell line were called euploid. Of note, 7-CCN profiles of both samples showed a clear shift of chromosome 13 (copy numbers of 2.40 and 2.48; an example is given in **Figure 3.21 C**). Because of the two false-negative results, test sensitivity was 93.94 %. In contrast, specificity was 100 % since all chromosomally normal samples were correctly identified as euploid.

A correct copy number was assigned to 97.5 % (314 / 322) of the chromosomes tested. Five aneuploidies were missed (samples 13, 20, 21, 35 and 37) and three euploid chromosomes were identified as abnormal (samples 11, 28 and 30). Therefore, sensitivity and specificity for CCN assignment was 87.8 % and 98.9 %, respectively. This assumes that the cell lines tested have a uniform karyotype in all cells.

Of the 46 samples pre-amplified in a ~15 µl reaction volume, one sample (sample 10) failed to amplify. The sex was determined correctly in the remaining 45 samples. Moreover, all samples were correctly identified as either being euploid or aneuploid resulting in a test diagnosis sensitivity and specificity of 100 %. Furthermore, a correct copy number was assigned to 99.7 % of all chromosomes tested (314 / 315). The test resulted in only one false-negative CCN call (sample 19) giving a sensitivity of 97.5 % and specificity of 100 % for CCN assignment.

The real-time qPCR method was primarily developed for the analysis of trophectoderm biopsies derived from blastocyst-stage embryos. However, following the promising results obtained from the 92 cell samples which consisted of three or five cells, performance of the method was also tested on single cells.

A total of 46 samples were tested, which were pre-amplified in a ~15 µl reaction volume. Following real-time qPCR, copy numbers were calculated as previously described. Of note, euploid cell samples from this sample set were used to generate the reference.

Results, examples of real-time qPCR 7-CCN profiles as well as calculations of sensitivity and specificity are presented in **Table 3.5**, in **Figures 3.22** and **3.23** as well as in **Table A.8** in **Appendix A**.

As expected, the method did not perform well in the single-cell sample set. Although only two samples failed to amplify (samples 3 and 22), accuracy rates were greatly reduced as compared to the accuracy obtained after testing of three- and five-cell samples. Only 79.6 % (35 / 44) of the samples were correctly classified as euploid or aneuploid (sensitivity = 81.8 %; specificity = 72.7 %). Moreover, of the 308 chromosomes assessed, copy number was wrongly assigned to 35 chromosomes (11.4 %; sensitivity = 46.1 %; specificity = 92.2%).

Table 3.3: Results obtained from three- and five-cell samples derived from a female and male control individual and nine different aneuploid cell lines (pre-amplified in ~25 µl reaction volume)

Samples	Cells	Karyotype		Agreement
		Expected	Real-time qPCR	
Lymphocyte samples from control individuals				
1	5	46,XX	46,XX	Yes
2	5		46,XX	Yes
3	5		46,XX	Yes
4	3		46,XX	Yes
5	3		46,XX	Yes
6	5	46,XY	46,XY	Yes
7	5		46,XY	Yes
8	5		46,XY	Yes
9	3		46,XY	Yes
10	3		46,XY	Yes
Fibroblast and chorionic villus samples from aneuploid cell lines				
11	5	48,XXY,+21	47,XXY,+21,-22	Partial
12	5		48,XXY,+21	Yes
13	3		47,XXY	Partial
14	3		48,XXY,+21	Yes
15	5	47,XYY	47,XYY	Yes
16	5		47,XYY	Yes
17	3		47,XYY	Yes
18	3		47,XYY	Yes
19	5	48,XY,+16,+21	48,XY,+16,+21	Yes
20	5		47,XY,+21	Partial
21	3		47,XY,+16	Partial
22	3		48,XY,+16,+21	Yes
23	5	46,XX,+Xq	46,XX	Yes[a]
24	5		46,XX	Yes[a]
25	3		47,XXX	Yes[b]
26	3		46,XX	Yes[a]
27	5	47,XX,+22	47,XX,+22	Yes
28	5		46,XX,-13,+22	Partial
29	3		47,XX,+22	Yes
30	3		47,XX,-13,+22	Partial
31	5	45,X0	45,X0	Yes
32	5		45,X0	Yes
33	3		45,X0	Yes
34	3		45,X0	Yes
35	5	47,XY,+13	46,XY	No

36	5		47,XY,+13	Yes
37	3		46,XY	No
38	3		48,XY,+13	Yes
39	5	47,XY,+18	47,XY,+18	Yes
40	5		47,XY,+18	Yes
41	3		48,XY,+18	Yes
42	3		47,XY,+18	Yes
43	5	47,XY,+21	47,XY,+21	Yes
44	5		47,XY,+21	Yes
45	3		47,XY,+21	Yes
46	3		47,XY,+21	Yes

a = two copies of X was considered true-negative. b = trisomy X was considered true-positive.

Table 3.4: Results obtained from three- and five-cell samples derived from a female and male control individual and nine different aneuploid cell lines (pre-amplified in ~15 µl reaction volume)

Samples	Cells	Karyotype		Agreement
		Expected	Real-time qPCR	
Lymphocyte samples from control individuals				
1	5	46,XX	46,XX	Yes
2	5		46,XX	Yes
3	5		46,XX	Yes
4	3		46,XX	Yes
5	3		46,XX	Yes
6	5	46,XY	46,XY	Yes
7	5		46,XY	Yes
8	5		46,XY	Yes
9	3		46,XY	Yes
10	3		No amplification	No result
Fibroblast and chorionic villus samples from aneuploid cell lines				
11	5	48,XXY,+21	48,XXY,+21	Yes
12	5		48,XXY,+21	Yes
13	3		48,XXY,+21	Yes
14	3		48,XXY,+21	Yes
15	5	47,XYY	47,XYY	Yes
16	5		47,XYY	Yes
17	3		47,XYY	Yes
18	3		47,XYY	Yes
19	5	48,XY,+16,+21	47,XY,+21	Partial
20	5		48,XY,+16,+21	Yes
21	3		48,XY,+16,+21	Yes

22	3		48,XY,+16,+21	Yes
23	5	46,XX,+Xq	46,XX	Yes[a]
24	5		46,XX	Yes[a]
25	3		46,XX	Yes[a]
26	3		46,XX	Yes[a]
27	5	47,XX,+22	47,XX,+22	Yes
28	5		47,XX,+22	Yes
29	3		47,XX,+22	Yes
30	3		47,XX,+22	Yes
31	5	45,X0	45,X0	Yes
32	3		45,X0	Yes
33	3		45,X0	Yes
34	3		45,X0	Yes
35	5	47,XY,+13	47,XY,+13	Yes
36	5		47,XY,+13	Yes
37	3		47,XY,+13	Yes
38	3		47,XY,+13	Yes
39	5	47,XY,+18	47,XY,+18	Yes
40	5		47,XY,+18	Yes
41	3		47,XY,+18	Yes
42	3		47,XY,+18	Yes
43	5	47,XY,+21	47,XY,+21	Yes
44	5		47,XY,+21	Yes
45	3		47,XY,+21	Yes
46	3		47,XY,+21	Yes

a = two copies of X was considered true-negative.

Table 3.5: Results obtained from single-cell samples derived from a female and male control individual and nine different aneuploid cell lines (pre-amplified in ~15 µl reaction volume)

Samples	Karyotype		Agreement
	Expected	Real-time qPCR	
Lymphocyte samples from control individuals			
1	46,XX	46,XX	Yes
2		46,XX	Yes
3		No amplification	No result
4		45,XX,-18	No
5		45,XX,-13	No
6	46,XY	46,XY	Yes
7		46,XY	Yes
8		46,XY	Yes

9		46,XY	Yes
10		47,XY,+13	No
Fibroblast and chorionic villus samples from aneuploid cell lines			
11	48,XXY,+21	47,XXY	Partial
12		46,XY	No
13		47,XXY	Partial
14		46,XY	No
15	47,XYY	47,XYY	Yes
16		46,XY	No
17		47,XYY	Yes
18		47,XYY,-16,+18	Partial
19	48,XY,+16,+21	46,XY,+16,-21	Partial
20		46,XY	No
21		46,XY	No
22		No amplification	No result
23	46,XX,+Xq	46,XX,-22	Partial[a]
24		47,XXX	Yes[b]
25		46,XX	Yes[a]
26		46,XX	Yes[a]
27	47,XX,+22	45,X0,-21,+22	Partial
28		47,XX,+22	Yes
29		47,XX,+22	Yes
30		46,XX	No
31	45,X0	45,X0	Yes
32		46,X0,+13	Partial
33		47,X0,+13,+18	Partial
34		45,X0,-16,+18	Partial
35	47,XY,+13	47,XY,+13	Yes
36		47,XY,+13	Yes
37		45,XY,+18,-21,-22	No
38		48,XY,+13	Yes
39	47,XY,+18	45,XY,+18,-21,-22	Partial
40		46,XY,+18,-16	Partial
41		48,XY,+18	Yes
42		47,XY,+18	Yes
43	47,XY,+21	46,XY,-16,+21	Partial
44		47,XY,+21	Yes
45		47,XY,+21	Yes
46		45,XY,-13	No

a = presence of two copies of X was considered true-negative. b = trisomy X was considered true-positive.

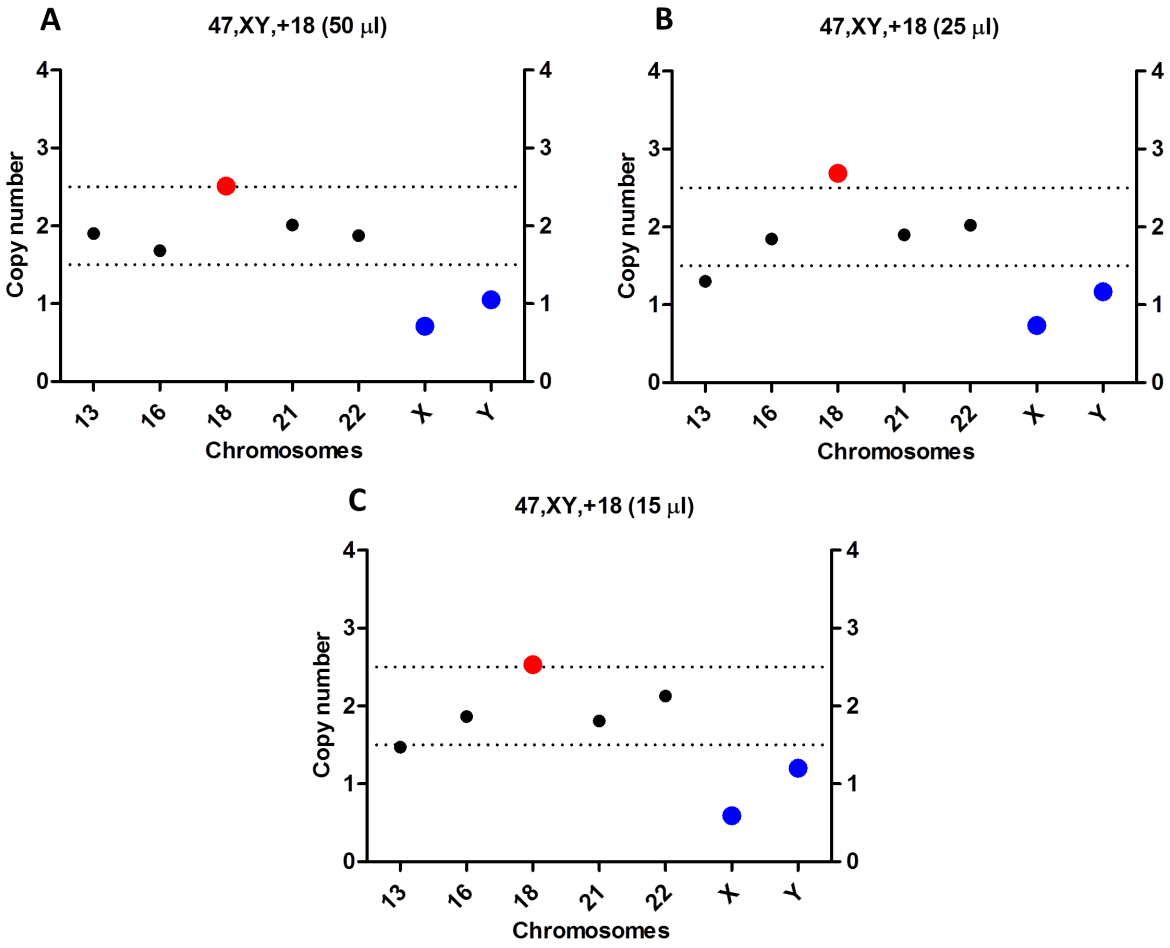


Figure 3.19: Real-time qPCR 7-CCN profiles of three-cell samples pre-amplified in three different multiplex pre-amplification reaction volumes. Areas between dotted lines indicate CCN of two (ranging from copy number 1.5 - 2.5). Black dots illustrate the copy number of euploid autosomes. Blue dots illustrate the copy number of the sex chromosomes. The expected trisomies of chromosome 18 are illustrated by red dots. **A**, **B** and **C** depict results obtained after pre-amplification in ~50 µl, ~25 µl and ~15 µl reaction volumes, respectively.

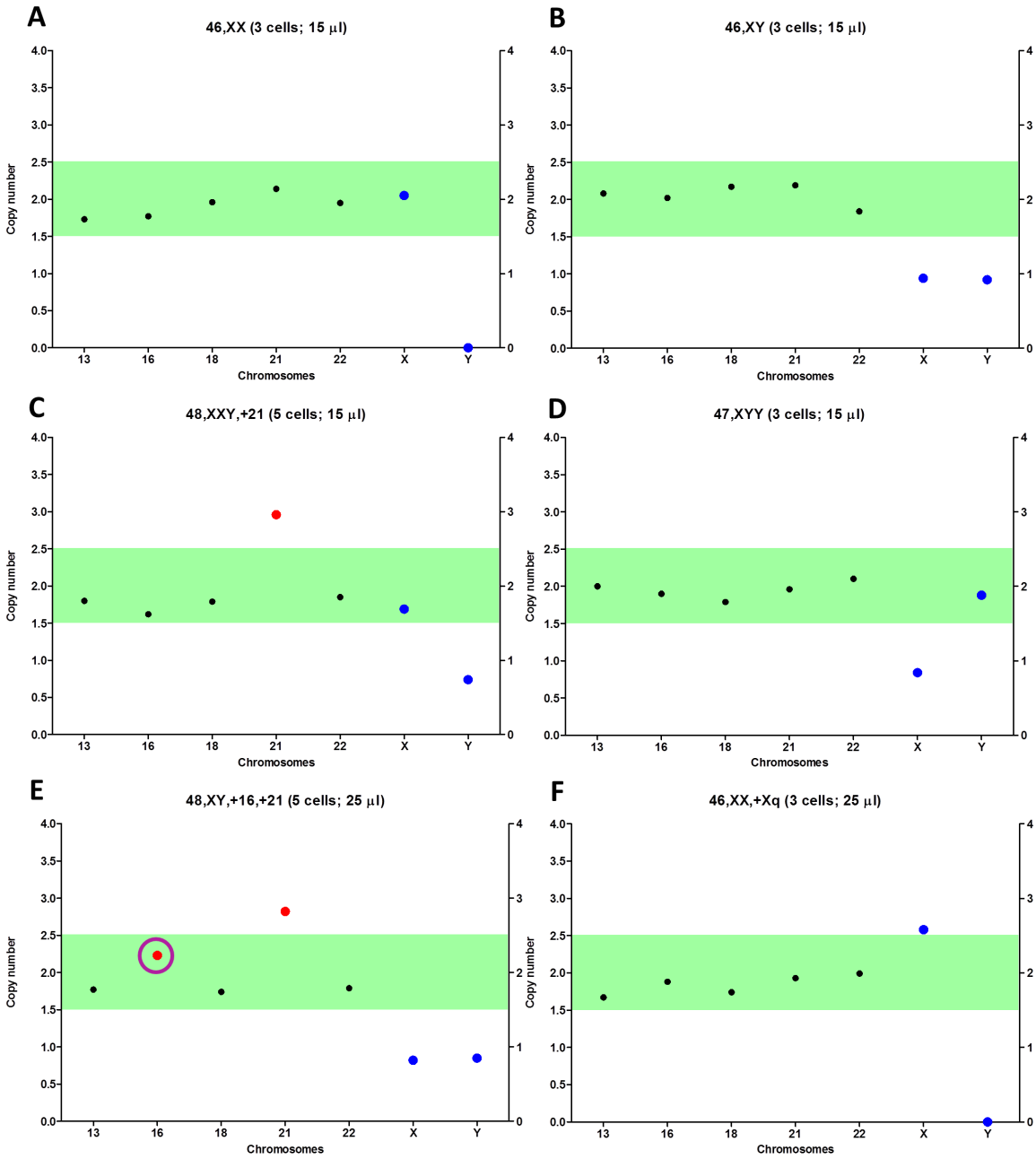


Figure 3.20: Examples of real-time qPCR 7-CCN profiles of euploid and aneuploid three- and five-cell samples. Areas shaded in green indicate CCN of two (ranging from copy number 1.5 - 2.5). Black dots illustrate the copy number of the euploid autosomes. Blue dots illustrate the copy number of the sex chromosomes. Expected autosomal trisomies are illustrated by red dots. The purple circle marks a chromosome which was falsely identified as euploid. Pictured cell line profiles: **A:** 46,XX; **B:** 46,XY; **C:** 48,XXY,+21; **D:** 47,XYY; **E:** 48,XY,+16,+21; **F:** 46,XX,+Xq.

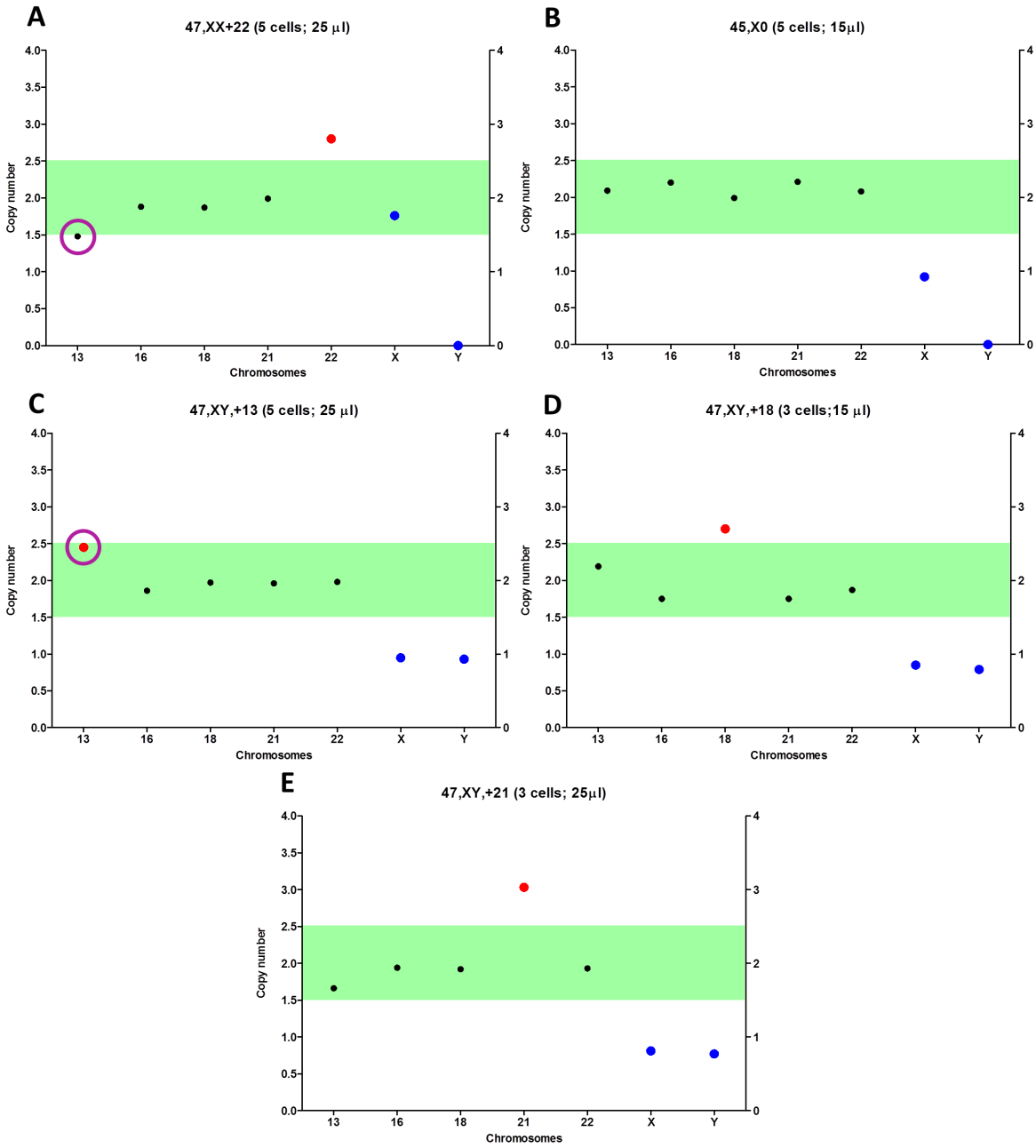


Figure 3.21: Examples of real-time qPCR 7-CCN profiles of aneuploid three- and five-cell samples. Areas shaded in green indicate CCN of two (ranging from copy number 1.5 - 2.5). Black dots illustrate the copy number of euploid autosomes. Blue dots illustrate the copy number of the sex chromosomes. Expected autosomal trisomies are illustrated by red dots. Purple circles indicate chromosomes which were falsely identified as aneuploid or euploid. Pictured cell line profiles: **A:** 47,XX,+22; **B:** 45,X0; **C:** 47,XY,+13; **D:** 47,XY,+18; **E:** 47,XY,+21.

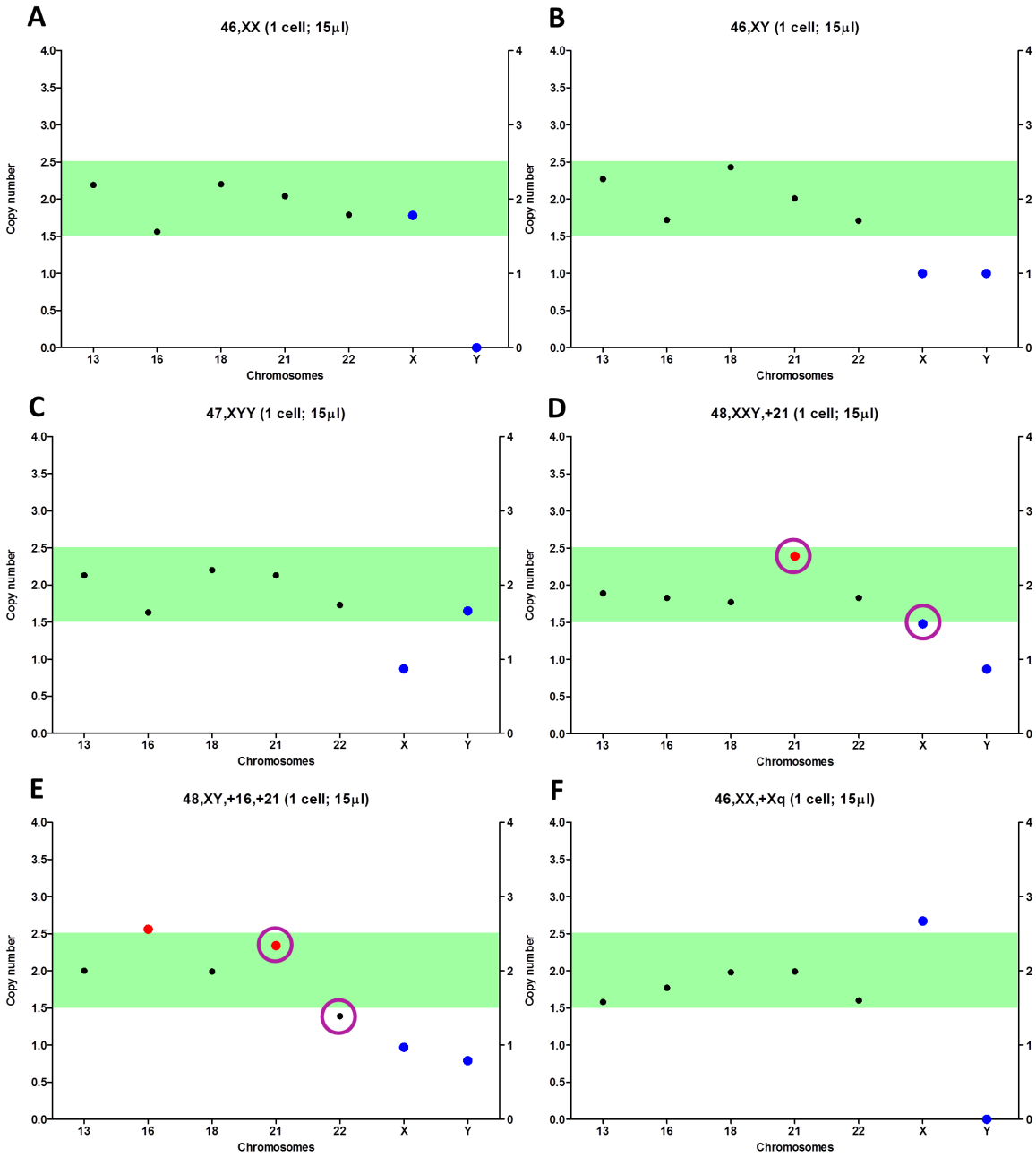


Figure 3.22: Examples of real-time qPCR 7-CCN profiles of euploid and aneuploid single-cell samples. Areas shaded in green indicate CCN of two (ranging from copy number 1.5 - 2.5). Black dots illustrate the copy number of the euploid autosomes. Blue dots illustrate the copy number of the sex chromosomes. Expected autosomal trisomies are illustrated by red dots. The purple circles mark chromosomes which were falsely identified as euploid or aneuploid. Pictured cell line profiles: **A:** 46,XX; **B:** 46,XY; **C:** 47,XYY; **D:** 48,XXY,+21; **E:** 48,XY,+16,+21; **F:** 46,XX,+Xq.

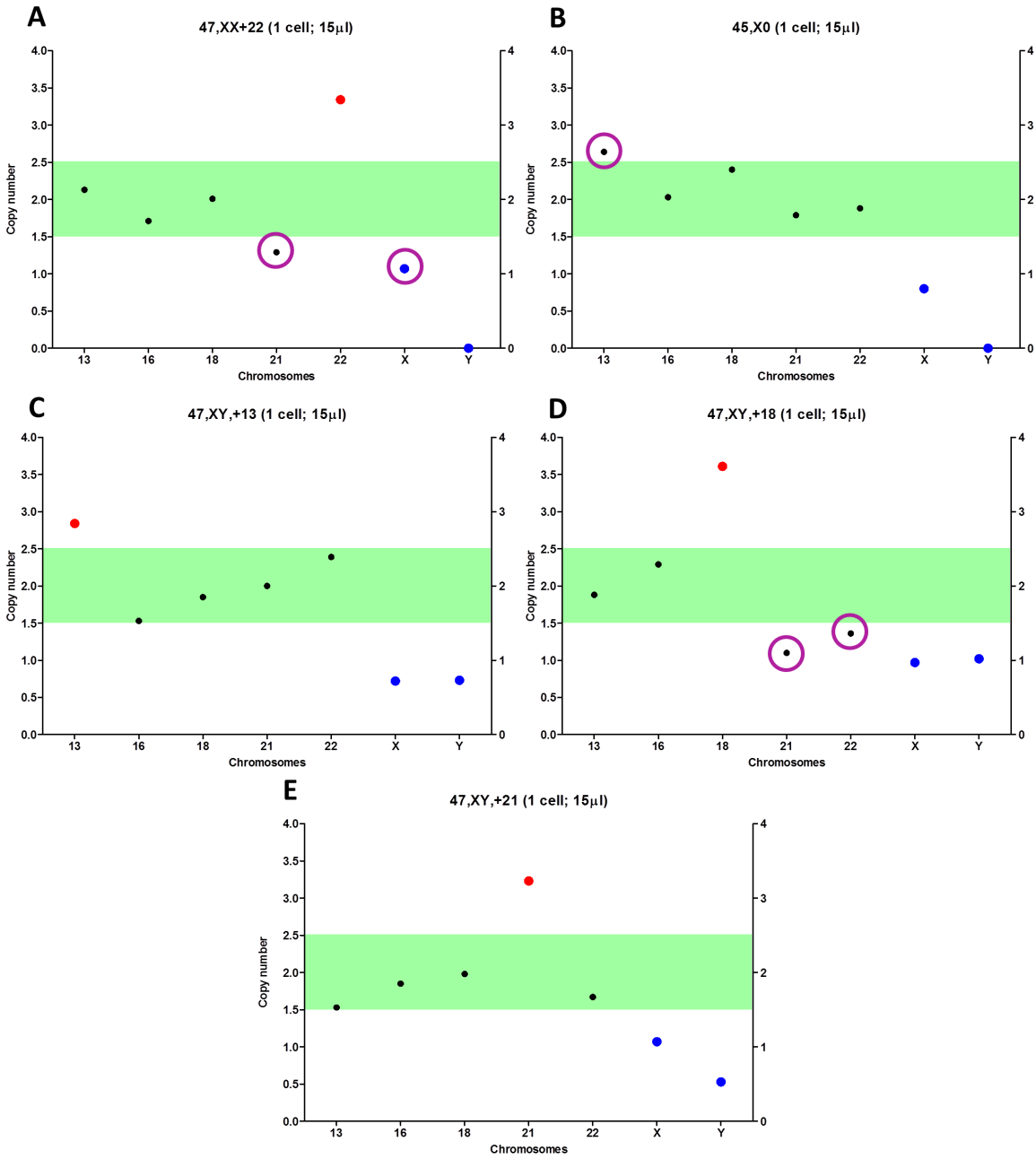


Figure 3.23: Examples of real-time qPCR 7-CCN profiles of aneuploid single-cell samples. Areas shaded in green indicate CCN of two (ranging from copy number 1.5 - 2.5). Black dots illustrate the copy number of euploid autosomes. Blue dots illustrate the copy number of the sex chromosomes. Expected autosomal trisomies are illustrated by red dots. Purple circles indicate chromosomes which were falsely identified as aneuploid. Pictured cell line profiles: **A:** 47,XX,+22; **B:** 45,X0; **C:** 47,XY,+13; **D:** 47,XY,+18; **E:** 47,XY,+21.

3.3.4 Phase 4 - Feasibility of OpenArray Technology for comprehensive chromosome copy number testing

3.3.4.1 Protocol design Phase 4

During Phase 4 of protocol development a new array was designed permitting comprehensive CCN analysis of all 24 chromosomes. The 12 (four sub-arrays per sample) x 224 (data-points) array design was chosen which allowed simultaneous processing of 12 samples and the analysis of 224 genomic regions (per sample) on a single array. Of the 224 genomic regions assessed per sample, 216 loci were selected for analysis of CCN (nine loci per chromosome). Extra copy number assays were again chosen on the basis of proximity to the chromosomes' telomere region while avoiding regions of known copy number variation. Additionally, few copy number assays which gave inconsistent results during previous validation phases were replaced by new assays.

Similarly, to previous experiments, two reference assays were included (TERT and RNase P). Furthermore, three assays (DGR.1, DGR.2 and DGR.3) targeting three different regions on the 22q11 cytoband of chromosome 22 were included in the array design to test if the method was applicable to DiGeorge microdeletion Syndrome testing. Additionally, three assays assays (M.1, M.2 and M.3) covering three different genomic loci on the mitochondrial genome were included for quantification of mtDNA copy number. The array design is illustrated in **Figure 3.24**. Assay IDs and genomic location of the selected copy number and reference assays as well as assays targeting the DiGeorg microdeletion region and the mitochondrial genome are presented in **Table A.9** in **Appendix A**.

CCN analysis using the newly designed 24-chromosome array format was directly evaluated on cell line-derived cell samples (rather than gDNA) following cell lysis and multiplex pre-amplification of all 224 loci in a ~15 µl reaction volume (rather than ~25 µl). Samples used during the evaluation of the new array design included a total of 72 single-, three- and five-cell samples which were isolated from peripheral blood of karyotypically normal individuals and from cell culture of nine different aneuploid cell lines (48,XXY,+21; 47,XYY; 48,XY,+16,+21; 46,XX,+Xq; 47,XX,+22; 45,X0; 47,XY,+13; 47,XY,+18; 47,XY,+21).

The previously established analysis algorithm was modified to allow comprehensive analysis of the entire chromosome set. Again, data analysis was performed in Microsoft Excel.

A flowchart describing Phase 4 of protocol development is shown in **Figure 3.25**.

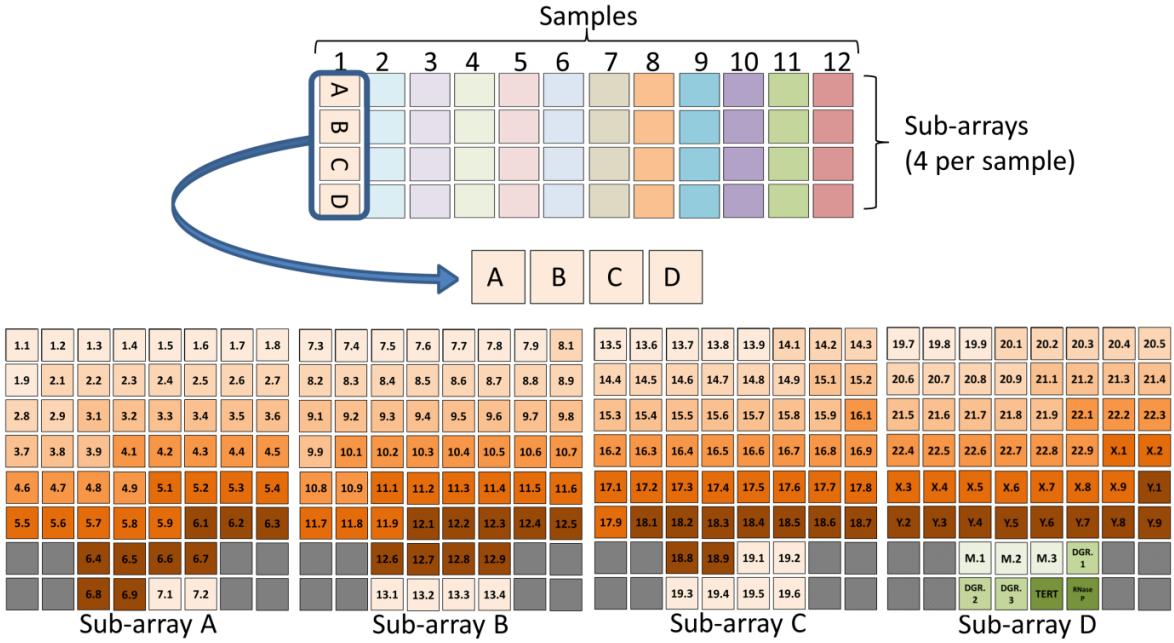


Figure 3.24: Array design for comprehensive CCN testing combined with DiGeorge microdeletion Syndrome testing and mtDNA quantification. A total of 12 samples can be processed simultaneously on one array. Four sub-arrays (A - D) are utilised per sample. Copy number assays (shown in orange shades) were spotted in ascending order (chromosome 1-22, X and Y) starting from sub-array A - D. Reference assays (TERT and RNase P), assays covering the DiGeorge microdeletion area (DGR.1, DGR.2 and DGR.3) as well as mtDNA assays (M.1, M.2 and M.3) were spotted on sub-array D (shown in green shades). Through-holes coloured in grey were left empty.

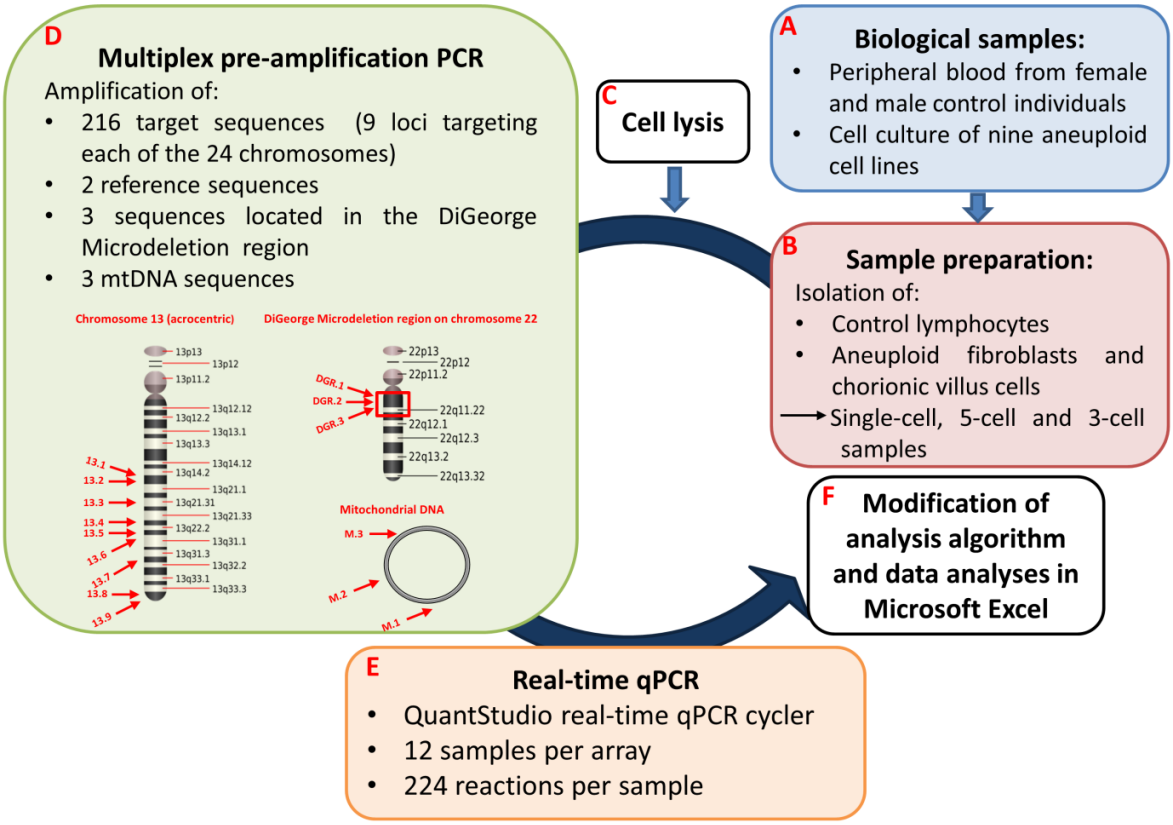


Figure 3.25: Flowchart describing Phase 4 of protocol development. A/B: Lymphocyte as well as fibroblast and chorionic villus-derived samples consisting of three and five as well as single cells were isolated from peripheral blood and cell culture, respectively. **C:** Cell samples were subjected to cell lysis followed by (**D**) multiplex pre-amplification of 224 loci, including 216 loci for CCN analysis, two reference sequences, three regions located in the DiGeorge microdeletion region and three loci located in the mitochondrial genome. **E:** After enrichment of nuclear and mitochondrial sequences, each locus was amplified separately during real-time qPCR on the OpenArray platform (as described in Figure **3.24**). **F:** CCN was calculated in Microsoft Excel. Chromosome images were obtained from Wikimedia Commons.

3.3.4.2 Data analysis Phase 4

The following section describes the 24-CCN analysis. Details on the detection of the DiGeorge microdeletion and calculation of mtDNA quantities are discussed in **Sections 3.3.5.2** and **3.3.6.2**, respectively.

To calculate CCNs of all 24 chromosomes, the analysis protocol utilised during Phase 2 and Phase 3 was modified to allow simultaneous assessment of all 24 chromosomes (rather than seven chromosomes). Again, samples derived from control

individuals [3 x 46,XX (1 cell); 3 x 46,XX (3 cells); 3 x 46,XX (5 cells); 3 x 46,XY (1 cell); 3 x 46,XY (3 cells); 3 x 46,XY (5 cells)] were used to create female and male reference data sets, whereby references consisting of results from single-cell samples or results from three- and five-cell samples were used for the analysis of single cells or clumps of cells, respectively.

Similarly to previous analysis protocols, Ct_{assay} values of each copy number assays were normalised to the $Ct_{reference}$ value (TERT) to obtain the ΔCt_{assay} value. Of note, the reference assay was separately amplified in sub-array D (as shown in **Figure 3.24**) and all 216 copy number assays, spread across sub-arrays A, B, C and D, were normalised to the same $Ct_{reference}$ value. Following Ct_{assay} value normalisation, the fold change of each ΔCt_{assay} value was determined by considering the ΔCt_{assay} value as the negative exponent of 2 ($2^{-\Delta Ctassay}$). Data smoothening was performed as previously described. In brief, multiplication factors used for the normalisation of each of the 216 $2^{-\Delta Ctassay}$ values were calculated from the results obtained from control samples. Following the multiplication by assay-specific multiplication factors, chromosome- and sample-specific LB and UB were computed and $2^{-\Delta Ctassay}$ values adjusted when necessary.

After data normalisation, the sum of the nine chromosome-specific $2^{-\Delta ctchromosome}$ values was formed and chromosome-specific values (in %) assigned by dividing each of the 24 $2^{-\Delta ctchromosome}$ values by the total amount of the 216 $2^{-\Delta Ctassay}$ values, multiplied by 100. Generation of CCNs of all autosomes and sex chromosomes was performed as previously described utilising the newly created female and male reference data sets. 24-CCN profiles were analysed manually and previously

established rules for copy number assignment applied (≤1.5 = single copy; ≥2.5 = three copies).

3.3.4.3 Results Phase 4

Samples processed during Phase 4 included a total of 18 karyotypically normal samples. The remaining 54 cell samples were derived from the same nine aneuploid cell lines used during previous protocol development phases.

Although results obtained during the first three phases of protocol development were promising, none of the 99 cell samples tested received a correct CCN assignment. In fact, 24-CCN plots showed chaotic chromosome profiles. Two examples are given in **Figure 3.26 A** which illustrates the results obtained from two three-cell samples derived from the 47,XY,+13 and 47,XX,+22 cell line. In the left plot (47,XY,+13) a gradual increase in autosomal copy numbers can be seen, while in the right profile (47,XX,+22) a gradual decrease in CCNs is present. Similar copy number changes were also observed in profiles of most of the other tested samples, which displayed either a continuous rise or drop in copy numbers. Examples of CCN profiles for each cell line and control samples are given in **Figure A.8** in **Appendix A**.

Unlike during Phase 2 and Phase 3 where only one sub-array was utilised per sample, the newly designed arrays comprised four sub-arrays per sample to accommodate additional assays utilised for comprehensive chromosome analysis. Since copy number assays were spotted in ascending chromosome order (from chromosome 1 - 22, X and Y, spotted in sub-arrays A - D), the observed gradual increase/decrease in CCNs suggested

that real-time qPCR reactions of the same sample performed differently between different sub-arrays.

Indeed, when examining the raw data (Ct values), a consistent variation in performance between the four sub-arrays was detected and Ct values were gradually declining from sub-array A to sub-array D. Two examples are shown in **Figure 3.26 B** which illustrates the stepwise decrease of Ct values between sub-arrays in samples derived from the 47,XY,+13 and 47,XX,+22 cell line (same samples as shown in **Figure 3.26 A**). Of note, the gradual decrease was observed across most of the tested samples (see **Figure A.9 A** in **Appendix A**).

Figure 3.26 C further illustrates the stepwise decrease in Ct values between assays targeting different chromosomes (data derived from same samples as depicted in **Figure 3.26 A** and **B**). For example, mean chromosome Ct values of assays amplifying sequences of chromosomes 1 - 6 (spotted on sub-array A) were consistently higher than those from assays targeting chromosomes 8 - 12 (spotted on sub-array B). Interestingly, mean Ct values of chromosomes whose assays were divided between different sub-arrays [e.g. chromosome 7; assays distributed between sub-arrays A and B (see **Figure 3.24**)] showed intermediate mean Ct values. Of note, similar patterns were also observed for the remaining 70 samples (illustrated in **Figure A.9 B** in **Appendix A**).

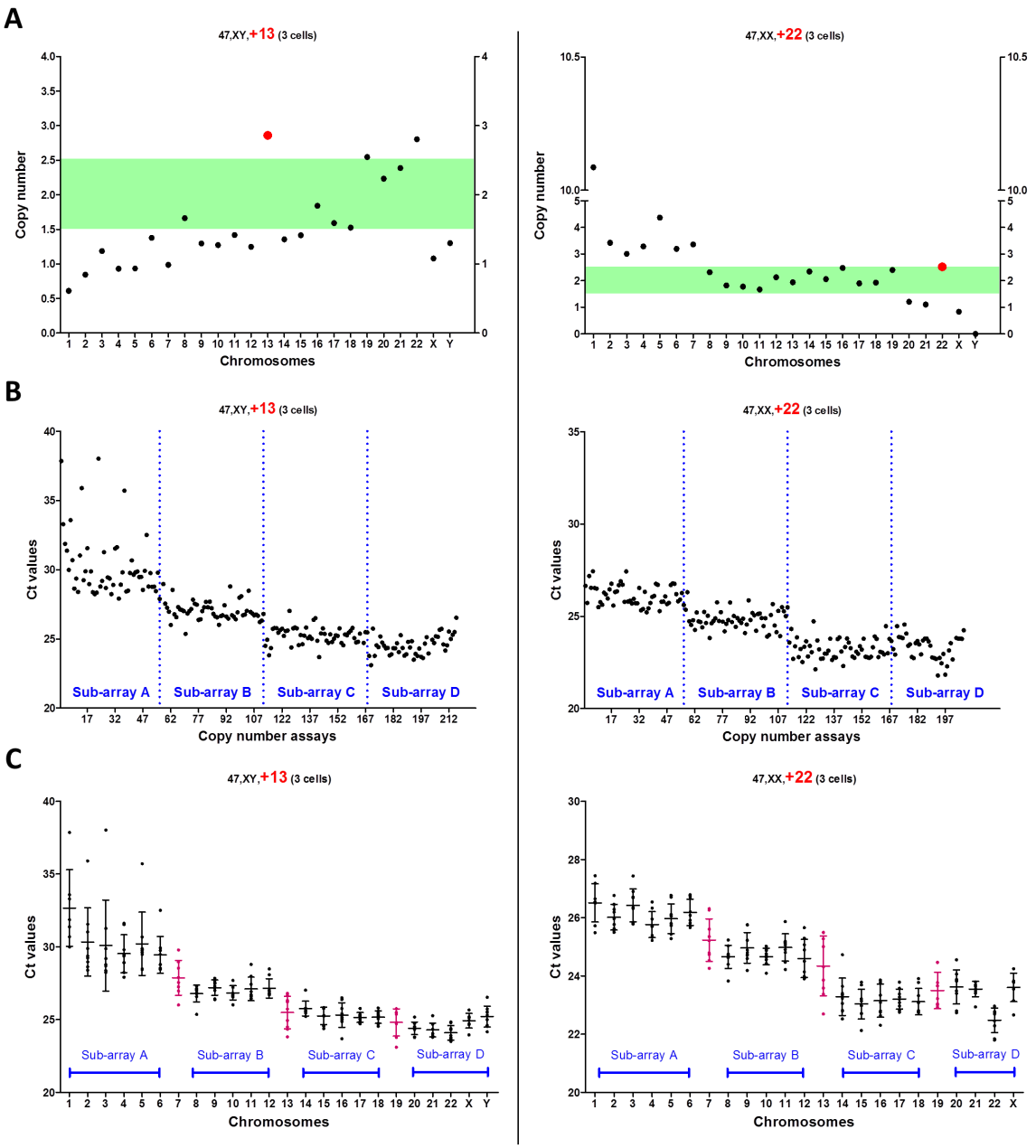


Figure 3.26: Examples of results obtained from samples processed during Phase 4 of protocol development. The left and right panel show results of two three-cell samples obtained from the 47,XY,+13 and 47,XX,+22 cell line, respectively. **A: Real-time qPCR 24-CCN profiles.** Areas shaded in green indicate CCN of two (ranging from copy number 1.5 - 2.5). Expected euploid chromosomes are shown by black dots. Expected aneuploid chromosomes are illustrated by red dots. **B: Distribution of obtained Ct values across sub-arrays A - D.** Each dot represents a single Ct value (total: 216). **C: Distribution of mean chromosome Ct values across sub-arrays A - D.** Ct values of chromosomes targeted by assays located on two different sub-arrays are coloured in pink. Dots represent single Ct values. Error bars indicate SD of assay Ct values of the same chromosome. The mean Ct value of each chromosome is indicated by the horizontal black line.

3.3.5 Phase 5 - Feasibility of OpenArray Technology for comprehensive chromosome copy number testing using a modified array design

3.3.5.1 Protocol design Phase 5

Following the adverse results obtained during Phase 4 of protocol development, the protocol and array design were re-assessed to identify possible deficiencies in the experimental set-up and/or the design of the arrays. After liaising with the technical support team from ThermoFisher, technical failures during array manufacturing (e.g. errors occurring during assay spotting) were eliminated as a potential cause of the sub-array dependent differences in Ct values. Instead, it was more likely that the variations between sub-arrays were attributed to an uneven distribution of sample DNA between the four different sub-arrays (e.g. lower amounts of DNA result in higher Ct values, whereas higher amounts typically result in lower Ct values). Hence, the protocol was revised and the steps following sample pre-amplification examined.

After pre-amplification, the sample DNA was diluted and then combined with TaqMan OpenArray Real-Time PCR Master Mix (described in **Section 2.5.3.1** in **CHAPTER 2**). The mixture was then equally distributed between four wells of a 384-well plate and from there dispensed into four dedicated sub-arrays by a robotic system (see **Figure A.10** in **Appendix A**). ThermoFisher recommended to combine sample DNA and Master Mix by gentle pipetting rather than vortexing, to avoid damage to reaction components by thorough mixing. However, improper mixing may have caused unequal loading of sample

DNA between wells and therefore between sub-arrays, which creates several inevitable problems during the analysis.

Firstly, an unequal distribution of sample DNA between sub-arrays is problematic when normalising copy number assay Ct values to the reference Ct value (TERT). During Phase 1, TERT was co-amplified along with each copy number assay. Similarly, during Phase 2 and Phase 3, TERT was amplified in the same sub-array as all other copy number assays in a sample. In contrast, in arrays utilised during Phase 4, TERT was spotted in a single copy on sub-array D and Ct values obtained from all copy number assays/sub-arrays were normalised to the same reference value.

Secondly, spotting of copy number assays in chromosome order (from 1 - 22, X and Y) may have further distorted copy number results and let to the characteristic profiles displaying a stepwise increase or decrease in CCNs.

Lastly, due to possible differences in DNA distribution between sub-arrays in test samples as well as reference samples, normalisation to reference data sets during the final stage of data processing might have further had a negative impact on accurate CCN prediction.

To address these issues, a new array for 24-CCN analysis was designed during Phase 5 of protocol development with the aim of reducing the impact of unequal sample loading between different sub-arrays. The same assays utilised during Phase 4 were used for the new array design, however, instead of spotting assays in chromosome order (from 1 - 22, X and Y), all assays for each chromosome were equally distributed between the four sub-arrays (**Figure 3.27**). For example, for chromosome 1, assays 1.1 and 1.2 were

spotted on sub-array A, assays 1.3 and 1.4 were spotted on sub-array B, assays 1.5 and 1.6 were spotted on sub-array C and assays 1.7, 1.8 and 1.9 were spotted on sub-array D.

Furthermore, the reference assays, TERT and RNase P, were omitted altogether and a new algorithm for data analysis was developed which did not rely on normalisation to a single reference assay. Similarly, the three assays targeting the mitochondrial genome (M.1, M.2 and M.3) were distributed between sub-arrays A, B and C. Furthermore, to allow for a more comprehensive analysis of the DiGeorge microdeletion region, four more assays (total of seven) were included in the array design, replacing the two reference assays and one assay targeting each of the sex chromosomes. Again, assays targeting the microdeletion region were distributed between the four sub-arrays. Information on additional assays is provided in **Table A.10** in **Appendix A**.

The newly designed array was then tested on cell samples which consisted of three and five cells. In addition, a large number of single-cell samples (frozen as well as freshly isolated) was processed to test if assessment of 24 chromosomes yields better results in single-cell samples as compared to the results obtained after testing of seven chromosomes only (**Figure 3.28**). Cell lysis and multiplex pre-amplification was performed in a ~15 µl reaction volume. To ensure a more equal distribution of sample DNA between sub-arrays, sample DNA/Master Mix mixtures were briefly vortexed prior to the transfer to the 384-well plates.

All cell samples (114 three- and five-cell samples, 53 single-cell samples), including karyotypically normal female and male cells, were isolated from cell culture. In addition to the aneuploid cell lines utilised for validation experiments during previous phases (48,XXY,+21; 47,XYY; 48,XY,+16,+21; 46,XX,+Xq; 47,XX,+22; 45,X0; 47,XY,+13; 47,XY,+18),

cell samples were also isolated from five cell lines harbouring structural chromosome abnormalities. Three of these cell lines (46,XX,-5p; 46,XY,-10p; 46,XX,-13q;) were characterised by structural chromosome losses. Furthermore, two cell lines were derived from individuals affected by the DiGeorge microdeletion Syndrome. In one of the individuals (cell line: 46,XY,+20p,-22q11) the deletion was caused by an unbalanced translocation. In the second individual (cell line: 46,XX,-22q11) the syndrome was caused by the microdeletion. Exact karyotypes (according to the International System for Human Cytogenetic Nomenclature, ISCN) are provided in **Table 1** in **Appendix A**.

During previous stages of protocol development, the real-time qPCR data was manually analysed in Microsoft Excel. To reduce the time required for data analysis, a PERL script was developed (by ThermoFisher), which enabled automated data processing. The script was written according to the analysis algorithm outlined in the following section (**Section 3.3.5.2**) and validated during initial runs by comparing to results obtained after manual analysis in Microsoft Excel.

The developed script utilised the raw data file generated by the QuantStudio real-time qPCR cycler and a reference file, which contained Ct values of the female and male reference data sets. The PERL programme generated a Microsoft Excel file containing CCNs of each of the assessed samples in tabular, as well as graphical output.

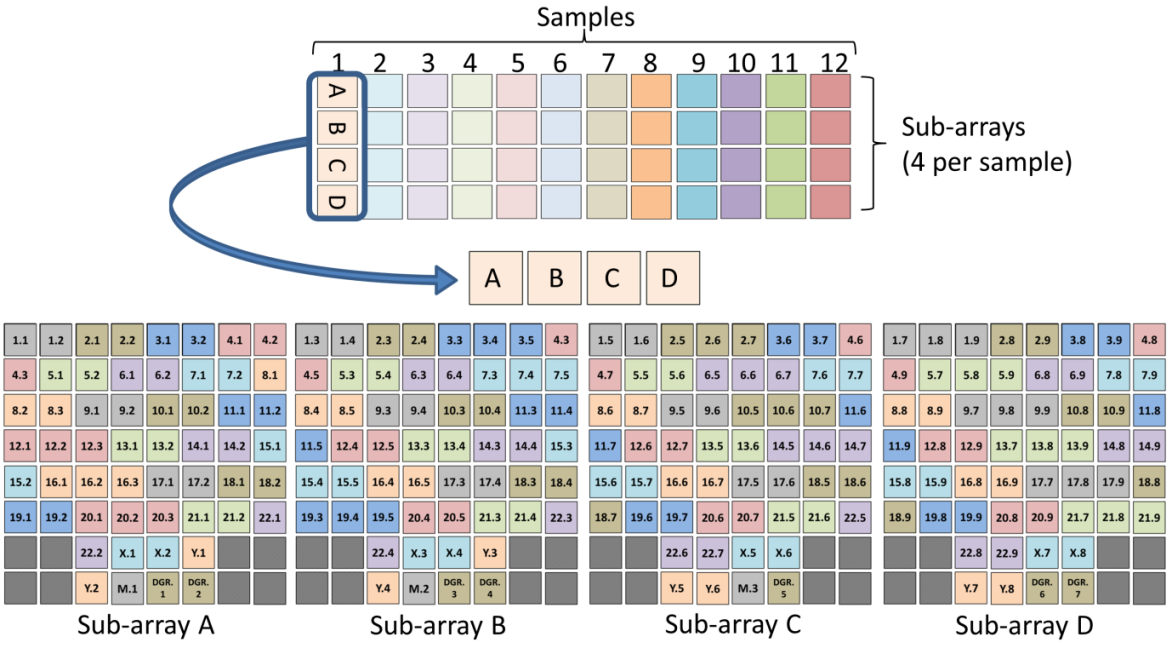


Figure 3.27: Revised array design for comprehensive CCN testing combined with DiGeorge microdeletion Syndrome testing and mtDNA quantification. A total of 12 samples can be processed on one array. Similarly to the previous array design (**Figure 3.24**), four sub-arrays (A - D) are utilised per sample. However, in contrast to the previous design, copy number assays of each chromosome were distributed between different sub-arrays. Assays targeting the DiGeorge microdeletion region as well as mtDNA assays were also distributed between sub-arrays. Trough-holes coloured in grey were left empty.

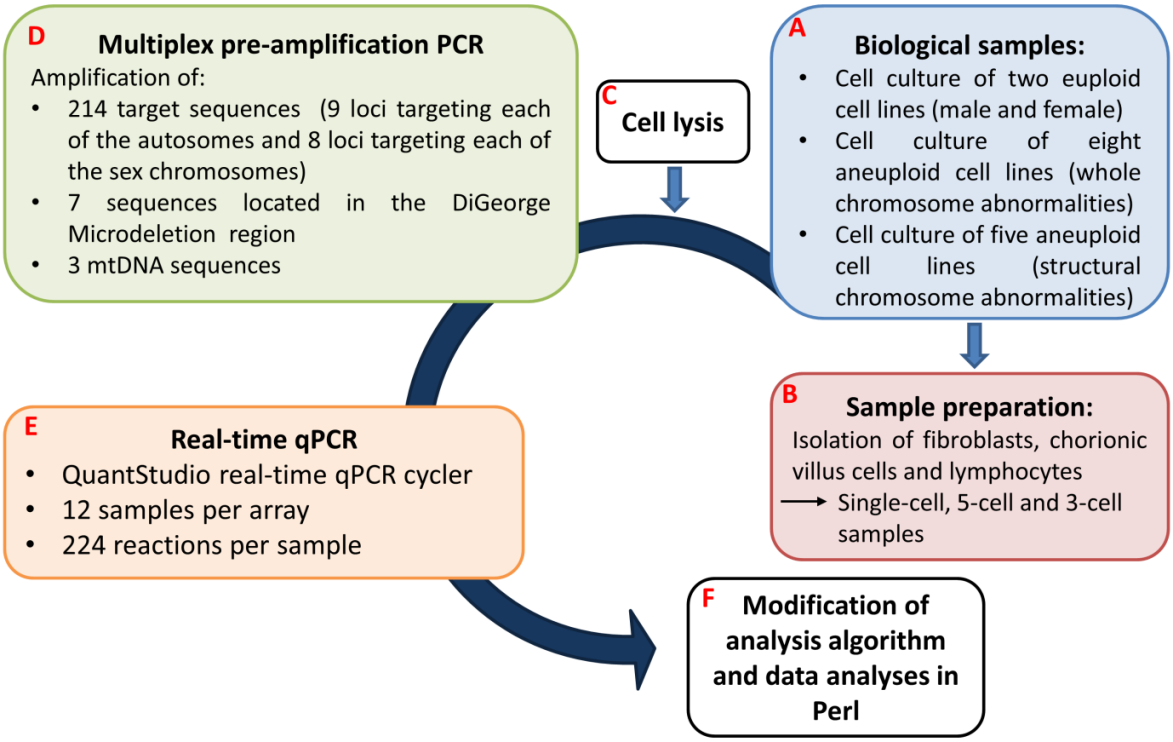


Figure 3.28: Flowchart describing Phase 5 of protocol development. A/B: Samples consisting of three and five as well as single cells were isolated from cell culture. **C:** Cell samples were subjected to cell lysis followed by (**D**) multiplex pre-amplification of 224 loci, including 214 loci for CCN analysis, seven regions located in the DiGeorge microdeletion region and three loci located in the mitochondrial genome. **E:** After enrichment of nuclear and mitochondrial sequences, each locus was amplified separately during real-time qPCR on the OpenArray platform (as described in **Figure 3.25**).**F:** CCN was calculated using the developed PERL script.

3.3.5.2 Data analysis Phase 5

The analysis algorithm used during Phase 4 was modified to accommodate the changes in the new array design. In order to lessen the impact of unequal sample loading between sub-arrays, Ct values were not normalised to a reference Ct value, but instead normalised to sub-array-specific normalisation factors. Normalisation factors for each sample/sub-array consisted of the mean Ct value obtained from the copy number assays spotted on each sub-array. Of note, Ct values derived from assays targeting the sex chromosomes, the DiGeorge microdeletion region and the mtDNA were not included in normalisation factor calculations.

As previously described, the obtained $\Delta_{Ctassay}$ values were again converted to $2^{-\Delta ctassay}$ values. Similarly to previous analysis protocols, a female and male reference data set consisting of data derived from a karyotypically normal female and male was established. Each reference data set consisted of eight female (4 x 3 cells and 4 x 5 cells) and eight male samples (4 x 3 cells and 4 x 5 cells).

After $2^{-\Delta Ctassay}$ normalisations, which was performed as previously described, the sum of the corrected $2^{-\Delta ctassay}$ values was calculated for each chromosome and a specific value (in %) assigned to each of the 24 chromosomes by dividing each $2^{-\Delta ctchromosome}$ value by the total amount of all $2^{-\Delta Ctassay}$ values, multiplied by 100 (same as previously described). The exact copy number of each chromosome was determined by normalising to reference data set values (as outlined before).

Computed CCNs were plotted in a graph depicting copy numbers of all 24 chromosomes and analysed manually by visually inspecting the copy number profiles. Autosomal chromosomes with copy numbers ranging from 1.5 - 2.5 were called euploid (CCN of two). Autosomal copy numbers above 2.5 were identified as trisomies (CCN of three). If values of chromosomes X and Y were in the range of 1.5 - 2.5, a copy number of two was assigned. If chromosome X and Y values were below 1.5, a copy number of one was assigned.

In addition to CCN analysis, a slightly modified algorithm for the analysis of the DiGeorge microdeletion was developed. To assess presence or absence of the microdeletion, the deleted locus was treated as a 25^{th} chromosome when calculation CCNs. The developed algorithm for DiGeorge microdeletion testing was based on the protocol outlined above. In brief, $\Delta_{Ctassay}$ values of all copy number assays, including assays targeting

the microdeletion region were calculated and converted into $2^{-\Delta ctassay}$ values. Normalisation steps were performed as previously described and the sum of the corrected $2^{-\Delta ctassay}$ values calculated for each of the chromosomes as well as the microdeletion region. Again, a specific value was assigned to each chromosome, including the microdeletion by dividing each of the 25 $2^{-\Delta Ctchromosome}$ values by the total amount of all $2^{-\Delta Ctassay}$ values, multiplied by 100. Results were again normalised to female and male reference data sets and plotted in graphs illustrating copy numbers of the 24 chromosomes as well as the DiGeorge microdeletion region. Previously established rules for CCN assignment were applied. Hence, if copy number of the DiGeorge locus was ≤1.5 the region was identified as being deleted.

3.3.5.3 Results Phase 5

Initially, a total of 114 cell samples (consisting of three or five cells) isolated from 15 cell lines were tested. Two cell lines were karyotypically normal (46,XX and 46,XY). Seven aneuploid cell lines carried whole chromosome abnormalities (48,XXY,+21; 47,XYY; 48,XY,+16,+21; 47,XX,+22; 45,X0; 47,XY,+13; 47,XY,+18) and six aneuploid cell lines carried structural chromosome abnormalities (46,XX,+Xq; 46,XY,+20p,-22q11; 46,XX,-5p; 46,XX,-22q11; 46,XY,-10p; 46,XX,-13q).

Obtained CCN results are presented in **Table 3.6**. Examples of 24-CCN profiles are shown in **Figures 3.29** (euploid samples), **3.30** (samples with whole chromosome abnormalities) and **3.31** (samples with structural chromosome abnormalities). Calculation of sensitivity and specificity is summarised in **Table A.11** in **Appendix A**.

Three samples (samples 35, 78 and 83) failed to amplify (2.6 %). The gender was assigned correctly in all samples. Of the 111 samples which gave a result, 110 (99.1 %) were diagnosed correctly as euploid or aneuploid, resulting in a sensitivity of 100 %. Specificity was slightly lower (97.9 %) due to one false-positive result (sample 7).

Among the 2664 (111 x 24) chromosomes analysed, copy number was assigned correctly to 2660 chromosomes (99.9 %). One aneuploidy was missed (sample 32) and three chromosomes were wrongly identified as abnormal (samples 7, 52 and 57), resulting in a sensitivity of 98.8 % and specificity of 99.9 %.

As stated before, the method cannot detect structural chromosome abnormalities since all copy number assays located on one specific chromosome are taken into account when calculating CCNs. Structural chromosome errors of the six cell lines which carried structural abnormalities varied in size and detection of these was largely dependent on the number of loci covering the affected chromosome areas (array CGH profiles obtained from cells derived from these cell lines are illustrated in **Figures A.11**, **A.12**, **A.13**, **A.14** and **A.15** in **Appendix A**).

For example, a monosomy of chromosome 13 was detected in all cell samples isolated from the 46,XX,-13p cell line because all of the nine copy number assays targeted regions located in the affected chromosome region. Furthermore, in about half of the samples where at least four loci covered the affected chromosome region, a loss/gain was detected. In contrast, in samples derived from the 46,XY,-10p cell line chromosome 10 appeared to be unaffected by an aneuploidy because only one of the assessed loci was located in the deleted chromosome region.

In addition to 24-CCN analysis, all three- and five-cell samples processed during Phase 5 were tested for presence or absence of the DiGeorge microdeletion. Presence of only one copy of the DiGeorge locus was detected in all 14 cell samples isolated from the two lines derived from two individuals with DiGeorge microdeletion Syndrome (8 x 46,XY,+20p,-22q11; 6 x 46,XX,-22q11). In contrast, the deletion was not detected in any of the other samples. Examples of '25-CCN' profiles (24 chromosomes + DiGeorge locus) are presented in **Figure 3.32**.

Following the good results obtained from the comprehensive analysis of cell samples consisting of three and five cells, the method was again tested on single cells (total: 53 samples). Initially, 41 single-cell samples were processed and analysed. These were isolated from the two karyotypically normal cell lines (46,XX and 46,XY), from seven aneuploid cell lines carrying whole chromosome abnormalities (48,XXY,+21; 47,XYY; 48,XY,+16,+21; 47,XX,+22; 45,X0; 47,XY,+13; 47,XY,+18) and six aneuploid cell lines carrying structural chromosome abnormalities (46,XX,+Xq; 46,XY,+20p,-22q11; 46,XX,-5p; 46,XX,-22q11; 46,XY,-10p; 46,XX,-13q). Following isolation, these samples were stored at -80 °C (usual procedure). To verify that freezing and thawing procedures as well as sample storage has no impact on CCN assignment, 12 more single-cell samples were processed immediately after isolation from cell culture (without freezing).

CCN results obtained from 'frozen' and 'fresh' single-cell samples are summarised in **Tables 3.7** and **3.8**, respectively. Examples of 24-CCN profiles of 'frozen' samples are shown in **Figures 3.33** (euploid samples), **3.34** (samples with whole chromosome abnormalities) and **3.35** (samples with structural chromosome abnormalities). Examples of 'fresh' single-cell sample results are illustrated in **Figure 3.36**. Calculation of test sensitivity

and specificity in 'frozen' cells is summarised in **Table A.12** in **Appendix A**. No calculations were performed in 'fresh' samples due to the small sample size.

The method did not give good results in 'frozen' samples consisting of one cell. One sample (sample 27) failed to amplify. Of the remaining 40 samples, only 30 (75.0 %) were diagnosed correctly as euploid or aneuploid. Although sensitivity was 100 %, specificity was greatly reduced (50.0 %).

Among the 960 (40 x 24) chromosomes analysed, copy number was wrongly assigned to 69 chromosomes (7.2 %), resulting in a sensitivity of 95.8 % and specificity of 95.2 %. Similar results were obtained for 'fresh' samples. One third of the samples (4 / 12; 33 %) was falsely identified as aneuploid.

Table 3.6: Results obtained from three- and five-cell samples derived from two euploid and 13 different aneuploid cell lines

Samples	Cells	Karyotype		Agreement
		Expected	Real-time qPCR	
Fibroblast samples from karyotypically normal individuals				
1	3	46,XX	46,XX	Yes
2	3		46,XX	Yes
3	3		46,XX	Yes
4	3		46,XX	Yes
5	3		46,XX	Yes
6	3		46,XX	Yes
7	3		45,XX,-4	No
8	3		46,XX	Yes
9	5		46,XX	Yes
10	5		46,XX	Yes
11	5		46,XX	Yes
12	5		46,XX	Yes
13	5		46,XX	Yes
14	5		46,XX	Yes
15	5		46,XX	Yes
16	3	46,XY	46,XY	Yes
17	3		46,XY	Yes

18	3		46,XY	Yes
19	3		46,XY	Yes
20	3		46,XY	Yes
21	3		46,XY	Yes
22	3		46,XY	Yes
23	3		46,XY	Yes
24	3		46,XY	Yes
25	5		46,XY	Yes
26	5		46,XY	Yes
27	5		46,XY	Yes
28	5		46,XY	Yes
29	5		46,XY	Yes
30	5		46,XY	Yes
31	5		46,XY	Yes
Fibroblast and chorionic villus samples from aneuploid cell lines (whole chromosome abnormalities)				
32	3	48,XXY,+21	47,XXY	Partial
33	3		48,XXY,+21	Yes
34	3		48,XXY,+21	Yes
35	3		No amplification	No result
36	5		48,XXY,+21	Yes
37	5		48,XXY,+21	Yes
38	5		48,XXY,+21	Yes
39	5		48,XXY,+21	Yes
40	3	47,XYY	47,XYY	Yes
41	3		47,XYY	Yes
42	3		47,XYY	Yes
43	5		47,XYY	Yes
44	5		47,XYY	Yes
45	5		47,XYY	Yes
46	5		47,XYY	Yes
47	5		47,XYY	Yes
48	3	48,XY,+16,+21	48,XY,+16,+21	Yes
49	3		48,XY,+16,+21	Yes
50	3		48,XY,+16,+21	Yes
51	3		48,XY,+16,+21	Yes
52	3		47,XY,+16,-20,+21	Partial
53	5		48,XY,+16,+21	Yes
54	5		48,XY,+16,+21	Yes
55	5		48,XY,+16,+21	Yes
56	5		48,XY,+16,+21	Yes
57	5		49,XY,+9,+16,+21	Partial

58	3	47,XX,+22	47,XX,+22	Yes
59	3		47,XX,+22	Yes
60	3		47,XX,+22	Yes
61	5		47,XX,+22	Yes
62	5		47,XX,+22	Yes
63	5		47,XX,+22	Yes
64	5		47,XX,+22	Yes
65	5		47,XX,+22	Yes
66	5		47,XX,+22	Yes
67	3	45,X0	45,X0	Yes
68	3		45,X0	Yes
69	5		45,X0	Yes
70	5		45,X0	Yes
71	5		45,X0	Yes
72	3	47,XY,+13	47,XY,+13	Yes
73	3		47,XY,+13	Yes
74	5		47,XY,+13	Yes
75	5		47,XY,+13	Yes
76	5		47,XY,+13	Yes
77	3	47,XY,+18	47,XY,+18	Yes
78	3		No amplification	No result
79	3		47,XY,+18	Yes
80	5		47,XY,+18	Yes
81	5		47,XY,+18	Yes
82	5		47,XY,+18	Yes
Fibroblast and lymphocyte samples from aneuploid cell lines (structural chromosome abnormalities)				
83	3	46,XX,+Xq	No amplification	No result
84	3		47,XXX	Yes[a]
85	5		47,XXX	Yes[a]
86	5		47,XXX	Yes[a]
87	3	46,XY,+20p,-22q11 (microdeletion)	47,XY,+20	Yes[a]
88	3		46,XY	Yes[b]
89	3		46,XY	Yes[b]
90	3		46,XY	Yes[b]
91	3		46,XY	Yes[b]
92	3		46,XY	Yes[b]
93	5		46,XY	Yes[b]
94	5		47,XY,+20	Yes[a]
95	3	46,XX,-5p	45,XX,-5	Yes[c]
96	3		45,XX,-5	Yes[c]
97	5		46,XX	Yes[b]

98	5		45,XX,-5	Yes[c]
99	3	46,XX,-22q11 (microdeletion)	46,XX	Yes[b]
100	3		46,XX	Yes[b]
101	3		46,XX	Yes[b]
102	3		46,XX	Yes[b]
103	5		46,XX	Yes[b]
104	5		46,XX	Yes[b]
105	5	46,XY,-10p	46,XY	Yes[b]
106	3		46,XY	Yes[b]
107	5		46,XY	Yes[b]
108	5		46,XY	Yes[b]
109	3	45,XX,-13q	45,XX,-13	Yes[c]
110	3		45,XX,-13	Yes[c]
111	3		45,XX,-13	Yes[c]
112	5		45,XX,-13	Yes[c]
113	5		45,XX,-13	Yes[c]
114	3		45,XX,-13	Yes[c]

Samples 1 - 4, 9 - 12, 16 - 19 and 25 - 28 were included in female and male reference data sets. a = presence of three copies of the expected aneuploid chromosome was considered 'true-positive'. b = presence of two copies of the expected aneuploid chromosome was considered 'true-negative'. c = presence of one copy of the expected aneuploid chromosome was considered 'true-positive'.

Table 3.7: Results obtained from frozen single-cell samples derived from two euploid and 13 different aneuploid cell lines

Samples	Karyotype		Agreement
	Expected	Real-time qPCR	
Fibroblast samples from karyotypically normal individuals			
1	46,XX	46,XX	Yes
2		46,XX	Yes
3		46,XX	Yes
4		45,X0	No
5		45,X0	No
6		47,X0,+7,-20,+22	No
7	46,XY	46,XY	Yes
8		43,XY,-7,-21,-22	No
9		46,XY	Yes
10		45,XY,-5,-9,+22	No
11		46,XY,-9,+22	No
Fibroblast and chorionic villus samples from aneuploid cell lines (whole chromosome abnormalities)			
12	48,XXY,+21	45,XXY,-4,-5,+6,-13,+14,-19,+21	Partial

13	47,XYY	48,XYY,+17	Partial
14	48,XY,+16,+21	48,XY,+16,+21	Yes
15		48,XY,+16,+21	Yes
16		47,XY,+21	Partial
17	47,XX,+22	46,XX,-4,+13,-15,+22	Partial
18		46,XX,+7,-14,-21,+22	Partial
19	45,X0	48,X0,+11,+18	Partial
20	47,XY,+13	48,XY,+13,+20	Partial
21		45,XY,-2,+13,-15	Partial
22	47,XY,+18	47,XY,+18	Yes
Fibroblast and lymphocyte samples from aneuploid cell lines (structural chromosome			
23	46,XX,+Xq	48,XX,+9,+13	No[b]
24	46,XY,+20p,-22q11 (microdeletion)	46,XY	Yes[b]
25		46,XY	Yes[b]
26		47,XY,+5,-8,+20	Partial[a]
27	46,XX,-5p	No amplification	No result
28		46,XX	Yes[b]
29		45,XX,-5	Yes[c]
30		46,XX,-5,-8	Partial[c]
31		46,XX,-5,+22	Partial[c]
32	46,XX,-22q11 (microdeletion)	45,XX,-14	No[b]
33		47,XX,-3,+8,+22	No[b]
34	46,XY,-10p	45,XY,-17	No[b]
35		46,XY	Yes[b]
36		46,XY	Yes[b]
37	45,XX,-13q	45,XX,-13	Yes[c]
38		44,XX,-13,-22	Partial[c]
39		45,XX,-13	Yes[c]
40		46,XX,+7,-13	Partial[c]
41		45,XX,-13	Yes[c]

Female and male reference data sets were identical to sets used with previous samples (see **Table 3.6**). a = presence of three copies of the expected aneuploid chromosome was considered 'true-positive'. b = presence of two copies of the expected aneuploid chromosome was considered 'true-negative'. c = presence of one copy of the expected aneuploid chromosome was considered 'true-positive'.

Table 3.8: Results obtained from freshly isolated single-cells derived from two euploid and four different aneuploid cell lines

Samples	Karyotype		Agreement
	Expected	Real-time qPCR	
Fibroblast samples from karyotypically normal individuals			

1	46,XX	46,XX	Yes
2		48,XX,+1,+9	No
3		47,XX,+11,-14,+22	No
4	46,XY	46,XY	Yes
5		45,XXY,-2,+10,-11,+12,+13,-17,-18,-19	No
6		45,XY,+3,-5,-17,-19,+20	No
Fibroblast samples from aneuploid cell lines			
7	48,XXY,+21	47,XXY,+19,+21	Partial
8	47,XX,+22	47,XX,+22	Yes
9	45,X0	45,X0	Yes
10		47,X0,+3,-5,+8,+13,-19	Partial
11	47,XY,+18	47,XY,+8,+18	Partial
12		47,XY,-7,+12,-13,+18,+21	Partial

Female and male reference data sets were identical to sets used with previous samples (see **Table 3.6**).

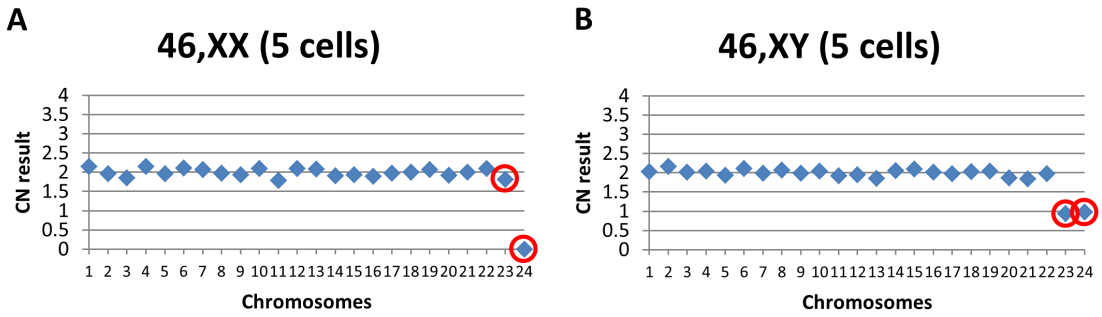


Figure 3.29: Examples of real-time qPCR 24-CCN profiles of euploid cell samples. Profiles were generated using the PERL programme. Blue diamond-shaped signs indicate CCNs. Chromosomes labelled '23' and '24' refer to chromosomes X and Y, respectively. Red circles highlight sex chromosomes. Pictured cell line profiles: **A:** 46,XX; **B:** 46,XY.

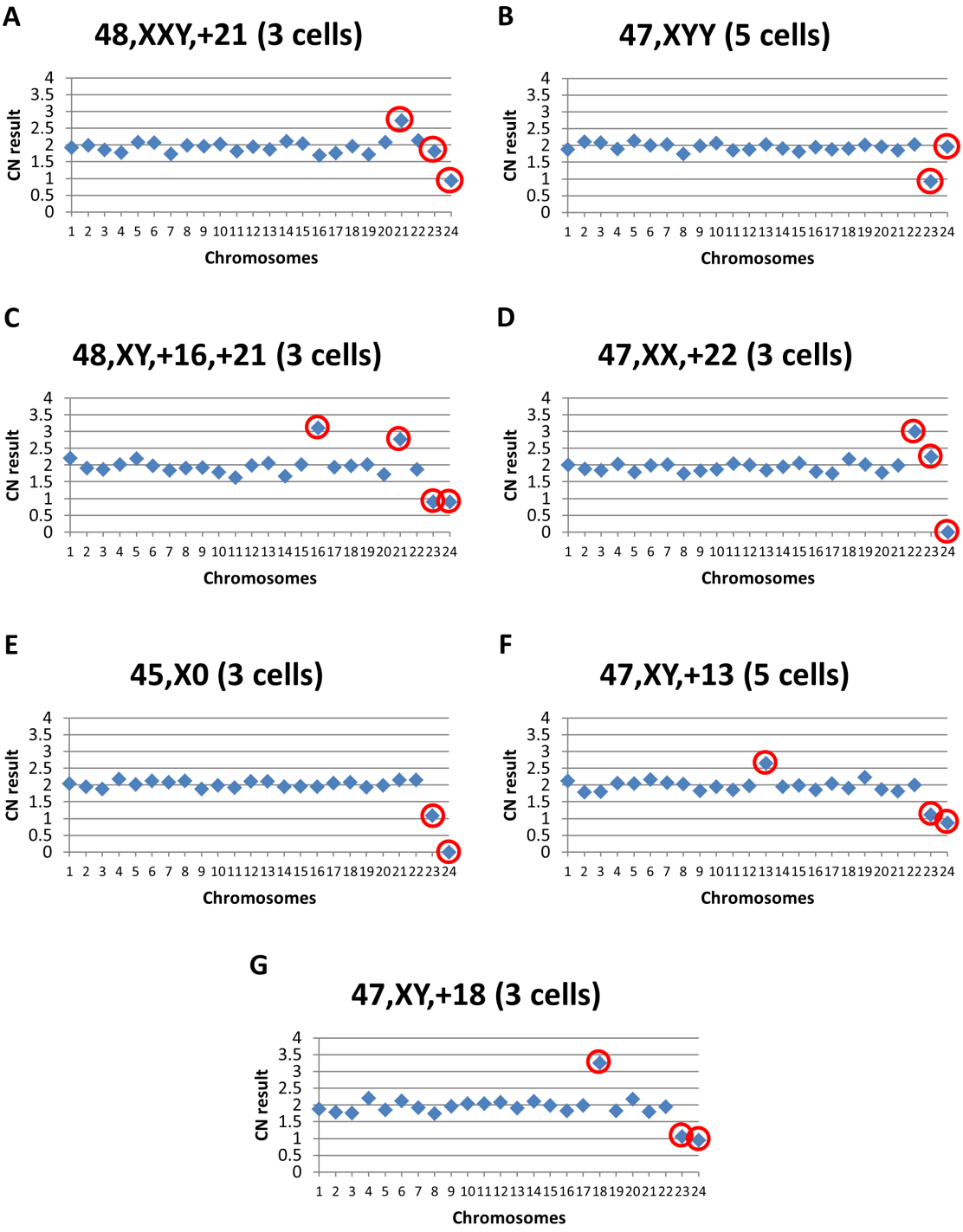


Figure 3.30: Examples of real-time qPCR 24-CCN profiles of aneuploid cell samples carrying aneuploidies affecting entire chromosomes. Profiles were generated using the PERL programme. Blue diamond-shaped signs indicate CCNs. Chromosomes labelled '23' and '24' refer to chromosomes X and Y, respectively. Red circles highlight sex chromosomes and expected aneuploid chromosomes. Pictured cell line profiles: **A:** 48,XXY,+21; **B:** 47,XYY; **C:** 48,XY,+16,+21; **D:** 47,XX,+22; **E:** 45,X0; **F:** 47,XY,+13; **G:** 47,XY,+18.

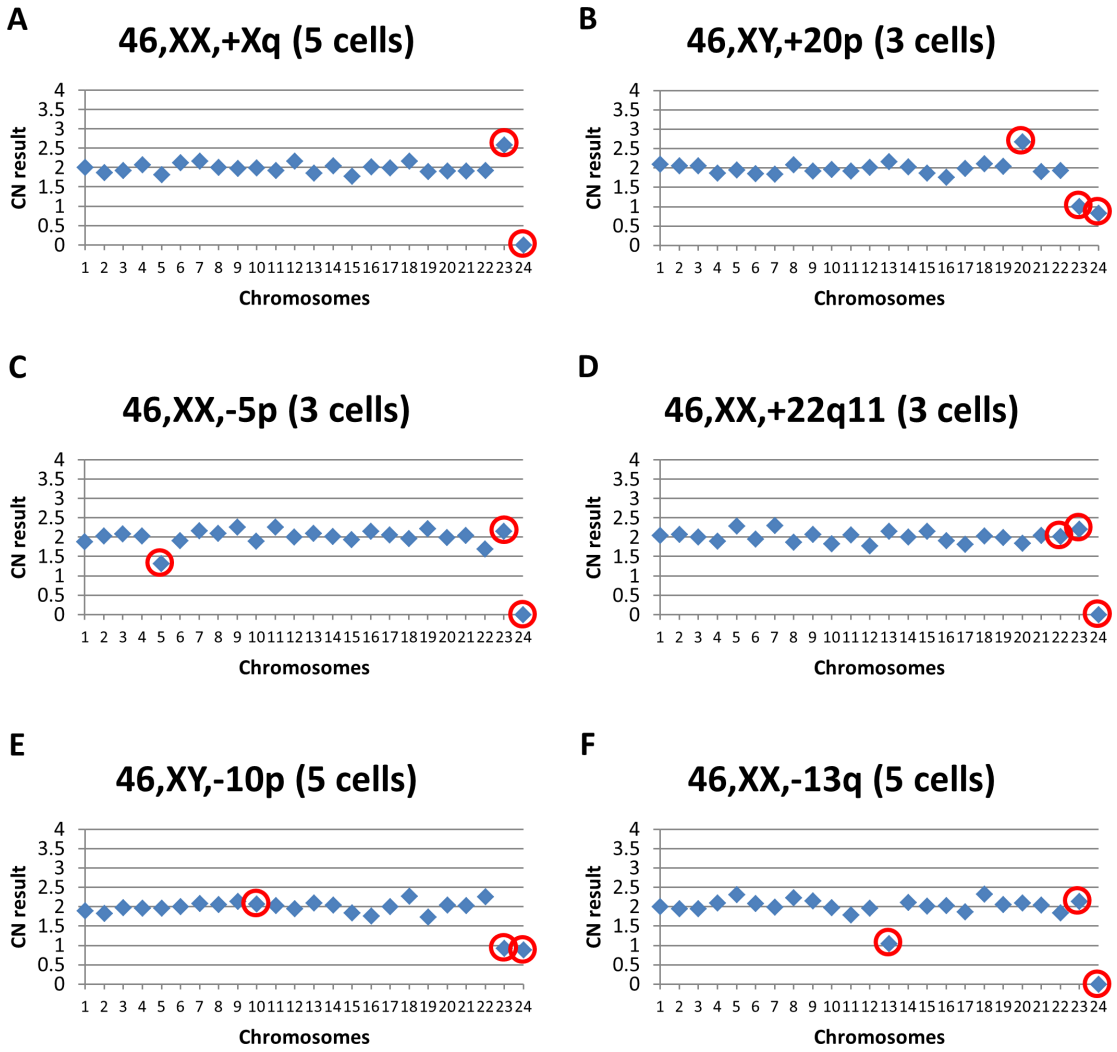


Figure 3.31: Examples of real-time qPCR 24-CCN profiles of aneuploid cell samples carrying aneuploidies affecting parts of chromosomes. Profiles were generated using the PERL programme. Blue diamond-shaped signs indicate CCNs. Chromosomes labelled '23' and '24' refer to chromosomes X and Y, respectively. Red circles highlight sex chromosomes and expected aneuploid chromosomes. Pictured cell line profiles: **A:** 46,XX,+Xq; **B:** 46,XY,+20p; **C:** 46,XX,-5p; **D:** 46,XX,+22q11; **E:** 46,XY,-10p; **F:** 46,XX,-13q.

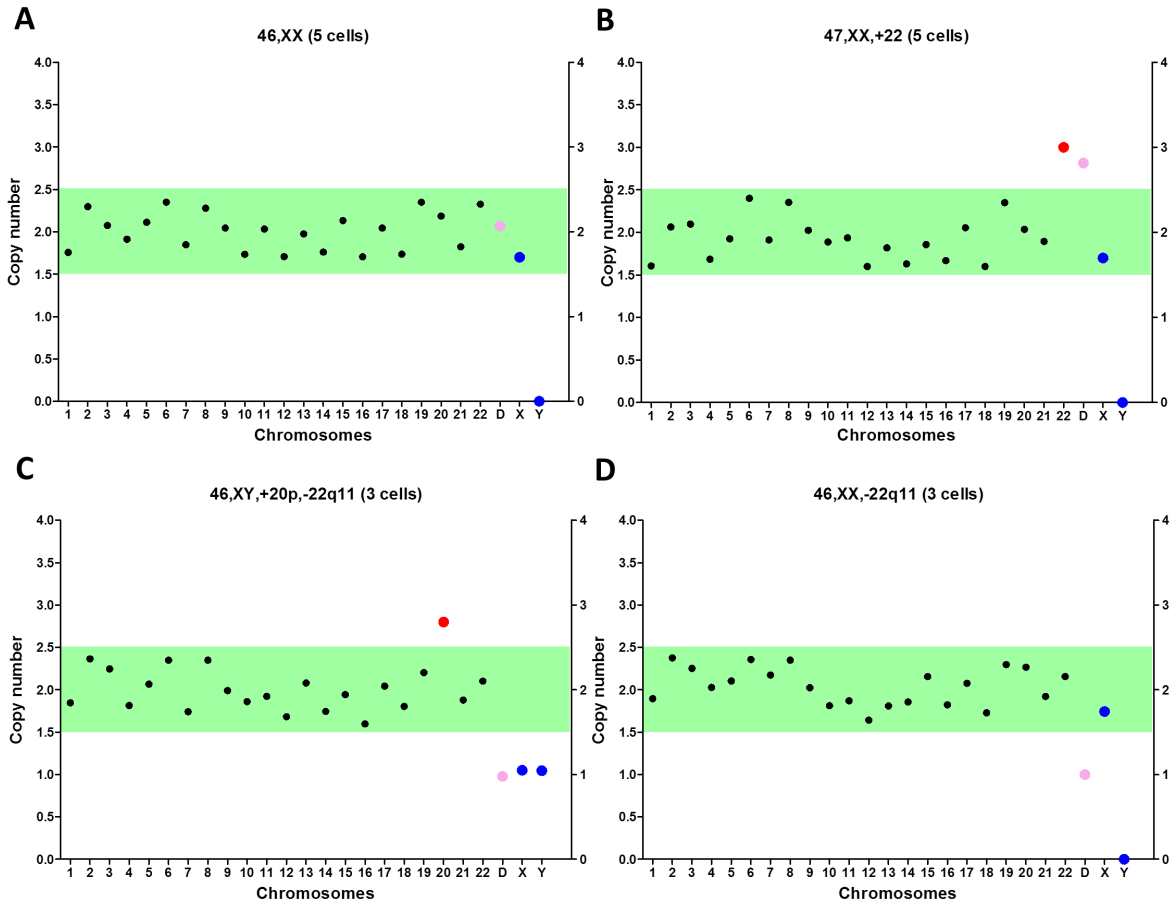


Figure 3.32: Examples of real-time qPCR '25-CCN' profiles illustrating copy number of the 24 chromosomes and the DiGeorge locus. Areas shaded in green indicate chromosome/DiGeorge locus copy number of two (ranging from copy number 1.5 - 2.5). Black dots illustrate the copy number of euploid autosomes. Blue dots illustrate the copy number of the sex chromosomes. Expected autosomal trisomies are illustrated by red dots. Pink dots show copy number of the DiGeorge locus (referred to as 'D'). Pictured cell line profiles: **A:** 46,XX; **B:** 47,XX,+22; **C:** 46,XY,+20p,-22q11; **D:** 46,XX,-22q11.

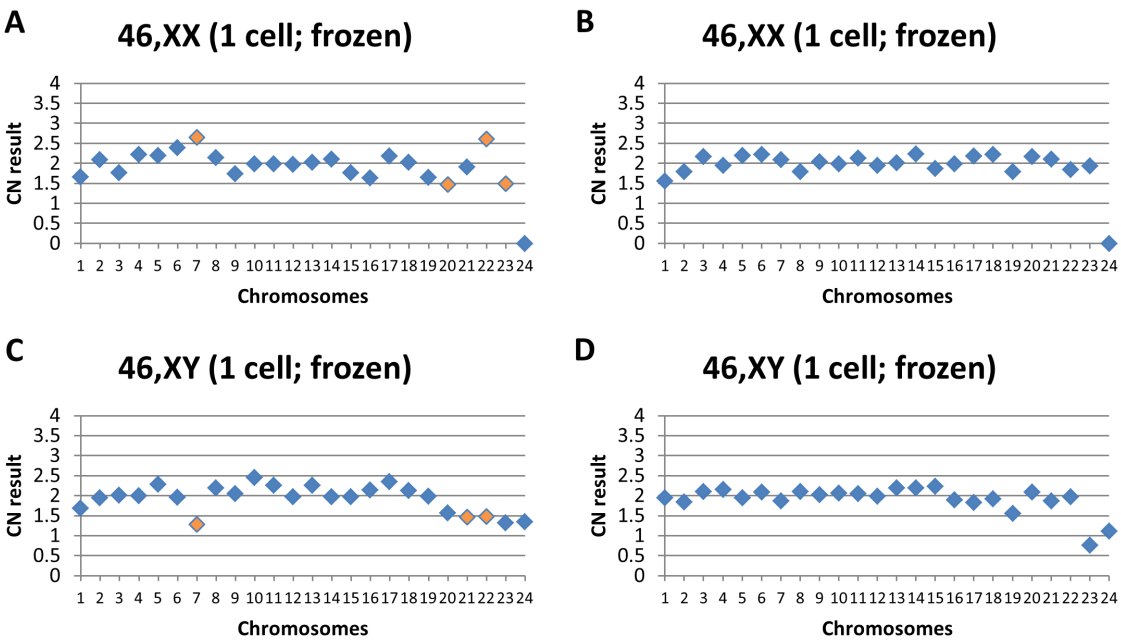


Figure 3.33: Examples of real-time qPCR 24-CCN profiles of euploid cell samples consisting of a single cell. Profiles were generated using the PERL programme. Diamond-shaped signs indicate CCNs. Orange diamond-shaped signs highlight chromosomes wrongly identified as aneuploid. Chromosomes labelled '23' and '24' refer to chromosomes X and Y, respectively. Pictured cell line profiles: **A/B:** 46,XX; **C/D:** 46,XY.

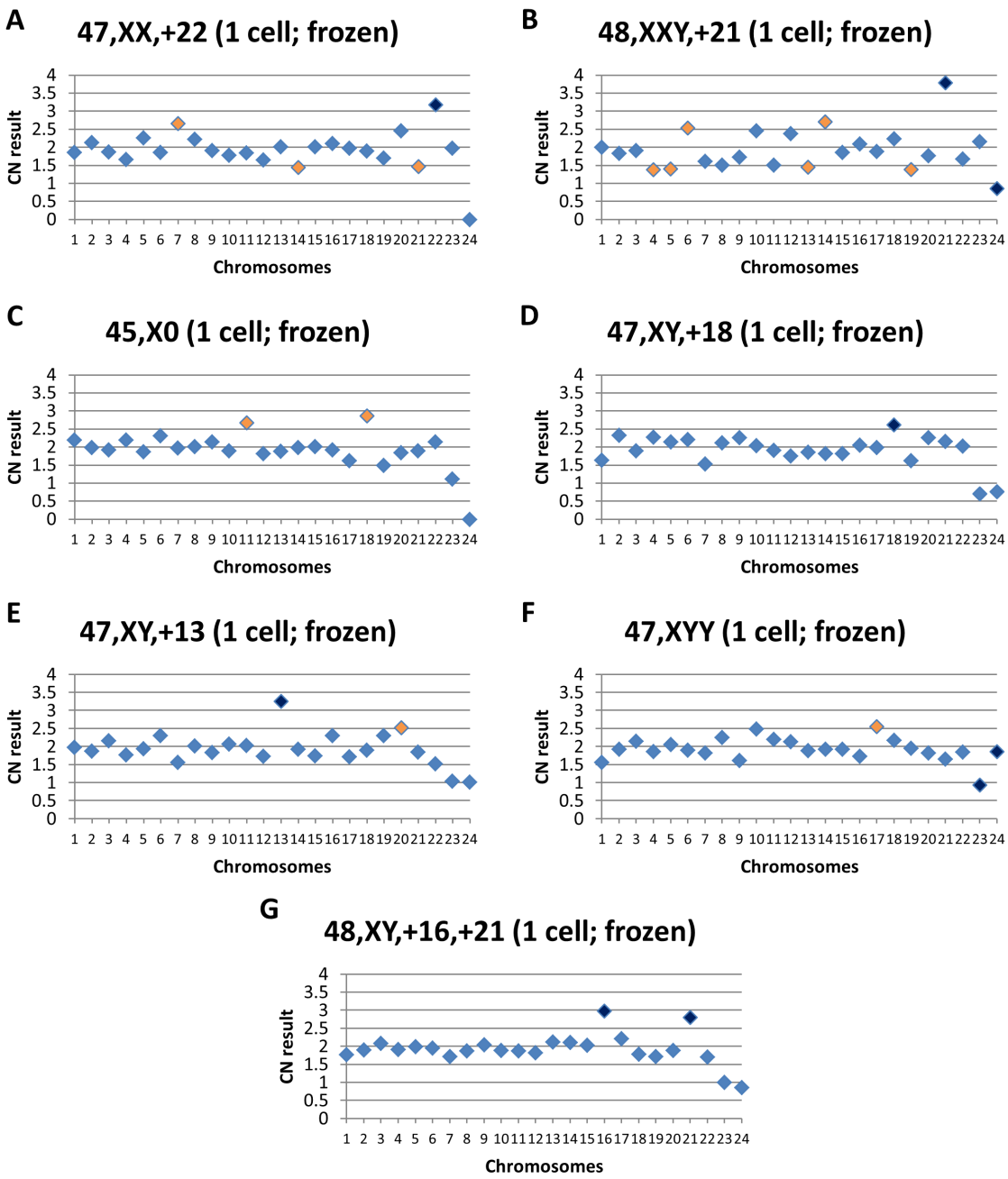


Figure 3.34: Examples of real-time qPCR 24-CCN profiles of aneuploid cell samples consisting of a single cell and carrying aneuploidies affecting entire chromosomes. Profiles were generated using the PERL programme. Diamond-shaped signs indicate CCNs. Orange diamond-shaped signs highlight chromosomes wrongly identified as aneuploid. Dark-blue diamond-shaped signs highlight expected aneuploid chromosomes. Chromosomes labelled '23' and '24' refer to chromosomes X and Y, respectively. Pictured cell line profiles: **A:** 47,XX,+22; **B:** 48,XXY,+21; **C:** 45,X0; **D:** 47,XY,+18; **E:** 47,XY,+13; **F:** 47,XYY; **G:** 48,XY,+16,+21.

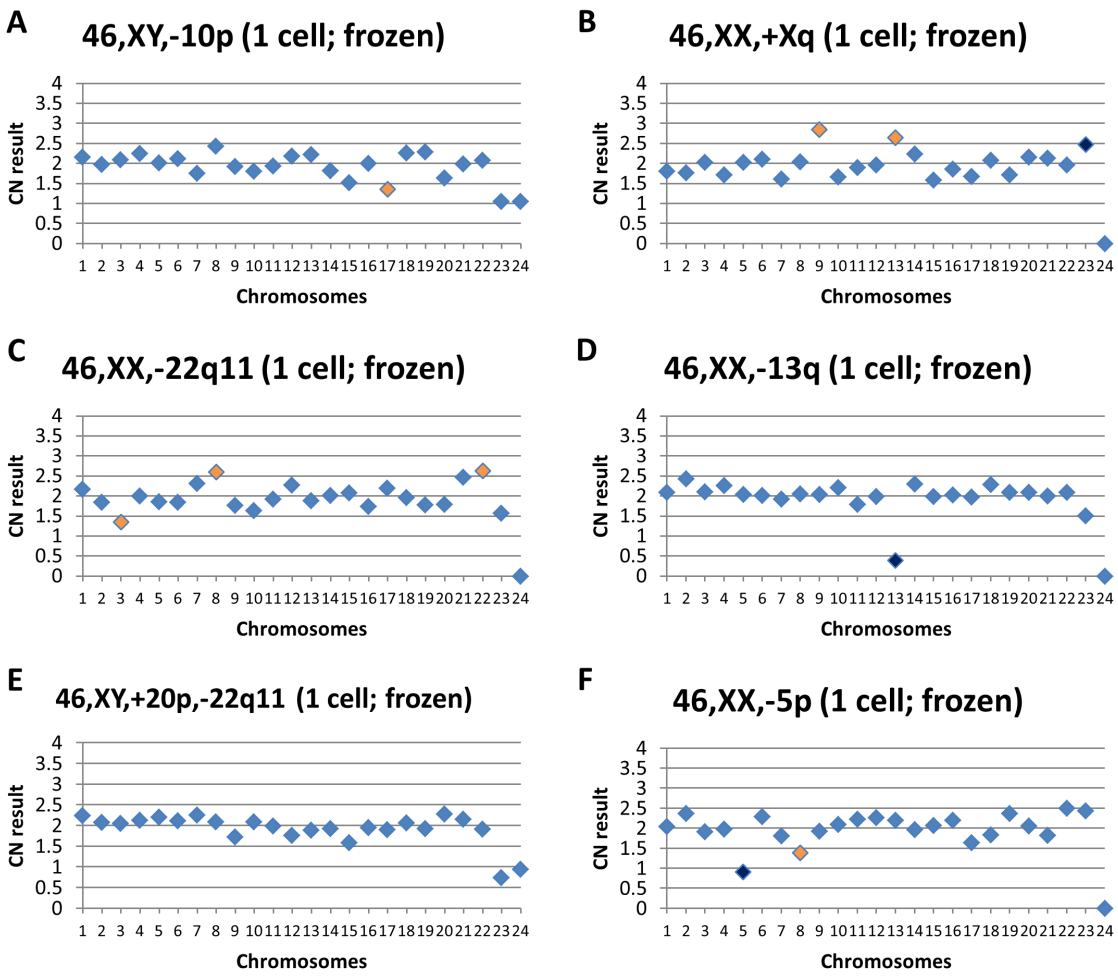


Figure 3.35: Examples of real-time qPCR 24-CCN profiles of aneuploid cell samples consisting of a single cell carrying aneuploidies affecting parts of chromosomes. Profiles were generated using the PERL programme. Diamond-shaped signs indicate CCNs. Orange diamond-shaped signs highlight chromosomes wrongly identified as aneuploid. Dark-blue diamond-shaped signs highlight expected aneuploid chromosomes. Chromosomes labelled '23' and '24' refer to chromosomes X and Y, respectively. Pictured cell line profiles: **A:** 46,XY,-10p; **B:** 46,XX,+Xq; **C:** 46,XX,-22q11; **D:** 46,XX,-13q; **E:** 46,XY,+20p,-22q11; **F:** 46,XX,-5p.

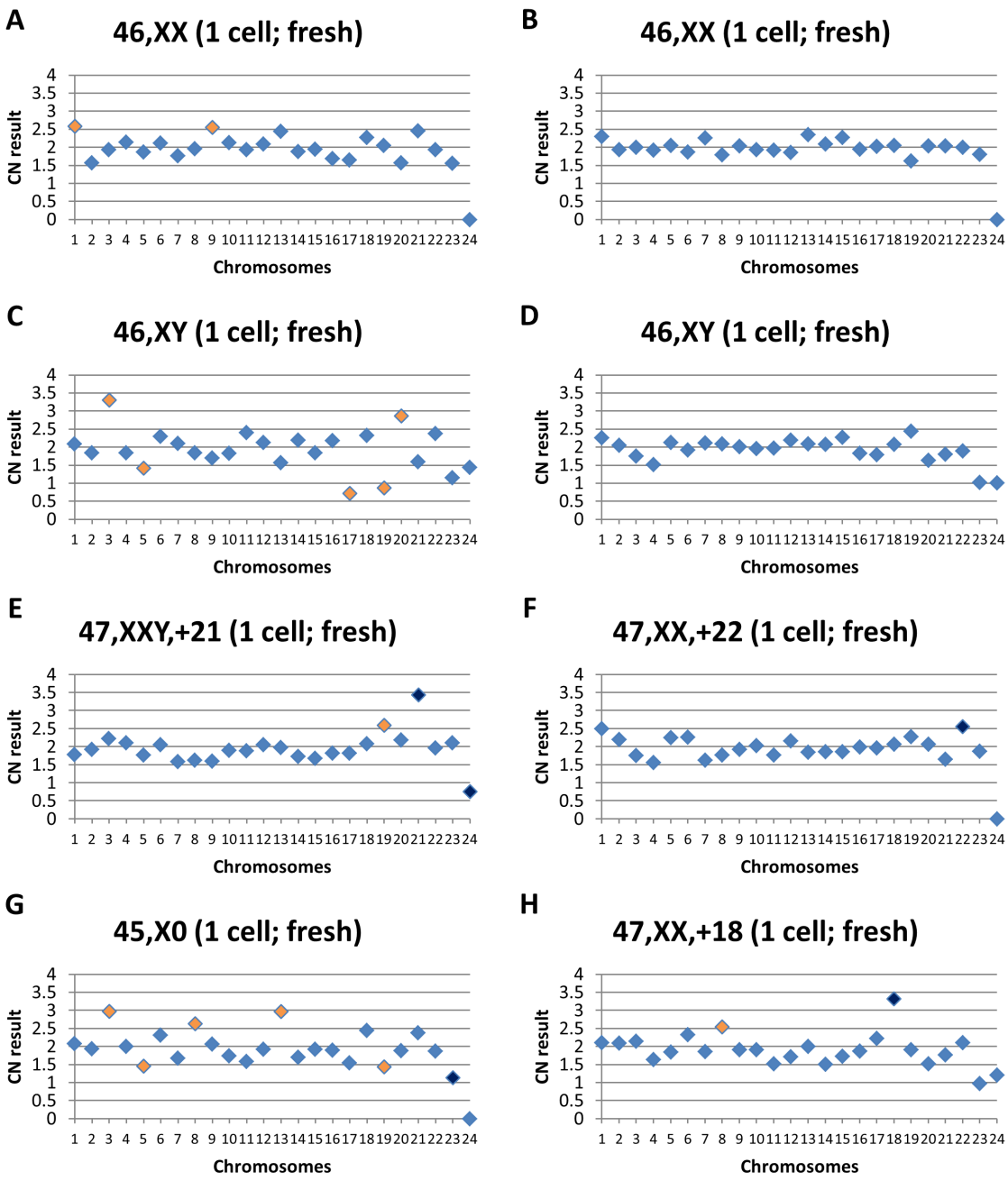


Figure 3.36: Examples of real-time qPCR 24-CCN profiles of freshly isolated euploid and aneuploid cell samples consisting of a single cell. Profiles were generated using the PERL programme. Diamond-shaped signs indicate CCNs. Orange diamond-shaped signs highlight chromosomes wrongly identified as aneuploid. Dark-blue diamond-shaped signs highlight expected aneuploid chromosomes. Chromosomes labelled '23' and '24' refer to chromosomes X and Y, respectively. Pictured cell line profiles: **A/B:** 46,XX; **C/D:** 46,XY; **E:** 47,XXY,+21; **F:** 47,XX,+22; **G:** 45,X0; **H:** 47,XX,+18.

3.3.6 Phase 6 - Pre-clinical validation study

3.3.6.1 Protocol design Phase 6

Following the high accuracy of the test obtained during Phase 5 of protocol development, a pre-clinical validation study was performed and the method tested on embryo biopsies.

A total of 52 donated embryos derived from 20 patients were included in the study. All embryos were biopsied at the blastocyst-stage. Biopsies and corresponding embryos were tubed separately. Entire embryos were tested for CCN using a well-established NGS-based CCS protocol and trophectoderm biopsies were tested using the developed real-time qPCR protocol. Although it is impossible to entirely avoid the issue of chromosomal mosaicism when testing preimplantation embryos, an effort was made to minimise this problem by restricting real-time qPCR tests to embryos where NGS-based CCS had not detected any evidence of mosaicism.

In addition to CCN testing, mtDNA quantities present in biopsied cells and corresponding embryos were determined and compared. Entire embryos were tested using a previously established and validated real-time qPCR protocol which utilises WGA products (see **Section 3.2.2**). MtDNA quantities present in embryo biopsies were inferred from the three mitochondrial assays (M.1, M.2 and M.3) spotted on the arrays utilised for real-time qPCR reactions.

Although mosaic embryos were excluded from the pre-clinical validation study, the real-time qPCR method's sensitivity in the detection of mosaic abnormalities was assessed.

Initially, cell samples consisting of mixtures of euploid and aneuploid cells at different ratios were assessed. Thereafter, real-time qPCR was performed on trophectoderm biopsies of the embryos previously determined via NGS to carry mosaic abnormalities.

3.3.6.2 Data analysis Phase 6

CCN in entire embryos following WGA and NGS-based CCS was determined as described in **Section 2.5.2** in **CHAPTER 2**.

Relative quantities of mtDNA present in WGA products of entire embryos were calculated using a modified version of the ΔΔCt method. Ct values of the mtDNA assays, 16s and MajArc, were initially normalised to the corresponding Alu Ct values:

$$\mathbf{\Delta Ct_{16s} = Ct_{16s} - Ct_{Alu}}$$

$$\mathbf{\Delta Ct_{MajArc} = Ct_{MajArc} - Ct_{Alu}}$$

After assigning a ΔCt value to each of the three replicates of the 16s and MajArc assays, the ΔCt_{mean} was calculated by dividing the sum of the three ΔCt values by three:

$$\mathbf{\Delta Ct_{mean} = (\Delta Ct_{replicate\ 1} + \Delta Ct_{replicate\ 2} + \Delta Ct_{replicate\ 3}) / 3}$$

The resulting ΔCt_{mean} values were used to determine the fold change by considering the ΔCt_{mean} values as the negative exponent of 2 ($2^{-\Delta Ct}$). Finally, relative mtDNA quantities were calculated by averaging the $2^{-\Delta Ct}$ values of 16s and MajArc.

Real-time qPCR CCN results of trophectoderm biopsies were generated as described in Phase 5 (**Section 3.3.5.2**) and normalised to the female and male reference data sets created during Phase 5 of protocol development. Furthermore, an algorithm for mtDNA quantification in the trophectoderm biopsies, assessed via real-time qPCR, was developed. Ct values of mtDNA assays M.1, M.2 and M.3 were initially normalised to the sample/sub-array-specific normalisation factors, which were calculated as described in **Section 3.3.5.2**. The obtained ΔCt_{assay} values were then converted to $2^{-\Delta Ctassay}$ values and the average of the M.1, M.2 and M.3 $2^{-\Delta Ctassay}$ values calculated.

3.3.6.2 Results Phase 6

Of the 52 embryos included in the study, 15 carried mosaic abnormalities only (according to NGS-based CCS performed in entire embryo) and were therefore excluded from the study. Obtained CCN results (NGS-VeriSeq and real-time qPCR) are presented in **Table 3.9**. Examples of 24-CCN profiles are shown in **Figure 3.37**. Sensitivity and specificity of the real-time qPCR test was again calculated on the basis of overall diagnostic accuracy (euploid or aneuploid sample) and on the basis of individual CCN assignment (euploid or aneuploid chromosome) in comparison to the NGS-VeriSeq results (**Table A.13** in **Appendix A**).

Of the 37 samples tested, eight samples failed to give a result (21.1 %; samples 1 - 4, 7, 13 and 35). Of note, the failure rate was unusually high and was most likely

caused by degenerated DNA present in the biopsies. Half of the failed samples were derived from 'poor quality' embryos. In addition, samples were shipped from the US and arrived at room temperature.

Of the 30 samples which gave a result, 29 (96.7 %) were correctly identified as euploid or aneuploid, resulting in a sensitivity of 100 % and slightly lower specificity of 96.2 % (due to one false-positive result; sample 19). A total of 720 chromosomes were assessed, of which 718 (99.7 %) were correctly identified. Two chromosomes were falsely called aneuploid, both in the same sample (sample 19). Therefore, sensitivity was 100 % and specificity 99.7 %.

In addition to CCN analysis, relative mtDNA quantities were determined in trophectoderm samples which gave a result during real-time qPCR and compared to the relative mtDNA content measured in the corresponding entire embryos.

Initially, correlation between the utilised mtDNA assays was assessed. **Figure 3.38 A** illustrates the correlation between the relative mtDNA quantities obtained from the 16s and MajArc assays which were utilised for mtDNA analysis in WGA products of entire embryos. **Figure 3.38 B** illustrates correlation between relative mtDNA quantities of assays M.1, M.2 and M.3 measured in trophectoderm biopsies. Importantly, assays used for mtDNA quantification performed equally well in both cases, which was evident by a very high and significant correlation between the different mtDNA quantities (16s versus MajArc: $r = 0.86$, $p < 0.0001$; M.1 versus M.2: $r = 0.91$, $p < 0.0001$; M.1 versus M.3: $r = 0.92$, $p < 0.0001$; M.2 versus M.3: $r = 0.93$; $p < 0.0001$) providing evidence that the utilised assays worked well.

Next, correlation between mean mtDNA quantities in trophectoderm biopsies and entire embryos was assessed (**Figure 3.39**). Overall a good correlation between biopsies and entire embryos was observed ($r = 0.45$, $p = 0.01$), suggesting that mtDNA quantities present in trophectoderm biopsies typically relate well to those present in the embryo proper.

Following the pre-clinical test validation, the possibility of detecting mosaic chromosome abnormalities was assessed. Initially, aneuploid/euploid cell line dilution experiments were performed whereby aneuploid cells were mixed with euploid cells to create samples consisting of five cells with 0 %, 20.0 %, 40.0 %, 60.0 % and 80.0 % mosaicism.

The obtained real-time qPCR results are summarised in **Table 3.10**. 24-CCN profiles of euploid cells mixed with aneuploid cells derived from cell lines 47,XX,+22, 48,XXY,+21 and 45,X0 are illustrated in **Figures 3.40**, **3.41** and **3.42**.

Interestingly, results obtained from the processed samples indicated that the real-time qPCR method is able to detect chromosomal mosaicism if it is present in about half of the sample's cells. For instance, the method was able to detect all expected aneuploidies when present at a rate of 60 % or higher (at least three out of five cells were aneuploid). Moreover, trisomy 22 in the cell sample with 47,XX,+22 cells was already detected at a level of 40 % (two out of five cells were aneuploid).

Next, real-time qPCR was performed in trophectoderm biopsies of the 15 embryos previously determined (via NGS) to carry mosaic abnormalities. NGS and real-time qPCR results are summarised in **Table 3.11**. Examples of NGS and real-time qPCR 24-CCN plots

obtained from entire embryos and corresponding trophectoderm biopsies, respectively, are illustrated in **Figures 3.43** and **3.44** and in **Figures A.16**, **A.17**, **A.18**, **A.19**, **A.20** and **A.21** in **Appendix A**.

Only few of the mosaic abnormalities observed via NGS in embryo reminders were also observed in trophectoderm biopsies following real-time qPCR analysis. For instance, embryo M.1 was identified to carry a mosaic gain of chromosome 4 which was confirmed via real-time qPCR (**Figure 3.43 A**). In contrast, mosaic monosomies of chromosomes 6 and 20 detected in embryo M.2 were not identified in the biopsy analysed via real-time qPCR. Similarly, mosaic abnormalities identified in embryos M.3 and M.4 were not detected in trophectoderm biopsies using real-time qPCR (**Figures 3.44 A** and **B**). Interestingly, however, the structural mosaic loss of part of the q-arm of chromosome 8 in embryo M.3 was detected via real-time qPCR, resulting in a loss of chromosome 8.

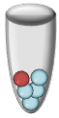
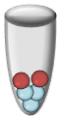
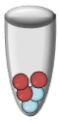
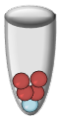
Table 3.9: NGS-VeriSeq and real-time qPCR results obtained from embryo specimens

Embryos	Karyotype		Agreement	Comment
	NGS-VeriSeq	Real-time qPCR		
1	46,XY	No amplification	NA	Poor quality
2	46,XX	No amplification	NA	-
3	46,XX	No amplification	NA	Poor quality
4	46,XY	No amplification	NA	-
5	46,XX	46,XX	Yes	-
6	46,XX	46,XX	Yes	-
7	46,XY	No amplification	NA	Poor quality
8	45.XY,-4,+8,-21	45,XY,-4,+8,-21	Yes	-
9	46,XX	46,XX	Yes	-
10	46,XX	46,XX	Yes	-
11	48,XX,+3(pentasomy),+21(mosaic)	47,XX,+3	Yes[a]	-
12	46,XY,-12q22qter	45,XY,-12	Yes[b]	-
13	46,XX	No amplification	NA	-
14	46,XY	46,XY	Yes	-
15	46,XY	46,XY	Yes	-
16	46,XX	46,XX	Yes	-

17	46,XX	46,XX	Yes	-
18	46,XY	46,XY	Yes	-
19	46,XY	46,XY,-5,+21	No	-
20	46,XY	46,XY	Yes	-
21	46,XX	46,XX	Yes	-
22	46,XX	46,XX	Yes	-
23	46,XX	46,XX	Yes	-
24	46,XX	46,XX	Yes	-
25	46,XY	46,XY	Yes	-
26	46,XY	46,XY	Yes	-
27	46,XY	46,XY	Yes	-
28	46,XY	46,XY	Yes	-
29	46,XY	46,XY	Yes	-
30	48,XY,+15,+16	48,XY,+15,+16	Yes	-
31	46,XX	46,XX	Yes	-
32	46,XX	46,XX	Yes	-
33	46,XX	46,XX	Yes	-
34	46,XX	46,XX	Yes	-
35	46,XX	No amplification	NA	Poor quality
36	46,XX	46,XX	Yes	-
37	46,XY	46,XY	Yes	-

NA = not applicable. a = real-time qPCR result of sample 11 was considered to be in agreement with the NGS-VeriSeq result, because trisomy 21 was mosaic. b = monosomy of chromosome 12 was considered true-positive.

Table 3.10: Real-time qPCR results of samples containing a mixture of euploid and aneuploid cell lines

Mosaicism		Aneuploid cell line		
		47,XX,+22[1]	**48,XXY,+21[2]**	**45,X0[1]**
	**20.0 %**	46,XX	46,XY	46,XX
	**40.0 %**	47,XX,+22	47,XY,+21	46,XX
	**60.0 %**	47,XX,+22	48,XXY,+21	45,X0
	**80.0 %**	47,XX,+22	48,XXY,+21	45,X0

1 = cell mixing was performed with cells from the 46,XX cell line. 2 = cell mixing was performed with cells from the 46,XY cell line.

Table 3.11: NGS-VeriSeq and real-time qPCR results obtained from mosaic embryo specimens

Embryos	Karyotype	
	NGS-VeriSeq (entire embryo)	**Real-time qPCR (biopsy)**
M.1	47,XX,+4(m)	47,XX,+4
M.2	44,XY,-6(m),-20(m)	46,XY
M.3	43,XX,-6(m),+8p,-8q,-16(m),-18(m),-21(m),+22(m)	45,XX,-8
M.4	46,XY,-9q (m)	46,XX
M.5	46,XY,-6q(m)	46,XY
M.6	47,XY,+6(m)	46,XY
M.7	45,XY,-21(m)	46,XY
M.8	45,XY,-18(m)	46,XY
M.9	46,XX+14q(m)	46,XX
M.10	46,XY,+11q(m)	46,XX
M.11	47,XX,-1q(m),+13q(m),+14q(m),+21(m)	46,XX
M.12	46,XX,-1p(m),+1p(m),+3q(m),-4p(m),-14q(m)	46,XX
M.13	45,XY,-13(m)	47,XY-13,+14,+16
M.14	47,XY,+3(m),-4q(m),-15(m),+22(m)	45,XY,-3,-4,+7
M.15	46,XX,-2p(m)	46,XX,-1,+3,+7,-12,+13,-17

m = mosaic. q = gain or loss of part or entire chromosome q-arm. p = gain or loss of part or entire chromosome p-arm.

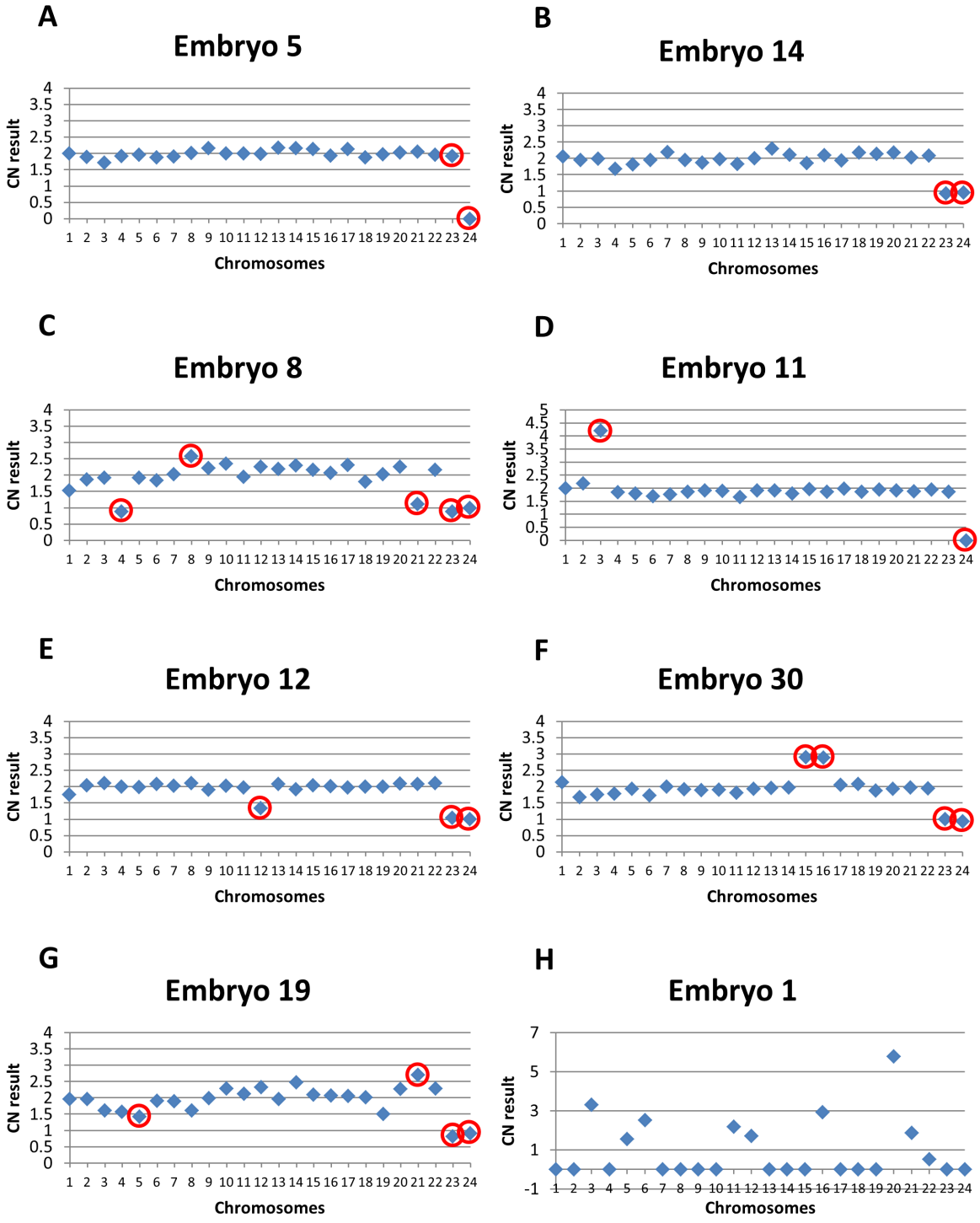
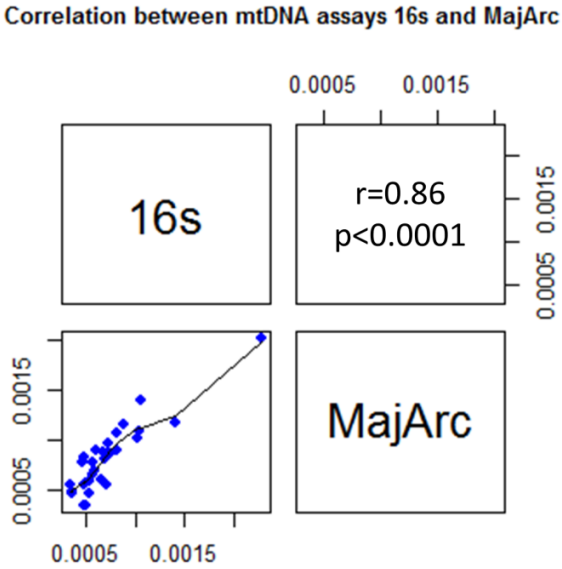


Figure 3.37: Examples of real-time qPCR 24-CCN profiles of trophectoderm biopsies. Profiles were generated using the PERL programme. Blue diamond-shaped signs indicate CCNs. Chromosomes labelled '23' and '24' refer to chromosomes X and Y, respectively. Red circles highlight sex chromosomes and detected aneuploid chromosomes. Profiles **A** and **B** show results of a euploid female and male embryo, respectively. Profiles **C**, **D**, **E**, **F** and **G** show results of aneuploid embryos. An example of a sample which failed to amplify is shown in profile **H**.

A



B

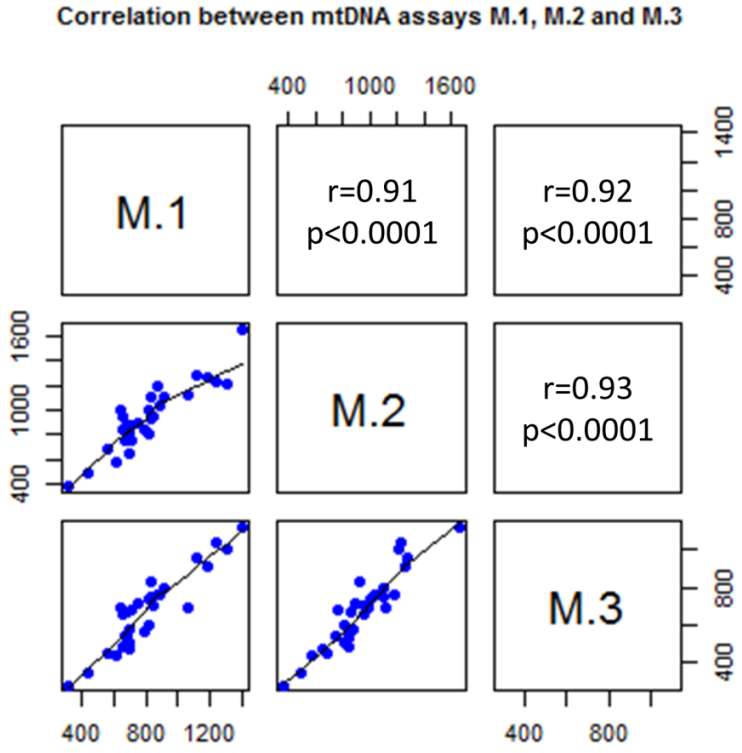


Figure 3.38: Scatterplot matrices illustrating correlations in mtDNA quantities between different assays. Blue symbols show calculated relative mtDNA quantities. **A:** Scatterplot illustrates correlation between assays 16s and MajArc which were used for mtDNA quantification in WGA products of entire embryos. r = Spearman's rank correlation coefficient with corresponding p-value. **B:** Scatterplot matrix illustrates correlation between assays (M.1, M.2 and M.3) utilised for mtDNA quantification in embryo biopsies. r = Pearson's rank correlation coefficients with corresponding p-values.

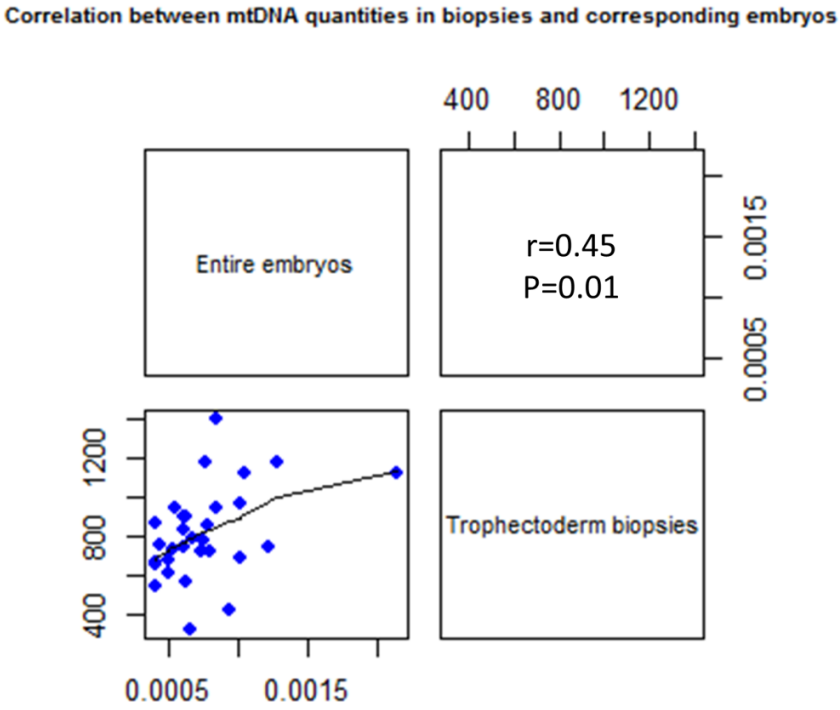


Figure 3.39: Scatterplot illustrating correlation of mtDNA content between trophectoderm biopsies and corresponding embryos. Blue symbols show calculated relative mtDNA quantities. r = Spearman's rank correlation coefficient with corresponding p-value.

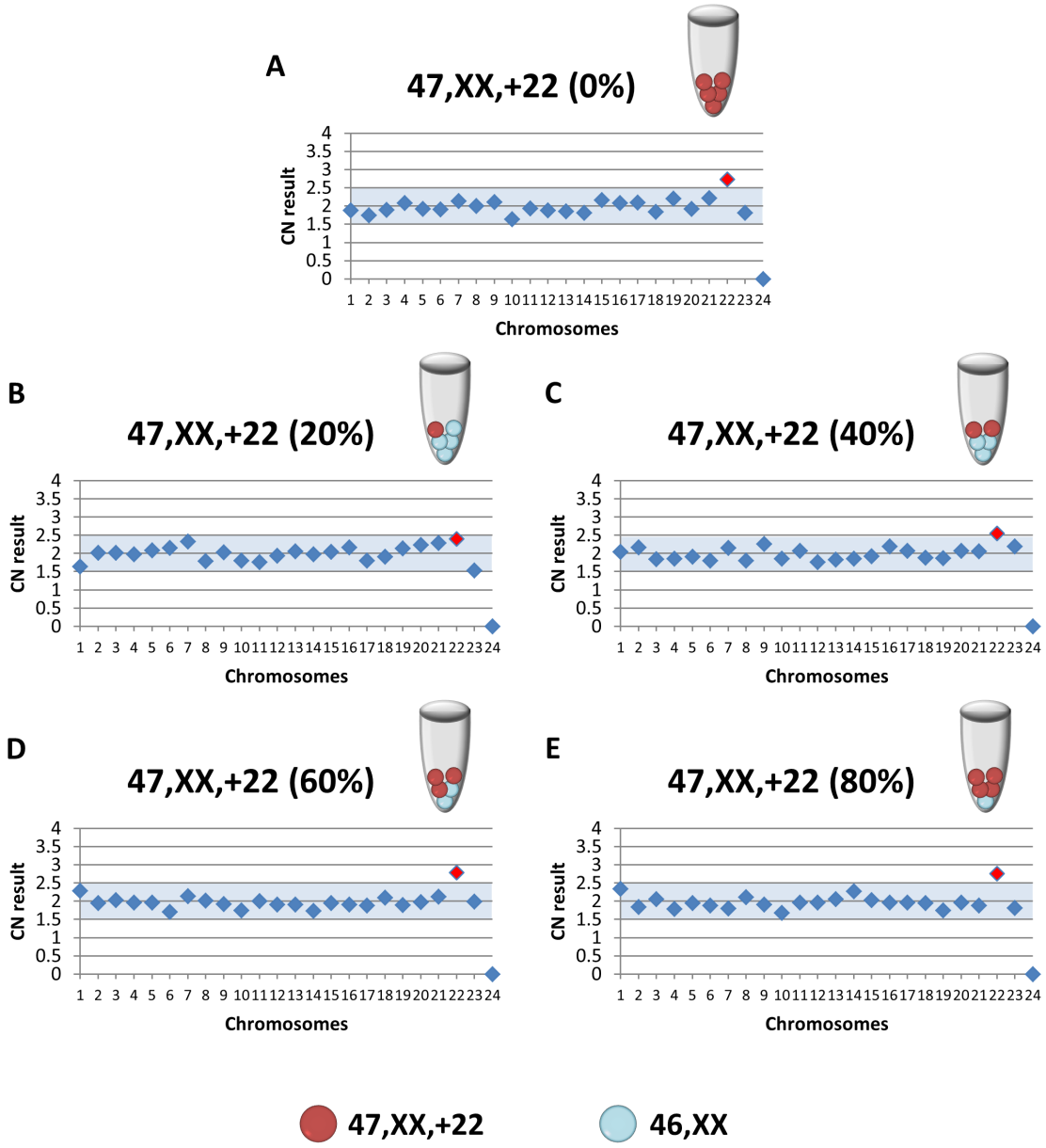


Figure 3.40: Real-time qPCR 24-CCN profiles of different levels of simulated mosaicism using the 47,XX,+22 and the 46,XX cell line. Profiles were generated using the PERL programme. Diamond-shaped signs indicate CCNs. Red diamond-shaped signs highlight expected aneuploid chromosome. Chromosomes labelled '23' and '24' refer to chromosomes X and Y, respectively. Profiles **A**, **B**, **C**, **D** and **E** refer to cell samples consisting of 0 %, 20.0 %, 40.0 %, 60.0 % and 80.0 % mosaicism, respectively. Each sample consisted of five cells.

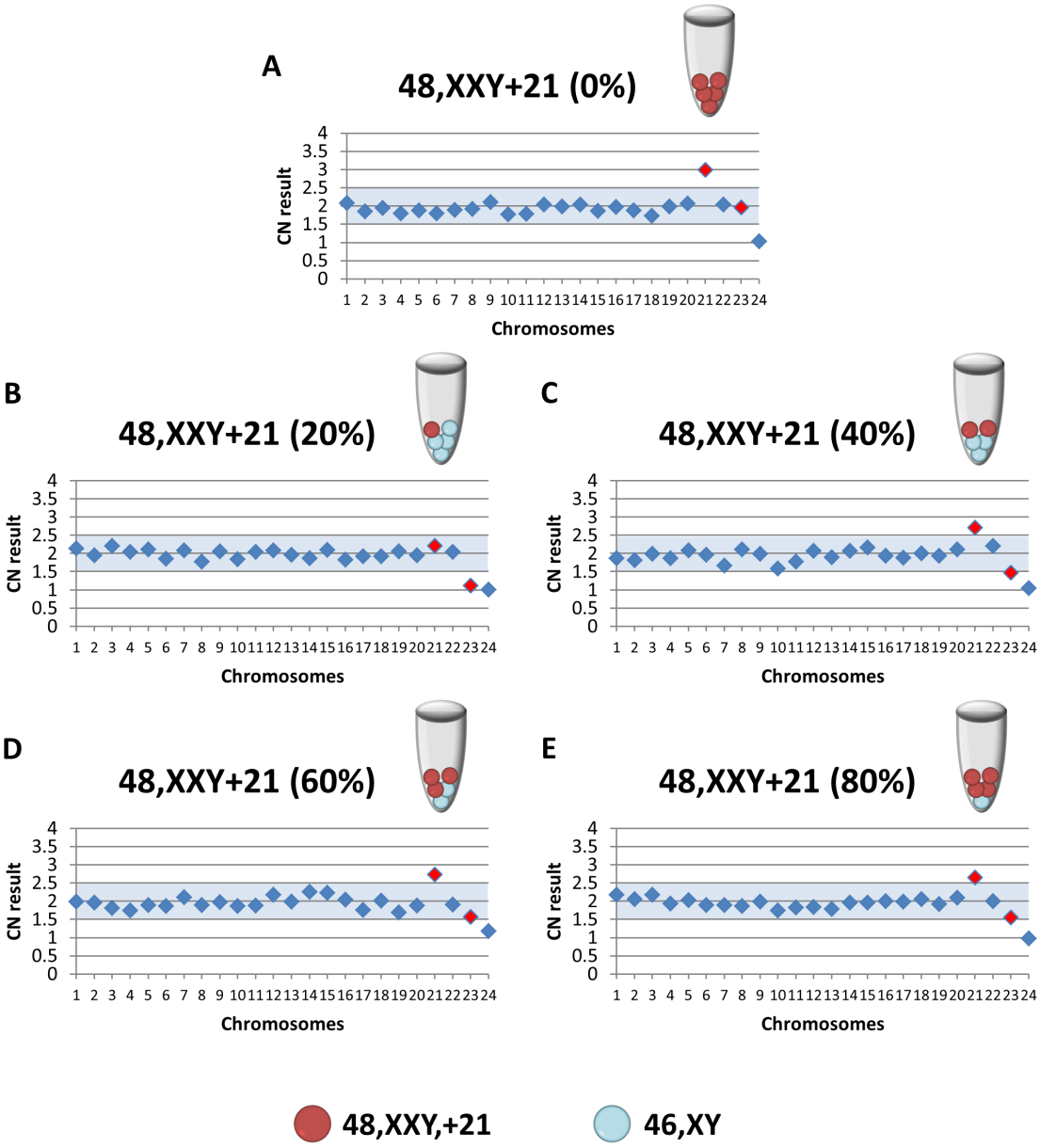


Figure 3.41: Real-time qPCR 24-CCN profiles of different levels of simulated mosaicism using the 48,XXY,+21 and the 46,XY cell line. Profiles were generated using the PERL programme. Diamond-shaped signs indicate CCNs. Red diamond-shaped signs highlight expected aneuploid chromosome. Chromosomes labelled '23' and '24' refer to chromosomes X and Y, respectively. Profiles **A**, **B**, **C**, **D** and **E** refer to cell samples consisting of 0 %, 20.0 %, 40.0 %, 60.0 % and 80.0 % mosaicism, respectively. Each sample consisted of five cells.

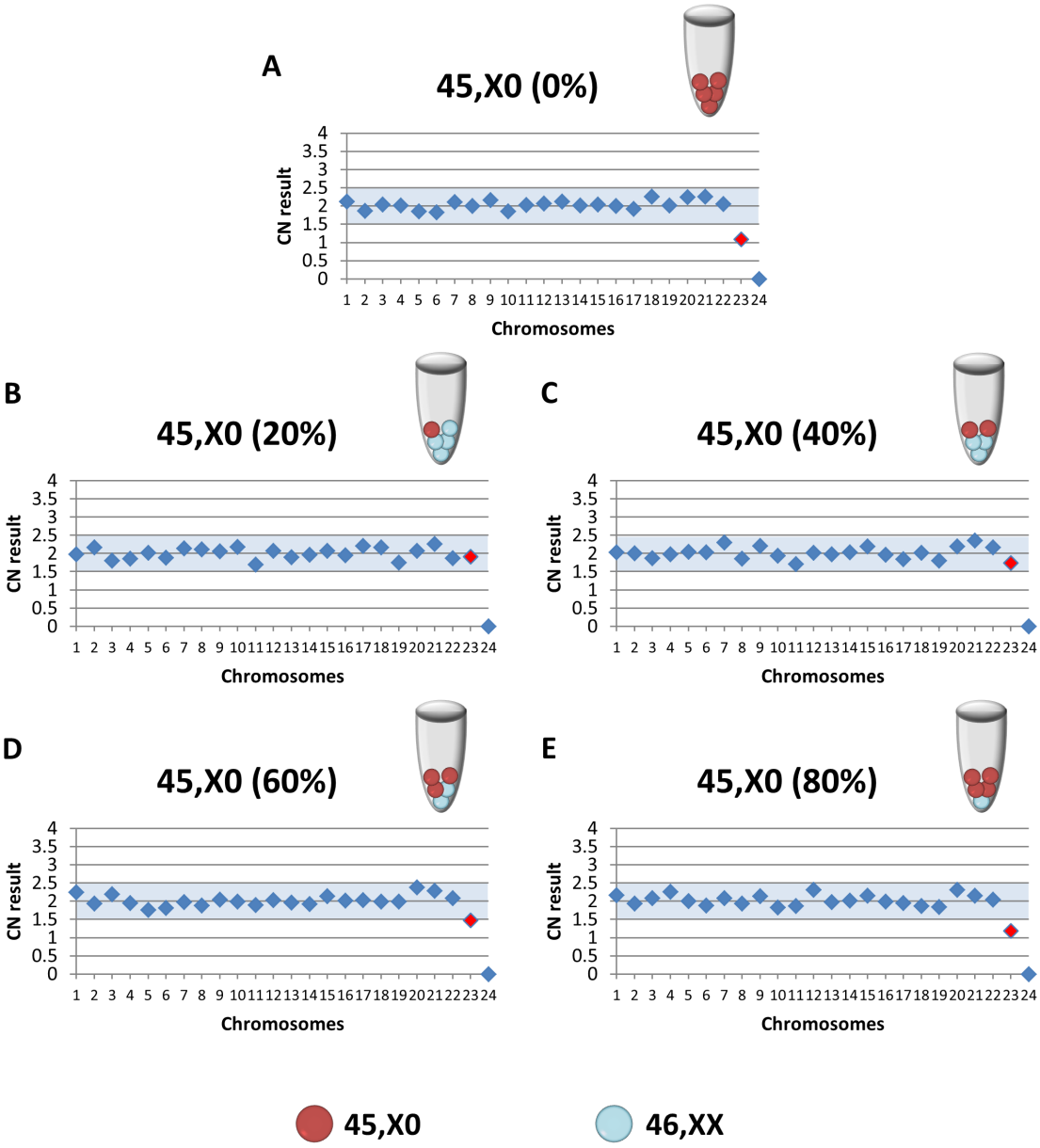


Figure 3.42: Real-time qPCR 24-CCN profiles of different levels of simulated mosaicism using the 45,X0 and the 46,XX cell line. Profiles were generated using the PERL programme. Diamond-shaped signs indicate CCNs. Red diamond-shaped signs highlight expected aneuploid chromosome. Chromosomes labelled '23' and '24' refer to chromosomes X and Y, respectively. Profiles **A**, **B**, **C**, **D** and **E** refer to cell samples consisting of 0 %, 20.0 %, 40.0 %, 60.0 % and 80.0 % mosaicism, respectively. Each sample consisted of five cells.

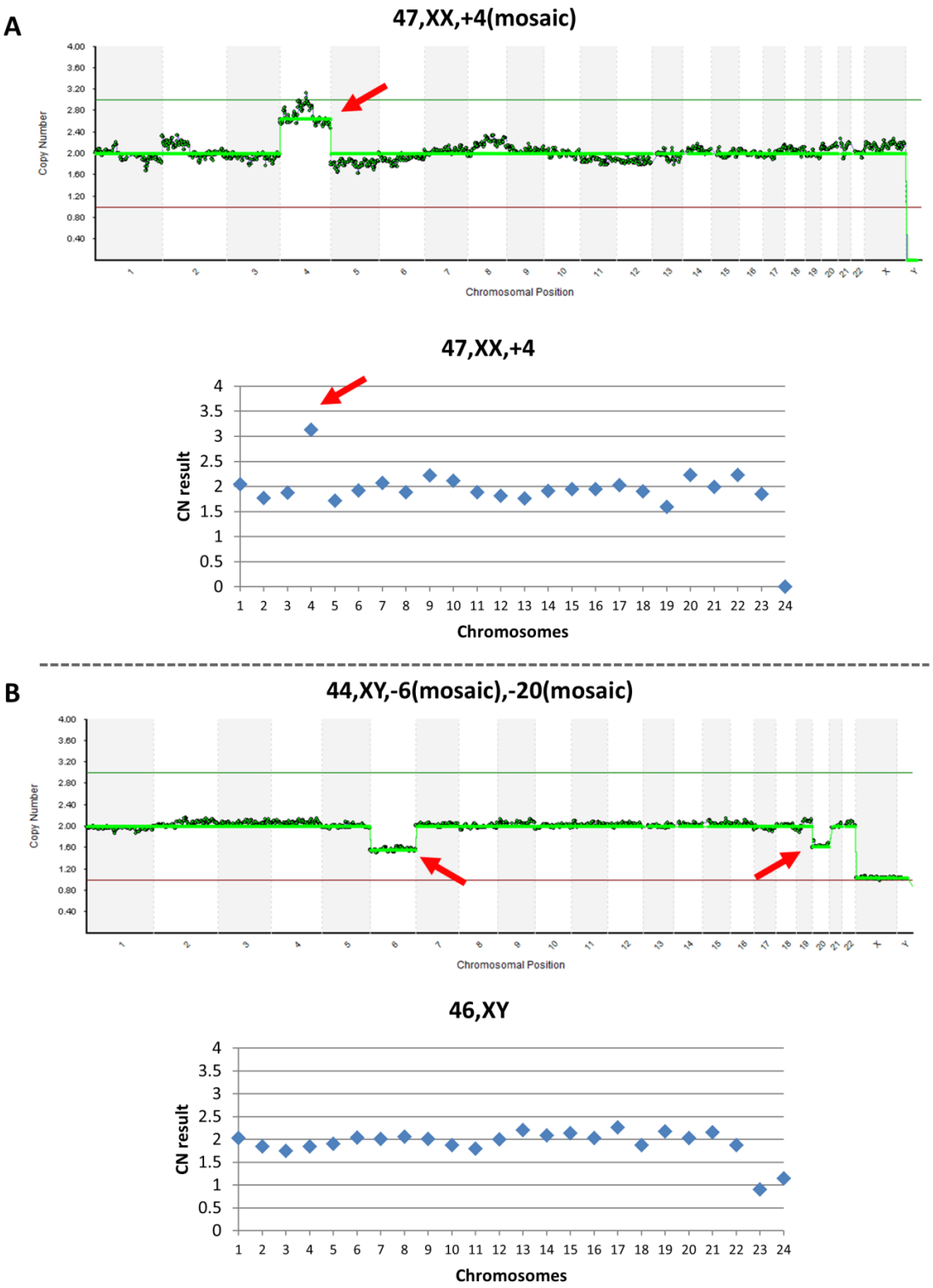


Figure 3.43: Comparison of NGS and real-time qPCR 24-CCN profiles of entire embryos M.1 and M.2 and corresponding trophectoderm biopsies. NGS profiles were generated with Bluefuse (for plot descriptions refer to **CHAPTER 2**, **Section 2.5.2**). Real-time qPCR profiles were generated using the PERL programme (for plot descriptions refer to previous plots). Red arrows mark aneuploid chromosomes. **A: Sample M.1.** NGS identified a mosaic gain of chromosome 4 (entire embryo). The abnormality was identified as gain with real-time qPCR (biopsy). **B: Sample M.2.** NGS identified a mosaic loss of chromosomes 6 and 20 (entire embryo). The abnormalities were not identified with real-time qPCR (biopsy).

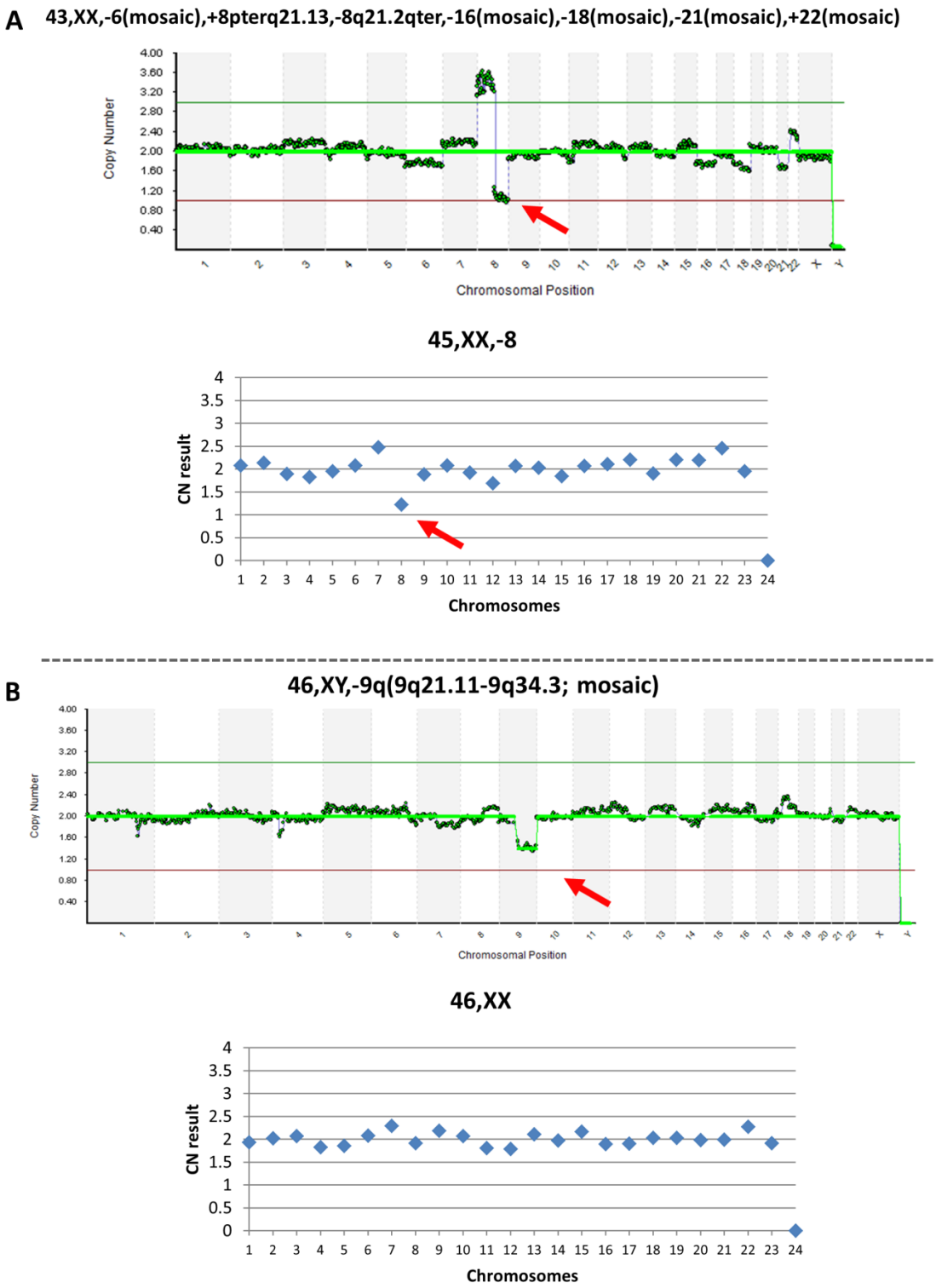


Figure 3.44: Comparison of NGS and real-time qPCR 24-CCN profiles of entire embryos M.3 and M.4 and corresponding trophectoderm biopsies. NGS profiles were generated with Bluefuse (for plot descriptions refer to **CHAPTER 2**, **Section 2.5.2**). Real-time qPCR profiles were generated using the PERL programme (for plot descriptions refer to previous plots). Red arrows mark aneuploid chromosomes. **A: Sample M.3.** Amongst other mosaic errors, NGS identified structural non-mosaic errors of chromosome 8 (entire embryo). The abnormalities were identified as loss with real-time qPCR (biopsy). **B: Sample M.4.** NGS identified a mosaic structural loss of chromosome 9 (entire embryo). This was not confirmed with real-time qPCR (biopsy).

3.4 Clinical application of the developed protocol - **CHAPTER 3**

Following high test accuracy obtained during Phase 5 and Phase 6 of protocol development, the test was applied clinically to blastocyst-stage embryos utilising the array-based real-time qPCR protocol developed during Phase 5. Clinical outcomes following real-time qPCR testing were compared to results obtained from patients referred for array CGH analysis from the same clinic. All findings are summarised in **Table 3.12**. Additionally, information on patient characteristics (female age and reason for referral), number of embryos tested per cycle, test results and embryos transferred is presented in **Tables A.14** (real-time qPCR cohort) and **A.15** (array CGH cohort) in **Appendix A**.

The real-time qPCR group included 123 embryos generated during the course of 35 cycles. The array CGH group comprised 180 embryos obtained during 45 IVF cycles. Women included in the real-time qPCR cohort were on average six month older than patients referred for array CGH testing (38.9 years of age versus 38.3, not significant). The mean number of embryos available for biopsy and genetic analysis per cycle was slightly lower in the real-time qPCR cohort (3.51 versus 4.0, not significant).

No diagnostic result was obtained from 8.1 % of all samples analysed with real-time qPCR (10 / 123), which was slightly higher compared to array CGH (5.6 %, 10 / 180), but not significant. Similarly, aneuploidy rates were comparable between groups [62.8 % (71 / 113) versus 58.8 % (100 / 180), not significant]. Approximately two thirds of all patients had at least one euploid embryo available for transfer following real-time qPCR (60.0 %, 21 / 35) or array CGH (62.2 %, 28 / 45) analysis and received a euploid embryo

transfer in the morning (real-time qPCR cohort) or afternoon (array CGH cohort) on day-6 post fertilisation.

A total of 23 embryos (1.1 per patient) were transferred in the real-time qPCR group and 34 embryos (1.2 per patient) in the array CGH cohort. Implantation rates were comparable between both groups [65.2 % (15 / 23) versus 61.8 % (21 / 34), not significant]. Two miscarriages were reported in each group. Hence, ongoing pregnancy rate per transfer in the real-time qPCR cohort was 57.1 % (12 / 21) which was slightly higher compared to the ongoing pregnancy rate in the array CGH cohort [50.0 % (14 / 28), not significant]. Similarly, ongoing pregnancy rate per cycle was slightly higher following real-time qPCR, which however was not significant [34.3 % (12 / 35) versus 31.1 % (14 / 45)].

The utilised array-based real-time qPCR protocol further permitted mtDNA quantification in embryo biopsies. Of note, mtDNA analysis was not part of the clinical investigation and will only be discussed briefly.

MtDNA content present in embryo biopsies was assessed in relation to female age as well as embryo status (aneuploid or euploid). Additionally, differences in mtDNA content between embryos that implanted and those that did not implant or miscarried was analysed. Relative mtDNA quantities were calculated as described in **Section 3.3.6.2**.

Initially, impact of advancing maternal age on relative mtDNA quantities was assessed. Interestingly, a positive correlation was observed between female age and relative mtDNA quantities which was significant when including embryos of the entire cohort ($n = 113$, $r = 0.34$, $p = 0.0002$; **Figure 3.45 A**), suggesting that advancing age leads to an increase in mtDNA content in blastocyst-stage embryos.

Since aneuploidy increases with advancing maternal age, the embryo cohort was divided into euploid and aneuploid embryos and relation between maternal age and mtDNA content assessed (**Figure 3.45 A**). Interestingly, an even higher correlation between maternal age and mtDNA content was observed in euploid embryos ($n = 42$, $r = 0.40$, $p = 0.0093$). In contrast, maternal age and mtDNA content was not correlated in chromosomally abnormal embryos ($n = 71$, $r = 0.14$, $p = 0.2348$).

Next, difference in mtDNA content between euploid and aneuploid embryos was analysed (**Figure 3.45 B**). Chromosomally abnormal embryos carried significantly higher amounts of mtDNA as compared to chromosomally normal embryos ($p = 0.0027$). This was not surprising since mtDNA was correlated with female age. Therefore, embryos were divided into three groups according to maternal age and mtDNA contents compared between euploid and aneuploid embryos. The first group included mtDNA results from embryos derived from patients aged 31 - 35. The second group consisted of results from embryos generated by patients aged 36 - 40 and the third group included results of patients aged 41 and above. Of note, average maternal age was not significantly different between euploid and aneuploid embryo groups in the first two age categories (31 - 35 and 36 - 40). However, average maternal age was significantly higher in the aneuploid embryo cohort in patients above the age of 40.

Interestingly, aneuploid embryos carried significantly higher amounts of mtDNA as compared to euploid embryos in the youngest age group ($p = 0.0244$). In contrast, no differences in mtDNA content between chromosomally normal and abnormal embryos was present in the two older age groups (36 - 40: $p = 0.9801$, >40: $p = 0.4298$).

Finally, relative mtDNA quantities were compared between embryos that implanted and let to an ongoing pregnancy to embryos that failed to implant or miscarried (**Figure 3.46**). Although, embryos that resulted in an ongoing pregnancy had on average lower amounts of mtDNA, no significant difference in mtDNA content was detected between the two groups (p = 0.6619).

Table 3.12: Comparison of patient/embryo characteristics and PGS outcomes following real-time qPCR or array CGH testing

Patient/Sample details and PGS outcomes	Array CGH	Real-time qPCR	p-value
Cycles: total (n)	45	35	NA
Female age: mean (y) ± SD; range (y)	38.3 ± 3.5; 30 - 44	38.9 ± 3.4; 31 - 45	0.39[a]
Embryos tested: total (n); per patient (mean n ± SD)	180; 4.0 ± 2.5	123; 3.5 ± 2.2	0.34[c]
Undiagnosed embryos: total (n); frequency (%)	10; 5.6	10; 8.1	0.48[b]
Aneuploid embryos: total (n); frequency (%)	100; 58.8	71; 62.8	0.54[b]
Patients with transfer: total (n); frequency (%)	28; 62.2	21; 60.0	1.00[b]
Embryos transferred: total (n); per patient (mean n ± SD)	34; 1.2 ± 0.4	23; 1.1 ± 0.3	0.28[c]
Embryos implanted: total (n); frequency (%)	21; 61.8	15; 65.2	1.00[b]
Pregnant patients: total (n)	16	14	NA
Miscarriages: total (n)	2	2	NA
Ongoing pregnancy rate per transfer: frequency (%)	50.0	57.1	0.56[b]
Ongoing pregnancy rate per cycle: frequency (%)	31.1	34.3	0.82[b]

n = number. NA = not applicable. y = years of age. a = unpaired t test. b = Fisher's exact test. c = Mann Whitney U test.

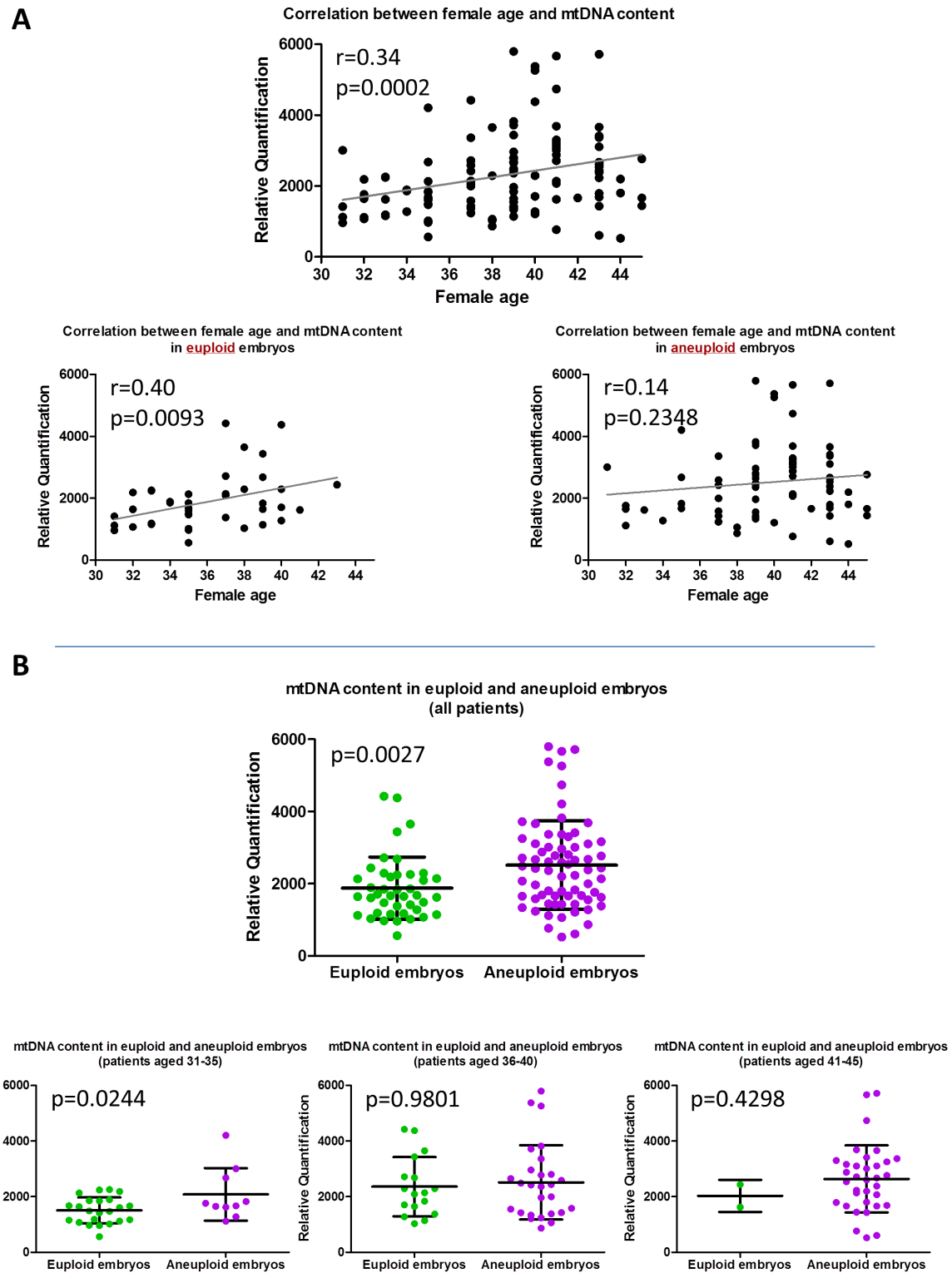


Figure 3.45: MtDNA content present in embryo biopsies. A: Correlation between female age and relative mtDNA quantities in the entire cohort, euploid embryos and aneuploid embryos. r = Spearman's rank correlation coefficient with corresponding p-value. **B: Relation between embryo status (euploid or aneuploid) and relative mtDNA quantities.** Scatter dot plots show distribution of mtDNA quantities, mean quantities and SD. Statistical data analysis was performed using Mann Whitney U test (entire cohort) or unpaired t test (age groups).

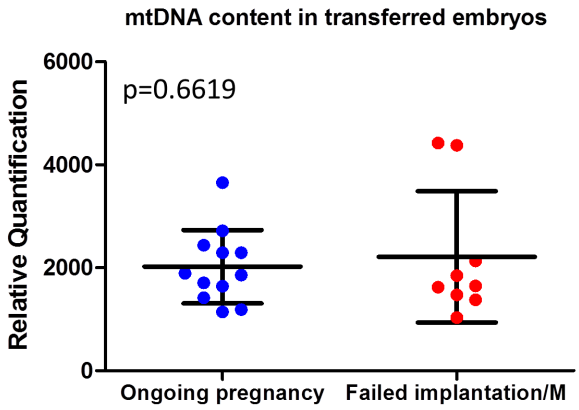


Figure 3.46: Comparison of mtDNA content present in embryos resulting in an ongoing pregnancy and embryos that failed to implant or miscarried. Scatter dot plots show distribution of mtDNA quantities, mean quantities and SD. Statistical data analysis was performed using the unpaired t test. M = miscarriage.

3.5 Discussion - **CHAPTER 3**

Aneuploidy screening has been proposed to assist in the identification of chromosomally normal embryos. Available cumulative evidence suggests that CCS performed at the blastocyststage improves certain IVF outcomes (Chen et al., 2015; Dahdouh et al., 2015b; Forman et al., 2013; E. Lee et al., 2015; Scott et al., 2013a; Yang et al., 2012). However, most widely used techniques, such as array- or NGS-based CCS methodologies, typically require 24 hours or more for result generation following embryo biopsy. Considering that some blastocysts are not sufficiently developed to be deemed ready for biopsy until later on day-5 or in some cases even day-6 post fertilisation, embryo cryopreservation is necessary to provide sufficient time for testing. The addition of cryopreservation represents an extra cost to PGS/IVF treatment, restricting patient access and introduces an additional risk factor for the embryo.

To address these problems, a novel technique for the assessment of CCN in blastocyst-stage embryos was developed, validated and applied during the course of the present study.

3.5.1 Development and validation of a robust quantitative real-time polymerase chain reaction protocol

During Phase 1 of protocol development, a proof-of-principal study was performed to test the feasibility of real-time qPCR for CCN detection. A robust algorithm was developed for the analysis of real-time qPCR data, which constituted the foundation for data analysis in later development phases. An important element of the generated algorithm is its capacity to take into account possible differences in amplification efficiencies between different copy number assays which can be in part due to differences in amplicon GC content and size. To reduce the impact of these variables, copy number assays are multiplied by an assay-specific multiplication factor. As a result, assays that under- or over-perform during amplification are detected and adjusted accordingly. Both normalisation steps lead to an overall data smoothening which was evident by observing considerably reduced SDs between single assays of the same chromosome and between copy numbers of individual chromosomes as well as cleaner CCN profiles.

Furthermore, the established algorithm takes into account possible variations across different experiments by assigning a specific value (in %) to each chromosome, which constitutes the final copy number assignment following comparison to reference values. This is important as it allows comparison of results between different experimental set-ups without the need of processing control samples along with the test samples.

Instead, a female and a male reference data set can be generated and used for normalisation of samples processed on different runs as well as different batches of arrays.

After obtaining an encouraging data set during Phase 1 where all reactions were performed on a traditional real-time qPCR cycler in 96-well plates, the methodology was transferred to a nano-scale array-based real-time qPCR system and tested during Phases 2 - 6. The OpenArray platform has several advantages over traditional real-time qPCR systems: (1) it enables analysis of more than 3,000 data points per array, which permits higher coverage of the genome, which should theoretically reduce the impact of technical artefacts associated with individual assays, thereby increasing test accuracy; (2) real-time qPCR reactions are performed in a volume of only 33 nl (per data point) which significantly decreases reagent costs; (3) the experimental set-up is streamlined and fully automated, which greatly reduces hands-on time; (4) it is high-throughput, allowing simultaneous processing of a large number of samples.

As a proof-of-principle, an array for the analysis of just seven chromosomes was designed, and initially tested on gDNA and cell samples (Phases 2 and 3). To further decrease reagent costs, smaller reaction volumes (~25 µl and ~15 µl) for pre-amplification of cell samples were tested. The test results obtained from the analysis of gDNA samples were reassuring. However, the expected karyotype was fully confirmed in only 16 out of 22 samples (72.7 %). Of note, all gDNA samples expected to be euploid were identified as being chromosomally normal.

A possible explanation for the decreased accuracy is that only a small number of chromosomes was tested. Since the analysis algorithm takes into account overall chromosome distribution when assigning CCNs, the presence of a trisomy automatically

lowers copy numbers of all other chromosomes. Importantly, the test accuracy was considerably improved when testing cell samples consisting of three and five cells, rather than gDNA, suggesting that the initial pre-amplification of cell samples led to an improved detection of aneuploidies. For example, 82.6 % (38 / 46) of cell samples pre-amplified in a ~25 µl reaction volume were classified correctly. Moreover, the expected karyotype in three- and five-cell samples processed in the smallest reaction volume of ~15 µl was confirmed in all, but one sample [97.8 % (44 / 45)]. In contrast, the method did not perform very well in single-cell samples, which was possibly due to low starting genetic material.

During the next stages of protocol development (Phases 4, 5 and 6), the method was extended to the analysis of all 24 chromosomes using a new array design. Initial results obtained during Phase 4 were surprisingly disappointing as none of the tested samples gave a correct CCN result. This was most likely caused by improper sample loading which was evident by the stepwise decrease in assay Ct values between sub-arrays.

To compensate for unequal sample DNA distribution between sub-arrays, a new array for 24-CCN analysis was designed and the analysis algorithm was revised and updated. The new protocol design was then extensively tested and validated on a large number of cell samples (Phase 5). This revised method proved to be highly accurate in CCN assignment in samples consisting of three and five cells. Real-time qPCR testing demonstrated 100 % sensitivity for aneuploid sample call, generating zero false-negative sample diagnoses. Importantly, all samples, besides of one, expected to be chromosomally normal were diagnosed as euploid (97.9 % specificity). A high accuracy was also obtained when assessing results at the chromosome level. Of all chromosomes tested, 99.9 % were correctly diagnosed as euploid or aneuploid, resulting in a sensitivity of 98.8 % and

specificity of 99.9 %. Of note, the method did not perform well in single-cell samples. Although100 % sensitivity was obtained, specificity was greatly reduced (40.0 %) due to a high number of false-positive calls.

Before implementation of any diagnostic or screening test into clinical practice it is essential to determine test accuracy in actual clinical samples. Therefore, a pre-clinical validation study was performed during the final validation phase (Phase 6) where the real-time qPCR test accuracy was evaluated on embryo biopsies derived from blastocyst-stage embryos. Chromosomal mosaicism is common at the blastocyst-stage (Van Echten-Arends et al., 2011). To avoid the impact of mosaicism on test results only embryos found to be euploid or carriers of non-mosaic chromosome abnormalities were included in the pre-clinical validation study.

The real-time qPCR results were compared to the results obtained from corresponding embryos which were analysed using a well-established and validated NGS-based CCS technique (VeriSeq, Illumina; Fiorentino et al., 2014a, Fiorentino et al., 2014b). The results demonstrated validity of the real-time qPCR protocol for aneuploidy screening in trophectoderm biopsies. In particular, 100 % sensitivity was achieved for overall embryo as well as chromosome diagnosis. In one biopsy, however, two aneuploidies were detected using real-time qPCR which were not present in the corresponding embryo, resulting in an overall slightly decreased specificity (96.2 % and 99.7 %). Of note, it was not clear if the detected errors were true false-positive chromosome calls or caused by euploid/aneuploid cells present in the biopsied sample.

It should be acknowledged that the test failure rate was relatively high as compared to the study performed in cell lines (21.1 % versus 2.6 %). This was likely due to

the higher amplification failure rate as a result of poor quality of some samples, most likely containing degraded DNA, a suggestion supported by data subsequently obtained after clinical implementation, which showed a considerably lower failure rate (8.1 %).

3.5.2 Clinical application

Following the development and validation phases, the real-time qPCR test was applied clinically and outcomes compared to results obtained from patients referred for PGS from the same clinic utilising a widely used and validated array CGH method. Importantly, patient characteristics, such as maternal age, referral indications and number of embryos biopsied were similar between the real-time qPCR and array CGH groups. In both groups, embryos were selected for transfer primarily based on PGS results. In cases where multiple chromosomally normal embryos were available, those with highest morphological scores were transferred. It is important to note that, while patients in the real-time qPCR cohort received a transfer early in the morning of day-6, patients in the array CGH group received a transfer in the afternoon of day-6.

The retrospective comparison of clinical outcomes demonstrated that real-time qPCR testing resulted in similarly high implantation rates as well as clinical and ongoing pregnancy rates as compared to the array CGH cohort, providing further evidence of test validity. In fact, although not significant, clinical outcomes appear to be slightly better in the real-time qPCR cohort (implantation rate: 65.2 % versus 61.8 %; ongoing pregnancy rate per transfer: 57.1 % versus 50.0 %; ongoing pregnancy rate per cycle: 34.3 % versus 31.1 %). These results are also in line with clinical outcomes reported in other studies

involving testing of blastocyst-stage embryos derived from infertile female patients of similar age (Fiorentino et al., 2014b; Forman et al., 2012; Scott et al., 2013a).

Thus far, clinical outcomes are promising. However, it should be acknowledged that the sample size of this pilot study was relatively small and validity of the proposed real-time qPCR protocol should be confirmed in a larger patient group. Furthermore, in any study which implements new technologies into clinical practice, it is essential to determine the ultimate end-point, live birth rate. This will be possible in a retrospective analysis once the clinical live birth rates become available in the real-time qPCR cohort. Nevertheless, overall clinical outcomes, including the live birth rate should ideally be evaluated in a randomised controlled trial in the future.

In addition, a potential benefit of early day-6 transfer as opposed to afternoon transfers on day-6 remains to be established. Accumulating evidence suggests that embryo transfers performed on day-5 lead to higher implantation rates compared to day-6 transfers (Barrenetxea et al., 2005; Khorram et al., 2000; Poulsen et al., 2017). In line with this notion, it is possible that any marginal improvement in implantation rates observed in the real-time qPCR cohort are attributable to earlier transfers (early on day-6), since these may be more likely to remain within the ideal window of optimal endometrial receptivity. An alternative explanation why embryos transferred later perform poorer could be that prolonged embryo culture, extended from day-5 to day-6, impacts on the implantation potential, as suggested by Poulsen et al. (2017). Importantly, the observed increase in implantation rate in the real-time qPCR cohort was not statistically significant and without confirmation in a larger population, no conclusions can be drawn.

3.5.3 Microdeletion detection

An advantage of real-time qPCR over methods such as array CGH and low-pass NGS is that it allows the addition of primers which can be used for different types of investigations in addition to CCS. In this study, primers targeting the DiGeorge chromosomal region on chromosome 22 were added to assess feasibility of microdeletion testing.

The 22q11.2 deletion (1.5 - 3 Mb in size) was chosen as a model for microdeletion testing since it is the most common microdeletion in humans with a prevalence of 1 in 4,000 live births (Driscoll, 2001). A proof-of-principle study was performed during Phase 5 of protocol development and all processed cell samples tested for the presence/absence of the deletion. Real-time qPCR confirmed presence of the microdeletion in all cell samples derived from the DiGeorge cell lines, while the deletion was not detectable in all other samples, providing evidence that real-time qPCR could be applied for the detection of common microdeletions. In the future, this approach could be extended to the detection of other microdeletion syndromes.

3.5.4 Mitochondrial DNA quantification

Aneuploidy is considered to be the single biggest cause of embryo implantation failure and miscarriage. Nevertheless, a relatively high proportion of euploid embryos fail to produce a viable pregnancy. Given the fact that mitochondrial function and adequate energy supply during preimplantation development is critical for embryo development, some researchers have hypothesised that mitochondrial deficiencies could explain loss of

viability affecting some embryos (Van Blerkom, 2011). Several recent studies have investigated the relationship between mtDNA copy number and implantation potential in blastocyst-stage embryos. Research undertaken by Fragouli et al. (2015) and Diez-Juan et al. (2015) has shown a correlation between elevated mtDNA content and decreased implantation potential in blastocyst-stage embryos, suggesting that mtDNA copy number could serve as a potential biomarker for assessing viability of euploid embryos. Consequently, qPCR assays targeting fragments of the mitochondrial genome were included in the later versions of the array design. The effectiveness of quantifying mtDNA content in embryo biopsies was initially tested during the pre-clinical validation phase and results obtained from trophectoderm biopsies compared with results obtained from corresponding entire embryos.

To determine the test accuracy, correlation analysis was performed. A high correlation in relative mtDNA quantities was obtained between the three mtDNA assays (M.1, M.2 and M.3) spotted on the arrays. Furthermore, the two assays (16s and MajArc) used for the quantification of mtDNA in WGA products of corresponding embryos performed equally well.

A significant but moderate correlation in mtDNA quantities was observed between biopsies and corresponding whole-embryo samples, suggesting that mtDNA content detected in the biopsy may not always be fully indicative of the mtDNA content in the entire embryo. However, as two different techniques were used for mtDNA quantification, the observed variations could have been partly due to differences in testing methodology.

MtDNA content was also assessed in clinical trophectoderm samples of patients referred for PGS utilising the real-time qPCR protocol. Interestingly, a significant correlation

between female age and mtDNA content was observed, which is in line with a previously published study by Fragouli et al. (2015). Importantly, a significant increase in mtDNA copy numbers was observed with advancing maternal age, even when assessing euploid embryos, thereby removing any potential biases associated with aneuploidy. A significant difference in mtDNA content was also observed between aneuploid and euploid embryos. However, when stratified for female age, a statistically significant difference was only observed in the youngest age group.

The observed correlation between mtDNA content and female age/embryo ploidy is in contrast to a recently published study by Victor et al. (2017) who found no such correlation. However when investigating the methodology of the Victor study, the observed absence of correlation could have been due to incorrect normalisation technique, where the obtained mtDNA values were normalised against a single nuclear reference, as opposed to a multi-copy nuclear references. It is clear that analysis of samples composed of small numbers of cells can only be accurately accomplished when normalisation is against multiple-copy nuclear targets, as shown by Ravichandran et al. (2017). Attempts to quantify mtDNA using NGS approaches are also challenging due to the failure of some commercially available methods to provide a sufficient number of reads from the mitochondrial genome for accurate measurement.

In the present study, the obtained mtDNA values were normalised against values obtained from all genomic regions amplified during real-time qPCR, with exception of sex chromosome and DiGeorge microdeletion assays, as these can be present in different copy number.

No difference in mtDNA content was observed between transferred embryos that resulted in an ongoing pregnancy and embryos that failed to implant or miscarried. This is possibly attributed to a small sample size and as the clinical sample size increases this should be evaluated retrospectively. Recent data suggests that fewer than 10 % of euploid blastocysts have elevated mtDNA levels, thus relatively large sample sizes are required in order to evaluate the impact of mtDNA on implantation potential (Ravichandran et al., 2017).

3.5.5 Advantages and limitations in comparison to currently available 24-chromosome screening techniques

A key strength of the developed protocol is that it allows rapid chromosome screening. Results can be generated within five hours following embryo biopsy or receipt of samples, permitting same day or early day-6 embryo transfer. The initial cell lysis and multiplex pre-amplification steps require approximately two hours, including processing and incubation times. The real-time qPCR set-up takes about 30 minutes, followed by two hours incubation in the real-time qPCR cycler. Results are readily available, which leaves 30 minutes for data analysis and reporting.

Overall, the test can be performed at substantially decreased turn-around times as compared to most other CCS techniques. For instance, the most commonly used array CGH protocol (24Sure, Illumina) requires approximately 12 hours for data generation (Handyside, 2013). In practice however, a 12 hour turn-around may not always be possible due to laboratory logistics, such as standard working hours. Therefore, a 24 hour turn-around might often be more feasible, particularly if the test is not performed in-house

but by a service provider based at a different location, as is the case for the majority of PGS cases performed worldwide.

The technique further allows scalability and high sample throughput. Twelve samples can be processed on a single array. A total of four arrays can be run simultaneously on the OpenArray platform which means that, if required a total of 48 samples can be analysed at the same time, which is of particular importance for laboratories which process a large number of samples. The high versatility in sample throughput is a significant advantage compared to other current high-throughput methodologies. For instance, the NGS-based PGS approach developed by Illumina (VeriSeq PGS) necessitates simultaneous processing of a large number of samples in order to be cost-effective.

While this is not the first rapid real-time qPCR protocol to be developed for the purpose of PGS, the only other published methodology suffers from poor scalability and is limited by the number of samples which can be processed per run (Treff et al., 2012b). That technique has been validated utilising a traditional real-time qPCR cycler which has significantly less capacity as compared to the OpenArray platform. For instance, in order to simultaneously process 48 samples the laboratory would have to be equipped with a total of 48 real-time qPCR cyclers provided that one embryo is processed per 384-well plate, as outlined in Treff et al. (2012b). However, this is not feasible for most laboratories/clinics. Problems with throughput have also made it difficult for previous qPCR platforms to introduce additional tests (e.g. microdeletion analysis and mtDNA quantification) into routine clinical practice.

Considering the cost of testing, the developed technique is comparable to the currently implemented CCS techniques, such as NGS, in terms of both, equipment and

reagent costs. Potential cost-effectiveness, however can only be achieved if arrays are loaded with maximum number of samples (e.g. 12, 24, 36 or 48). Importantly, staff costs associated with the new array-based real-time qPCR strategy are very much lower than those associated with any other CCS technology, requiring less than 40 minutes of hands-on time in the laboratory. Finally, similarly to NGS-based screening, the developed technique does not require control samples to be processed along with the test samples as opposed to array CGH.

As the qPCR method stands, it is likely that the presence of mosaicism can be detected when aneuploidy is present in more than half of the cells. However, it is not possible to differentiate between mosaic and non-mosaic abnormalities. This is in contrast to NGS methods which have recently been validated for this purpose and have been shown to be particularly good at detecting mosaicism at low levels and to differentiate between mosaic and non-mosaic errors (Fragouli et al., 2017a; Vera-Rodríguez et al., 2016).

Stringent rules are applied during data analysis of real-time qPCR data, with autosomal chromosomes below a copy number of 1.5 or above a copy number of 2.5 being classified as monosomies and trisomies, respectively. This means that in some occasions when chromosomes are identified as aneuploid, the aneuploidy may actually be present in a mosaic form, probably affecting the majority of cells in the biopsy specimen. Conversely, in other instances where mosaic embryos have low proportions of aneuploid cells in their biopsies, they may receive a 'normal' assignment.

Although preliminary data generated from samples containing a mix of cells derived from euploid and aneuploid cell lines demonstrated that the developed method is capable of detection of mosaicism levels greater than or equal to 60 %. Further

experiments are warranted in order to obtain a better understanding of the impact of chromosomal mosaicism on real-time qPCR test results. It is worth noting that a similar study has recently been reported by the group that developed the first real-time qPCR test for CCS (Treff et al., 2012b). The results obtained from their established real-time qPCR protocol demonstrate feasibility of detecting mosaicism in aneuploid/euploid cell line mixture models using real-time qPCR (Goodrich et al., 2016).

The failure to detect the extend of mosaic aneuploidy can be considered a limitation of the qPCR method, which may be clinically relevant. Recent publications have indicated that blastocysts associated with a mosaic trophectoderm biopsy specimen have intermediate outcomes with respect to embryos with fully euploid biopsies (highest potential) and those with no normal cells detected (lowest potential) (Fragouli et al., 2017a; Greco et al., 2015). However, some clinics find the reporting of mosaicism to be problematic, as there remains some uncertainty concerning the fate of affected embryos. Their viability is difficult to quantify with any certainty, as is the risk that their transfer will result in an abnormal pregnancy/birth. Consequently some doctors and patients favour the more simplistic, binary results produced by the real-time qPCR approach detailed here.

A further limitation of the developed technique is its inability to detect segmental chromosome abnormalities, due to its low resolution. This means that segmental aneuploidy can be undetected or be incorrectly characterised as gains or losses affecting entire chromosomes, depending on the size of the structural abnormality and the chromosomal locations of the amplified loci used for real-time qPCR. In contrast, array- and NGS-based methods have significantly higher sensitivity in calling structural chromosome

abnormalities (Fiorentino et al., 2014a; Fiorentino et al., 2014b; Fragouli et al., 2017a; Handyside, 2011; Handyside, 2013; Yin et al., 2013).

Furthermore, as with other CCS techniques, the detection of haploidy or polyploidy is not possible using real-time qPCR since the total DNA content is balanced.

Lastly, the methodology can only be reliably applied to multiple cells. Analysis of polar bodies or blastomeres is not reliable using the current method.

3.5.6 Conclusion - **CHAPTER 3**

In conclusion, results presented in this study demonstrate high accuracy of the final iteration of the developed array-based real-time qPCR technology in the detection of whole chromosome abnormalities. In addition, the technique has the capacity of quantifying the mtDNA content, which may provide extra information on embryo viability, as well as detecting the DiGeorge microdeletion.

The actual hands-on experimental set-up, not including incubation periods when samples are lysed, pre-amplified and run on the qPCR OpenArray platform, requires less than one hour. This, as well as the fact that the process is simple, cost-effective and not labour-intensive, is of great advantage to clinical genetic laboratories and makes the possibility for an in-house facility much more practicable for IVF centres.

The technique is clinically applicable and has been translated from research into routine clinical use. While the number of cases undertaken is still relatively small, outcomes are promising and seem to be as good or better than those achieved after PGS using array CGH.

CHAPTER 4: Design, validation and first clinical application of a protocol for preimplantation genetic testing of mitochondrial DNA disease combined with comprehensive chromosome screening

This chapter describes the design, validation and clinical application of a novel test to combine detection of mtDNA mutations and chromosome aneuploidy in embryo specimens. The chapter is divided into five sections. A brief introduction is followed by a materials and methods section which states the ethics, the patient characteristics, the study design and the applied methods. The third part describes the development and validation of the test. The fourth section describes the results and outcomes obtained following clinical implementation. In the last section, the developed test and clinical results are discussed.

4.1 Introduction - **CHAPTER 4**

Different reproductive options are available to families affected by mtDNA disease which include adoption, IVF using donated oocytes, prenatal diagnosis (PND) and PGD (reviewed by Poulton et al., 2009). PGD has several advantages over the proposed reproductive strategies. PGD allows patients harbouring mtDNA mutations to have a genetically related child. Furthermore, since PGD is performed prior to the establishment of a pregnancy, patients can avoid the risk of possible pregnancy termination following PND (reviewed by Smeets et al., 2015).

The aim of PGD of mtDNA disease is to minimise the risk of disease transmission from mother to child by identifying and selecting preimplantation embryos for transfer, which are unlikely to develop a disease phenotype. Ideally, only embryos which are found to be free of the disease-causing mutation are transferred. If no mutation-free embryo is available, those with lowest mutation load may be chosen for transfer to reduce the risk of disease transmission (reviewed by Poulton et al., 2010).

The accuracy of currently available techniques for PGD of mtDNA disease has been questioned due to technical difficulties (Mitalipov et al., 2014). Moreover, to date, no technique has been developed or validated that can combine mtDNA mutation load and aneuploidy assessment in a single embryo biopsy. However, aneuploidy is common in preimplantation embryos and significantly contributes to poor IVF outcomes [e.g. implantation failure, miscarriage and aneuploid pregnancy (reviewed by Wilton, 2005; reviewed by Nagaoka et al., 2012)]. Therefore, a protocol for simultaneous mtDNA mutation and aneuploidy detection would be beneficial in order to increase the chance of healthy offspring in women at risk of transmitting a mtDNA disease.

CCS is most commonly performed in WGA products using well-validated techniques, such as array CGH or NGS-based testing. To combine both procedures, CCS and PGD of mtDNA mutation detection, a protocol utilising NGS was designed and validated to accurately detect mtDNA variant levels in embryo specimens which have previously been subjected to WGA. The flow chart presented in **Figure 4.1** illustrates the proposed protocol.

Following the successful validation of the protocol, the test was clinically applied to embryo specimens of four patients. Three patients were referred for PGD of maternally inherited Leigh Syndrome (MILS; OMIM #256000). Each of these patients had one child affected by the syndrome. In two cases the syndrome was caused by the m.8993T>G mutation in the mitochondrially encoded ATP synthase membrane subunit 6 (MT-ATP6) gene and in one case by the m.10191T>G mutation in the mitochondrially encoded NADH:ubiquinone oxidoreductase core subunit 3 (MT-ND3) gene. The fourth patient had no child at the time of referral but had been diagnosed with mitochondrial myopathy

caused by the m.3243A>G mutation in the mitochondrially encoded tRNA-Leu (UUA/G) 1 (MT-TL1) gene.

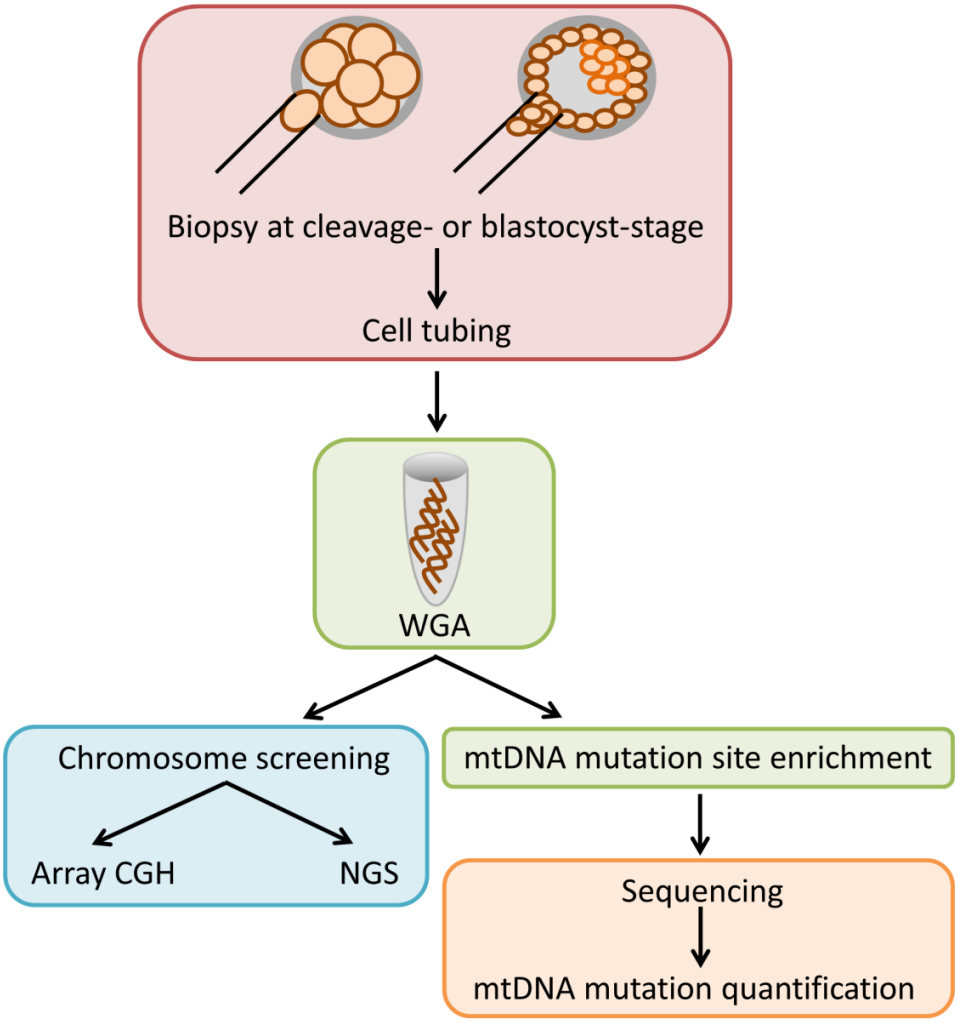


Figure 4.1: Design of the protocol for mtDNA mutation analysis combined with CCS. After embryo biopsy at the cleavage- or blastocyst-stage, cells are tubed and subjected to WGA. The amplification product is then split into two parts. One part is used for CCS using either array CGH or NGS. The other part is used for mtDNA mutation analysis using NGS. In order to enrich the mtDNA region of interest a PCR is performed prior to sequencing using primers flanking the mutation site.

4.2 Materials and methods - **CHAPTER 4**

4.2.1 Ethics regarding test development and clinical application

Two patients were referred for PGD by clinics in the US (NYU Fertility Center, New York, Center for Reproductive Medicine, Orlando). Two patients were referred by Oxford Fertility, UK. The technique was developed and validated using cell and gDNA samples derived from the referred patients and the patients' affected children, if applicable. The technique was then applied to embryo specimens of patients.

PGD of mtDNA disease is licensed by the Human Fertilisation and Embryology Authority (HFEA, http://guide.hfea.gov.uk/pgd/). By necessity, the vast majority of all PGD protocols used worldwide are unique, created for individual families using a wide array of different molecular genetic techniques. Patient counselling and signed informed consent are important and required elements of PGD, but specific ethical approvals are not sought for the development of protocols for individual families. PGD is not considered an experimental intervention and it is accepted that most protocols used will be novel. All PGD tests created in accredited laboratories follow a set strategy for the design, optimisation and validation, common to all PGD methods. The PGD tests developed as part of this thesis were conducted within such an accredited laboratory (Reprogenetics UK). From communications with the Institutional Review Board of New York University, it was confirmed that the situation in the US is the same as that in the UK and that no institutional review board approvals are required for the development of new PGD protocols. Written

consent for the use of cell and DNA samples for the work towards the creation and subsequent application of the new PGD test was obtained in all cases.

Prior to the PGD test development and initiation of treatment, all patients were counselled either by a genetic counsellor or by the referring physician. US-based patients were counselled by Amy Jordan, a Board Certified genetic counsellor and manager of Clinical Genetic Services for Reprogenetics US. UK-based patients were counselled by Joanna Poulton, Professor and Honorary Consultant in Mitochondrial Genetics, Oxford.

During the counselling process, patients were informed that limited experience with PGD of mtDNA disease exists in general. Furthermore, patients were informed that the diagnostic method is new and consequently no clinical data on the accuracy of the test was available at the time. Patients were also made aware of the potential outcomes associated with PGD of mtDNA disease, e.g. possibility of not identifying a 'healthy' embryo or remaining risk of disease transmission because the biopsy specimen might not reflect the mutation load in tissues of the body at birth or later in life. Patients were also advised to perform follow-up prenatal testing in case of embryo transfer and pregnancy to confirm the previous diagnosis.

Furthermore, all patients were provided with counselling regarding the IVF process and PGS utilising array CGH or NGS and informed consent was obtained in all cases. Counselling includes a description of treatment procedures as well as purpose, limitations, risks and benefits associated.

4.2.2 Patient details

Pedigrees of the four patients referred for PGD are shown in **Figure 4.2**. Patients A, B, and C have/had one child severely affected by mtDNA disease. Of note, no known family history of mtDNA disease was present in these patients and the possibility of mtDNA disease transmission only became apparent after affected children were born and confirmed to carry pathogenic mtDNA variants at levels associated with a disease phenotype. Hence, Patients A, B and C underwent genetic testing prior to initiating IVF treatment to assess their carrier status. In one case (Patient B) the patient's mother (the diseased child's grandmother) was also tested. The fourth patient, Patient D, has not had a child at the time of referral, however was diagnosed with mitochondrial myopathy caused by a mtDNA mutation.

Patient A (28 years of age when initiating treatment) lost her daughter when she was nine months old. The daughter was a homoplasmic carrier of the m.8993G mtDNA variant (assessed in a blood sample). Although Patient A was asymptomatic at the time of testing, the mutation was detected in her blood cells at a level of approximately 56.0 %.

Patient B (33 years of age when initiating treatment) has a son who was diagnosed with Leigh Syndrome at the age of 11 months caused by 95.0 % mutation load of the m.8993G variant (detection performed in a blood sample). Due to the inheritance through the maternal lineage, both, Patient B and the patient's mother underwent genetic testing, however the mutation was either not present or levels too low to be detected in the tested samples (blood, urine sample and buccal cells).

Patient C (38 years of age when initiating treatment) was referred for PGD due to the presence of 78.0 % heteroplasmy of m.10191T>C in the muscle biopsy of her diseased daughter who was nine months at the time of testing. The mutation was not detectable in the patient's blood or urine.

Patient D (33 years of age when initiating treatment) was referred for PGD due to 28 % heteroplasmy of the m.3243A>G mutation in her muscle biopsy. The patient suffers from mitochondrial myopathy resulting in ptosis and restricted eye movement. Although the patient's mother and brother were not genetically tested, both present with hearing and vision loss, symptoms frequently associated with the m.3243A>G mutation (reviewed by Kokotas et al., 2007; reviewed by Finsterer et al., 2017).

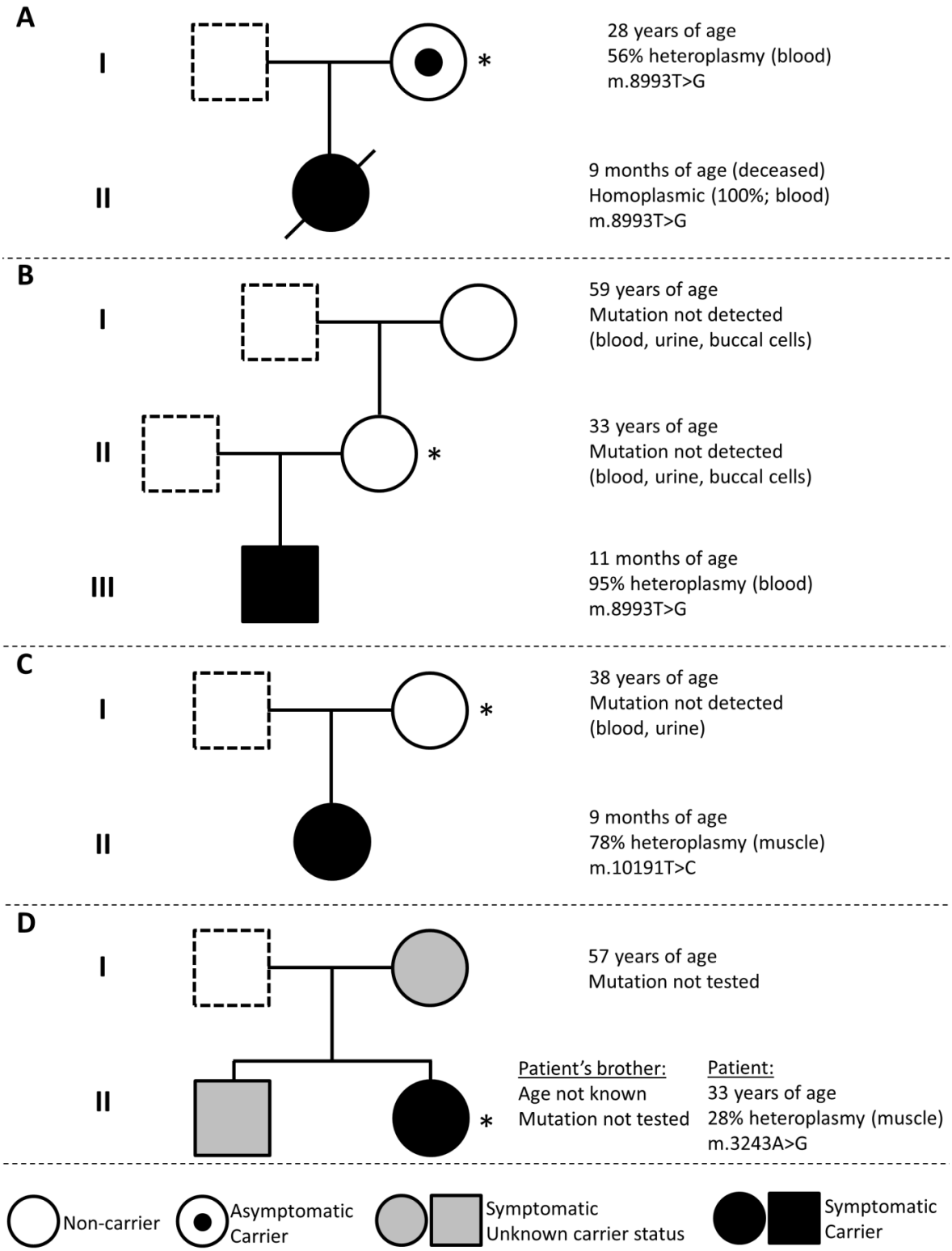


Figure 4.2: Pedigrees of the four patients referred for PGD of mtDNA disease. Pedigrees **A**, **B**, **C** and **D** refer to families of Patients A, B, C and D, respectively. Roman numerals refer to family generations. Patients are indicated by an asterisk.

4.2.3 Design of test development, validation and clinical application

The test was designed to detect mutation loads in embryo specimens previously subjected to WGA. The most commonly used WGA techniques are SurePlex and MDA. Both techniques can be used with array CGH- and NGS-based CCS. To verify that WGA generates sufficient quantities of the mitochondrial genome, both protocols were initially tested on single control cells (**Section 4.3.1**). To assess if mtDNA amplification was successful, a PCR was performed on SurePlex- and MDA-amplified products using primers specific to the mitochondrial genome and amplification products visualised on an agarose gel.

To establish accuracy and sensitivity of the NGS protocol in terms of mutation detection and quantification, artificial sample mixtures containing various heteroplasmy levels ranging from 0.0 % - 100 % were generated (see **Section 4.3.2** for a full description) and subjected to conventional PCR to generate amplicons of the mtDNA locus of interest. Obtained sequencing results were then compared to the theoretical values. Furthermore, to test if WGA introduces any distortion in the ratio of mutant and wild-type sequences, same sample mixtures were subjected to WGA followed by conventional PCR and the obtained ratios were compared to those expected.

To ensure consistency of the sequencing protocol the test was further applied to gDNA samples derived from referred patients and their affected children, if applicable, and results (with and without WGA) compared to previously established mutation levels (see **Section 4.3.3**). Furthermore, to confirm findings in gDNA and to ensure that the test can be applied to single or few cells, cell samples (lymphocytes and/or buccal cells) from patients

and affected children were assessed and heteroplasmy levels determined prior and after WGA.

The test was then clinically applied to embryo biopsies performed at the cleavage- and blastocyst-stage (**Section 4.4**). Furthermore, to determine transmission risk, unfertilised or abnormally fertilised oocytes and arrested embryos were tested. This sort of supplementary analysis is recommended in all PGD tests undertaken for the avoidance of mtDNA disorders, as the investigation of a greater number of samples (oocytes and/or embryos) greatly improves the estimation of likely recurrence risk, assisting patient counselling and clinical decision making. Additionally, to further validate mtDNA testing at the single-cell level, relevant to PGD at the cleavage- and blastocyst-stage, the uniformity of heteroplasmy levels between individual embryonic cells and between clumps of cells of some of the patients' arrested cleavage-stage embryos was tested.

One patient delivered a child following IVF-PGD treatment. To confirm the previous diagnosis, newborn gDNA samples derived from cord blood and buccal swabs were analysed.

4.2.4 Preparation of samples for test development and validation

GDNA and cell samples were obtained from buccal and/or peripheral blood samples (see **Sections 2.1.2** and **2.1.3** in **CHAPTER 2**). Newborn gDNA was isolated from cord blood and buccal swabs. GDNA isolation was performed as described in **Sections 2.2.2.2** and **2.2.2.3** (**CHAPTER 2**). Buccal cells and lymphocytes were isolated as

described in **Sections 2.2.1.2** and **2.2.1.3** in **CHAPTER 2**. Cells from the UK patients were isolated by either Dr Jonas Sarasa or Dr Araz Raberi. Cells and gDNA from both US patients were isolated by Dr Michalis Konstantinidis and members of the Reprogenetics US team.

4.2.5 IVF treatment, embryo culture and biopsy

IVF treatment, embryo culture and biopsy was performed as described in **Sections 2.1.4** and **2.2.1.4** in **CHAPTER 2** and took place in referring clinics. Embryos from Patients A, B and D were biopsied at the blastocyst-stage on day-5 or day-6 post fertilisation. Embryos from Patient C were biopsied at the cleavage-stage. Unfertilised/abnormally fertilised oocytes and arrested embryo samples were tubed on the day of embryo biopsy. All developmentally competent embryos were vitrified following the biopsy to allow sufficient time for sample processing and data analysis.

4.2.6 Sample processing procedures

Procedures involved in the NGS protocol (preparation of libraries, sequencing and data analysis) were performed as described in **Section 2.6** (**CHAPTER 2**). A negative and positive control sample was included in each sequencing run.

Prior to library preparation and sequencing, a conventional PCR was performed on all samples to enrich the mtDNA mutation site of interest. The PCR protocol was performed as described in **Section 2.3.2** (**CHAPTER 2**) using primers flanking the mutation site. Primer sequences are described in **Table B.1** in **Appendix B**.

Prior to conventional PCR, WGA (SurePlex) was performed on all embryo specimens as well as biopsy negative controls (described in **Section 2.3.1.1** in **CHAPTER 2**). To test presence of exogenous DNA contamination, negative controls were run on an agarose gel and amplification products visually inspected. SurePlex was also performed on gDNA and cell samples derived from a control individual as well as samples derived from referred patients and their children. MDA was performed on control cells as described in **Section 2.3.1.2** (**CHAPTER 2**).

4.2.7 Comprehensive chromosome screening protocols

To determine chromosome content in embryo specimens array CGH or NGS was utilised and performed according to **Sections 2.5.1** and **2.5.2** (**CHAPTER 2**), respectively. CCS of embryos from US-based patients was performed at the Reprogenetics US laboratory. Aliquots of WGA products were then shipped to Reprogenetics UK for further analysis of the mtDNA. All procedures involving samples from UK patients were performed at Reprogenetics UK.

4.2.8 Statistical data analysis

Statistical data analysis was conducted using GraphPad Prism v5.00 (GraphPad Software, La Jolla California, USA). Data was tested for normal distribution using the D'Agostino & Pearson omnibus normality test. Linear regression analysis was performed to assess linearity of obtained mutation ratios in initial validation experiments. The Pearson's

rank correlation coefficient was calculated to assess consistency between expected and obtained heteroplasmy levels during method validation. One-way ANOVA was used to compare heteroplasmy levels at different stages of preimplantation development. All data analysis tests were performed two-tailed with a 95 % CI. A p-value < 0.05 was considered significant.

4.3 Protocol development and validation - **CHAPTER 4**

4.3.1 Assessment of whole genome amplification protocols

Initially, two different WGA protocols were assessed, SurePlex and MDA. Each WGA protocol was performed on six control lymphocyte samples, each containing a single cell. After WGA, a conventional PCR was performed using the primer set flanking the mtDNA sequence containing the m.8993 mutation site (**Figure 4.3 A**).

Both WGA methods resulted in bands specific to the mtDNA sequence of interest (135 bp) in all samples tested. Since SurePlex is a standard routine technique applied for aneuploidy screening using either array CGH or NGS, SurePlex was selected for further development of the protocol.

To verify that the method also enables amplification of the m.10191 and m.3243 mutation sites, conventional PCRs using primers targeting these regions were performed on SurePlex products of single lymphocytes (**Figures 4.3 B** and **4.3 C**). Again, PCRs resulted in amplicons of the desired sizes (124 bp and 108 bp).

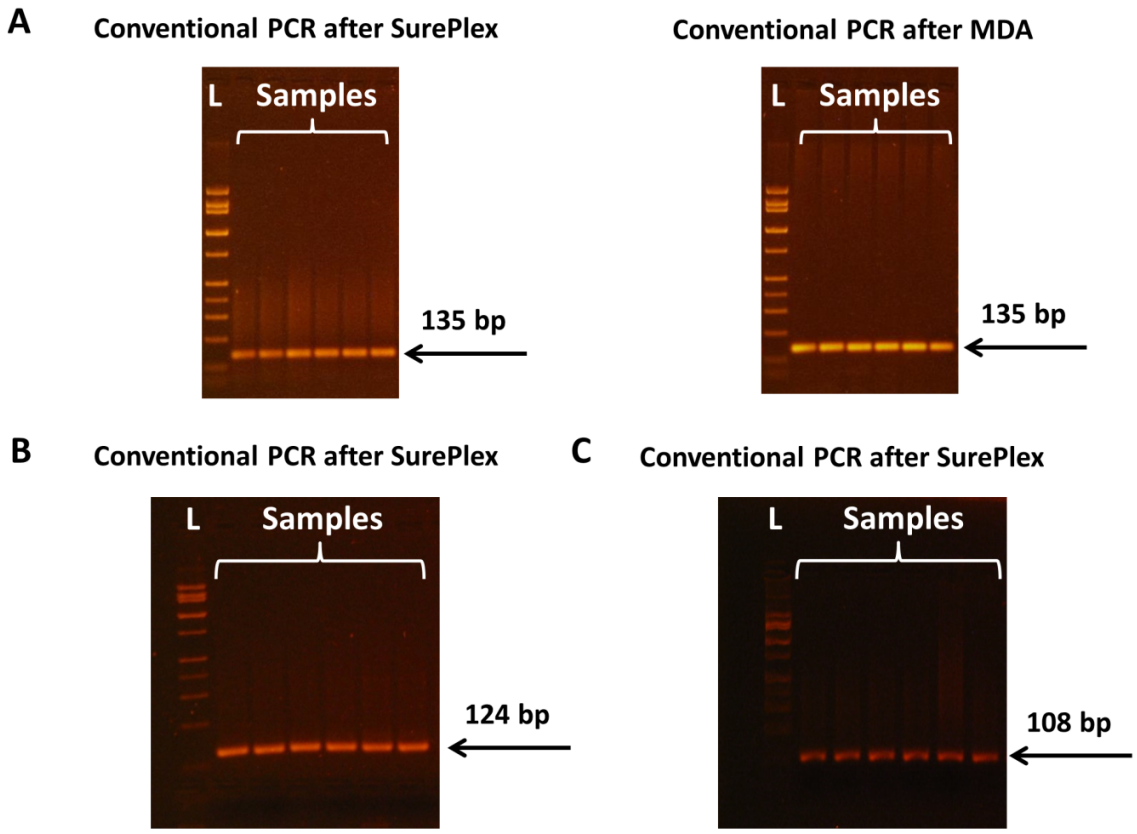


Figure 4.3: Gel images of amplification products after WGA followed by conventional PCR. Single control lymphocytes ('Samples') were subjected to WGA followed by conventional PCR targeting the (**A**) m.8993 mutation site (SurePlex and MDA) resulting in 135 bp products, the (**B**) m.10191 mutation site resulting in 124 bp products and the (**C**) m.3243 mutation site resulting in 108 bp products. L = ladder.

4.3.2 Assessment of accuracy and sensitivity of the designed test

Accuracy as well as sensitivity of the designed sequencing method in quantifying heteroplasmy levels was assessed. To do this, mixtures of two gDNA samples of equal concentration were created to obtain samples with varying levels of heteroplasmy at position m.8993 (T>G): 5.0 %, 10.0 %, 20.0 %, 40.0 %, 60.0 % and 80.0 %. GDNA samples were obtained from a control individual (100 % homoplasmic and wild-type at the m.8993 mutation site) and the deceased daughter of Patient A, who was 100 % homoplasmic for

the m.8993G variant. All gDNA samples, sample mixtures as well as undiluted gDNA samples of both individuals (representing 0.0 % and 100 % mutation load) were subjected to conventional PCR to enrich the m.8993 mtDNA region, followed by library preparation and sequencing.

Figure 4.4 illustrates the obtained heteroplasmy levels at position m.8993 plotted against the expected heteroplasmy ratios. Raw data and sequencing depths at position m.8993 are presented in **Tables B.2** and **B.3** in **Appendix B**, respectively.

The method proved to be highly accurate. Observed and expected ratios were almost identical (mean difference: 2.4 % ± 2.8 % SD) resulting in a correlation coefficient of 0.9972 ($p < 0.0001$). Furthermore, ratios of mutant and wild-type mtDNA species were linear ($r^2 = 0.9944$). Of note, undiluted samples which were homoplasmic for either the mutant or the wild-type mtDNA variant, showed exactly 100 % or 0.0 % of the mutation, respectively. Furthermore, the method proved to be highly sensitive and heteroplasmy levels could be detected at the lowest level assessed.

Next, the same series of gDNA mixtures as well as undiluted samples from the control individual and the homoplasmic carrier of the mutant mtDNA variant (m.8993G) were subjected to WGA followed by conventional PCR. This was important to rule out possible amplification bias caused during WGA (prior to conventional PCR) which may result in over- or under-representation of either the mutant or wild-type allele.

The results after sequencing are illustrated in **Figure 4.5**. The obtained heteroplasmy levels were plotted against the heteroplasmy levels observed during the

previous experiment. Raw data and sequencing depths are presented in **Table B.4** and **B.5** in **Appendix B**, respectively.

A strong correlation was observed between obtained heteroplasmy levels detected after WGA followed by conventional PCR and those measured after PCR only ($r = 0.9987$, $p < 0.0001$). Observed ratios were nearly identical to ratios observed in the previous experiment (mean difference: 1.8 % ± 1.9 % SD) and resulted in an almost perfect linear regression ($r^2 = 0.9975$). Again, samples consisting of either 100 % mutant or 100 % wild-type mtDNA variants presented with 100 % or 0.0 % mutation load, respectively. Of note, the sample with the lowest mtDNA mutation proportion was nearly equivalent to the previously obtained result (3.2 % versus 3.4 %), differing by only 0.2 %. This indicated that the use of WGA does not lead to distortion of the relative quantities of wild-type and mutant mtDNA molecules.

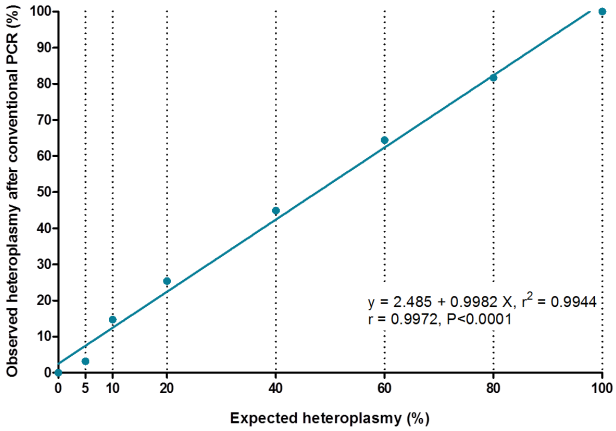


Figure 4.4: Correlation of observed and expected heteroplasmy levels at position m.8993. The graph shows the detected heteroplasmy levels after sequencing (dots) and the corresponding best-fit line. r^2 indicates r-squared value after linear regression analysis. The equation of the best-fit line is shown. r indicates Pearson's rank correlation coefficient with the corresponding p-value.

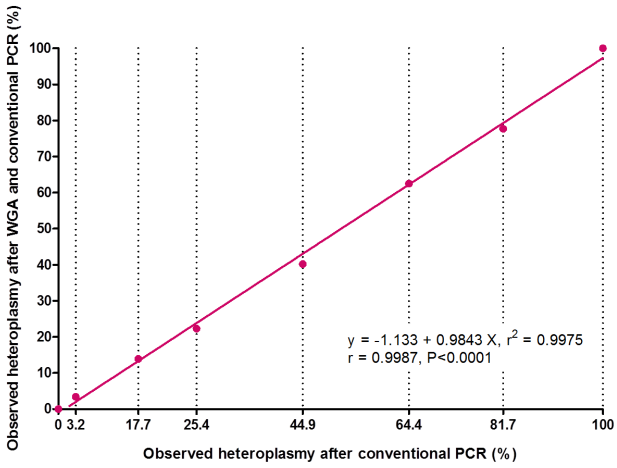


Figure 4.5: Correlation of observed heteroplasmy levels after WGA and conventional PCR and observed heteroplasmy levels after conventional PCR at position m.8993. The graph shows the detected heteroplasmy levels after sequencing of WGA samples (dots) and the corresponding best-fit line. r^2 indicates r-squared value after linear regression analysis. The equation of the best-fit line is shown. r indicates Pearson's rank correlation coefficient with the corresponding p-value.

4.3.3 Assessment of patient and carrier samples

Prior to the clinical application of the PGD protocol the method was tested on gDNA and cell samples derived from the patients and their affected children. This was important to ensure test reliability. Furthermore, testing on samples consisting of few cells or single cells was critical to mimic the amount of DNA/cells present in an embryo biopsy.

4.3.3.1 Patient A

Patient A (56.0 % heteroplasmic for m.8993T>G) provided a buccal swab and a blood sample. GDNA was isolated from both sample types. In addition, cell samples consisting of one, three and five lymphocytes were prepared from her blood sample. A gDNA sample was also obtained from her deceased child (100 % homoplasmic for m.8993G) from the laboratory which performed the previous diagnosis.

Initially, gDNA extracted from blood and buccal samples of Patient A was amplified via conventional PCR only, targeting the m.8993 mutation site, followed by sequencing. Results were then compared to the expected heteroplasmy level of 56.0 %, which has previously been established by a reference laboratory.

Next, 100 pg of gDNA (equivalent to approximately 17 cells) from both sample types (buccal swab and blood) were amplified via WGA followed by conventional PCR and compared to the expected ratio and to the ratio obtained from the previous experiment. This was done to provide further confirmation that WGA prior to conventional PCR does not introduce errors or cause amplification bias. Results of both experiments are shown in **Figure 4.6**. Raw data and sequencing depth at position m.8993 are given in **Tables B.6** and **B.7** in **Appendix B**.

Analysis of four aliquots of gDNA derived from blood and buccal samples (two aliquots per sample type) showed a mean mutation load of 54.4 % ± 1.9 % SD (blood: 53.5 % ± 2.2 SD; buccal cells: 55.4 % ± 1.3 SD) after conventional PCR (**Figure 4.6 A**). Analysis of eight aliquots (four per sample type) subjected to WGA and PCR showed a mean mutation ratio of 55.9 % ± 5.8 % SD (blood: 55.6 % ± 5.5 SD; buccal cells: 56.1 % ± 6.9 SD; **Figure 4.6 B**). Mean mutation loads of both experiments were close to the expected value of 56.0 %. Furthermore, mean values of extracted gDNA prior and after WGA were consistent and differed only slightly between both experiments (~1.5 %).

Of note, the SD was higher in samples subjected to WGA prior to conventional PCR as compared to those subjected to PCR only. This was most likely due to the low input amount of gDNA (100 pg) which might have resulted in slight variations in heteroplasmy levels between the processed samples.

Next, the method was tested on lymphocyte samples from Patient A, which were obtained from the same blood draw as the gDNA used in the above described experiments. Cell samples were again either amplified by conventional PCR or by WGA followed by PCR. In each experiment (with and without prior WGA), two samples either consisting of a single cell, three cells or five cells were processed (total of six samples per experiment). The obtained results are illustrated in **Figure 4.7**. Raw data, including sequencing depths are presented in **Tables B.8** and **B9** in **Appendix B**.

A wide range in mutation load was detected between individual samples ranging from 0.0 % - 97.3 % (**Figure 4.7 A**) and 0.0 % - 100 % (**Figure 4.7 B**) in samples processed via PCR or via WGA and PCR, respectively. Of note, the widest variation was seen in samples consisting of single cells.

Intercellular variation is common in heteroplasmic individuals. Therefore, in order to compare results obtained from cell samples to the expected ratio (56 %) and to the results obtained from the patient's gDNA the mean mutation loads were calculated.

To get an accurate estimate on the mean mutation rate in lymphocytes, the average heteroplasmy levels were calculated by taking into account the number of cells present in each sample. Therefore, mutation loads were multiplied by a specific factor to reach the lowest common multiple (30). Single cells were multiplied by 30, 3-cell samples by 10 and 5-cell samples by 6. The sum of all samples was then divided by 92. This resulted in calculated means of 54.3 % ± 42.9 % SD and 53.7 % ± 43.0 % SD before and after WGA, respectively.

Calculated means were close to the expected ratio and most importantly almost identical to ratios obtained in Patient A's gDNA, differing by 0.1 % (after PCR) and 2.2 % (after WGA and PCR).

Figure 4.8 summarises the findings of all experiments performed in samples derived from Patient A. In summary, results obtained from different sample types and amplification procedures were consistent and close to the expected heteroplasmy level, confirming that the developed test could accurately predict the mutation load.

No cells were available from the deceased child. Therefore, only gDNA was processed. Conventional PCR was performed on two aliquots. Similarly, WGA followed by conventional PCR was performed on two samples each consisting of 100 pg input gDNA. The raw data and number of sequencing reads are given in **Table B.10** in **Appendix B**.

In all four samples 100 % mutation load was detected which was consistent with the previously established homoplasmy for m.8993G.

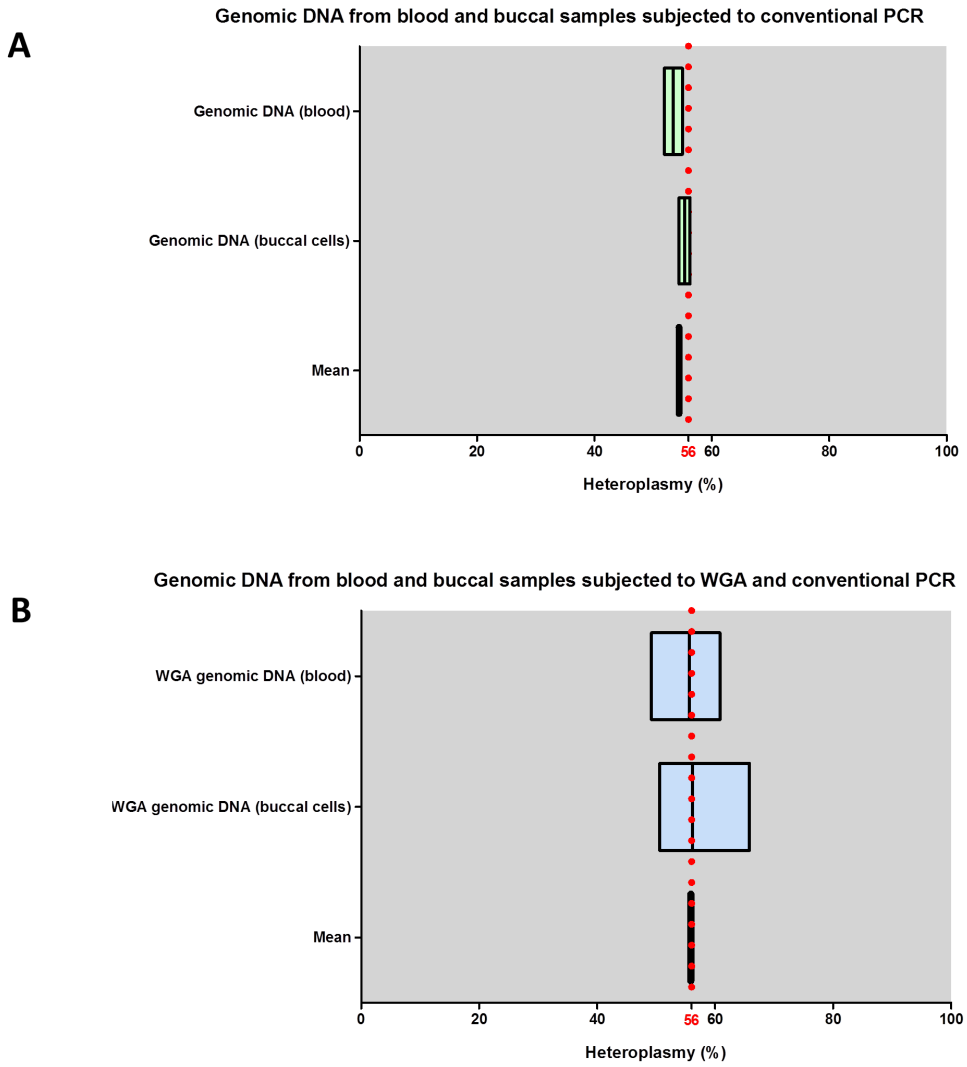


Figure 4.6: Obtained heteroplasmy levels in gDNA extracted from blood and buccal samples of Patient A. Floating bars (green and blue) show the lowest and highest detected mutation load (left and right border, respectively). Mean mutation ratios are indicated by the central vertical line in each floating bar. Black bars show mean mutation ratios, calculated from all samples in each experiment (**A** or **B**). Dotted lines (red) indicate the expected heteroplasmy level of 56.0 %. Graph **A** illustrates results obtained after conventional PCR (two samples per sample type). Graph **B** shows results obtained after WGA followed by conventional PCR (four samples per sample type).

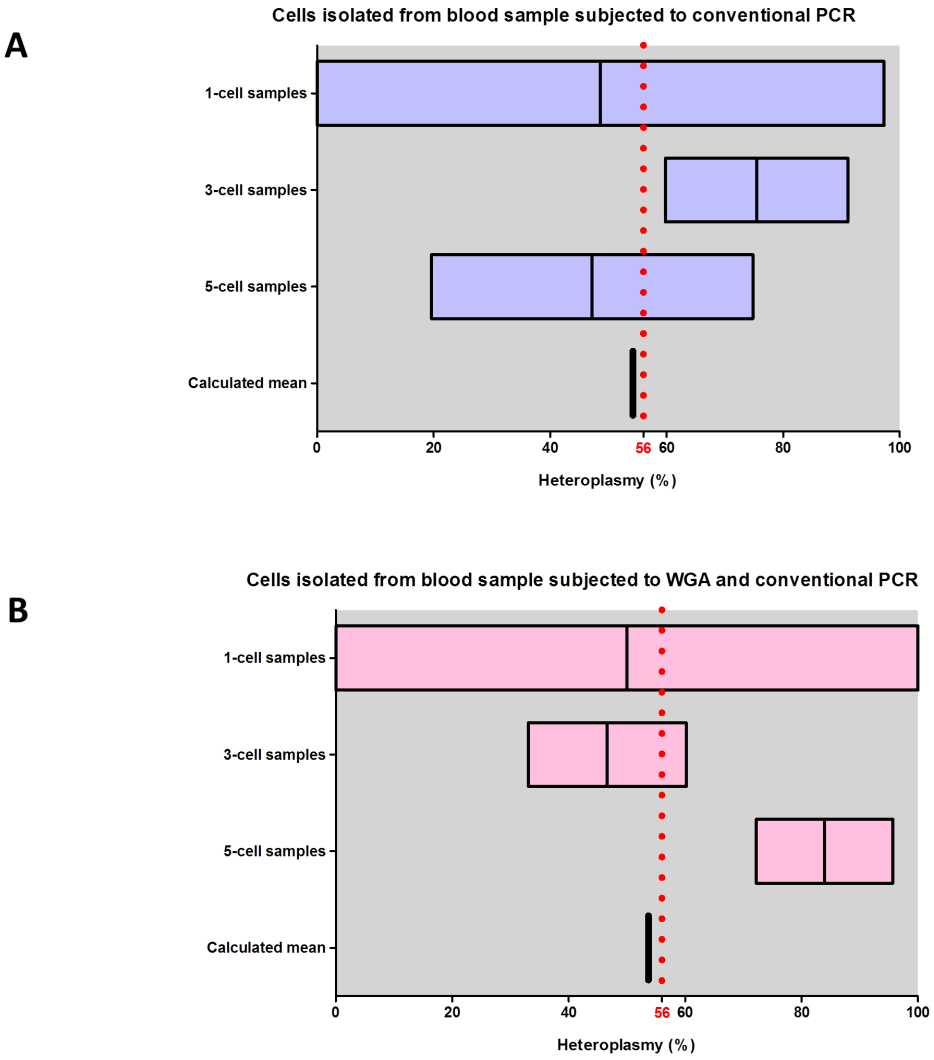


Figure 4.7: Obtained heteroplasmy levels in lymphocyte samples of Patient A. Floating bars (purple and pink) show the lowest and highest detected mutation load (left and right border, respectively). Mean mutation ratios are indicated by the central vertical line in each floating bar. Black bars show mean mutation ratios calculated from all cell samples in each experiment (**A** or **B**). Dotted lines (red) indicate the expected heteroplasmy level of 56.0 %. Graph **A** illustrates results obtained after conventional PCR (two samples per sample type). Graph **B** shows results obtained after WGA followed by conventional PCR (two samples per sample type).

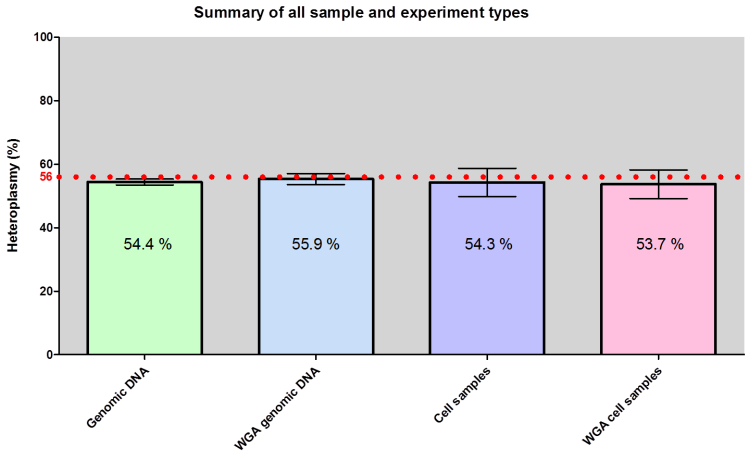


Figure 4.8: Summary of obtained mean heteroplasmy levels in gDNA and lymphocyte samples of Patient A. Obtained mean heteroplasmy levels were consistent between different sample types (gDNA and cell samples) and experiment types (conventional PCR and WGA followed by PCR). Furthermore, heteroplasmy levels were consistently close to the expected ratio of 56.0 % (red dotted line). Error bars depict standard error of the mean (SEM).

4.3.3.2 Patient B

A blood sample was obtained from Patient B (0.0 % heteroplasmic for m.8993T>G) and the son of Patient B (95.0 % heteroplasmic for m.8993T>G). GDNA and single cells were isolated from both samples. Similarly to the validation experiments performed for Patient A, mutation load was assessed in gDNA and single cells of both individuals, prior and after WGA.

Samples assessed from Patient B included one aliquot of gDNA processed via conventional PCR, two aliquots of gDNA (100 pg) amplified via SurePlex followed by PCR, three single lymphocyte cells amplified via PCR and six single lymphocytes subjected to WGA and PCR. Raw data and sequencing depths are presented in **Tables B.11**, **B.12**, **B.13** and **B.14** in **Appendix B**.

In concordance with the previous diagnosis, all samples assessed showed 0.0 % mutation load at position m.8993.

Next, samples from the affected son were analysed. Results obtained from his gDNA are illustrated in **Figure 4.9**. Raw data and number of sequencing reads are given in **Tables B.15** and **B.16** in **Appendix B**.

A heteroplasmy level of 97.1 % was detected in his gDNA (one aliquot) following conventional PCR which was close to the previously established value of 95.0 % (**Figure 4.9 A**). Three aliquots of gDNA (each containing 100 pg of gDNA) were sequenced after WGA followed by PCR, resulting in a mean mutation load of 95.6 % ± 3.4 % SD (**Figure 4.9 B**). Again, results were very similar to the result obtained from gDNA and nearly identical to the previously established mutation load.

Results obtained from samples consisting of single lymphocytes are shown in **Figure 4.10**. Raw data and sequencing depths are shown in **Tables B.17** and **B.18** (**Appendix B**).

Three single cell samples were sequenced after amplification of the m.8993 mutation site following conventional PCR. The mean mutation load was 97.6 % ± 4.0 % SD, ranging from 93.0 % - 100 % (**Figure 4.10 A**). A total of nine cell samples were analysed after WGA followed by PCR. Mean heteroplasmy was 92.8 % ± 20.0 % SD, ranging from 39.5 % - 100 %. The mean mutation load was slightly lower and a wider intercellular variation was observed, as shown in **Figure 4.10 B**. This was caused by a single sample with a low variant mtDNA level (39.5 %). Mutant load in the remaining eight samples ranged from 98.0 % - 100 %.

Figure 4.11 summarises the results obtained from all processed samples from the son of Patient B. Results obtained from gDNA and single cells prior and after WGA were very similar and close to the previously measured mutation value, confirming that the test could accurately predict the mutation load.

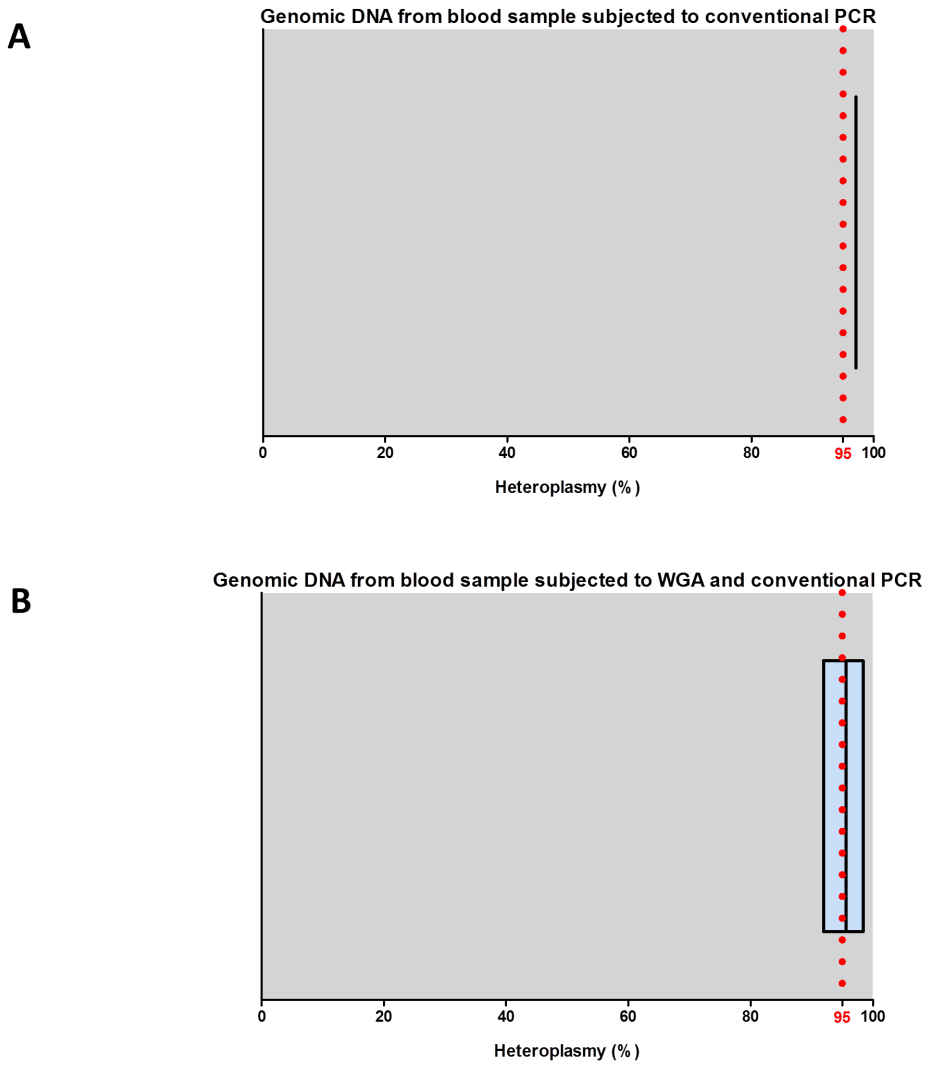


Figure 4.9: Obtained heteroplasmy levels in gDNA extracted from the blood sample of the son of Patient B. Dotted lines (red) indicate the expected heteroplasmy level of 95.0 %. Graph **A** illustrates the result obtained after conventional PCR in one sample. Graph **B** shows results obtained after WGA followed by conventional PCR (three samples). The blue floating bar shows the lowest and highest detected mutation load (left and right border, respectively). The mean mutation ratio is indicated by the central vertical line in the floating bar.

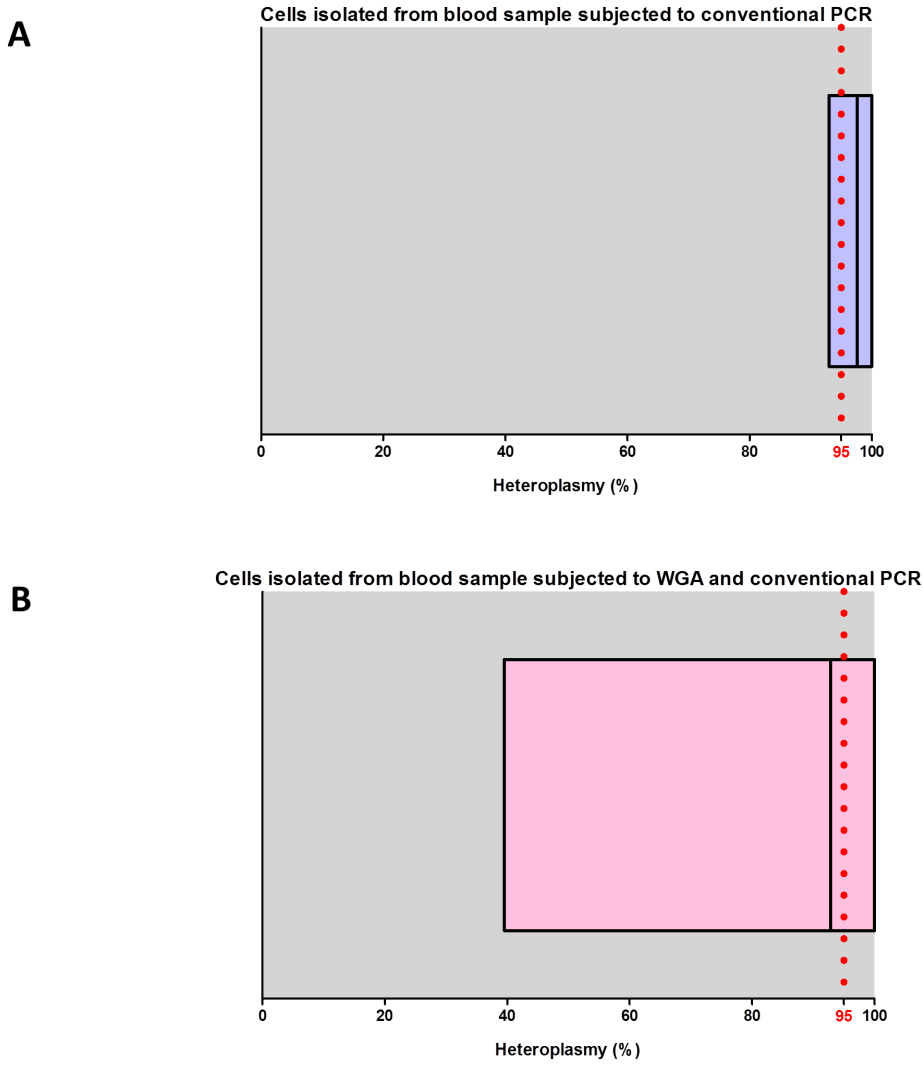


Figure 4.10: Obtained heteroplasmy levels in lymphocyte samples of the son of Patient B. Floating bars (purple and pink) show the lowest and highest detected mutation load (left and right border, respectively). Mean mutation ratios are indicated by the central vertical line in each floating bar. Dotted lines (red) indicate the expected heteroplasmy level of 95.0 %. Graph **A** illustrates results obtained after conventional PCR (three samples). Graph **B** shows results obtained after WGA followed by conventional PCR (nine samples).

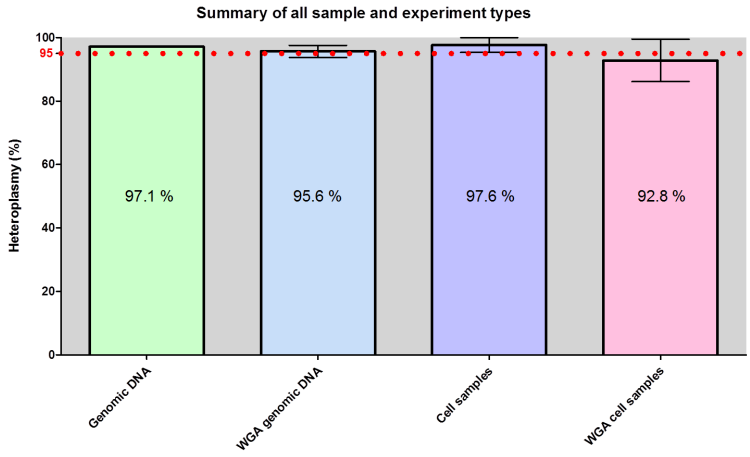


Figure 4.11: Summary of obtained heteroplasmy levels in gDNA and lymphocyte samples of the son of Patient B. Obtained mean heteroplasmy levels were consistent between different sample types (gDNA and cell samples) and experiment types (conventional PCR and WGA followed by PCR). Furthermore, heteroplasmy levels were consistently close to the expected ratio of 95.0 % (red dotted line). Error bars depict SEM.

4.3.3.3 Patient C

A blood and buccal sample was obtained from Patient C (0.0 % heteroplasmic for m.10191T>C). GDNA and single lymphocytes were isolated from her blood sample. Additionally, single buccal cells were isolated from her buccal swab. Buccal samples were also obtained from her daughter (78.0 % heteroplasmic for m.10191T>C) and gDNA as well as single cells isolated. Again, mutation load was assessed in gDNA and cells of both individuals after conventional PCR targeting the m.10191 mutation site and after WGA combined with PCR.

Analysis of Patient C's gDNA after conventional PCR and after WGA combined with PCR was performed in triplicate and duplicate, respectively. A single buccal cell and a single lymphocyte were subjected to PCR and analysed. Moreover, three buccal cells and three

lymphocytes were analysed after WGA and PCR. Results and sequencing outputs are presented in **Tables B.19**, **B.20**, **B.21** and **B.22** in **Appendix B**.

As expected, the assessed mutation was not detected in any of the samples from Patient C, consistent with previous findings.

A mean mutation load of 84.7 % ± 0.5 % SD was detected in the gDNA of Patient C's daughter, which was almost 7.0 % higher as compared to the previously established value (78.0 %) by a reference lab (**Figure 4.12**). Of note, three aliquots were processed which gave all almost identical results. Moreover, a similar result was obtained from five different gDNA aliquots. Following WGA and conventional PCR a mean mutation load of 83.9 % ± 1.6 % SD was obtained, which differed by less than 1.0 % compared to the results obtained after PCR.

Raw data and sequencing outputs after analyses of gDNA samples are presented in **Tables B.23** and **B24** in **Appendix B**.

The observed findings of relatively high heteroplasmy levels in her gDNA were also confirmed after the analysis of single buccal cells. Four single cell samples were sequenced following conventional PCR. This resulted in a mean mutation load of 89.0 % ± 5.1 % SD, ranging from 83.5 % - 93.5 %. Furthermore, six single cells were subjected to WGA and conventional PCR resulting in a mean heteroplasmy level of 82.0 % ± 7.2 % SD, ranging from 77.3 % - 94.3 %.

Results are shown in **Figure 4.13**. Raw data and sequencing results are presented in **Tables B.25** and **B.26** in **Appendix B**.

Figure 4.14 summarises the findings obtained from Patient C's daughter. Although heteroplasmy levels were higher than expected in her gDNA and cells isolated from buccal samples, obtained results were consistent and gDNA and cell samples comparable.

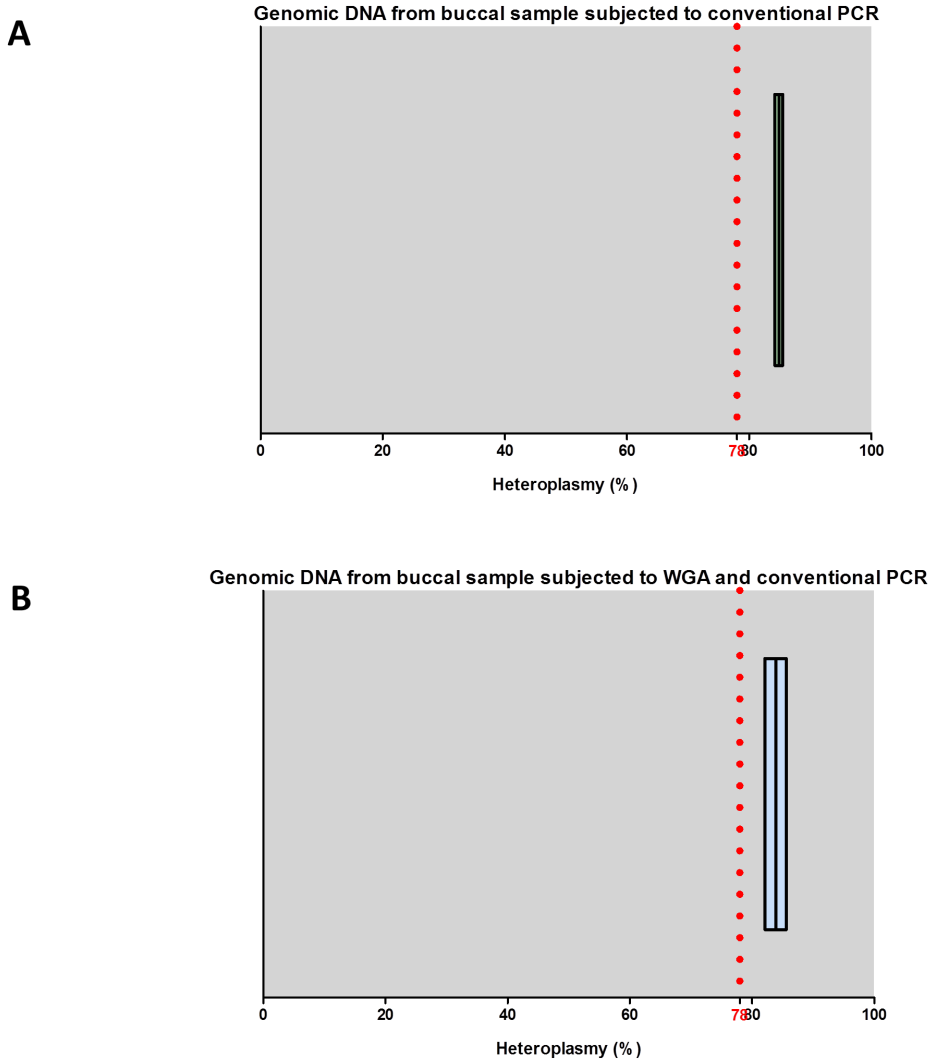


Figure 4.12: Obtained heteroplasmy levels in gDNA extracted from the buccal sample of the daughter of Patient C. Floating bars (green and blue) show the lowest and highest detected mutation load (left and right border, respectively). Mean mutation ratios are indicated by the central vertical line in each floating bar. Dotted lines (red) indicate the expected heteroplasmy level of 78.0 %. Graph **A** illustrates results obtained after conventional PCR (three samples). Graph **B** shows results obtained after WGA followed by conventional PCR (five samples).

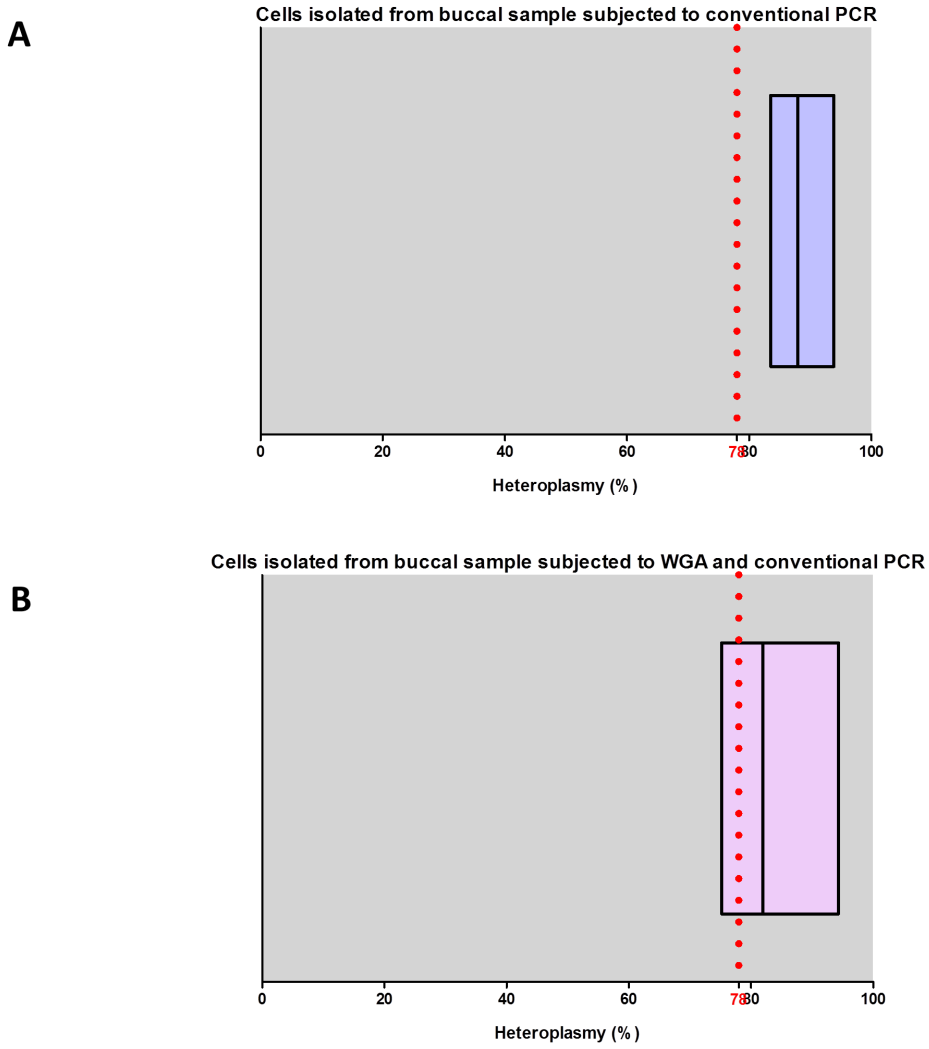


Figure 4.13: Obtained heteroplasmy levels in cell samples (buccal cells) of the daughter of Patient C. Floating bars (purple and pink) show the lowest and highest detected mutation load (left and right border, respectively). Mean mutation ratios are indicated by the central vertical line in each floating bar. Dotted lines (red) indicate the expected heteroplasmy level of 78.0 %. Graph **A** illustrates results obtained after conventional PCR (four samples). Graph **B** shows results obtained after WGA followed by conventional PCR (six samples).

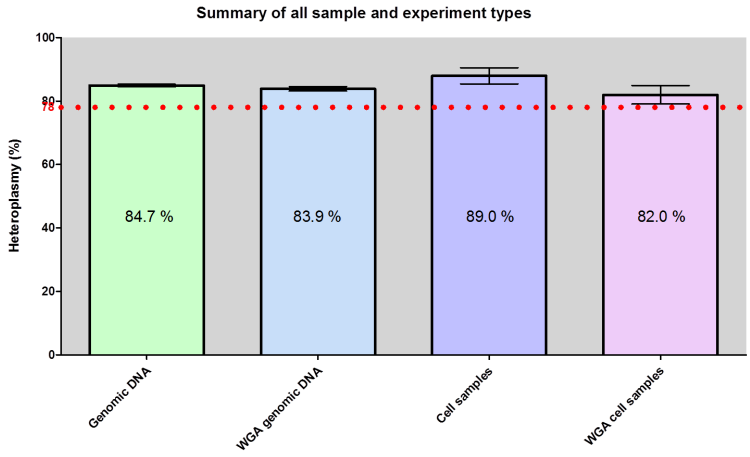


Figure 4.14: Summary of obtained heteroplasmy levels in gDNA and buccal cell samples of the daughter of Patient C. Obtained mean heteroplasmy levels were higher compared to the expected value of 78.0 % (red dotted line), however this was consistent between different sample types (gDNA and cell samples) and experiment types (conventional PCR and WGA followed by PCR). Error bars depict SEM.

4.3.3.4 Patient D

One blood sample and two buccal swabs were obtained from Patient D (28.0 % heteroplasmic for m.3243A>G). GDNA and single lymphocytes were isolated from her blood sample. GDNA was also extracted from one buccal sample and single buccal cells were isolated from the other sample. Mutation loads were assessed in gDNA and cell samples of both sample types following conventional PCR targeting the m.3243A>G mutation site and after WGA combined with PCR.

Results obtained from gDNA and cell samples are shown in **Figures 4.15** and **4.16**, respectively. Raw data and sequencing depths at position m.3243 obtained from gDNA and cell samples which were processed with or without initial WGA are given in **Tables B.27**, **B.28**, **B.29** and **B.30** in **Appendix B**, respectively.

A mean mutation load of 9.6 % ± 5.1 % SD (**Figure 4.15 A**) was detected in Patient D`s gDNA following conventional PCR. Of note, the mutation load in gDNA extracted from buccal cells was more than twice as high as compared to the level detected in the blood sample (13.2 % versus 6.0 %). Moreover, the detected mutation levels were substantially lower than the levels previously identified in a muscle biopsy.

Importantly, these findings were in concordance with the results obtained after analysis of gDNA subjected to WGA and conventional PCR (**Figure 4.15 B**) and after the analysis of cell samples (**Figure 4.16 A**). Almost identical mutation levels of 6.7 % and 14.7 % were detected in gDNA of blood and buccal samples, respectively, resulting in a mean mutation load of 10.7 % ± 5.7 % SD. Similarly, single cells (six lymphocytes and six buccal cells) had an overall mean mutation load of 12.7 % ± 23.5 % SD (lymphocytes: 8.2 % ± 20 % SD; buccal cells: 17.2 % ± 27.7 % SD). Of note, a large intercellular variation was observed. Of all lymphocytes analysed, only one carried mutated mtDNA copies (49.0 %) and of all buccal cells analysed only two carried the mutation (39.1 % and 63.8 %).

Similar variations were also observed in cells subjected to WGA and PCR (**Figure 4.16 B**). Of the six lymphocytes analysed, only one carried the mutation (49.7 % heteroplasmy). Of the six buccal cells analysed, half carried the mutation. Of note, heteroplasmy levels were low (1.2 %, 13.0 % and 1.6 %) resulting in an overall mean mutation rate of 4.5 % ± 14.3 % SD (lymphocytes: 8.3 % ± 20.3 % SD; buccal cells: 0.7 % ± 0.8 % SD).

Figure 4.17 summarises the findings of Patient D's gDNA and cell samples. Although heteroplasmy levels differed between sample types and were also lower than the

previously established level in her muscle tissue, obtained results were consistent and comparable.

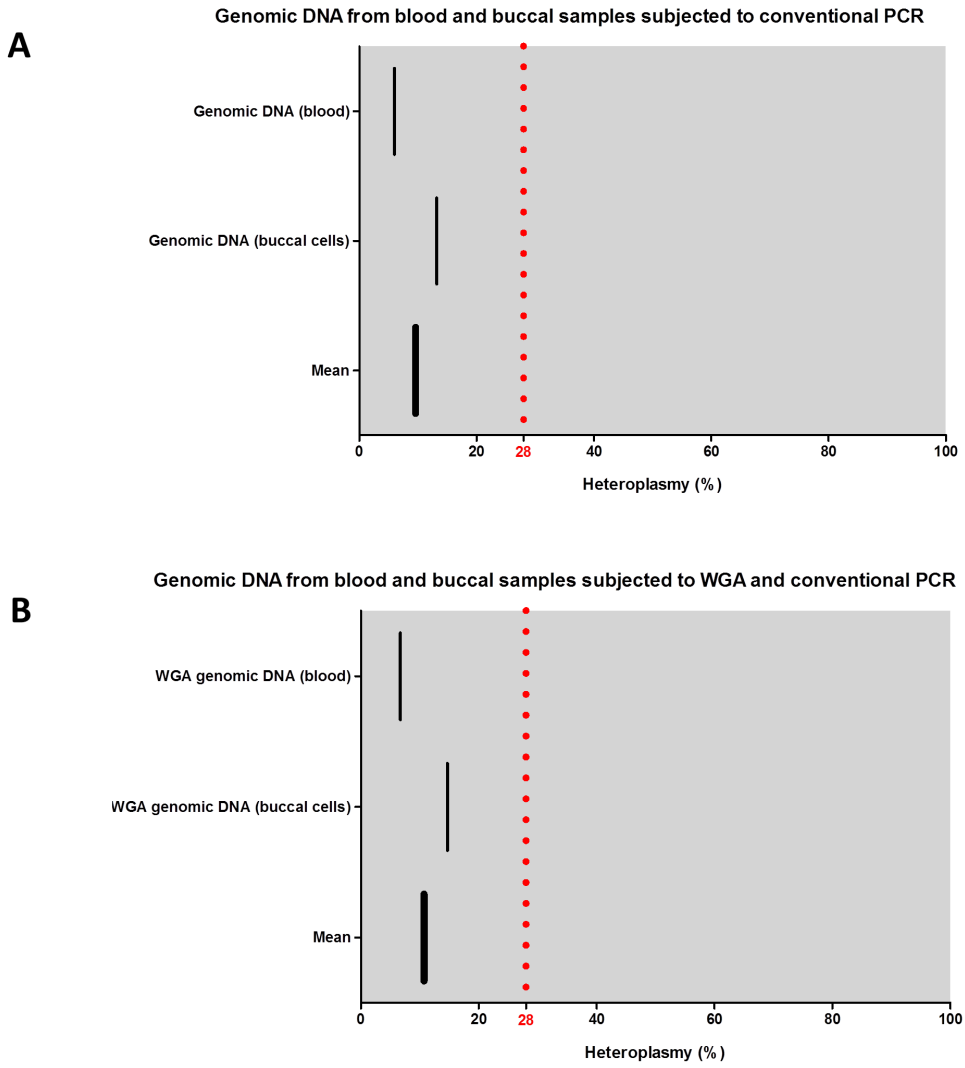


Figure 4.15: Obtained heteroplasmy levels in gDNA extracted from blood and buccal samples of Patient D. Dotted lines (red) indicate the expected heteroplasmy level of 28.0 %. Graph **A** illustrates the results obtained after conventional PCR in gDNA of blood and buccal samples (one sample per sample type). Graph **B** shows results obtained after WGA followed by conventional PCR in gDNA of blood and buccal samples (one sample per sample type).

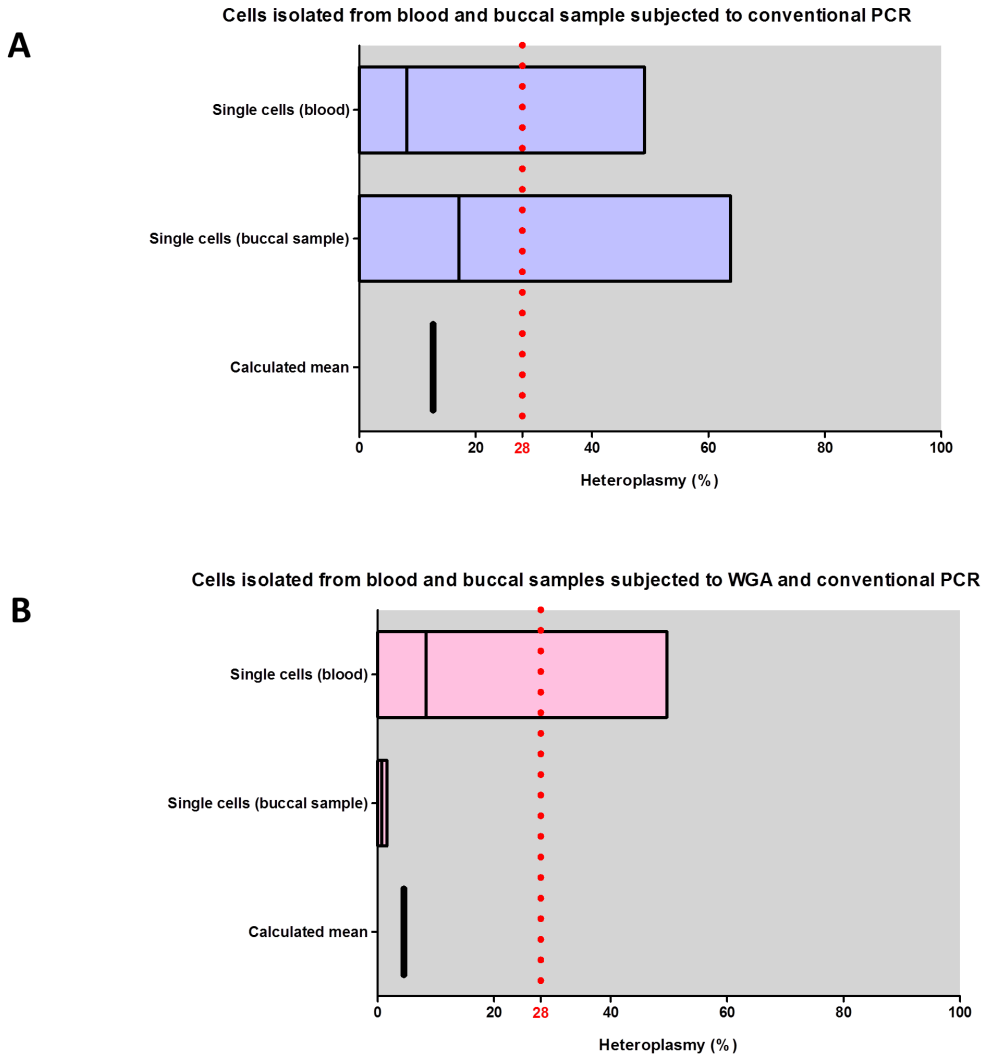


Figure 4.16: Obtained heteroplasmy levels in cell samples (lymphocytes and buccal cells) of Patient D. Floating bars (purple and pink) show the lowest and highest detected mutation load (left and right border, respectively). Mean mutation ratios are indicated by the central vertical line in each floating bar. Black bars indicate mean mutation ratios calculated from all cell samples in each experiment (**A** or **B**). Dotted lines (red) indicate the expected heteroplasmy level of 28.0 %. Graph **A** illustrates results obtained after conventional PCR (six samples per sample type). Graph **B** shows results obtained after WGA followed by conventional PCR (six samples per sample type).

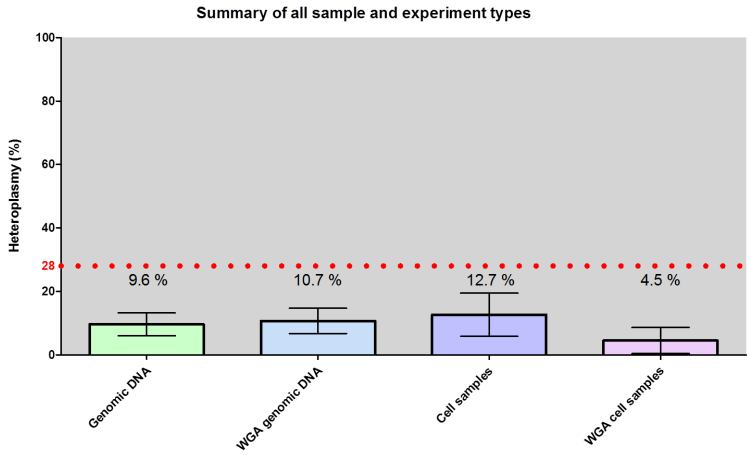


Figure 4.17: Summary of obtained heteroplasmy levels in gDNA and cell samples of Patient D. Obtained mean heteroplasmy levels were lower as compared to the expected value of 28.0 % (red dotted line). These findings were consistent between different sample and experiment types. Error bars depict SEM.

4.4 Clinical application of the developed protocol - **CHAPTER 4**

4.4.1 Case report Patient A

Patient A underwent two consecutive IVF cycles. Two oocytes were collected after the first cycle (IDs 1 and 2) and two oocytes after her second cycle (IDs 3 and 4). Three oocytes fertilised successfully (IDs 1, 2 and 3) and one oocyte failed to fertilise (ID 4). Of the three fertilised oocytes, one zygote (ID 1) developed to the blastocyst-stage. Embryos 2 and 3 (from zygotes 2 and 3) arrested during development. A trophectoderm biopsy was performed on embryo 1 on day-5 post fertilisation and the embryo vitrified. The unfertilised oocyte and both arrested embryos were placed whole into individual tubes.

All samples and four negative controls, consisting of approximately 2 µl wash buffer from the last wash drop of each sample, were subjected to SurePlex amplification. Amplification products were visualised on an agarose gel. Successful amplification was obtained from the oocyte and all embryonic samples. No amplification was observed in negative controls, confirming absence of possible exogenous DNA contamination.

Analysis of mtDNA mutation load at position m.8993 was performed in the trophectoderm biopsy and in the arrested embryos and the unfertilised oocyte. CCS was performed in the TE biopsy and the arrested embryos using array CGH. Results are presented in **Table 4.1**. Sequencing depths are presented in **Table B.31** in **Appendix B**.

No mutation was detected in the trophectoderm biopsy derived from embryo 1. However, an abnormal chromosome content was identified (48,XXY,+16). Hence, no embryo transfer was performed. One of the arrested embryos (ID 2) was found to be free of the mutation and to be euploid. The second arrested embryo (ID 3) was aneuploid and in addition carried high levels of the mutation (88.7 %). Similarly, the unfertilised oocyte carried high levels of the mutation (91.2 %).

Table 4.1: Mutation load at position m.8993 (T>G) and karyotype detected in clinical samples of Patient A

ID	Sample type	Mutation load (%)	Predicted karyotype	Interpretation
1	Trophectoderm biopsy	0.0	48,XXY,+16	Mutation not detected; aneuploid
2[1]	Whole embryo	0.0	46,XX	Mutation not detected; euploid
3[1]	Whole embryo	88.7	47,XXY,5,+6	Mutation detected; aneuploid
4	Unfertilised oocyte	91.2	Not tested	Mutation detected

1 = arrested at cleavage-stage.

4.4.2 Case report Patient B

Patient B underwent one cycle of IVF treatment. A total of 18 oocytes were collected (IDs 1 - 18) and subjected to ICSI. One oocyte failed to fertilise (ID 16). Two embryos arrested at the cleavage-stage (IDs 11 and 13). Single blastomeres of both embryos were separated and tubed individually. Embryo 11 consisted of five blastomeres (IDs 11a - 11e). Embryo 13 contained eleven blastomeres (IDs 13a - 13k). One embryo arrested during blastocyst formation (ID 14) and was tubed in whole. A total of 14 zygotes (IDs 1 - 10, 12, 15, 17 and 18) developed into competent blastocyst-stage embryos, which were biopsied followed by cryopreservation.

SurePlex was performed on the unfertilised oocyte, all single sister blastomere samples, the arrested blastocyst-stage embryo and all trophectoderm biopsies. Additionally, WGA amplification was performed on all biopsy negative controls. All samples amplified which was evident by a smear on the agarose gel. Moreover, no contamination was detected in the negative controls.

Analysis of mtDNA mutation load at position m.8993 as well as CCS utilising array CGH was performed on all samples. Obtained results are presented in **Table 4.2**. Sequencing outputs are given in **Table B.32** in **Appendix B**. All of the single sister blastomere samples of the arrested embryo 13 carried more than four chromosome abnormalities and were defined as 'complex abnormal'. A detailed karyotype analysis of those samples is provided in **Table B.33** in **Appendix B**.

Interestingly, no mutation was present at detectable levels in any of the assessed samples. Of note, four of the 14 blastocysts were found to be chromosomally abnormal.

The patient received a transfer of a euploid male embryo and became pregnant. No pregnancy complications were reported and the patient delivered a healthy boy at 40 weeks of gestation.

To confirm the previous diagnosis, cord blood was collected at birth. Furthermore, buccal swabs were collected from the newborn at two and three weeks of age. GDNA was isolated from both sample types and sequenced (without prior WGA). No mutant variant was detected at position m.8993 in any of the newborn's samples confirming previous PGD diagnosis. Sequencing outputs are presented in **Table B.34** in **Appendix B**.

It is also worth mentioning, that although all sister blastomeres of embryos 11 and 13 were aneuploid, a high presence of mosaicism was detected and blastomeres carried meiotic abnormalities (e.g. loss of chromosome 15 in embryo 11) as well as abnormalities that arose during the cleavage divisions.

Table 4.2: Mutation load at position m.8993 (T>G) and karyotype detected in clinical samples of Patient B

ID		Sample type	Mutation load (%)	Predicted karyotype	Interpretation
1		Trophectoderm biopsy	0.0	46,XY	Mutation not detected; euploid
2		Trophectoderm biopsy	0.0	46,XX	Mutation not detected; euploid
3		Trophectoderm biopsy	0.0	46,XX	Mutation not detected; euploid
4		Trophectoderm biopsy	0.0	46,XY	Mutation not detected; euploid
5		Trophectoderm biopsy	0.0	45,XY,-16	Mutation not detected; aneuploid
6		Trophectoderm biopsy	0.0	46,XY	Mutation not detected; euploid
7		Trophectoderm biopsy	0.0	45,XY,-11	Mutation not detected; aneuploid
8		Trophectoderm biopsy	0.0	46,XY	Mutation not detected; euploid
9		Trophectoderm biopsy	0.0	46,XX	Mutation not detected; euploid
10		Trophectoderm biopsy	0.0	46,XX	Mutation not detected; euploid
11[1]	a	Blastomere	0.0	45,XYY,-6,-15	Mutation not detected; aneuploid
	b	Blastomere	0.0	44,XYY,-2,-6,-15	Mutation not detected; aneuploid
	c	Blastomere	0.0	45,XY,-15	Mutation not detected; aneuploid
	d	Blastomere	0.0	47,XYY,+3,-6,-15,+22	Mutation not detected; aneuploid
	e	Blastomere	0.0	47,XYY,-15,+22	Mutation not detected; aneuploid
12		Trophectoderm biopsy	0.0	46,XX	Mutation not detected; euploid
13[1]	a[3]	Blastomere	0.0	Complex abnormal	Mutation not detected; aneuploid
	b[3]	Blastomere	0.0	Complex abnormal	Mutation not detected; aneuploid
	c[3]	Blastomere	0.0	Complex abnormal	Mutation not detected; aneuploid
	d[3]	Blastomere	0.0	Complex abnormal	Mutation not detected; aneuploid
	e[3]	Blastomere	0.0	Complex abnormal	Mutation not detected; aneuploid
	f[3]	Blastomere	0.0	Complex abnormal	Mutation not detected; aneuploid
	g[3]	Blastomere	0.0	Complex abnormal	Mutation not detected; aneuploid
	h[3]	Blastomere	0.0	Complex abnormal	Mutation not detected; aneuploid
	i[3]	Blastomere	0.0	Complex abnormal	Mutation not detected; aneuploid
	j[3]	Blastomere	0.0	Complex abnormal	Mutation not detected; aneuploid
	k[3]	Blastomere	0.0	Complex abnormal	Mutation not detected; aneuploid
14[2]		Whole embryo	0.0	47,XX,+16	Mutation not detected; aneuploid
15		Trophectoderm biopsy	0.0	47,XX,+22	Mutation not detected; aneuploid
16		Unfertilised oocyte	0.0	24,X,+16	Mutation not detected; aneuploid
17		Trophectoderm biopsy	0.0	45,XX,-16	Mutation not detected; aneuploid
18		Trophectoderm biopsy	0.0	46,XX	Mutation not detected; euploid

1 = arrested at cleavage-stage. 2 = arrested at blastocyst-stage. 3 = ≥4 chromosome errors.

4.4.3 Case report Patient C

Patient C underwent two separate IVF-PGD cycles. Three oocytes were collected during her first cycle (IDs 1 - 3). Two oocytes fertilised after ICSI (IDs 1 and 3). Oocyte 2 failed to fertilise. Embryo 1 stopped developing at the 4-cell stage and blastomeres were separated and tubed individually (IDs 1a - 1d). A single blastomere was biopsied from embryo 3 on day-3 post fertilisation and the embryo cryopreserved.

The unfertilised oocyte, single sister blastomeres, the cleavage-stage biopsy as well as negative controls were subjected to SurePlex amplification. Besides of the negative controls, all samples amplified successfully.

NGS-based CCS was performed on the WGA product of the blastomere removed from embryo 1. Mutation analysis was performed on all samples.

Sequencing and NGS-based CCS results are shown in **Table 4.3**. Information on sequencing depths is provided in **Table B.35** in **Appendix B**.

No mutation was detected at position m.10191 in any of the clinical samples analysed for Patient C. In addition, the biopsied blastomere obtained from embryo 3 was identified as euploid. Hence, the patient received a frozen embryo transfer. However, the embryo failed to implant.

Patient C underwent a second PGD cycle. This time, nine oocytes were collected and subjected to ICSI (IDs 4 - 11). Oocytes 10 and 11 did not fertilise. Embryos 4, 7 and 8 arrested during development and entire embryos were tubed. Zygotes 5, 6 and 9

developed to the cleavage-stage, when blastomere biopsy was performed on day-3 post fertilisation, followed by embryo freezing.

Again, all samples, including biopsy negative controls were subjected to WGA. No exogenous DNA contamination was observed and unfertilised oocytes and all other embryonic samples amplified successfully.

Results of mutation analysis are shown in **Table 4.4**. Raw data is presented in **Table B.36** in **Appendix B**. In one of the cleavage-stage biopsies (embryo 9) more than four chromosome aneuploidies were detected and it was therefore termed as 'complex abnormal'. A detailed karyotype analysis of this sample is provided in **Table B.37** in **Appendix B**.

Similarly to the patient's first cycle, no mutant variant was detected at position m.10191 in any of her samples. However, two of the three cleavage-stage embryos were identified as being chromosomally abnormal (IDs 6 and 9). Hence, the patient received a transfer of embryo 5. The embryo implanted which was evident by a positive pregnancy test. However, the pregnancy was lost shortly after and no fetal heartbeat was detectable at her follow-up visit to the referring clinic.

Because no mutant variant was detected in any of Patient C's embryo specimens, it is clear that the risk of recurrence (having another affected child) is very low for this patient. After discussing the results with her genetic counsellor, Patient C decided to try and conceive naturally and to perform PND in case of pregnancy. The patient became pregnant after a natural conception. She underwent PND (performed via chorionic villus

sampling) at 11 weeks of pregnancy. No mutant variant at position m.10191 was detected and a healthy boy was delivered at 40 weeks of gestation.

Table 4.3: Mutant load at position m.10191 (T>C) and karyotype detected in clinical samples of Patient C (1st cycle)

ID		Sample type	Mutation load (%)	Predicted karyotype	Interpretation
1[1]	a	Blastomere	0.0	Not tested	Mutation not detected
	b	Blastomere	0.0	Not tested	Mutation not detected
	c	Blastomere	0.0	Not tested	Mutation not detected
	d	Blastomere	0.0	Not tested	Mutation not detected
2		Unfertilised oocyte	0.0	Not tested	Mutation not detected
3		Blastomere biopsy	0.0	46,XX	Mutation not detected; euploid

1 = arrested at cleavage-stage.

Table 4.4: Mutant load at position m.10191 (T>C) and karyotype detected in clinical samples of Patient C (2nd cycle)

ID	Sample type	Mutation load (%)	Predicted karyotype	Interpretation
4	Whole embryo[1]	0.0	Not tested	Mutation not detected
5	Blastomere biopsy	0.0	46,XY	Mutation not detected; euploid
6	Blastomere biopsy	0.0	43,XX,-6,-15,-20	Mutation not detected; aneuploid
7[1]	Whole embryo	0.0	Not tested	Mutation not detected
8[1]	Whole embryo	0.0	Not tested	Mutation not detected
9[2]	Blastomere biopsy	0.0	Complex abnormal	Mutation not detected; aneuploid
10	Unfertilised oocyte	0.0	Not tested	Mutation not detected
11	Unfertilised oocyte	0.0	Not tested	Mutation not detected

1 = arrested at cleavage-stage. 2 = ≥4 chromosome errors.

4.4.4 Case report Patient D

Patient D underwent one cycle of IVF treatment. A total of 20 oocytes (IDs 1 - 20) were subjected to ICSI. One oocyte (ID 6) failed to fertilise. Of the fertilised oocytes, nine developed to the blastocyst-stage. Blastocysts were biopsied on day-5 (IDs 1, 3, 9, 11 and 16) or day-6 (IDs 7, 12, 13 and 14) post fertilisation and then vitrified. One embryo (ID 5) developed to the blastocyst-stage but due to abnormal fertilisation (zygote with

three pronuclei) the entire blastocyst was tubed. The remaining embryos arrested during the cleavage divisions. All arrested embryos were split into two parts and cells placed into two tubes (IDs 2a, 2b, 4a, 4b, 8a, 8b, 10a, 10b, 15a, 15b, 17a, 17b, 18a, 18b, 19a, 19b, 20a and 20b).

All tubed samples were amplified using the SurePlex protocol. Besides of sample 15b, all samples amplified successfully. Analysis of mtDNA mutation load at position m.3243 was performed in all amplified samples. CCS using array CGH was performed in trophectoderm biopsies of viable blastocysts. Results are presented in **Table 4.5**. Information on sequencing depths is presented in **Table B.38** in **Appendix B**. In one of the trophectoderm biopsies (embryo 3) more than four chromosome aneuploidies were detected and it was therefore termed as 'complex abnormal'. A detailed karyotype analysis of this sample is provided in **Table B.39** in **Appendix B**.

The mutation was detected in more than one third of all embryos (7 / 19; IDs 1, 2, 3, 8, 10, 17 and 19) as well as in the unfertilised oocyte (ID 6). A wide variation in mutation levels was observed, with a mean mutation load of 9.9 % ± 15.6 % SD, ranging from 3.1 % - 39.6 %. Importantly, almost identical mutation levels were observed between the two parts of arrested cleavage-stage embryos (mean difference of 1.8 % ± 1.3 % SD, ranging from 0.2 % - 3.2 %). Moreover, when wild-type homoplasmy was detected in one embryo half it was always detected in the other half.

The distribution of variant and wild-type alleles at different stages of preimplantation development is illustrated in **Figure 4.18**. Interestingly, although not significant, mutation frequencies steadily declined during preimplantation development, from the time of fertilisation to the blastocyst-stage. The highest mutation rate was

detected in the unfertilised oocyte (37.5 %). In contrast, a mean mutation ratio of 13.0 % ± 18.2 % SD was detected in all cleavage-stage embryos. Of note, four out of nine embryos (44.4 %) carried the mutation. Mean mutation load in these embryos was 29.3 % ± 15.7 % SD, ranging from 5.7 % - 38.0 %. The lowest mutation rate was detected in samples obtained at the blastocyst-stage. On average, a mutation load of 4.4 % ± 9.4 % SD was detected. Also noteworthy, only three out of ten embryos (30.0 %) were identified as carriers at the blastocyst-stage, carrying a mean mutation frequency of 14.6 % ± 13.3 % SD, ranging from 3.1 % - 29.2 %. These embryos were also found to be aneuploid.

Of the six mutation-free blastocysts, two embryos (IDs 7 and 11) were identified as euploid and eligible for transfer. A frozen single embryo transfer was performed (embryo 7). Although the embryo implanted and a fetal heartbeat was seen, the patient miscarried at eight weeks of gestation. A second frozen embryo transfer was performed (embryo 11). Again, a pregnancy was established. However the patient miscarried after eight weeks of pregnancy.

Table 4.5: Mutation load at position m.3243 (A>G) and karyotype detected in clinical samples of Patient D

ID		Sample type	Mutation load (%)	Predicted karyotype	Interpretation
1		Trophectoderm biopsy	29.2	47,XX,-4,-6p,+8,+20	Mutation detected; aneuploid
2[1]	a	Half embryo	37.0	Not tested	Mutation detected
	b	Half embryo	35.6	Not tested	
3[3]		Trophectoderm biopsy	11.5	Complex abnormal	Mutation detected; aneuploid
4[1]	a	Half embryo	0.0	Not tested	Mutation not detected
	b	Half embryo	0.0	Not tested	
5[2]		Whole embryo	0.0	Not tested	Mutation not detected
6		Unfertilised oocyte	37.5	Not tested	Mutation detected
7		Trophectoderm biopsy	0.0	46,XX	Mutation not detected; euploid
8[1]	a	Half embryo	37.1	Not tested	Mutation detected
	b	Half embryo	36.9	Not tested	
9		Trophectoderm biopsy	3.1	46,XY	Mutation detected; euploid
10[1]	a	Half embryo	0.0	Not tested	Mutation not detected
	b	Half embryo	0.0	Not tested	
11		Trophectoderm biopsy	0.0	46,XX	Mutation not detected; euploid
12		Trophectoderm biopsy	0.0	47,XX,+18	Mutation not detected; aneuploid
13		Trophectoderm biopsy	0.0	45,XX,+1,-3,-10	Mutation not detected; aneuploid
14		Trophectoderm biopsy	0.0	48,XX,+4,+16	Mutation not detected; aneuploid
15[1]	a	Half embryo	0.0	Not tested	Mutation not detected
	b	Half embryo	No amplification		
16		Trophectoderm biopsy	0.0	45,XX,-9	Mutation not detected; aneuploid
17[1]	a	Half embryo	39.6	Not tested	Mutation detected
	b	Half embryo	36.4	Not tested	
18[1]	a	Half embryo	0.0	Not tested	Mutation not detected
	b	Half embryo	0.0	Not tested	
19[1]	a	Half embryo	4.6	Not tested	Mutation detected
	b	Half embryo	6.8	Not tested	
20[1]	a	Half embryo	0.0	Not tested	Mutation not detected
	b	Half embryo	0.0	Not tested	

1 = arrested at cleavage-stage. 2 = arrested at blastocyst-stage. 3 = ≥4 chromosome errors.

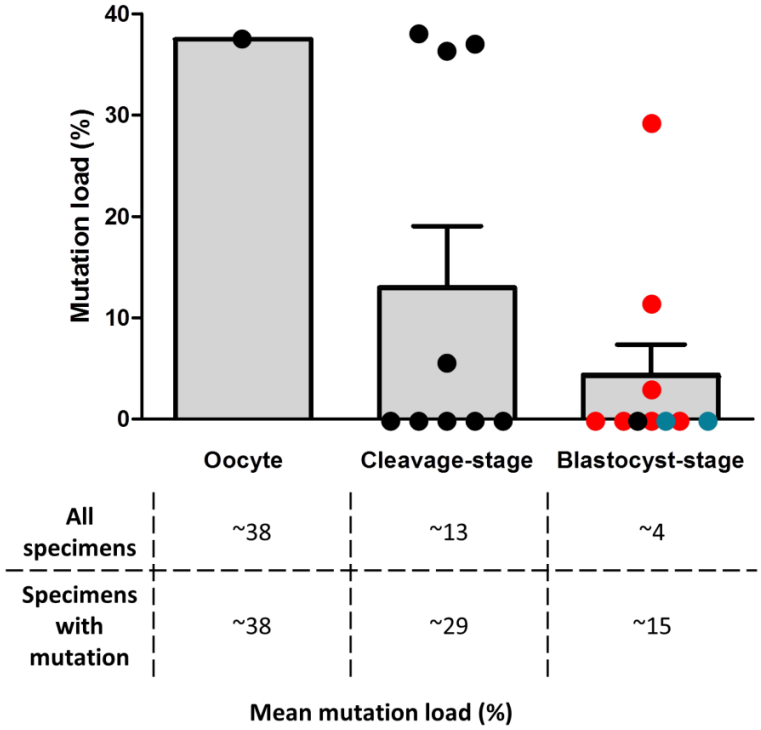


Figure 4.18: Mutation loads detected in embryo specimens of Patient D. Dots represent assessed samples. Colours indicate CCS results, whereby red indicates aneuploidy and blue euploidy. Black dots refer to samples which were not tested via CCS. Grey bars show mean mutation load detected in all assessed samples. Error bars depict SEM. For each cleavage-stage embryo the mean mutation load of embryo halves was plotted. The table summarises results and states mean mutation loads detected in all assessed samples and in samples found to carry the mutation. Differences between developmental stages were not significant (One-way ANOVA).

4.6 Discussion - **CHAPTER 4**

CCS is currently not incorporated in PGD protocols for mtDNA mutation analysis (Monnot et al., 2011; Treff et al., 2012a; Sallevelt et al., 2013; Tajima et al., 2007). However, combination of mtDNA mutation analysis and CCS provides an additional measure of embryo viability, enhancing identification of viable embryos. Euploid embryos can be prioritised for transfer, which not only increases a patient's chance of pregnancy but also reduces the risk of early miscarriage (reviewed by Dahdouh et al., 2015a). Furthermore, CCS allows gender identification and therefore the selection of male embryos for transfer

(if available), which eliminates the transmission of mtDNA disease to future generations (Bredenoord et al., 2010). This is particularly relevant if no embryo entirely free of the mtDNA mutation can be identified and an embryo with low (ideally subclinical) levels of mutant mitochondria is transferred. In contrast, for some mtDNA mutations, such as m.11778G>A causing Leber's Hereditary Optic Neuropathy (LHON) Syndrome, transfer of a female embryo is advisable, if no mutation-free embryo is available, because disease expression is much higher in males (reviewed by Poulton et al., 2010).

Most of currently available CCS techniques, such as array CGH or NGS-based CCS are performed on WGA products. In order to combine both techniques, a sequencing approach performed on WGA products was explored as an alternative method to detect mtDNA mutations in embryo specimens.

NGS, sometimes referred to as massive parallel sequencing, is a term used to describe recently developed technologies that allow high-throughput sequencing within a relatively short time and at relatively low cost. Several NGS platforms are available which differ in sequencing chemistry and technological approach. Since NGS technologies enable the generation of vast amounts of sequencing data, it is increasingly being used as a clinical diagnostic tool and of particular use in mtDNA research, diagnostics and forensic genetics, because it allows reliable assessment of low frequencies of mtDNA variants (McElhoe et al., 2014; Mikkelsen et al., 2014; Parson et al., 2013; Ye et al., 2014).

4.6.1 Protocol design and validation

WGA technologies utilised for the amplification of low input DNA, such as DNA present in single or few embryonic cells, have primarily been developed for the

amplification of the nuclear genome. To determine whether WGA also produces mtDNA quantities sufficient for PGD of mtDNA disease, two different WGA protocols, SurePlex and MDA were tested prior to the validation of the sequencing approach.

SurePlex utilises random primers and generates relatively short amplicons (200 - 1,000 bp). In contrast, MDA is a non-PCR based, isothermal amplification method and results in much longer fragments (up to 10,000 bp). MDA was tested in addition to SurePlex because it might have been more likely to cover the mtDNA regions of interest. Both protocols were tested on cell samples followed by conventional PCR targeting the mtDNA region of interest and both protocols resulted in bands specific for the amplified mtDNA loci. Since SurePlex is routinely used in combination with CCS and recommended for the use with array CGH and NGS-based CCS platforms, SurePlex was selected for further validation of the protocol.

In addition to WGA, the protocol included a second amplification step targeting the mtDNA sequences of interest. This was followed by the preparation of sequencing libraries. Samples were then processed on the PGM. The obtained sequencing data was analysed using the TVC plugin, which has previously been utilised for the analysis of mtDNA sequencing data generated on the PGM system (Parson et al., 2013). The TVC software was specifically developed for the analysis of data generated by the PGM sequencer. The software aligns the obtained sequences to the reference genome and reports presence, frequency and coverage of variants in the assessed mtDNA loci. Most importantly, the software is capable of distinguishing between instrumental sequencing errors, which are filtered prior to the analysis, to enable detection of true low-frequency variants.

To test whether the TVC software could accurately quantify mtDNA sequencing variants and to ensure that both amplification steps (WGA and conventional PCR) do not introduce errors in the mtDNA sequence, extensive validation experiments were performed prior to clinical application.

Initially, accuracy and sensitivity of the NGS test were established using artificial mixtures of gDNA which contained various levels of mtDNA heteroplasmy ranging from 0.0 % - 100 %. The method proved to be highly accurate and an excellent correlation between expected and obtained variant ratios was achieved. Of note, a mean difference of about 2.4 % between theoretical and measured levels was observed. Although gDNA samples were mixed at equal concentrations, it was not possible to take into account overall mtDNA copy numbers present in each of the gDNA samples. Mitochondrial copy number, and hence the proportion of the total cellular DNA attributable to mitochondria, can differ between individuals which might have caused the slight discrepancies. The NGS test further proved to be highly sensitive and was able to detect the lowest mutant/wild-type combination (5 %) tested.

To ensure that the method can also accurately detect mtDNA variant frequencies following WGA and conventional PCR, the same sample mixtures were subjected to SurePlex amplification. Again, an excellent correlation between previously determined and obtained heteroplasmy levels was obtained. Moreover, the mean difference between expected and measured values was further reduced as compared to previous experiments and differed only by about 1.8 %. Additionally, the lowest tested variant frequency was nearly identical between both experiments, indicating that the PGD test can safely be performed on SurePlex products with high accuracy and sensitivity.

The protocol was then tested on gDNA and cell samples derived from patients and their affected children. This was important to verify that the proposed PGD test can accurately detect wild-type/mutant ratios in samples consisting of single or few cells, as is the case for embryo biopsies. Data obtained from cell samples were then compared to results of the individual's gDNA to get an estimate on test accuracy.

Results obtained from the analysis of gDNA and cell samples derived from individuals previously diagnosed as homoplasmic for either wild-type or mutant (son of Patient A: 100 % m.8993G; Patient B: 100 % m.8993T; Patient C: 100 % m.10191C) were consistent throughout all tests and homoplasmy for either the wild-type or mutant molecule was obtained in all processed samples.

The PGD test also proved to be reliable in mutation detection in samples derived from heteroplasmic mtDNA mutation carriers (Patient A: 56 % m.8993G; son of Patient B: 95 % m.8993G; daughter of Patient C: 78 % m.10191C; Patient D: 28 % m.3243G). Importantly, the obtained mtDNA mutation ratios in gDNA samples of all four carriers were confirmed when analysing cell samples. Of note, in all cases cell samples were obtained on the same day as the assessed gDNA samples and lymphocytes were isolated from the same blood draw as the gDNA.

The mean mutation ratios detected in gDNA of Patient A and the son of Patient B, both heteroplasmic carriers of m.8993G, were almost identical to the previously established frequencies by reference laboratories. Most importantly, agreement was also obtained when gDNA was subjected to WGA, providing further evidence that WGA does not cause amplification bias.

Also noteworthy, detected mutation ratios between gDNA extracted from blood and buccal samples of Patient A were highly consistent. In fact, the m.8993G variant is known to be relatively uniformly distributed across different tissue types (White et al., 1999b). In contrast, some mtDNA mutations are known to display a tissue-specific variation in heteroplasmy levels (Lestienne & Ponsot, 1988; Dubeau et al., 2000).

For instance, heteroplasmy levels of the 10191T>C mutation are known to vary widely between different organs and tissues of the same individual (Nesbitt et al., 2012; Levy et al., 2014), which is in agreement with the findings of this study. A tissue-dependent variation was identified in the daughter of Patient C who carries the m.10191C variant. The mutation load detected in her gDNA, isolated from buccal cells, was about 7 % higher than the level previously diagnosed in her muscle tissue. Of note, three aliquots of the child's gDNA were processed separately and consistent results were achieved with a very low SD of 0.5 %. Moreover, five aliquots were sequenced after performing WGA and again, a similarly high mean mutation load was observed.

Similarly, the m.3243G variant (carried by Patient D) is known to fluctuate considerably between tissue types (Monnot et al., 2011; Poulton et al., 2010; Shanske et al., 2004). A high variation in heteroplasmy levels was detected in the gDNA of Patient D's samples. The mutation load in gDNA from buccal cells was twice as high as in gDNA from blood cells, however, still significantly lower than in the patient's muscle tissue, in which the original diagnosis was made. These findings are in line with previously published studies, reporting significant tissue-dependent differences in m.3243G levels, being lowest in leucocytes followed by buccal cells and then skeletal muscle cells (Chinnery et al., 1999; Frederiksen et al., 2006).

In addition to the tissue-specific differences in heteroplasmy levels observed in some of the mtDNA mutation carriers, a wide distribution of mutation frequencies was observed in the cell samples of all four carriers. Importantly, average mutation loads of the cell samples were always close to mutation loads of the individuals' gDNA. These results were obtained irrespectively of the mode of amplification performed prior to sequencing, which further demonstrated reliability of the test in samples consisting of low DNA quantities.

Of note, intercellular variation in mutation levels, which is thought to be caused by unequal segregation of wild-type and mutant mitochondria during mitotic cell divisions, is a common phenomenon in mtDNA mutation carriers (Gigarel et al., 2005; Steffann et al., 2006; Tajima et al., 2007; Monnot et al., 2011; Saitoh et al., 1999; Vandewoestyne et al., 2011). For instance, levels of the m.8993G variant detected in lymphocyte samples of Patient A and the son of Patient B ranged considerably. This was most pronounced in samples consisting of a single cell, ranging from 0.0 % - 100 %. Similarly, the 10191C variant levels detected in single buccal cells from the daughter of Patient C differed between samples, ranging from approximately 77.0 % - 94.0 %. This variation was also observed in cell samples of Patient D, where the m.3243G variant was either absent or present at up to about 60 %.

4.6.2 Clinical cases

Three of the four patients involved in this study were referred for PGD of MILS, which is a common mtDNA disorder. Leigh Syndrome can be caused by mutations occurring in the nuclear as well as the mitochondrial genome and to date, more than 60 different

genes involved in the disease development have been identified (reviewed by Gerards et al., 2016). Leigh Syndrome is a progressive neurodegenerative disorder with poor prognosis and often results in death before the age of three years (Lee et al., 2009).

The most common mtDNA mutation in children is a base change from T>G or T>C in the MT-ATP6 gene at position m.8993. This base change is also the most common cause of MILS (Rahman et al., 1996; Santorelli et al., 1993). For both mutation types (T>G and T>C), a mutation ratio of 60 % - 80 % usually results in NARP (neuropathy, ataxia, and retinitis pigmentosa; OMIM #551500) Syndrome. NARP is milder as compared to Leigh Syndrome, which usually presents at >90 % heteroplasmy (Holt et al., 1990; De Vries et al., 1993). Individuals which carry less than 60 % heteroplasmy are usually asymptomatic (Mäkelä-bengs et al., 1995; White et al., 1999a).

For instance, Patient A, who carries approximately 56 % of the m.8993G variant, is unaffected by the disease. In contrast, her son, who carried 100 % of the variant, died at the age of nine months. Due to the high risk of disease transmission to future children, Patient A underwent two consecutive IVF-PGD cycles, which ultimately resulted in the generation of one blastocyst. Although the embryo was found to be free of the mutation, it was chromosomally abnormal and no embryo transfer took place. The embryo carried a sex chromosome abnormality (XXY) and a trisomy 16 which could have potentially resulted in implantation and subsequent miscarriage if CCS was not performed and the embryo transferred. One of her other two embryos, which unfortunately arrested during development was identified as euploid with 0.0 % mutation load. In contrast, the second arrested embryo and the unfertilised oocyte carried very high levels of the mutation (both approximately 90 %).

A skew in heteroplasmy levels in samples of patients referred for PGD due to m.8993T>G has been reported previously and it is often the case that oocytes or embryonic samples show either a very low or very high rate of the mutation, rather than intermediate levels (Blok et al., 1997; Steffann et al., 2006). The fact that Patient A's deceased son carried only the mutant variant and two of her tested samples carried very high mutant levels, further reflects the potential for rapid purifying segregation of m.8993 mutant alleles within a single generation. This phenomenon has been observed in other studies, reporting a rapid shift in m.8993 heteroplasmy levels close towards homoplasmy within few generations (Ferlin et al., 1997; Degoul et al., 1997).

Patient B, on the other hand, who was referred for PGD due to the same mutation as Patient A, generated only blastocysts which were free of the mutation. Moreover, all other assessed sample types (one unfertilised oocyte, one arrested blastocyst and 16 sister blastomeres) were found to be free of the mutation. Although children of mothers who carry intermediate levels of the m.8993 mutation are at high risk of carrying levels above the disease-causing threshold, disease recurrence has been estimated to be much lower for children of females in which the mutant variant was not present or too low to be detected in somatic tissues (White et al., 1999a). Although Patient B had a severely affected son (95 % heteroplasmy), the mutation was not detected prior to PGD in any of her tested samples (blood, urine and buccal cells), nor in the samples of her mother (affected child's grandmother). Hence, it is possible that the m.8993 mutation present in her affected son, was either caused by a *de novo* mutation which occurred during oogenesis or early embryonic development or due to the presence of few mutation variants in the mother's gametes, as has been suggested in previous studies (White et al. 1999b; Playán et al., 2002;

Tulinius et al., 1995). Most of Patient B's embryos were also chromosomally normal and the transfer of a euploid male embryo let to the birth of a healthy son, who was found to be free of the mutation following birth (cord blood and buccal swab).

In many other cases of MILS, the disease is caused by pathogenic point mutations present in the MT-ND3 gene (Nesbitt et al., 2012), which also includes the m.10191T>C mutation which was present at high levels in the daughter of Patient C. Similarly to Patient B, Patient C was not identified as a carrier, however high levels of the m.10191C mutation were detected in her daughter's muscle biopsy. Again, no mutant load was detected in any of her clinical samples (three unfertilised oocytes, three arrested embryos, four sister blastomeres and four cleavage-stage biopsies).

Since no mutant alleles were detected in gDNA and cell samples of Patient C as well as in her clinical samples, it is possible that the daughter's mutation could be attributed to a *de novo* mutation. An absence of the m.10191T>C mutation in mothers and other female relatives of children identified with high heteroplasmy levels at position m.10191 has previously been reported, suggesting that the mutation occurs sporadically, possible due to an event occurring during oogenesis or shortly after fertilisation (Nesbitt et al., 2012; Sallevelt et al., 2017).

Although transfer of two euploid embryos did not result in an ongoing pregnancy, PGD tests following two cycles of IVF treatment revealed a low risk of disease transmission. Hence, after two failed IVF cycles, the patient opted to conceive naturally. The patient delivered a healthy child who was tested to be free of the pathogenic m.10191C variant.

Unlike the first three patients, who were referred for PGD because of their diseased children, Patient D was referred for PGD due to the diagnosis of mitochondrial myopathy caused by the m.3243A>G mutation resulting in ptosis and restricted movement of her right eye.

The m.3243A>G mutation, which occurs in the MT-TL1 gene, is the most common pathogenic mtDNA mutation (reviewed by Gorman et al., 2016).The mutation can cause a variety of disorders and syndromes, including maternally inherited diabetes and deafness (MIDD; OMIM #520000), mitochondrial encephalopathy, lactic acidosis, and stroke-like episodes Syndrome (MELAS; OMIM #540000), chronic progressive external ophthalmoplegia (CPEO), myoclonic epilepsy associated with ragged-red fibers (MERRF; OMIM #545000) and other less severe clinical phenotypes (Nesbitt et al., 2013). Unlike in other frequent pathogenic mtDNA mutations, mutation frequency of the m.3243G variant is not a reliable predictor of disease expression, onset, type or severity (Pickett et al., 2018). Hence it is preferable to transfer embryos which are free of the mutation.

Although Patient D generated a large number of embryos, ultimately only two blastocysts were identified to be free of aneuploidy and the tested mtDNA mutation and were therefore eligible for transfer. Unfortunately, the patient miscarried twice at eight weeks of gestation. Of note, pregnancy complications are not uncommon in women suffering from mitochondrial disease. In fact, pregnancy complications have been reported in women suffering from MIDD or mitochondrial myopathy caused by the m.3243G mutation (Aggarwal et al., 2001; Donovan & Severin, 2006; Hosono et al., 2001).

Valuable data was obtained from the analysis of arrested cleavage-stage embryos of Patient D which demonstrated that mutation levels of m.3243G are likely to be uniformly

distributed in embryonic cells. This finding is particularly important in the context of PGD as it demonstrates that mtDNA mutation load detected in biopsies is representative of the entire embryo. Only limited data on the distribution of the m.3243G mutation in human embryos and fetuses is available. Of note, a uniform distribution has been reported in tissue samples of human fetuses, suggesting that m.3243G mutation levels remain stable during the prenatal stage of development (Matthews et al., 1994; Cardaioli et al., 2000; Monnot et al., 2011). These findings further suggest that the variation in tissue-specific distribution occurs only after birth.

Approximately one third of the embryos generated by Patient D carried the mutation. Interestingly, the percentage of mutated mtDNA molecules was highest in the unfertilised oocyte and in arrested cleavage-stage embryos and lowest in embryos that developed to the blastocyst-stage. This is an important finding as it appears that there is a negative selection against embryos carrying high levels of the mutation during preimplantation development. This is in sharp contrast to the m.8993T>G mutation, which is frequently found in high percentages, close towards homoplasmy in human embryos.

4.6.3 Conclusion - **CHAPTER 4**

The study showed that NGS can reliably be utilised for the quantification of mtDNA heteroplasmy in single or few cells following WGA and, hence, enables combination of CCS and mtDNA mutation analysis, increasing a patient's chance of pregnancy. The technique proved to be robust and reproducible, yielding results from 100 % of the clinical samples tested and, in instances where several cells from the same embryo were analysed, showing concordance between all samples. The method was also shown to be highly accurate and

sensitive, with a near-perfect linear relationship between known proportions of mtDNA mutation in samples and the amounts estimated from testing. Heteroplasmy levels could be accurately quantified even when the proportion of mutant mtDNA molecules was as low as ~5 %.

Results obtained from patient and carrier samples supported previous findings of a wide variation in mutant load in the somatic cells of heteroplasmic mtDNA mutation carriers. The clinical results also indicated that disease recurrence risk is likely to be relatively low in female patients presenting with zero mutant load. This contrasts with the wide variability of mutant load seen in the oocytes/embryos of two heteroplasmic mtDNA mutation carriers, suggestive of a relatively high risk of recurrence.

Aneuploidy was demonstrated to be common, affecting approximately half of the embryos tested in this study. The chromosomal abnormalities were of types typically associated with implantation failure and/or miscarriage. Identifying and avoiding the transfer of these aneuploid embryos represents a significant advantage of the protocol reported here in comparison to previous PGD tests for mtDNA disorders.

Furthermore, data obtained from the analysis of the m.3243G mutation in preimplantation embryo specimens suggests that high mutation levels result in impaired embryo development.

CHAPTER 5: Concluding remarks

This chapter summarises the background and the achievements of the study and discusses the developed as well as other techniques in the context of improving ART as well as embryo selection and viability.

5.1 Evolution of preimplantation genetic testing

The past three decades marked a period of major technological advancements in the field of clinical genetics. These have also found their application in the continuously growing field of genetic testing of preimplantation embryos. Ever since its first applications in the 1990s, the PGT field has undergone a major transformation. The first PGD approaches to prevent inheritance of X-linked disorders relied on the amplification of Y-chromosome fragments (Handyside et al., 1990). Soon after, FISH was implemented for embryo sexing and for the detection of structural rearrangements and numerical abnormalities of few chromosomes (Munné et al., 1993b; Griffin et al., 1994; Munné, 2001), which gave rise to earliest versions of PGS.

However, due to numerous limitations, FISH failed to improve pregnancy outcomes (Mastenbroek et al., 2011) and was soon replaced by CCS methods based on CGH, SNP analysis and most recently real-time qPCR and NGS (reviwed by Sueoka, 2016).

For PGD, conventional PCR approaches, alongside with SNP arrays, targeted haplotyping and most recently targeted sequencing of mutations/genes using NGS have been employed.

As a consequence of the numerous techniques being available, the utilisation of PGS and PGD increased dramatically and patient access to these treatments grew (reviewed by Vermeesch et al., 2016).

The study presented here focused on the development/design, the validation and clinical application of two novel methods for PGS and PGD of mtDNA disease.

5.2 Assisted reproductive techniques to improve embryo selection

In the first part of the study, a robust nano-scale, array-based real-time qPCR method was developed, extensively validated and clinically implemented. It is a unique method which is streamlined, rapid, versatile and less labour-intensive compared to current techniques. In consequence, it has the potential to become an in-house component of an IVF laboratory. This would mean rapid turn-around time and increased accessibility for the patient, omitting the need for embryo cryopreservation. In the pool of techniques, the majority of which require freezing, this is a valuable option.

Although clinical utility of embryo selection tools, in particular tests based on aneuploidy screening, are under constant debate, it can be expected that the number and availability of embryo selection tools is continuing to grow. In fact, the development of non-invasive techniques is currently a topic of great interest because concerns have been raised about potential damage to the embryo caused by biopsy procedures necessary for conventional PGT. Hence, to prevent damage to the embryo, alternative sources of

embryonic DNA, such as the blastocoel fluid or culture media are being explored (Ho et al., 2018; Kuznyetsov et al., 2018; Li et al., 2018).

In addition to the chromosome complement, other important factors, such as epigenetics, energy generation, as well as maternal proteins and transcripts contribute to embryo competence and may therefore potentially be used as biomarkers to predict ART outcomes in future (reviewed by Vermeesch et al., 2016).

5.3 Assisted reproductive techniques to prevent mitochondrial DNA disease transmission

The complexities surrounding accurate detection of mtDNA disease in preimplantation embryos lies in the difficulty of developing tests, which are sensitive enough to quantify mtDNA mutation load in embryo specimens. Therefore, the second part of the study aimed to deliver a sensitive PGD protocol which is fully compatible with CCS. The developed protocol proved to be successful in achieving these goals and a healthy child was born after its clinical application.

The use of PGD to minimise the possibility of mtDNA disease is widely accepted to be a valuable option to women at risk of transmitting pathogenic mtDNA mutations to their children (Bredenoord et al., 2008). Nevertheless, several factors need to be considered prior to its application.

Although, the primary aim is to transfer mutation-free embryos, it may not always be possible to identify an embryo with zero mutation load following IVF-PGD treatment. In

these cases, embryos with a mutation load predicted to be below the disease-causing threshold may be considered for transfer (Greenfield et al., 2017). However, it is not always possible to determine a safe threshold for transfer, which is often dependent on the type of mtDNA mutation (Poulton et al., 2010). In several mtDNA disorders, mutation load and disease phenotype correlate well, as is the case for mutations present at positions m.8993 or m.3460 causing NARP/MILS or LHON (leber hereditary optic neuropathy; OMIM #535000) Syndrome (Black et al., 1996; White et al., 1999a). Often, however, disease expression and variant frequency correlate only poorly. For example, mtDNA diseases such as MELAS and MERRF, commonly caused by mutations present at positions m.3243 and m.8344, show a wide variation in clinical phenotypes independently of mutation load. Moreover, these mutations are known to exhibit a variation in mutation load between different organs and tissues which, in addition, can increase over time (Chinnery et al., 1997). Additionally, for private mutations, which are less common and may only be present in few families, a threshold can often not be assigned due to the lack of sufficient data regarding the relationship of mutation load and phenotype (Poulton et al., 2010).

It also needs to be emphasised that even if a mutation-free embryo is transferred, a small recurrence risk remains. PGD of mtDNA disease cannot guarantee that all embryonic cells are completely mutation-free or that the detected mutation load in the biopsy fully reflects the whole embryo.

Moreover, in cases where a female embryo is transferred, PGD may be necessary in the next generation due to the rapid segregation of mutant mtDNA variants during germ cell development.

Finally, in some cases of mtDNA disorders PGD may not be applicable. For instance, if the disorder is caused by a homoplasmic mtDNA mutation, as is often the case in LHON (reviewed by Jacobs et al., 2006), the mutation is always passed on to all children. PGD may also not be a valuable option for patients that do not generate embryos with mutation levels below a safe threshold for transfer.

More recently, to circumvent the issues associated with PGD of mtDNA disease, alternative techniques, often referred to as mitochondrial replacement therapy (MRT) techniques, are being investigated to prevent transmission of mtDNA disease to children (reviewed by Wolf et al., 2015). MRT techniques aim to create mutation-free oocytes/zygotes by combining the patient's nuclear genetic information with the mtDNA of a female donor. To do this, several different techniques have been developed. The two most widely used MRT research techniques are maternal spindle transfer (MST; **Figure C.1 A** in **Appendix C**) and pronuclear transfer (PNT; **Figure C.1 B** in **Appendix C**). During MST the spindle-chromosome complexes are removed from the female donor's oocytes and are replaced by spindle-chromosome complexes of the prospective mother. In contrast, during PNT the donor's and patient's oocytes are fertilised followed by the replacement of the pronuclei of the donor's zygotes by pronuclei of the prospective mother (reviewed by Wolf et al., 2015).

To date, MRT techniques have mostly been studied in animal models (reviewed by Greenfield et al., 2017). Results obtained from these studies demonstrated that MRT techniques are generally safe resulting in normal embryo development and healthy offspring as long as mtDNA carry-over rates were low (Neupane et al., 2014a; Tachibana et al., 2009; Wang et al., 2014).

These findings encouraged MRT studies in human oocytes and zygotes and promising results were obtained in preclinical studies (Craven et al., 2010; Kang et al., 2016; Paull et al., 2012; Tachibana et al., 2012; Yamada et al., 2016). However, these studies also highlight the importance of PNT and MST technique optimisations and refinements in order to reduce the mtDNA carry-over rate and to establish safety of MRT prior to clinical implementation (reviewed by Greenfield et al., 2017).

Although MRT is still considered to be experimental, it has been applied clinically and the world's first MRT baby was born in 2016. The birth of the child, conceived following MST, was first reported at the annual meeting of the American Society for Reproductive Medicine (ASRM) in Salt Lake City in October 2016 (J. Zhang et al., 2016) and published later in the journal of Reproductive BioMedicine Online (Zhang et al., 2017). In brief, MRT was performed on oocytes from a patient carrying the m.8993T>G mutation, who had previously lost two children due to Leigh Syndrome. Spindle transfer was performed in five oocytes, of which four developed to the blastocyst-stage. Of these, three were found to be aneuploid. Transfer of the only euploid embryo resulted in a pregnancy and birth of an apparently healthy boy.

The study faced strong criticism from the scientific community (Reardon, 2017). For instance, ethical aspects of the study were criticised. Although the MST technique itself was performed at the New Hope Fertility clinic in New York, the actual embryo transfer took place in Mexico, known for its lax regulations in regards to embryo manipulation techniques. Furthermore, concerns about the health of the child were raised. It was also not clear from the report if the patients received appropriate counselling in regards to MRT safety risks. The reported mtDNA carry-over rate was relatively high (approximately 6 %).

In addition, distribution of mutated mtDNA frequencies was 2 % - 9 % in different neonatal tissues. Of note, the child's parents refused any future testing or monitoring of the child which makes it hard to determine whether the treatment was safe (Alikani et al., 2017). It was also not clear from the study, why mtDNA mutation rates were not measured in the maternal enucleated oocytes and in the non-transferred embryos.

Overall, the obvious limitations and weaknesses of the discussed study highlight the need of specialised expertise when providing MRT to assess efficacy and safety of the different techniques.

More recently, the use of MRT has been explored to treat fertility caused by defects in the cytoplasm of oocytes (Costa-Borges et al., 2017). This idea is not new. In fact, already two decades ago, studies were conducted that aimed at improving embryo development by transplanting ooplasm from donor oocytes to oocytes of infertile patients (Cohen et al., 1998; Lanzendorf et al., 1999).

Success of oocyte fertilisation and proper early embryo development is greatly dependent on adequate supply of maternal transcripts, proteins and functional mitochondria, since the embryos own genome is still in an inactive state during the first days of development (reviewed by Minami et al., 2007). In particularly advanced female age is associated with poor oocyte quality. Hence there is potential to rejuvenate compromised oocytes using MRT and donated oocytes of young women (reviewed by Wolf et al., 2015).

For instance, in order to test feasibility of MRT in improving oocyte/embryo competence, MST was tested in a mouse model and employed to compromised mouse

oocytes. Successful results were obtained from this study providing evidence that embryo developmental arrest can be overcome by MST (Costa-Borges et al., 2017). Of note, the PGD technique for detection of mtDNA mutations, which was developed during the course of this study, was applied to determine the efficacy and safety of the MST technique used in the described mouse model.

Initially, the technique was validated to detect variant frequencies in embryo specimens born following spindle transfer (**Figure C.2** in **Appendix C**). This was followed by analysis of carry-over rates of mtDNA in adult mouse tissue samples (**Figure C.3** in **Appendix C**).

In summery the developed PGD method for detection of mtDNA disease has been clinically applied, resulting in the birth of a healthy child. Moreover, the developed technique has been implemented as a research tool to assess the success of MRT methods.

Bibliography

Aggarwal, P., Gill-Randall, R., Wheatley, T., Buchalter, M. B., Metcalfe, J., & Alcolado, J. C. (2001). Identification of mtDNA mutation in a pedigree with gestational diabetes, deafness, Wolff-Parkinson-White syndrome and placenta accreta. Human Heredity, 51(1–2), 114–116. doi:10.1159/000022950

Alfarawati, S., Fragouli, E., Colls, P., Stevens, J., Gutiérrez-Mateo, C., Schoolcraft, W. B. et al. (2011). The relationship between blastocyst morphology, chromosomal abnormality, and embryo gender. Fertility and sterility, 95(2), 520–4. doi:10.1016/j.fertnstert.2010.04.003

Alikani, M., Fauser, B. C. J., García-Valesco, J. A., Simpson, J. L., & Johnson, M. H. (2017). First birth following spindle transfer for mitochondrial replacement therapy: hope and trepidation. Reproductive BioMedicine Online, 34(4), 333–336. doi:10.1016/J.RBMO.2017.02.004

Anderson, S., Bankier, A. T., Barrell, B. G., de Bruijn, M. H., Coulson, A. R., Drouin, J. et al. (1981). Sequence and organization of the human mitochondrial genome. Nature, 290(5806), 457–65

Aparicio-Ruiz, B., Romany, L., & Meseguer, M. (2018). Selection of preimplantation embryos using time-lapse microscopy in in vitro fertilization: State of the technology and future directions. Birth Defects Research, 110(8), 648–653. doi:10.1002/bdr2.1226

Baart, E.B., Martini, E., Van den Berg, I., Macklon, N. S., Galjaard, R. J., Fauser, B. C., Van Opstal, D. (2006). Preimplantation genetic screening reveals a high incidence of aneuploidy and mosaicism in embryos from young women undergoing IVF. Human Reproduction, 21, 223–233. doi:10.1093/humrep/dei291

Barrenetxea, G., López de Larruzea, A., Ganzabal, T., Jiménez, R., Carbonero, K., & Mandiola, M. (2005). Blastocyst culture after repeated failure of cleavage-stage embryo transfers: a comparison of day 5 and day 6 transfers. Fertility and sterility, 83(1), 49–53. doi:10.1016/j.fertnstert.2004.06.049

Black, G. C., Morten, K., Laborde, A., & Poulton, J. (1996). Leber's hereditary optic neuropathy: heteroplasmy is likely to be significant in the expression of LHON in families with the 3460 ND1 mutation. The British journal of ophthalmology, 80(10), 915–7

Blok, R. B., Gook, D. A., Thorburn, D. R., & Dahl, H. H. (1997). Skewed segregation of the mtDNA nt 8993 (T>G) mutation in human oocytes. American journal of human genetics, 60(6), 1495–501

Braude, P., Bolton, V., & Moore, S. (1988). Human gene expression first occurs between the four- and eight-cell stages of preimplantation development. Nature, 332(6163), 459–461. doi:10.1038/332459a0

Bredenoord, A. L., Dondorp, W., Pennings, G., De Die-Smulders, C. E. M., & De Wert, G. (2008). PGD to reduce reproductive risk: the case of mitochondrial DNA disorders. Human reproduction, 23(11), 2392–401. doi:10.1093/humrep/den290

Bredenoord, A. L., Dondorp, W., Pennings, G., & De Wert, G. (2010). Avoiding transgenerational risks of mitochondrial DNA disorders: a morally acceptable reason for sex selection? Human Reproduction, 25(6), 1354–1360. doi:10.1093/humrep/deq077

Briggs, D., Power, N., Lamb, V., Rutherford, A., & Gosden, R. (2000). Amplification of DNA sequences in polar bodies from human oocytes for diagnosis of mitochondrial disease. The Lancet, 355(9214), 1520–1521. doi:10.1016/S0140-6736(00)02171-1

Brown, D. T., Samuels, D. C., Michael, E. M., Turnbull, D. M., & Chinnery, P. F. (2001). Random genetic drift determines the level of mutant mtDNA in human primary oocytes. American journal of human genetics, 68(2), 533–6. doi:10.1086/318190

Brown, W. M., George, M., & Wilson, A. C. (1979). Rapid evolution of animal mitochondrial DNA. Proceedings of the National Academy of Sciences of the United States of America, 76(4), 1967–71

Calhaz-Jorge, C., De Geyter, C., Kupka, M. S., De Mouzon, J., Erb, K., Mocanu, E. et al. (2017). Assisted reproductive technology in Europe, 2013: Results generated from

European registers by ESHRE. Human Reproduction, 32(10), 1957–1973. doi:10.1093/humrep/dex264

Calvo, S. E., Clauser, K. R., & Mootha, V. K. (2016). MitoCarta2.0: an updated inventory of mammalian mitochondrial proteins. Nucleic acids research, 44(D1), D1251-7. doi:10.1093/nar/gkv1003

Cao, L., Shitara, H., Horii, T., Nagao, Y., Imai, H., Abe, K. et al. (2007). The mitochondrial bottleneck occurs without reduction of mtDNA content in female mouse germ cells. Nature Genetics, 39(3), 386–390. doi:10.1038/ng1970

Capalbo, A., Rienzi, L., Cimadomo, D., Maggiulli, R., Elliott, T., Wright, G. et al. (2014). Correlation between standard blastocyst morphology, euploidy and implantation: an observational study in two centers involving 956 screened blastocysts. Human Reproduction, 29(6), 1173–1181. doi:10.1093/humrep/deu033

Cardaioli, E., Fabrizi, G. M., Grieco, G. S., Dotti, M. T., & Federico, A. (2000). Heteroplasmy of the A3243G transition of mitochondrial tRNA(Leu(UUR)) in a MELAS case and in a 25-week-old miscarried fetus. Journal of neurology, 247(11), 885–7

Carling, P. J., Cree, L. M., & Chinnery, P. F. (2011). The implications of mitochondrial DNA copy number regulation during embryogenesis. Mitochondrion, 11(5), 686–692. doi:10.1016/j.mito.2011.05.004

Chappel, S. (2013). The role of mitochondria from mature oocyte to viable blastocyst. Obstetrics and gynecology international, 2013, 183024. doi:10.1155/2013/183024

Chen, M., Wei, S., Hu, J., & Quan, S. (2015). Can comprehensive chromosome screening technology improve IVF/ICSI outcomes? A Meta-Analysis. PloS one, 10(10), e0140779. doi:10.1371/journal.pone.0140779

Chinnery, P. F., Howell, N., Lightowlers, R. N., & Turnbull, D. M. (1997). Molecular pathology of MELAS and MERRF. The relationship between mutation load and clinical phenotypes. Brain, 120(10), 1713–1721. doi:10.1093/brain/120.10.1713

Chinnery, P. F., Johnson, M. A., Wardell, T. M., Singh-Kler, R., Hayes, C., Brown, D. T. et al. (2000). The epidemiology of pathogenic mitochondrial DNA mutations. Annals of neurology, 48(2), 188–93

Chinnery, P. F., Zwijnenburg, P. J., Walker, M., Howell, N., Taylor, R. W., Lightowlers, R. N. et al. (1999). Nonrandom tissue distribution of mutant mtDNA. American journal of medical genetics, 85(5), 498–501

Cohen, J., Scott, R., Alikani, M., Schimmel, T., Munné, S., Levron, J. et al. (1998). Ooplasmic transfer in mature human oocytes. Molecular human reproduction, 4(3), 269–80

Cohen, J., Wells, D., & Munné, S. (2007). Removal of 2 cells from cleavage stage embryos is likely to reduce the efficacy of chromosomal tests that are used to enhance implantation rates. Fertility and Sterility, 87(3), 496–503. doi:10.1016/j.fertnstert.2006.07.1516

Colls, P., Escudero, T., Fischer, J., Cekleniak, N. A., Ben-Ozer, S., Meyer, B. et al. (2012). Validation of array comparative genome hybridization for diagnosis of translocations in preimplantation human embryos. Reproductive biomedicine online, 24(6), 621–9. doi:10.1016/j.rbmo.2012.02.006

Costa-Borges, N. L., Mestres, E., Miguel-Escalada, I., Basalmeda, R., Garcia, M., Vanrell, I. et al. (2017). Meiotic spindle transfer overcomes embryo developmental arrest in compromised oocytes: proof of concept in the mouse model. Fertility and Sterility, 108(3), e41. doi:10.1016/j.fertnstert.2017.07.133

Craven, L., Tuppen, H. A., Greggains, G. D., Harbottle, S. J., Murphy, J. L., Cree, L. M. et al. (2010). Pronuclear transfer in human embryos to prevent transmission of mitochondrial DNA disease. Nature, 465(7294), 82–85. doi:10.1038/nature08958

Cree, L. M., Samuels, D. C., de Sousa Lopes, S. C., Rajasimha, H. K., Wonnapinij, P., Mann, J. R. et al. (2008). A reduction of mitochondrial DNA molecules during embryogenesis explains the rapid segregation of genotypes. Nature Genetics, 40(2), 249–254. doi:10.1038/ng.2007.63

Cummins, J. (1998). Mitochondrial DNA in mammalian reproduction. Reviews of Reproduction, 3(3), 172–182. doi:10.1530/ror.0.0030172

Dahdouh, E. M., Balayla, J., & García-Velasco, J. A. (2015a). Comprehensive chromosome screening improves embryo selection: a meta-analysis. Fertility and sterility, 104(6), 1503–12. doi:10.1016/j.fertnstert.2015.08.038

Dahdouh, E. M., Balayla, J., & García-Velasco, J. A. (2015b). Impact of blastocyst biopsy and comprehensive chromosome screening technology on preimplantation genetic screening: a systematic review of randomized controlled trials. Reproductive biomedicine online, 30(3), 281–9. doi:10.1016/j.rbmo.2014.11.015

Dahdouh, E. M., Qc, M., Balayla, J., Audibert, F., Wilson, R. D., Ab, Calgary et al. (2015c). Technical Update: Preimplantation Genetic Diagnosis and Screening. J Obstet Gynaecol Can, 37(232), 451–463. doi:10.1016/S1701-2163(15)30261-9

Darin, N., Oldfors, A., Moslemi, A. R., Holme, E., & Tulinius, M. (2001). The incidence of mitochondrial encephalomyopathies in childhood: clinical features and morphological, biochemical, and DNA abnormalities. Annals of neurology, 49(3), 377–83

Dean, N. L., Battersby, B. J., Ao, A., Gosden, R. G., Tan, S. L., & Shoubridge, E. A. (2003). Prospect of preimplantation genetic diagnosis for heritable mitochondrial DNA diseases. Molecular Human Reproduction, 9(10), 631–638. doi:10.1093/molehr/gag077

Debrock, S., Melotte, C., Spiessens, C., Peeraer, K., Vanneste, E., Meeuwis, L. et al. (2010). Preimplantation genetic screening for aneuploidy of embryos after in vitro fertilization in women aged at least 35 years: a prospective randomized trial. Fertility and Sterility, 93(2), 364–373. doi:10.1016/j.fertnstert.2008.10.072

Degoul, F., François, D., Diry, M., Ponsot, G., Desguerre, I., Héron, B. et al. (1997). A near homoplasmic T8993G mtDNA mutation in a patient with atypic Leigh syndrome not present in the mother's tissues. Journal of inherited metabolic disease, 20(1), 49–53

De Vos, A., Staessen, C., De Rycke, M., Verpoest, W., Haentjens, P., Devroey, P. et al. (2009). Impact of cleavage-stage embryo biopsy in view of PGD on human blastocyst

implantation: a prospective cohort of single embryo transfers. Human Reproduction, 24(12), 2988–96. doi:10.1093/humrep/dep251

De Vos, A., & Van Steirteghem, A. (2001). Aspects of biopsy procedures prior to preimplantation genetic diagnosis. Prenatal diagnosis, 21(9), 767–80

De Vries, D. D., van Engelen, B. G. M., Gabreëls, F. J. M., Ruitenbeek, W., & van Oost, B. A. (1993). A second missense mutation in the mitochondrial ATPase 6 gene in Leigh's syndrome. Annals of Neurology, 34(3), 410–412. doi:10.1002/ana.410340319

Diez-Juan, A., Rubio, C., Marin, C., Martinez, S., Al-Asmar, N., Riboldi, M. et al. (2015). Mitochondrial DNA content as a viability score in human euploid embryos: less is better. Fertility and sterility, 104(3), 534–41.e1. doi:10.1016/j.fertnstert.2015.05.022

Dobson, A. T., Raja, R., Abeyta, M. J., Taylor, T., Shen, S., Haqq, C. et al. (2004). The unique transcriptome through day 3 of human preimplantation development. Human Molecular Genetics, 13(14), 1461–1470. doi:10.1093/hmg/ddh157

Donovan, L. E., & Severin, N. E. (2006). Maternally inherited diabetes and deafness in a north american kindred: tips for making the diagnosis and review of unique management issues. The Journal of Clinical Endocrinology & Metabolism, 91(12), 4737–4742. doi:10.1210/jc.2006-1498

Driscoll, D. A (2001). Prenatal diagnosis of the 22q11.2 deletion syndrome. Genetics in medicine, 3(1), 14–8. doi:10.109700125817-200101000-00004

Dubeau, F., De Stefano, N., Zifkin, B. G., Arnold, D. L., & Shoubridge, E. A. (2000). Oxidative phosphorylation defect in the brains of carriers of the tRNAleu(UUR) A3243G mutation in a MELAS pedigree. Annals of neurology, 47(2), 179–85

Elliott, H. R., Samuels, D. C., Eden, J. A., Relton, C. L., & Chinnery, P. F. (2008). Pathogenic mitochondrial DNA mutations are common in the general population. American journal of human genetics, 83(2), 254–60. doi:10.1016/j.ajhg.2008.07.004

Ferlin, T., Landrieu, P., Rambaud, C., Fernandez, H., Dumoulin, R., Rustin, P., & Mousson, B. (1997). Segregation of the G8993 mutant mitochondrial DNA through

generations and embryonic tissues in a family at risk of Leigh syndrome. The journal of paediatrics. doi.org/10.1016/S0022-3476(97)80074-1

Finsterer, J., Mancuso, M., Pareyson, D., Burgunder, J.-M., & Klopstock, T. (2017). Mitochondrial disorders of the retinal ganglion cells and the optic nerve. Mitochondrion. doi:10.1016/J.MITO.2017.10.003

Fiorentino, F., Biricik, A., Bono, S., Spizzichino, L., Cotroneo, E., Cottone, G. et al. (2014a). Development and validation of a next-generation sequencing–based protocol for 24-chromosome aneuploidy screening of embryos. Fertility and Sterility, 101(5), 1375-1382.e2. doi:10.1016/j.fertnstert.2014.01.051

Fiorentino, F., Biricik, A., Nuccitelli, A., De Palma, R., Kahraman, S., Iacobelli, M. et al. (2006). Strategies and clinical outcome of 250 cycles of Preimplantation Genetic Diagnosis for single gene disorders. Human reproduction, 21(3), 670–84. doi:10.1093/humrep/dei382

Fiorentino, F., Bono, S., Biricik, A., Nuccitelli, A., Cotroneo, E., Cottone, G. et al. (2014b). Application of next-generation sequencing technology for comprehensive aneuploidy screening of blastocysts in clinical preimplantation genetic screening cycles. Human Reproduction, 29(12), 2802–2813. doi:10.1093/humrep/deu277

Fiorentino, F., Spizzichino, L., Bono, S., Biricik, A., Kokkali, G., Rienzi, L. et al. (2011). PGD for reciprocal and Robertsonian translocations using array comparative genomic hybridization. Human Reproduction, 26(7), 1925–1935. doi:10.1093/humrep/der082

Forman, E. J., Hong, K. H., Ferry, K. M., Tao, X., Taylor, D., Levy, B. et al. (2013). In vitro fertilization with single euploid blastocyst transfer: a randomized controlled trial. Fertility and sterility, 100(1), 100–7.e1. doi:10.1016/j.fertnstert.2013.02.056

Forman, E. J., Tao, X., Ferry, K. M., Taylor, D., Treff, N. R., & Scott, R. T. (2012). Single embryo transfer with comprehensive chromosome screening results in improved ongoing pregnancy rates and decreased miscarriage rates. Human reproduction, 27(4), 1217–22. doi:10.1093/humrep/des020

Fragouli, E., Alfarawati, S., Spath, K., Babariya, D., Tarozzi, N., Borini, A. et al. (2017a). Analysis of implantation and ongoing pregnancy rates following the transfer of mosaic diploid–aneuploid blastocysts. Human Genetics. doi:10.1007/s00439-017-1797-4

Fragouli, E., Alfarawati, S., Spath, K., Jaroudi, S., Sarasa, J., Enciso, M. et al. (2013). The origin and impact of embryonic aneuploidy. Human Genetics, 132(9). doi:10.1007/s00439-013-1309-0

Fragouli, E, Alfarawati, S., Spath, K., & Wells, D. (2014). Morphological and cytogenetic assessment of cleavage and blastocyst stage embryos. Molecular human reproduction, 20(2), 117–26. doi:10.1093/molehr/gat073

Fragouli, E., McCaffrey, C., Ravichandran, K., Spath, K., Grifo, J. A., Munné, S. et al. (2017b). Clinical implications of mitochondrial DNA quantification on pregnancy outcomes: a blinded prospective non-selection study. Human Reproduction, 32(11), 2340–2347. doi:10.1093/humrep/dex292

Fragouli, E., Spath, K., Alfarawati, S., Kaper, F., Craig, A., Michel, C.-E. et al. (2015). Altered levels of mitochondrial DNA are associated with female age, aneuploidy, and provide an independent measure of embryonic implantation potential. PLoS Genetics, 11(6). doi:10.1371/journal.pgen.1005241

Franasiak, J. M., Forman, E. J., Hong, K. H., Werner, M. D., Upham, K. M., Treff, N. R., Scott, R. T. (2014). The nature of aneuploidy with increasing age of the female partner: a review of 15,169 consecutive trophectoderm biopsies evaluated with comprehensive chromosomal screening. Fertility and Sterility, 101, 656–663. doi: 10.1016/j.fertnstert.2013.11.004

Frederiksen, A. L., Andersen, P. H., Kyvik, K. O., Jeppesen, T. D., Vissing, J., & Schwartz, M. (2006). Tissue specific distribution of the 3243A>G mtDNA mutation. Journal of Medical Genetics, 43(8), 671–677. doi:10.1136/jmg.2005.039339

Garrisi, J. G., Colls, P., Ferry, K. M., Zheng, X., Garrisi, M. G., & Munné, S. (2009). Effect of infertility, maternal age, and number of previous miscarriages on the outcome of

preimplantation genetic diagnosis for idiopathic recurrent pregnancy loss. Fertility and Sterility, 92(1), 288–295. doi:10.1016/j.fertnstert.2008.05.056

Gerards, M., Sallevelt, S. C. E. H., & Smeets, H. J. M. (2016). Leigh syndrome: Resolving the clinical and genetic heterogeneity paves the way for treatment options. Molecular Genetics and Metabolism, 117(3), 300–312. doi:10.1016/j.ymgme.2015.12.004

Gigarel, N., Hesters, L., Samuels, D. C., Monnot, S., Burlet, P., Kerbrat, V. et al. (2011). Poor correlations in the levels of pathogenic mitochondrial DNA mutations in polar bodies versus oocytes and blastomeres in humans. American journal of human genetics, 88(4), 494–8. doi:10.1016/j.ajhg.2011.03.010

Gigarel, N., Ray, P. F., Burlet, P., Frydman, N., Royer, G., Lebon, S. et al. (2005). Single cell quantification of the 8993T>G NARP mitochondrial DNA mutation by fluorescent PCR. Molecular genetics and metabolism, 84(3), 289–92. doi:10.1016/j.ymgme.2004.10.008

Giles, R. E., Blanc, H., Cann, H. M., & Wallace, D. C. (1980). Maternal inheritance of human mitochondrial DNA. Proceedings of the National Academy of Sciences of the United States of America, 77(11), 6715–9

Goodrich, D., Tao, X., Bohrer, C., Lonczak, A., Xing, T., Zimmerman, R. et al. (2016). A randomized and blinded comparison of qPCR and NGS-based detection of aneuploidy in a cell line mixture model of blastocyst biopsy mosaicism. Journal of Assisted Reproduction and Genetics, 33(11), 1473–1480. doi:10.1007/s10815-016-0784-3

Gorman, G. S., Chinnery, P. F., DiMauro, S., Hirano, M., Koga, Y., McFarland, R. et al. (2016). Mitochondrial diseases. Nature Reviews Disease Primers, 2, 16080. doi:10.1038/nrdp.2016.80

Gorman, G. S., Schaefer, A. M., Ng, Y., Gomez, N., Blakely, E. L., Alston, C. L. et al. (2015). Prevalence of nuclear and mitochondrial DNA mutations related to adult mitochondrial disease. Annals of Neurology, 77(5), 753–759. doi:10.1002/ana.24362

Greaves, L. C., Reeve, A. K., Taylor, R. W., & Turnbull, D. M. (2012). Mitochondrial DNA and disease. The Journal of pathology, 226(2), 274–86. doi:10.1002/path.3028

Greco, E., Bono, S., Ruberti, A., Lobascio, A. M., Greco, P., Biricik, A. et al. (2014). Comparative genomic hybridization selection of blastocysts for repeated implantation failure treatment: a pilot study. BioMed research international, 2014, 457913. doi:10.1155/2014/457913

Greco, E., Minasi, M. G., & Fiorentino, F. (2015). Healthy Babies after intrauterine transfer of mosaic aneuploid blastocysts. The New England journal of medicine, 373(21), 2089–90. doi:10.1056/NEJMc1500421

Greenfield, A., Braude, P., Flinter, F., Lovell-Badge, R., Ogilvie, C., & Perry, A. C. F. (2017). Assisted reproductive technologies to prevent human mitochondrial disease transmission. Nature Biotechnology, 35(11), 1059–1068. doi:10.1038/nbt.3997

Griffin, D. K., Handyside, A. H., Harper, J. C., Wilton, L. J., Atkinson, G., Soussis, I. et al. (1994). Clinical experience with preimplantation diagnosis of sex by dual fluorescent in situ hybridization. Journal of assisted reproduction and genetics, 11(3), 132–43

Gutiérrez-Mateo, C., Colls, P., Sánchez-García, J., Escudero, T., Prates, R., Ketterson, K. et al. (2011). Validation of microarray comparative genomic hybridization for comprehensive chromosome analysis of embryos. Fertility and Sterility, 95(3), 953–958. doi:10.1016/j.fertnstert.2010.09.010

Handyside, A. H. (2011). PGD and aneuploidy screening for 24 chromosomes by genome-wide SNP analysis: seeing the wood and the trees. Reproductive biomedicine online, 23(6), 686–91. doi:10.1016/j.rbmo.2011.09.012

Handyside, A. H. (2013). 24-chromosome copy number analysis: a comparison of available technologies. Fertility and sterility, 100(3), 595–602. doi:10.1016/j.fertnstert.2013.07.1965

Handyside, A. H., Harton, G. L., Mariani, B., Thornhill, A. R., Affara, N., Shaw, M.-A. et al. (2010). Karyomapping: a universal method for genome wide analysis of genetic

disease based on mapping crossovers between parental haplotypes. Journal of medical genetics, 47(10), 651–8. doi:10.1136/jmg.2009.069971

Handyside, A. H., Kontogianni, E. H., Hardy, K., & Winston, R. M. (1990). Pregnancies from biopsied human preimplantation embryos sexed by Y-specific DNA amplification. Nature, 344(6268), 768–70. doi:10.1038/344768a0

Hardarson, T., Hanson, C., Lundin, K., Hillensjo, T., Nilsson, L., Stevic, J. et al. (2008). Preimplantation genetic screening in women of advanced maternal age caused a decrease in clinical pregnancy rate: a randomized controlled trial. Human Reproduction, 23(12), 2806–2812. doi:10.1093/humrep/den217

Harper, J. C., & SenGupta, S. B. (2012). Preimplantation genetic diagnosis: State of the ART 2011. Human Genetics, 131(2), 175–186. doi:10.1007/s00439-011-1056-z

Harton, G. L., Magli, M. C., Lundin, K., Montag, M., Lemmen, J., & Harper, J. C. (2011). ESHRE PGD Consortium/Embryology Special Interest Group--best practice guidelines for polar body and embryo biopsy for preimplantation genetic diagnosis/screening (PGD/PGS). Human Reproduction, 26(1), 41–6. doi:10.1093/humrep/deq265

Harton, G. L., Munné, S., Surrey, M., Grifo, J., Kaplan, B., McCulloh, D. H. et al. (2013). Diminished effect of maternal age on implantation after preimplantation genetic diagnosis with array comparative genomic hybridization. Fertility and sterility, 100(6), 1695–703. doi:10.1016/j.fertnstert.2013.07.2002

Hassold, T., & Hunt, P. (2001). To err (meiotically) is human: the genesis of human aneuploidy. Nature Reviews Genetics, 2(4), 280–291. doi:10.1038/35066065

Heindryckx, B., Neupane, J., Vandewoestyne, M., Christodoulou, C., Jackers, Y., Gerris, J. et al. (2014). Mutation-free baby born from a mitochondrial encephalopathy, lactic acidosis and stroke-like syndrome carrier after blastocyst trophectoderm preimplantation genetic diagnosis. Mitochondrion (Band 18). doi:10.1016/j.mito.2014.08.005

HFEA (2018). Fertility treatment 2014-2016 Trends and figures. Human Fertilisation & Embryology Authority

Ho, J. R., Arrach, N., Rhodes-Long, K., Ahmady, A., Ingles, S., Chung, K. et al. (2018). Pushing the limits of detection: investigation of cell-free DNA for aneuploidy screening in embryos. Fertility and Sterility, 110(3), 467-475.e2. doi:10.1016/j.fertnstert.2018.03.036

Holt, I. J., Harding, A. E., Petty, R. K., & Morgan-Hughes, J. A. (1990). A new mitochondrial disease associated with mitochondrial DNA heteroplasmy. American journal of human genetics, 46(3), 428–33

Hosono, T., Suzuki, M., & Chiba, Y. (2001). Contraindication of magnesium sulfate in a pregnancy complicated with late-onset diabetes mellitus and sensory deafness due to mitochondrial myopathy. The Journal of maternal-fetal medicine, 10(5), 355–6.

Howell, N. (1983). Origin, cellular expression, and cybrid transmission of mitochondrial CAP-R, PYR-IND, and OLI-R mutant phenotypes. Somatic cell genetics, 9(1), 1–24.

Jacobs, L. J. A. M., de Wert, G., Geraedts, J. P. M., de Coo, I. F. M., & Smeets, H. J. M. (2006). The transmission of OXPHOS disease and methods to prevent this. Human Reproduction Update, 12(2), 119–136. doi:10.1093/humupd/dmi042

Jansen, R. P., & de Boer, K. (1998). The bottleneck: mitochondrial imperatives in oogenesis and ovarian follicular fate. Molecular and Cellular Endocrinology, 145(1–2), 81–88. Elsevier. doi:10.1016/S0303-7207(98)00173-7

Jansen, R. P. S., Bowman, M. C., de Boer, K. A., Leigh, D. A., Lieberman, D. B., & McArthur, S. J. (2008). What next for preimplantation genetic screening (PGS)? Experience with blastocyst biopsy and testing for aneuploidy. Human Reproduction, 23(7), 1476–1478. doi:10.1093/humrep/den129

Jeppesen, T. D., Schwartz, M., Frederiksen, A. L., Wibrand, F., Olsen, D. B., Vissing, J. et al. (2006). Muscle phenotype and mutation load in 51 persons with the 3243A>G

mitochondrial DNA mutation. Archives of Neurology, 63(12), 1701. doi:10.1001/archneur.63.12.1701

Kang, E., Wu, J., Gutierrez, N. M., Koski, A., Tippner-Hedges, R., Agaronyan, K. et al. (2016). Mitochondrial replacement in human oocytes carrying pathogenic mitochondrial DNA mutations. Nature, 540(7632), 270–275. doi:10.1038/nature20592

Khan, N. A., Govindaraj, P., Meena, A. K., & Thangaraj, K. (2015). Mitochondrial disorders: challenges in diagnosis & treatment. The Indian journal of medical research, 141(1), 13–26

Khorram, O., Shapiro, S. S., & Jones, J. M. (2000). Transfer of nonassisted hatched and hatching human blastocysts after in vitro fertilization. Fertility and sterility, 74(1), 163–5.

Kokkali, G., Vrettou, C., Traeger-Synodinos, J., Jones, G. M., Cram, D. S., Stavrou, D. et al. (2005). Birth of a healthy infant following trophectoderm biopsy from blastocysts for PGD of beta-thalassaemia major. Human reproduction, 20(7), 1855–9. doi:10.1093/humrep/deh893

Kokotas, H., Petersen, M., & Willems, P. (2007). Mitochondrial deafness. Clinical Genetics, 71(5), 379–391. doi:10.1111/j.1399-0004.2007.00800.x

Krisher, R. L., Schoolcraft, W. B., & Katz-Jaffe, M. G. (2015). Omics as a window to view embryo viability. Fertility and Sterility, 103(2), 333–341. doi:10.1016/j.fertnstert.2014.12.116

Kuznyetsov, V., Madjunkova, S., Antes, R., Abramov, R., Motamedi, G., Ibarrientos, Z. et al. (2018). Evaluation of a novel non-invasive preimplantation genetic screening approach. PLOS ONE, 13(5), e0197262. doi:10.1371/journal.pone.0197262

Lanzendorf, S. E., Mayer, J. F., Toner, J., Oehninger, S., Saffan, D. S., & Muasher, S. (1999). Pregnancy following transfer of ooplasm from cryopreserved-thawed donor oocytes into recipient oocytes. Fertility and Sterility, 71(3), 575–577. doi:10.1016/S0015-0282(98)00504-4

Lathi, R. B., Westphal, L. M., & Milki, A. A. (2008). Aneuploidy in the miscarriages of infertile women and the potential benefit of preimplanation genetic diagnosis. Fertility and Sterility, 89(2), 353–357. doi:10.1016/j.fertnstert.2007.02.040

Lee, E., Illingworth, P., Wilton, L., & Chambers, G. M. (2015). The clinical effectiveness of preimplantation genetic diagnosis for aneuploidy in all 24 chromosomes (PGD-A): systematic review. Human reproduction, 30(2), 473–83. doi:10.1093/humrep/deu303

Lee, H.-F., Tsai, C.-R., Chi, C.-S., Lee, H.-J., & Chen, C. C.-C. (2009). Leigh syndrome: clinical and neuroimaging follow-up. Pediatric neurology, 40(2), 88–93. doi:10.1016/j.pediatrneurol.2008.09.020

Lee, H.-L., McCulloh, D. H., Hodes-Wertz, B., Adler, A., McCaffrey, C., & Grifo, J. A. (2015). In vitro fertilization with preimplantation genetic screening improves implantation and live birth in women age 40 through 43. Journal of assisted reproduction and genetics, 32(3), 435–44. doi:10.1007/s10815-014-0417-7

Lestienne, P., & Ponsot, G. (1988). Kearns-Sayre syndrome with muscle mitochondrial DNA deletion. Lancet, 1(8590), 885

Levy, R. J., Ríos, P. G., Akman, H. O., Sciacco, M., Vivo, D. C. De, & DiMauro, S. (2014). Long survival in patients with leigh syndrome and the m.10191T>C mutation in MT-ND3 : a case report and review of the literature. Journal of child neurology, 29(10), NP105-10. doi:10.1177/0883073813506783

Li, P., Song, Z., Yao, Y., Huang, T., Mao, R., Huang, Jun et al. (2018). Preimplantation genetic screening with spent culture medium/blastocoel fluid for in vitro fertilization. Scientific Reports, 8(1), 9275. doi:10.1038/s41598-018-27367-4

Lightowlers, R. N., Chinnery, P. F., Turnbull, D. M., & Howell, N. (1997). Mammalian mitochondrial genetics: heredity, heteroplasmy and disease. Trends in genetics, 13(11), 450–5

Livak, K. J., & Schmittgen, T. D. (2001). Analysis of Relative Gene Expression Data Using Real-Time Quantitative PCR and the 2−ΔΔCT Method. Methods, 25(4), 402–408. doi:10.1006/meth.2001.1262

Machtinger, R., & Racowsky, C. (2013). Morphological systems of human embryo assessment and clinical evidence. Reproductive BioMedicine Online, 26(3), 210–221. doi:10.1016/j.rbmo.2012.10.021

Macklon, N. S., Geraedts, J. P. M., & Fauser, B. C. J. M. (2002). Conception to ongoing pregnancy: the „black box“ of early pregnancy loss. Human reproduction update, 8(4), 333–43

Magli, M. C., Gianaroli, L., Ferraretti, A. P., Lappi, M., Ruberti, A., & Farfalli, V. (2007). Embryo morphology and development are dependent on the chromosomal complement. Fertility and Sterility, 87(3), 534–541. doi:10.1016/j.fertnstert.2006.07.1512

Mäkelä-bengs, P., Suomalainen, A., Majander, A., Rapola, J., Kalimo, H., Nuutila, A. et al. (1995). Correlation between the clinical symptoms and the proportion of mitochondrial DNA carrying the 8993 point mutation in the NARP Syndrome. Pediatric Research, 37(5), 634–639. doi:10.1203/00006450-199505000-00014

Mantikou, E., Wong, K. M., Repping, S., & Mastenbroek, S. (2012). Molecular origin of mitotic aneuploidies in preimplantation embryos. Biochimica et Biophysica Acta (BBA) - Molecular Basis of Disease, 1822(12), 1921–1930. doi:10.1016/J.BBADIS.2012.06.013

Manwaring, N., Jones, M. M., Wang, J. J., Rochtchina, E., Howard, C., Mitchell, P. et al. (2007). Population prevalence of the MELAS A3243G mutation. Mitochondrion, 7(3), 230–233. doi:10.1016/j.mito.2006.12.004

Mastenbroek, S., Twisk, M., van Echten-Arends, J., Sikkema-Raddatz, B., Korevaar, J. C., Verhoeve, H. R. et al. (2007). In Vitro Fertilization with Preimplantation Genetic Screening. New England Journal of Medicine, 357(1), 9–17. doi:10.1056/NEJMoa067744

Mastenbroek, S., Twisk, M., van der Veen, F., & Repping, S. (2011). Preimplantation genetic screening: a systematic review and meta-analysis of RCTs. Human Reproduction Update, 17(4), 454–466. doi:10.1093/humupd/dmr003

Matthews, P. M., Hopkin, J., Brown, R. M., Stephenson, J. B., Hilton-Jones, D., & Brown, G. K. (1994). Comparison of the relative levels of the 3243 (A>G) mtDNA mutation in heteroplasmic adult and fetal tissues. Journal of medical genetics, 31(1), 41–4

May-Panloup, P., Chretien, M., Malthiery, Y., & Reynier, P. (2007). Mitochondrial DNA in the Oocyte and the Developing Embryo. Current topics in developmental biology (Band 77, S. 51–83). doi:10.1016/S0070-2153(06)77003-X

McArthur, S. J., Leigh, D., Marshall, J. T., de Boer, K. A., & Jansen, R. P. S. (2005). Pregnancies and live births after trophectoderm biopsy and preimplantation genetic testing of human blastocysts. Fertility and sterility, 84(6), 1628–36. doi:10.1016/j.fertnstert.2005.05.063

McElhoe, J. A., Holland, M. M., Makova, K. D., Su, M. S.-W., Paul, I. M., Baker, C. H. et al. (2014). Development and assessment of an optimized next-generation DNA sequencing approach for the mtgenome using the Illumina MiSeq. Forensic science international. Genetics, 13, 20–9. doi:10.1016/j.fsigen.2014.05.007

Mersereau, J. E., Pergament, E., Zhang, X., & Milad, M. P. (2008). Preimplantation genetic screening to improve in vitro fertilization pregnancy rates: a prospective randomized controlled trial. Fertility and Sterility, 90(4), 1287–1289. doi:10.1016/j.fertnstert.2007.08.010

Meyer, L. R., Klipstein, S., Hazlett, W. D., Nasta, T., Mangan, P., & Karande, V. C. (2009). A prospective randomized controlled trial of preimplantation genetic screening in the “good prognosis” patient. Fertility and Sterility, 91(5), 1731–1738. doi:10.1016/j.fertnstert.2008.02.162

Mikkelsen, M., Frank-Hansen, R., Hansen, A. J., & Morling, N. (2014). Massively parallel pyrosequencing of the mitochondrial genome with the 454 methodology in

forensic genetics. Forensic science international. Genetics, 12, 30–7. doi:10.1016/j.fsigen.2014.03.014

Minami, N., Suzuki, T., & Tsukamoto, S. (2007). Zygotic gene activation and maternal factors in mammals. The Journal of reproduction and development, 53(4), 707–15

Mitalipov, S., Amato, P., Parry, S., & Falk, M. J. (2014). Limitations of preimplantation genetic diagnosis for mitochondrial DNA diseases. Cell Reports, 7(4), 935–937. doi:10.1016/j.celrep.2014.05.004

Monk, D. (2015). Germline-derived DNA methylation and early embryo epigenetic reprogramming: The selected survival of imprints. The International Journal of Biochemistry & Cell Biology, 67, 128–138. doi:10.1016/J.BIOCEL.2015.04.014

Monnot, S., Gigarel, N., Samuels, D. C., Burlet, P., Hesters, L., Frydman, N. et al. (2011). Segregation of mtDNA throughout human embryofetal development: m.3243A>G as a model system. Human mutation, 32(1), 116–25. doi:10.1002/humu.21417

Montag, M., Toth, B., & Strowitzki, T. (2013). New approaches to embryo selection. Reproductive BioMedicine Online, 27(5), 539–546. doi:10.1016/J.RBMO.2013.05.013

Morales, C., Sánchez, A., Bruguera, J., Margarit, E., Borrell, A., Borobio, V. et al. (2008). Cytogenetic study of spontaneous abortions using semi-direct analysis of chorionic villi samples detects the broadest spectrum of chromosome abnormalities. American Journal of Medical Genetics Part A, 146A(1), 66–70. doi:10.1002/ajmg.a.32058

Munné, S. (2001). Preimplantation genetic diagnosis of structural abnormalities. Molecular and cellular endocrinology, S55-8

Munné, S., Chen, S., Colls, P., Garrisi, J., Zheng, X., Cekleniak, N. et al. (2007). Maternal age, morphology, development and chromosome abnormalities in over 6000 cleavage-stage embryos. Reproductive biomedicine online, 14(5), 628–34

Munné, S., Chen, S., Fischer, J., Colls, P., Zheng, X., Stevens, J. et al. (2005). Preimplantation genetic diagnosis reduces pregnancy loss in women aged 35 years and older with a history of recurrent miscarriages. Fertility and Sterility, 84(2), 331–335. doi:10.1016/j.fertnstert.2005.02.027

Munné, S, Fragouli, E., Colls, P., Katz-Jaffe, M., Schoolcraft, W., & Wells, D. (2010a). Improved detection of aneuploid blastocysts using a new 12-chromosome FISH test. Reproductive biomedicine online, 20(1), 92–7. doi:10.1016/j.rbmo.2009.10.015

Munné, S., Grifo, J., Cohen, J., & Weier, H. U. (1994). Chromosome abnormalities in human arrested preimplantation embryos: a multiple-probe FISH study. American journal of human genetics, 55(1), 150–9

Munné, S., Lee, A., Rosenwaks, Z., Grifo, J., & Cohen, J. (1993a). Diagnosis of major chromosome aneuploidies in human preimplantation embryos. Human reproduction, 8(12), 2185–91

Munné, S., Weier, H. U., Stein, J., Grifo, J., & Cohen, J. (1993b). A fast and efficient method for simultaneous X and Y in situ hybridization of human blastomeres. Journal of assisted reproduction and genetics, 10(1), 82–90

Munné, Santiago, Wells, D., & Cohen, J. (2010b). Technology requirements for preimplantation genetic diagnosis to improve assisted reproduction outcomes. Fertility and sterility, 94(2), 408–30. doi:10.1016/j.fertnstert.2009.02.091

Nagaoka, So I., Hassold, T. J., & Hunt, P. A. (2012). Human aneuploidy: mechanisms and new insights into an age-old problem. Nature Reviews Genetics, 13(7), 493–504. doi:10.1038/nrg3245

Nesbitt, V., Morrison, P. J., Crushell, E., Donnelly, D. E., Alston, C. L., He, L. et al. (2012). The clinical spectrum of the m.10191T>C mutation in complex I-deficient Leigh syndrome. Developmental Medicine & Child Neurology, 54(6), 500–506. doi:10.1111/j.1469-8749.2012.04224.x

Nesbitt, V., Pitceathly, R. D. S., Turnbull, D. M., Taylor, R. W., Sweeney, M. G., Mudanohwo, E. E. et al. (2013). The UK MRC Mitochondrial Disease Patient Cohort Study: clinical phenotypes associated with the m.3243A>G mutation--implications for diagnosis and management. Journal of Neurology, Neurosurgery & Psychiatry, 84(8), 936–938. doi:10.1136/jnnp-2012-303528

Neupane, J., Vandewoestyne, M., Ghimire, S., Lu, Y., Qian, C., Van Coster, R. et al. (2014a). Assessment of nuclear transfer techniques to prevent the transmission of heritable mitochondrial disorders without compromising embryonic development competence in mice. Mitochondrion, 18, 27–33. doi:10.1016/j.mito.2014.09.003

Neupane, J., Vandewoestyne, M., Heindryckx, B., Ghimire, S., Lu, Y., Qian, C. et al. (2014b). A systematic analysis of the suitability of preimplantation genetic diagnosis for mitochondrial diseases in a heteroplasmic mitochondrial mouse model. Human reproduction, 29(4), 852–9. doi:10.1093/humrep/deu016

Niakan, K. K., Han, J., Pedersen, R. A., Simon, C., & Pera, R. A. R. (2012). Human pre-implantation embryo development. Development, 139(5), 829–41. doi:10.1242/dev.060426

Okae, H., Chiba, H., Hiura, H., Hamada, H., Sato, A., Utsunomiya, T. et al. (2014). Genome-wide analysis of DNA methylation dynamics during early human development. PLoS Genetics, 10(12), e1004868. doi:10.1371/journal.pgen.1004868

Parson, W., Strobl, C., Huber, G., Zimmermann, B., Gomes, S. M., Souto, L. et al. (2013). Evaluation of next generation mtGenome sequencing using the Ion Torrent Personal Genome Machine (PGM). Forensic Science International: Genetics, 7(5), 543–549. doi:10.1016/j.fsigen.2013.06.003

Paull, D., Emmanuele, V., Weiss, K. A., Treff, N., Stewart, L., Hua, H. et al. (2012). Nuclear genome transfer in human oocytes eliminates mitochondrial DNA variants. Nature, 493(7434), 632–637. doi:10.1038/nature11800

Pickett, S. J., Grady, J. P., Ng, Y. S., Gorman, G. S., Schaefer, A. M., Wilson, I. J. et al. (2018). Phenotypic heterogeneity in m.3243A>G mitochondrial disease: The role of

nuclear factors. Annals of clinical and translational neurology, 5(3), 333–345. doi:10.1002/acn3.532

Pinborg, A. (2005). IVF/ICSI twin pregnancies: risks and prevention. Human Reproduction Update, 11(6), 575–593. doi:10.1093/humupd/dmi027

Pinto, M., & Moraes, C. T. (2015). Mechanisms linking mtDNA damage and aging. Free radical biology & medicine, 85, 250–8. doi:10.1016/j.freeradbiomed.2015.05.005

Playán, A., Solano-Palacios, A., González de la Rosa, J. B., Merino-Arribas, J. M., Andreu, A. L., López-Pérez, M. et al. (2002). [Leigh syndrome resulting from a de novo mitochondrial DNA mutation (T8993G)]. Revista de neurologia, 34(12), 1124–6

Poulsen, V., Ingerslev, H. J., & Kirkegaard, K. (2017). Elective embryo transfers on Day 6 reduce implantation compared with transfers on Day 5. Human Reproduction, 1–6. doi:10.1093/humrep/dex059

Poulton, J., Bredenoord, A. L., Thorburn, D., Wilton, L., Stock-Myer, S., Jacobs, L. J. et al. (2010). 174th ENMC International Workshop: Applying pre-implantation genetic diagnosis to mtDNA diseases: Implications of scientific advances 19–21 March 2010, Naarden, The Netherlands. Neuromuscular Disorders, 20(8), 559–563. doi:10.1016/j.nmd.2010.05.008

Poulton, J., Kennedy, S., Oakeshott, P., & Wells, D. (2009). Preventing transmission of maternally inherited mitochondrial DNA diseases. BMJ (Clinical research ed.), 338, b94. doi:10.1136/BMJ.B94

Pyle, A., Hudson, G., Wilson, I. J., Coxhead, J., Smertenko, T., Herbert, M. et al. (2015). Extreme-depth re-sequencing of mitochondrial DNA finds no evidence of paternal transmission in humans. PLoS genetics, 11(5), e1005040. doi:10.1371/journal.pgen.1005040

Rahman, S., Blok, R. B., Dahl, H. H., Danks, D. M., Kirby, D. M., Chow, C. W. et al. (1996). Leigh syndrome: clinical features and biochemical and DNA abnormalities. Annals of neurology, 39(3), 343–51. doi:10.1002/ana.410390311

Ravichandran, K., McCaffrey, C., Grifo, J., Morales, A., Perloe, M., Munne, S. et al. (2017). Mitochondrial DNA quantification as a tool for embryo viability assessment: retrospective analysis of data from single euploid blastocyst transfers. Human Reproduction, 1–11. doi:10.1093/humrep/dex070

Reardon, S. (2017). Genetic details of controversial „three-parent baby“ revealed. Nature, 544(7648), 17–18. doi:10.1038/nature.2017.21761

Reynier, P., May-Panloup, P., Chrétien, M. F., Morgan, C. J., Jean, M., Savagner, F. et al. (2001). Mitochondrial DNA content affects the fertilizability of human oocytes. Molecular human reproduction, 7(5), 425–9

Saitoh, S., Momoi, M. Y., Yamagata, T., Nakauchi, H., Nihei, K., & Fujii, M. (1999). Single-cell analysis of mitochondrial DNA in patients and a carrier of the tRNA(Leu)(UUR) gene mutation. Journal of inherited metabolic disease, 22(5), 608–14

Sallevelt, S. C. E. H., de Die-Smulders, C. E. M., Hendrickx, A. T. M., Hellebrekers, D. M. E. I., de Coo, I. F. M., Alston, C. L. et al. (2017). De novo mtDNA point mutations are common and have a low recurrence risk. Journal of medical genetics, 54(2), 73–83. doi:10.1136/jmedgenet-2016-103876

Sallevelt, S. C. E. H., Dreesen, J. C. F. M., Drüsedau, M., Spierts, S., Coonen, E., van Tienen, F. H. J. et al. (2013). Preimplantation genetic diagnosis in mitochondrial DNA disorders: challenge and success. Journal of medical genetics, 50(2), 125–32. doi:10.1136/jmedgenet-2012-101172

Santorelli, F. M., Shanske, S., Macaya, A., DeVivo, D. C., & DiMauro, S. (1993). The mutation at nt 8993 of mitochondrial DNA is a common cause of Leigh’s syndrome. Annals of neurology, 34(6), 827–34. doi:10.1002/ana.410340612

Sato, A., Kono, T., Nakada, K., Ishikawa, K., Inoue, S.-I., Yonekawa, H. et al. (2005). Gene therapy for progeny of mito-mice carrying pathogenic mtDNA by nuclear transplantation. Proceedings of the National Academy of Sciences of the United States of America, 102(46), 16765–70. doi:10.1073/pnas.0506197102

Schaefer, A. M., McFarland, R., Blakely, E. L., He, L., Whittaker, R. G., Taylor, R. W. et al. (2008). Prevalence of mitochondrial DNA disease in adults. Annals of Neurology, 63(1), 35–39. doi:10.1002/ana.21217

Schatten, H., Sun, Q.-Y., & Prather, R. (2014). The impact of mitochondrial function/dysfunction on IVF and new treatment possibilities for infertility. Reproductive biology and endocrinology, 12, 111. doi:10.1186/1477-7827-12-111

Schoolcraft, W. B., Fragouli, E., Stevens, J., Munne, S., Katz-Jaffe, M. G., & Wells, D. (2010). Clinical application of comprehensive chromosomal screening at the blastocyst stage. Fertility and sterility, 94(5), 1700–6. doi:10.1016/j.fertnstert.2009.10.015

Schoolcraft, W. B., & Katz-Jaffe, M. G. (2013). Comprehensive chromosome screening of trophectoderm with vitrification facilitates elective single-embryo transfer for infertile women with advanced maternal age. Fertility and Sterility, 100(3), 615–619. doi:10.1016/j.fertnstert.2013.07.1972

Schoolcraft, W. B., Katz-Jaffe, M. G., Stevens, J., Rawlins, M., & Munne, S. (2009). Preimplantation aneuploidy testing for infertile patients of advanced maternal age: a randomized prospective trial. Fertility and Sterility, 92(1), 157–162. doi:10.1016/j.fertnstert.2008.05.029

Scott, R. T., Upham, K. M., Forman, E. J., Hong, K. H., Scott, K. L., Taylor, D. et al. (2013a). Blastocyst biopsy with comprehensive chromosome screening and fresh embryo transfer significantly increases in vitro fertilization implantation and delivery rates: a randomized controlled trial. Fertility and sterility, 100(3), 697–703. doi:10.1016/j.fertnstert.2013.04.035

Scott, R. T., Upham, K. M., Forman, E. J., Zhao, T., & Treff, N. R. (2013b). Cleavage-stage biopsy significantly impairs human embryonic implantation potential while blastocyst biopsy does not: a randomized and paired clinical trial. Fertility and sterility, 100(3), 624–30. doi:10.1016/j.fertnstert.2013.04.039

Shanske, S., Pancrudo, J., Kaufmann, P., Engelstad, K., Jhung, S., Lu, J. et al. (2004). Varying loads of the mitochondrial DNA A3243G mutation in different tissues: implications

for diagnosis. American journal of medical genetics. Part A, 130A(2), 134–7. doi:10.1002/ajmg.a.30220

Shoubridge, E. A., & Wai, T. (2007). Mitochondrial DNA and the mammalian oocyte. Current Topics in Developmental Biology, 77, 87–111. doi:10.1016/S0070-2153(06)77004-1

Singh, R., Ellard, S., Hattersley, A., & Harries, L. W. (2006). Rapid and sensitive real-time polymerase chain reaction method for detection and quantification of 3243A>G mitochondrial point mutation. The Journal of molecular diagnostics, 8(2), 225–30. doi:10.2353/jmoldx.2006.050067

Skladal, D., Halliday, J., & Thorburn, D. R. (2003). Minimum birth prevalence of mitochondrial respiratory chain disorders in children. Brain : a journal of neurology, 126(Pt 8), 1905–12. doi:10.1093/brain/awg170

Smeets, Hubert J M, Sallevelt, S. C. E. H., Dreesen, J. C. F. M., De Die-Smulders, C. E. M., De Coo, I. F. M., & Smeets, H J M (2015). Preventing the transmission of mitochondrial DNA disorders using prenatal or preimplantation genetic diagnosis. Ann. N.Y. Acad. Sci. doi:10.1111/nyas.12866

Smith, Z. D., Chan, M. M., Humm, K. C., Karnik, R., Mekhoubad, S., Regev, A. et al. (2014). DNA methylation dynamics of the human preimplantation embryo. Nature, 511(7511), 611–615. doi:10.1038/nature13581

Steffann, J., Frydman, N., Gigarel, N., Burlet, P., Ray, P. F., Fanchin, R. et al. (2006). Analysis of mtDNA variant segregation during early human embryonic development: a tool for successful NARP preimplantation diagnosis. Journal of medical genetics, 43(3), 244–7. doi:10.1136/jmg.2005.032326

Stewart, J. B., & Chinnery, P. F. (2015). The dynamics of mitochondrial DNA heteroplasmy: implications for human health and disease. Nature Reviews Genetics, 16(9), 530–542. doi:10.1038/nrg3966

Sueoka, K. (2016). Preimplantation genetic diagnosis: an update on current technologies and ethical considerations. Reproductive Medicine and Biology, 15(2), 69–75. doi:10.1007/s12522-015-0224-6

Suomalainen, A. (2011). Therapy for mitochondrial disorders: little proof, high research activity, some promise. Seminars in fetal & neonatal medicine, 16(4), 236–40. doi:10.1016/j.siny.2011.05.003

Tachibana, M., Amato, P., Sparman, M., Woodward, J., Sanchis, D. M., Ma, H. et al. (2012). Towards germline gene therapy of inherited mitochondrial diseases. Nature, 493(7434), 627–631. doi:10.1038/nature11647

Tachibana, M., Sparman, M., Sritanaudomchai, H., Ma, H., Clepper, L., Woodward, J. et al. (2009). Mitochondrial gene replacement in primate offspring and embryonic stem cells. Nature, 461(7262), 367–372. doi:10.1038/nature08368

Tajima, H., Sueoka, K., Moon, S. Y., Nakabayashi, A., Sakurai, T., Murakoshi, Y. et al. (2007). The development of novel quantification assay for mitochondrial DNA heteroplasmy aimed at preimplantation genetic diagnosis of Leigh encephalopathy. Journal of assisted reproduction and genetics, 24(6), 227–32. doi:10.1007/s10815-007-9114-0

Tan, Y.-Q., Tan, K., Zhang, S.-P., Gong, F., Cheng, D.-H., Xiong, B. et al. (2013). Single-nucleotide polymorphism microarray-based preimplantation genetic diagnosis is likely to improve the clinical outcome for translocation carriers. Human Reproduction, 28(9), 2581–2592. doi:10.1093/humrep/det271

Thorburn D, Wilton L, S.-M. S. (2009). Healthy baby girl born following preimplantation genetic diagnosis for mitochondrial DNA m.8993T>G Mutation. Mol Genet Metab, (89), 5–6

Thorburn, D. R., & Dahl, H. H. (2001). Mitochondrial disorders: genetics, counseling, prenatal diagnosis and reproductive options. American journal of medical genetics, 106(1), 102–14. doi:10.1002/ajmg.1380

Treff, N. R., Campos, J., Tao, X., Levy, B., Ferry, K. M., & Scott, R. T. (2012a). Blastocyst preimplantation genetic diagnosis (PGD) of a mitochondrial DNA disorder. Fertility and Sterility, 98(5), 1236–1240. doi:10.1016/j.fertnstert.2012.07.1119

Treff, N. R., Northrop, L. E., Kasabwala, K., Su, J., Levy, B., & Scott, R. T. (2011). Single nucleotide polymorphism microarray–based concurrent screening of 24-chromosome aneuploidy and unbalanced translocations in preimplantation human embryos. Fertility and Sterility, 95(5), 1606-1612.e2. doi:10.1016/j.fertnstert.2010.11.004

Treff, N. R., Su, J., Tao, X., Levy, B., & Scott Jr., R. T. (2010). Accurate single cell 24 chromosome aneuploidy screening using whole genome amplification and single nucleotide polymorphism microarrays. Fertility and Sterility, 94(6), 2017–2021. doi:10.1016/j.fertnstert.2010.01.052

Treff, N. R., Tao, X., Ferry, K. M., Su, J., Taylor, D., & Scott, R. T. (2012b). Development and validation of an accurate quantitative real-time polymerase chain reaction–based assay for human blastocyst comprehensive chromosomal aneuploidy screening. Fertility and Sterility, 97(4), 819-824.e2. doi:10.1016/j.fertnstert.2012.01.115

Treff, N. R., Zhan, Y., Tao, X., Olcha, M., Han, M., Rajchel, J. et al. (2017). Levels of trophectoderm mitochondrial DNA do not predict the reproductive potential of sibling embryos. Human Reproduction, 1–9. doi:10.1093/humrep/dex034

Tulinius, M. H., Houshmand, M., Larsson, N. G., Holme, E., Oldfors, A., Holmberg, E. et al. (1995). De novo mutation in the mitochondrial ATP synthase subunit 6 gene (T8993G) with rapid segregation resulting in Leigh syndrome in the offspring. Human genetics, 96(3), 290–4

Uyar, A., & Seli, E. (2014). Metabolomic assessment of embryo viability. Seminars in reproductive medicine, 32(2), 141–52. doi:10.1055/s-0033-1363556

Van Blerkom, J. (2004). Mitochondria in human oogenesis and preimplantation embryogenesis: engines of metabolism, ionic regulation and developmental competence. Reproduction, 128(3), 269–80. doi:10.1530/rep.1.00240

Van Blerkom, J. (2011). Mitochondrial function in the human oocyte and embryo and their role in developmental competence. Mitochondrion, 11(5), 797–813. doi:10.1016/j.mito.2010.09.012

Van Blerkom, J., Davis, P., & Alexander, S. (2000). Differential mitochondrial distribution in human pronuclear embryos leads to disproportionate inheritance between blastomeres: relationship to microtubular organization, ATP content and competence. Human reproduction, 15(12), 2621–33

Van der Giezen, M., & Tovar, J. (2005). Degenerate mitochondria. EMBO reports, 6(6), 525–30. European Molecular Biology Organization. doi:10.1038/sj.embor.7400440

Vandewoestyne, M., Heindryckx, B., De Gheselle, S., Lepez, T., Neupane, J., Gerris, J. et al. (2012). Poor correlation between polar bodies and blastomere mutation load in a patient with m.3243A>G tRNALeu(UUR) point mutation. Mitochondrion. doi:10.1016/j.mito.2012.04.002

Vandewoestyne, M., Heindryckx, B., Lepez, T., Van Coster, R., Gerris, J., De Sutter, P. et al. (2011). Polar body mutation load analysis in a patient with A3243G tRNALeu(UUR) point mutation. Mitochondrion (Band 11). doi:10.1016/j.mito.2011.03.123

Van Echten-Arends, J., Mastenbroek, S., Sikkema-Raddatz, B., Korevaar, J. C., Heineman, M. J., van der Veen, F. et al. (2011). Chromosomal mosaicism in human preimplantation embryos: a systematic review. Human Reproduction Update, 17(5), 620–627. doi:10.1093/humupd/dmr014

Vanneste, E., Voet, T., Melotte, C., Debrock, S., Sermon, K., Staessen, C. et al. (2009). What next for preimplantation genetic screening? High mitotic chromosome instability rate provides the biological basis for the low success rate. Human Reproduction, 24(11), 2679–2682. doi:10.1093/humrep/dep266

Vera-Rodríguez, M., Michel, C.-E., Mercader, A., Bladon, A. J., Rodrigo, L., Kokocinski, F. et al. (2016). Distribution patterns of segmental aneuploidies in human blastocysts identified by next-generation sequencing. Fertility and sterility, 105(4), 1047-1055.e2. doi:10.1016/j.fertnstert.2015.12.022

Verlinsky, Y., Cieslak, J., Ivakhnenko, V., Evsikov, S., Wolf, G., White, M., Lifchez, A., Kaplan, B., Moise, J., Valle, J., Ginsberg, N., Strom, C., Kuliev A (2001). Chromosomal abnormalities in the first and second polar body. Molecular and Cellular Endocrinology, 183, 47—49

Verlinsky, Y., & Kuliev, A. (1996). Preimplantation polar body diagnosis. Biochemical and molecular medicine, 58(1), 13–7.

Vermeesch, J. R., Voet, T., & Devriendt, K. (2016). Prenatal and pre-implantation genetic diagnosis. Nature Reviews Genetics, 17(10), 643–656. doi:10.1038/nrg.2016.97

Victor, A. R., Brake, A. J., Tyndall, J. C., Griffin, D. K., Zouves, C. G., Barnes, F. L. et al. (2017). Accurate quantitation of mitochondrial DNA reveals uniform levels in human blastocysts irrespective of ploidy, age, or implantation potential. Fertility and Sterility, 107(1), 34-42.e3. doi:10.1016/j.fertnstert.2016.09.028

Wai, T., Teoli, D., & Shoubridge, E. A. (2008). The mitochondrial DNA genetic bottleneck results from replication of a subpopulation of genomes. Nature genetics, 40(12), 1484–8. doi:10.1038/ng.258

Wallace, D. C., Luft, R., Ikkos, D., Palmieri, G., Ernster, L., Afzelius, B. A. et al. (1999). Mitochondrial diseases in man and mouse. Science, 283(5407), 1482–8. doi:10.1126/science.283.5407.1482

Wang, T., Sha, H., Ji, D., Zhang, H. L., Chen, D., Cao, Y. et al. (2014). Polar body genome transfer for preventing the transmission of inherited mitochondrial diseases. Cell, 157(7), 1591–1604. doi:10.1016/j.cell.2014.04.042

Wells, D., Kaur, K., Grifo, J., Glassner, M., Taylor, J. C., Fragouli, E. et al. (2014). Clinical utilisation of a rapid low-pass whole genome sequencing technique for the diagnosis of aneuploidy in human embryos prior to implantation. Journal of Medical Genetics, 51(8), 553–562. doi:10.1136/jmedgenet-2014-102497

Wells, D., Sherlock, J. K., Handyside, A. H., & Delhanty, J. D. (1999). Detailed chromosomal and molecular genetic analysis of single cells by whole genome amplification and comparative genomic hybridisation. Nucleic acids research, 27(4), 1214–8

White, S. L., Collins, V. R., Wolfe, R., Cleary, M. A., Shanske, S., DiMauro, S. et al. (1999a). Genetic counseling and prenatal diagnosis for the mitochondrial DNA mutations at nucleotide 8993. American journal of human genetics, 65(2), 474–82. doi:10.1086/302488

White, S. L., Shanske, S., McGill, J. J., Mountain, H., Geraghty, M. T., DiMauro, S. et al. (1999b). Mitochondrial DNA mutations at nucleotide 8993 show a lack of tissue- or age-related variation. Journal of inherited metabolic disease, 22(8), 899–914

Wilton, L. (2002). Preimplantation genetic diagnosis for aneuploidy screening in early human embryos: a review. Prenatal diagnosis, 22(6), 512–8. doi:10.1002/pd.388

Wilton, L. (2005). Preimplantation genetic diagnosis and chromosome analysis of blastomeres using comparative genomic hybridization. Human Reproduction Update, 11(1), 33–41. doi:10.1093/humupd/dmh050

Wilton, L., Williamson, R., McBain, J., Edgar, D., & Voullaire, L. (2001). Birth of a healthy infant after preimplantation confirmation of euploidy by comparative genomic hybridization. New England Journal of Medicine, 345(21), 1537–1541. doi:10.1056/NEJMoa011052

Wolf, D. P., Mitalipov, N., & Mitalipov, S. (2015). Mitochondrial replacement therapy in reproductive medicine. Trends in molecular medicine, 21(2), 68–76. doi:10.1016/j.molmed.2014.12.001

Yamada, M., Emmanuele, V., Sanchez-Quintero, M. J., Sun, B., Lallos, G., Paull, D. et al. (2016). Genetic Drift Can Compromise Mitochondrial Replacement by Nuclear Transfer in Human Oocytes. Cell Stem Cell, 18(6), 749–754. doi:10.1016/j.stem.2016.04.001

Yamanaka, M., Hashimoto, S., Amo, A., Ito-Sasaki, T., Abe, H., & Morimoto, Y. (2011). Developmental assessment of human vitrified-warmed blastocysts based on oxygen consumption. Human Reproduction, 26(12), 3366–3371. doi:10.1093/humrep/der324

Yang, Z., Liu, J., Collins, G. S., Salem, S. A., Liu, X., Lyle, S. S. et al. (2012). Selection of single blastocysts for fresh transfer via standard morphology assessment alone and with array CGH for good prognosis IVF patients: results from a randomized pilot study. Molecular cytogenetics, 5(1), 24. doi:10.1186/1755-8166-5-24

Ye, F., Samuels, D. C., Clark, T., & Guo, Y. (2014). High-throughput sequencing in mitochondrial DNA research. Mitochondrion, 17, 157–63. doi:10.1016/j.mito.2014.05.004

Yin, X., Tan, K., Vajta, G., Jiang, H., Tan, Y., Zhang, ChunLei et al. (2013). Massively parallel sequencing for chromosomal abnormality testing in trophectoderm cells of human blastocysts. Biology of Reproduction, 88(3), 69. doi:10.1095/biolreprod.112.106211

Youssry, M., Ozmen, B., Zohni, K., Diedrich, K., & Al-Hasani, S. (2008). Current aspects of blastocyst cryopreservation. Reproductive biomedicine online, 16(2), 311–20

Zhang, J., Liu, H., Luo, S., Chavez-Badiola, A., Liu, Z., yang, m. et al. (2016). First live birth using human oocytes reconstituted by spindle nuclear transfer for mitochondrial DNA mutation causing Leigh syndrome. Fertility and Sterility, 106(3), e375–e376. Elsevier. doi:10.1016/j.fertnstert.2016.08.004

Zhang, J., Liu, H., Luo, S., Lu, Z., Chávez-Badiola, A., Liu, Z. et al. (2017). Live birth derived from oocyte spindle transfer to prevent mitochondrial disease. Reproductive BioMedicine Online, 34(4), 361–368. doi:10.1016/j.rbmo.2017.01.013

Zhang, W., Liu, Y., Wang, L., Wang, H., Ma, M., Xu, M. et al. (2016). Clinical application of next-generation sequencing in preimplantation genetic diagnosis cycles for Robertsonian and reciprocal translocations. Journal of Assisted Reproduction and Genetics, 33(7), 899–906. doi:10.1007/s10815-016-0724-2

Appendices

Appendix A

Table A.1: Established cell lines utilised during protocol development. The exact nomenclature used by the Coriell Institute of cell lines carrying structural abnormalities is given below the table.

Cell line	Culture type	Coriell catalogue ID	Repository
47,XY,+13	Fibroblast	GM00526	NIGMS
47,XY,+18	Fibroblast	GM01359	NIGMS
47,XY,+21	Fibroblast	GM02067	NIGMS
45,X0	Fibroblast	GM00857	NIGMS
48,XY,+16,+21	Fibroblast	GM04435	NIGMS
48,XXY,+21	Fibroblast	GM04965	NIGMS
47,XX,+22	Chorionic villus	GM10315	NIGMS
47,XYY	Fibroblast	GM11337	NIGMS
46,XX,+Xq[a]	Fibroblast	GM01730	NIGMS
46,XX,-5p[b]	B-Lymphocyte	GM14130	NIGMS
46,XX,-13q[c]	Fibroblast	GM00509	NIGMS
46,XY,-10p[d]	Fibroblast	GM03047	NIGMS
46,XY,+20p,-22q11[e]	Fibroblast	GM02944	NIGMS
46,XX,-22q11[f]	Fibroblast	GM13325	NIGMS
46,XX	Fibroblast	ND34769	NINDS
46,XY	Fibroblast	ND34770	NINDS

a = 46,XX,der(21)(21qter>21p11::Xq11>Xqter)mat.
b = 46,XX,del(5)(p13.3).ish del(5)(p15.33p13.3)(D5S23-).arr 5p15.33p13.3(68519-33959668)x1,5p13.3p13.2(33961858-35306549)x3.
c = 46,XX,del(13)(pter>q14:).
d = 46,XY,del(10)(p14p12).ish del(10)(p14p12)(D10S2488+,D10S2490+).arr 10p14p12.1(8879757-28099697)x1.
e = 46,XY,+der(20)t(20;22)(20pter->20q11.1::22q11.2->22qter),-22.arr[hg19]20p13p11.1(61662-26305567)x3,22q11.1q11.21(16864885-20311905)x1.
f = 46,XX.ish del(22)(q11.2q11.2)(D22S75-).arr 22q11.21(17256415-19795660)x1.

Table A.2: Copy number assays and reference assay utilised during Phase 1 of protocol development

Chromosome	Assay ID	ThermoFisher catalogue ID	Cytoband position
1	1.1	Hs03193256_cn	1p35.3
	1.2	Hs00876448_cn	1p36.13
	1.3	Hs03178347_cn	1q42.12
	1.4	Hs07226270_cn	1q42.2
2	2.1	Hs04692736_cn	2p23.3
	2.2	Hs04658573_cn	2p25.1
	2.3	Hs04716535_cn	2q24.3
	2.4	Hs01702970_cn	2q31.1
3	3.1	Hs01278165_cn	3p24.2
	3.2	Hs00493458_cn	3p25.3
	3.3	Hs03491014_cn	3q23
	3.4	Hs02815441_cn	3q25.33
4	4.1	Hs05959876_cn	4p12
	4.2	Hs05920128_cn	4p14
	4.3	Hs02075730_cn	4q26
	4.4	Hs01271024_cn	4q31.21
5	5.1	Hs01044784_cn	5p15.31
	5.2	Hs02178036_cn	5p15.31
	5.3	Hs06001079_cn	5q34
	5.4	Hs06047048_cn	5q35.1
6	6.1	Hs04902228_cn	6p24.1
	6.2	Hs02988007_cn	6p25.2
	6.3	Hs06798399_cn	6q21
	6.4	Hs02761573_cn	6q22.32
7	7.1	Hs04339214_cn	7p21.3
	7.2	Hs02418225_cn	7p22.1
	7.3	Hs03114237_cn	7q34
	7.4	Hs03113881_cn	7q34
8	8.1	Hs00275884_cn	8p12
	8.2	Hs06163596_cn	8p23.1
	8.3	Hs00310789_cn	8q24.22
	8.4	Hs01241456_cn	8q24.22
9	9.1	Hs00956247_cn	9p21.1
	9.2	Hs00113964_cn	9p24.3
	9.3	Hs02334579_cn	9q34.13
	9.4	Hs01254139_cn	9q34.3
10	10.1	Hs01210989_cn	10p13
	10.2	Hs05189556_cn	10p15.1

	10.3	Hs07226388_cn	10q26.2
	10.4	Hs07226389_cn	10q26.2
11	11.1	Hs01644358_cn	11p15.4
	11.2	Hs01423651_cn	11p15.4
	11.3	Hs03194732_cn	11q23.1
	11.4	Hs03176196_cn	11q23.1
12	12.1	Hs03194239_cn	12p13.31
	12.2	Hs01557728_cn	12p13.31
	12.3	Hs00213327_cn	12q24.33
	12.4	Hs01436960_cn	12q24.33
13	13.1	Hs03861872_cn	13q31.3
	13.2	Hs00614394_cn	13q32.1
	13.3	Hs00216560_cn	13q34
	13.4	Hs00201890_cn	13q34
14	14.1	Hs02968347_cn	14q32.12
	14.2	Hs02269694_cn	14q32.32
	14.3	Hs02277899_cn	14q32.33
	14.4	Hs02330595_cn	14q32.33
15	15.1	Hs05389092_cn	15q26.1
	15.2	Hs05351793_cn	15q26.1
	15.3	Hs00689935_cn	15q26.1
	15.4	Hs02820990_cn	15q26.3
16	16.1	Hs01480069_cn	16p13.3
	16.2	Hs03055169_cn	16p13.3
	16.3	Hs00150593_cn	16q21
	16.4	Hs03934353_cn	16q24.1
17	17.1	Hs02194326_cn	17p13.1
	17.2	Hs03181823_cn	17p13.2
	17.3	Hs03181459_cn	17q25.1
	17.4	Hs03184552_cn	17q25.1
18	18.1	Hs02106900_cn	18p11.31
	18.2	Hs00488766_cn	18p11.32
	18.3	Hs01306949_cn	18q23
	18.4	Hs06498356_cn	18q23
19	19.1	Hs01413810_cn	19p13.3
	19.2	Hs01339946_cn	19p13.3
	19.3	Hs02995438_cn	19q13.43
	19.4	Hs00566496_cn	19q13.43
20	20.1	Hs07203821_cn	20p12.1
	20.2	Hs00358577_cn	20p12.2
	20.3	Hs00624199_cn	20q13.13

	20.4	Hs02620199_cn	20q13.2
21	21.1	Hs01167169_cn	21q22.3
	21.2	Hs04068763_cn	21q22.3
	21.3	Hs02427310_cn	21q22.3
	21.4	Hs04498861_cn	21q22.3
22	22.1	Hs07226295_cn	22q13.31
	22.2	Hs02065601_cn	22q13.31
	22.3	Hs02311370_cn	22q13.31
	22.4	Hs05561659_cn	22q13.33
X	X.1	Hs03194350_cn	Xp22.2
	X.2	Hs00982082_cn	Xp22.2
	X.3	Hs02022459_cn	Xq27.3
	X.4	Hs02497197_cn	Xq28
Y	Y.1	Hs01090783_cn	Yp11.31
	Y.2	Hs01026408_cn	Yp11.31
	Y.3	Hs01079454_cn	Yq11.221
	Y.4	Hs05704387_cn	Yq11.221
5	Reference	TERT	5p15.33

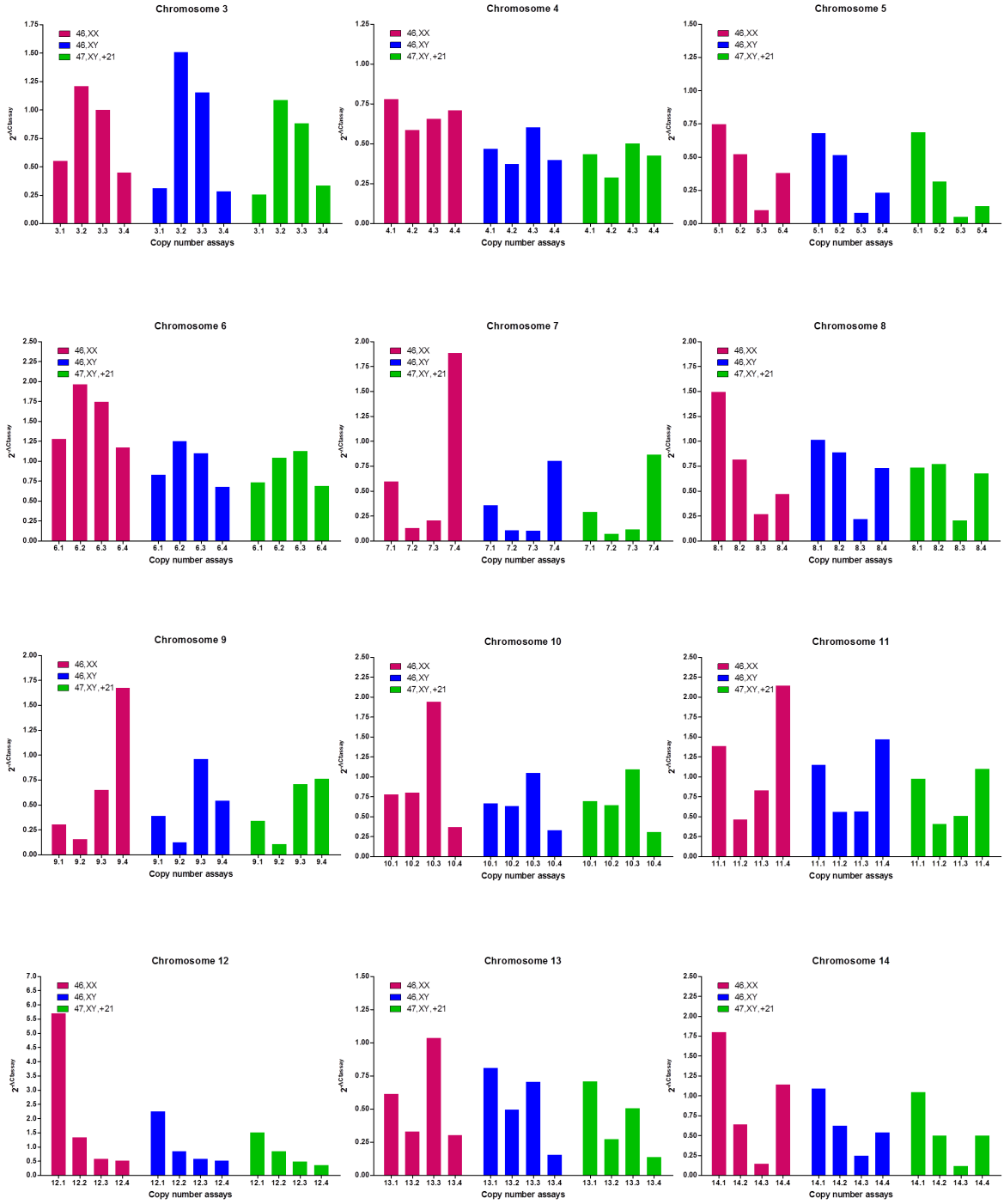


Figure A.1: Pattern of $2^{-\Delta Ctassay}$ values of chromosomes 3 - 14 obtained from three different samples (46,XX; 46,XY; 47,XY,+21)

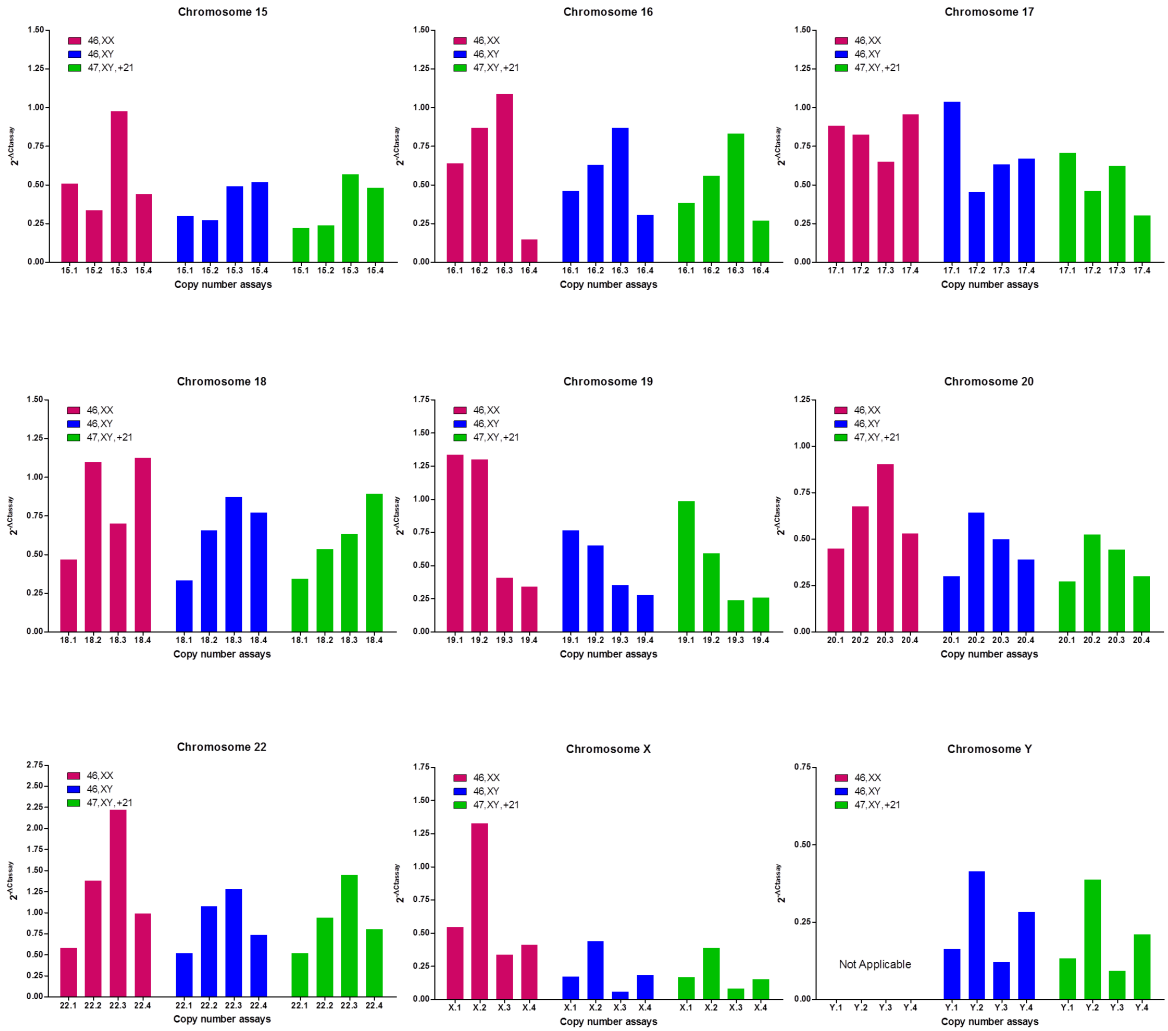


Figure A.2: Pattern of $2^{-\Delta Ctassay}$ values of chromosomes 15 - 20, 22, X and Y obtained from three different samples (46,XX; 46,XY; 47,XY,+21)

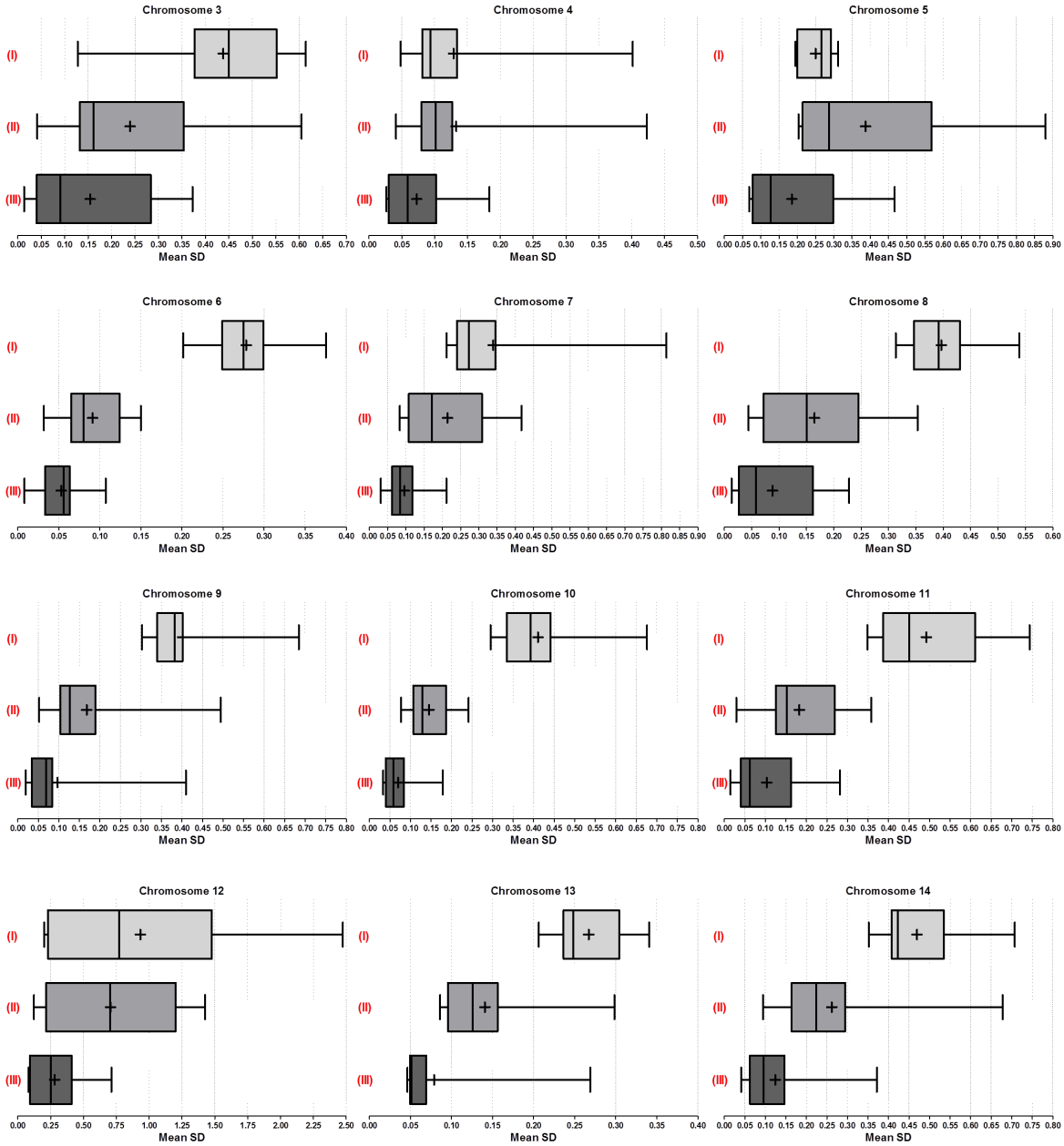


Figure A.3: Box and whisker plots depicting the SD of $2^{-\Delta Ctassay}$ values before and after each of the normalisation steps of chromosomes 3 - 14. Graphs illustrate mean SDs of $2^{-\Delta Ctassay}$ values which were calculated from the nine control samples processed in Phase 1 (5x 46,XX; 4x 46,XY). Vertical lines in the middle of boxes depict median SDs. + signs indicate mean SDs. Error bars show smallest and largest SD value. **I:** Mean SDs prior to normalisation. **II:** Mean SDs after first normalisation (multiplication by assay-specific multiplication factor). **III:** Mean SDs after second normalisation (outlier correction).

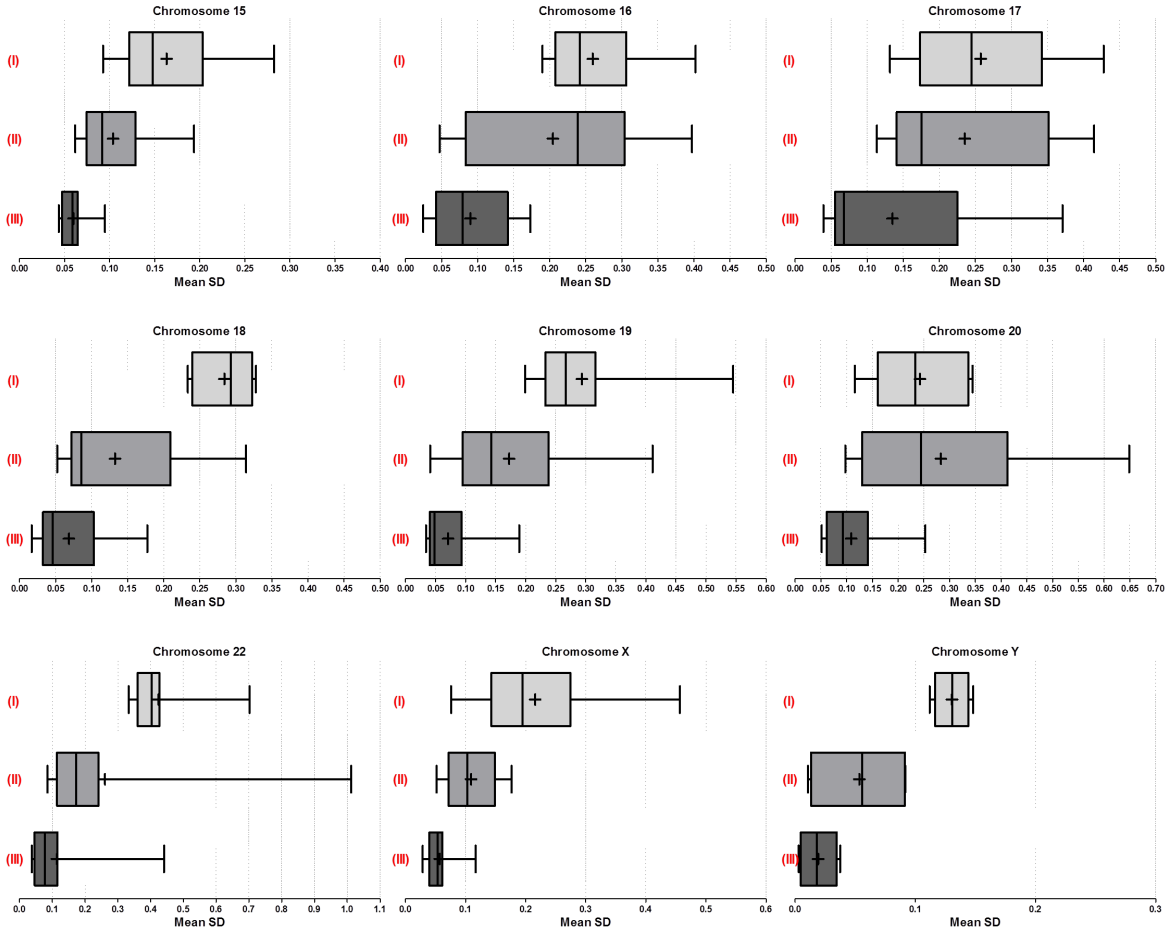


Figure A.4: Box and whisker plots depicting the SD of $2^{-\Delta Ctassay}$ values before and after each of the normalisation steps of chromosomes 15 - 20, X and Y. Graphs illustrate mean SDs of $2^{-\Delta Ctassay}$ values which were calculated from the nine control samples processed in Phase 1 (5x 46,XX; 4x 46,XY). Vertical lines in the middle of boxes depict median SDs. + signs indicate mean SDs. Error bars show smallest and largest SD value. **I:** Mean SDs prior to normalisation. **II:** Mean SDs after first normalisation (multiplication by assay-specific multiplication factor). **III:** Mean SDs after second normalisation (outlier correction).

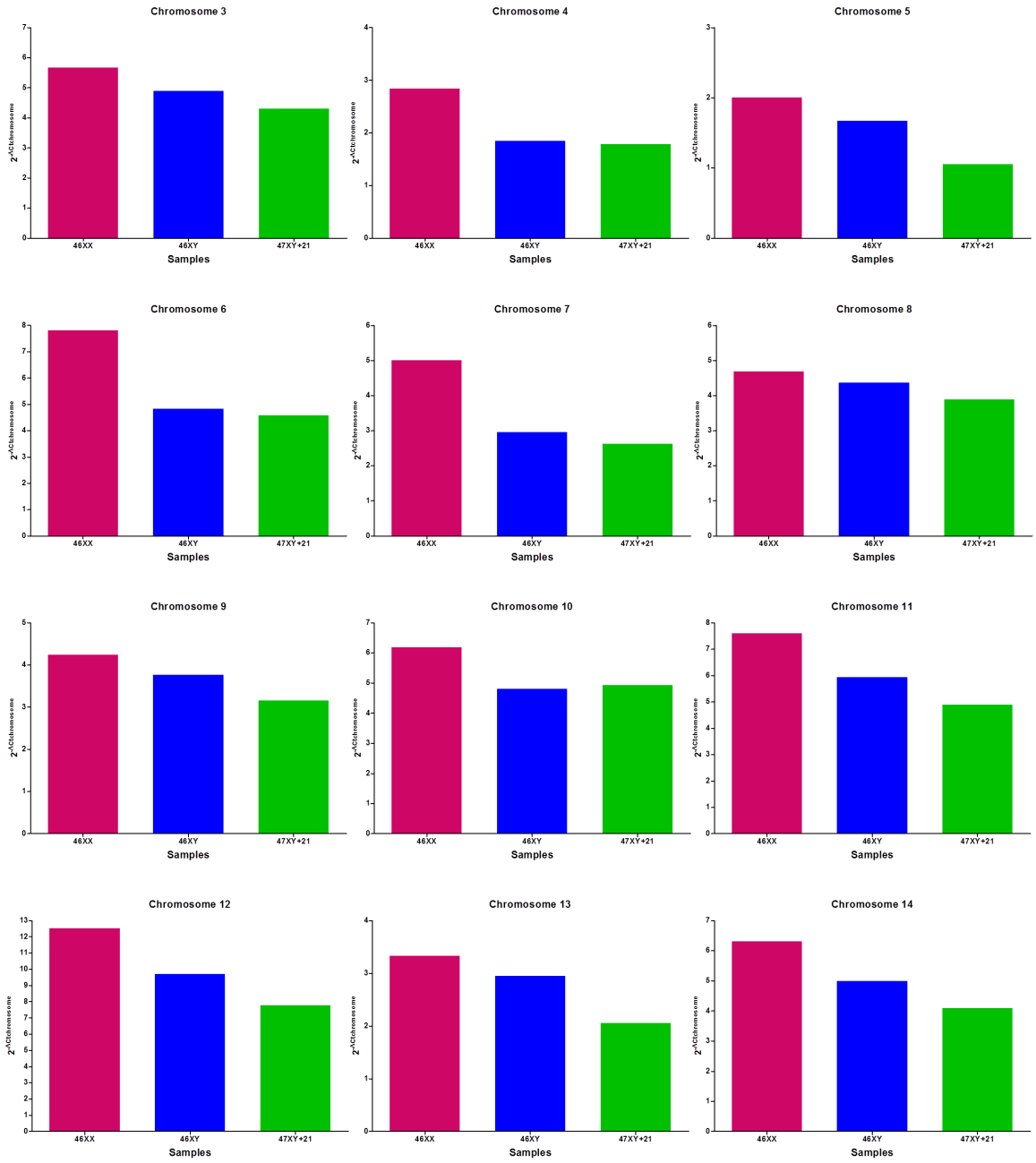


Figure A.5: Chromosome-specific $2^{-\Delta Ctchromosome}$ values of chromosomes 3 - 14 obtained from three different samples (46,XX; 46,XY; 47,XY,+21)

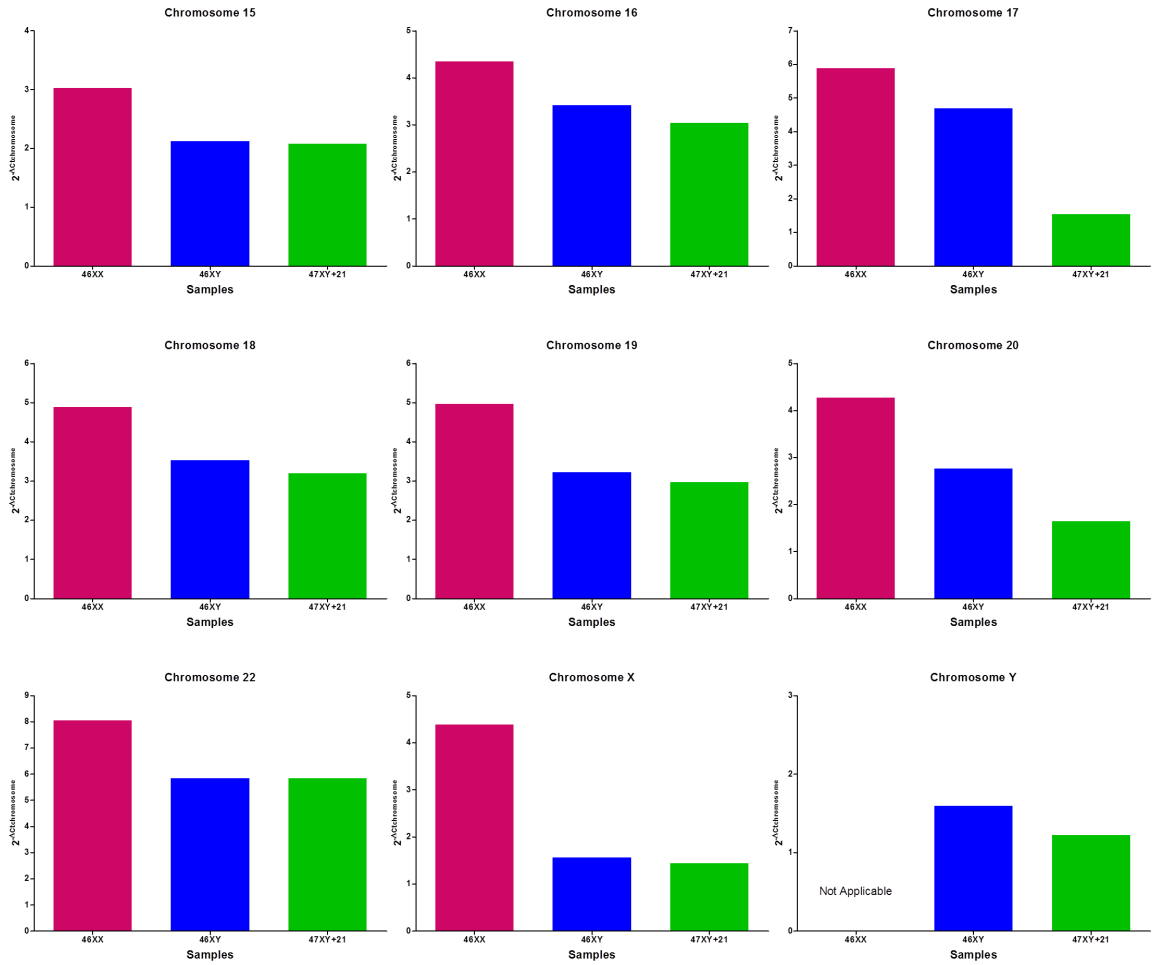


Figure A.6: Chromosome-specific $2^{-\Delta Ctchromosome}$ values of chromosomes 15 - 20, 22, X and Y obtained from three different samples (46,XX; 46,XY; 47,XY,+21)

Table A.3: Calculation of sensitivity and specificity of results obtained from samples processed during Phase 1

Sample diagnosis		**Chromosome diagnosis**	
Samples	14	Chromosomes	336
True-negatives	9	True-negatives	331
True-positives	5	True-positives	5
False-negatives	0	False-negatives	0
False-positives	0	False-positives	0
Sensitivity	100 %(47.82 % - 100 %)	**Sensitivity**	100 %(47.82 % - 100 %)
Specificity	100 %(66.37 % - 100 %)	**Specificity**	100 %(98.89 % - 100 %)

Values in brackets show 95 % CIs.

Table A.4: Copy number assays and reference assays utilised during Phase 2 of protocol development

Chromosome	Assay ID	ThermoFisher catalogue ID	Cytoband position
13	13.1	Hs03846573_cn	13q14.2
	13.2	Hs03189778_cn	13q14.3
	13.3	Hs02596417_cn	13q22.1
	13.4	Hs00854748_cn	13q22.3
	13.5	Hs03861872_cn	13q31.3
	13.6	Hs00614394_cn	13q32.1
	13.7	Hs00216560_cn	13q34
	13.8	Hs00201890_cn	13q34
16	16.1	Hs01103036_cn	16p12.3
	16.2	Hs05431908_cn	16p13.3
	16.3	Hs01480069_cn	16p13.3
	16.4	Hs03055169_cn	16p13.3
	16.5	Hs05466164_cn	16q11.2
	16.6	Hs07226330_cn	16q12.1
	16.7	Hs00150593_cn	16q21
	16.8	Hs03934353_cn	16q24.1
18	18.1	Hs03031102_cn	18p11.21
	18.2	Hs02106900_cn	18p11.31
	18.3	Hs00488766_cn	18p11.32
	18.4	Hs06507696_cn	18q21.33
	18.5	Hs01500302_cn	18q21.33
	18.6	Hs01245024_cn	18q22.3
	18.7	Hs01306949_cn	18q23
	18.8	Hs06498356_cn	18q23
21	21.1	Hs00227140_cn	21q22.13
	21.2	Hs00549243_cn	21q22.13
	21.3	Hs02062007_cn	21q22.13
	21.4	Hs02363779_cn	21q22.2
	21.5	Hs01167169_cn	21q22.3
	21.6	Hs04068763_cn	21q22.3
	21.7	Hs02427310_cn	21q22.3
	21.8	Hs04498861_cn	21q22.3
22	22.1	Hs01179019_cn	22q13.1
	22.2	Hs01010485_cn	22q13.1
	22.3	Hs01941283_cn	22q13.31
	22.4	Hs07226293_cn	22q13.31
	22.5	Hs07226295_cn	22q13.31
	22.6	Hs02065601_cn	22q13.31

	22.7	Hs02311370_cn	22q13.31
	22.8	Hs05561659_cn	22q13.33
X	X.1	Hs02913910_cn	Xp22.13
	X.2	Hs02363770_cn	Xp22.2
	X.3	Hs03194350_cn	Xp22.2
	X.4	Hs00982082_cn	Xp22.2
	X.5	Hs01936821_cn	Xq26.3
	X.6	Hs01196599_cn	Xq26.3
	X.7	Hs02022459_cn	Xq27.3
	X.8	Hs02497197_cn	Xq28
Y	Y.1	Hs07226066_cn	Yp11.2
	Y.2	Hs01075564_cn	Yq11.21
	Y.3	Hs01090783_cn	Yp11.31
	Y.4	Hs01026408_cn	Yp11.31
	Y.5	Hs01079454_cn	Yq11.221
	Y.6	Hs05704387_cn	Yq11.221
5	Reference	TERT	5p15.33
14	Reference	RNase P	14q11.2

Assays shaded in grey are newly added assays.

Table A.5: Calculation of sensitivity and specificity of results obtained from samples processed during Phase 2

Sample diagnosis		**Chromosome diagnosis**	
Samples	22	Chromosomes	154
True-negatives	4	True-negatives	128
True-positives	16[a]	True-positives	18[a]
False-negatives	1	False-negatives	3
False-positives	1	False-positives	5
Sensitivity	94.12 %(71.31 % - 99.85 %)	**Sensitivity**	85.71 %(63.66 % - 96.95 %)
Specificity	80.00 %(28.36 % - 99.49 %)	**Specificity**	96.24 %(91.44 % - 98.77 %)

a = trisomy X detected in the sample derived from the 46,XX,+Xq cell line (sample 11) was considered true-positive. 95 % CIs are shown in brackets.

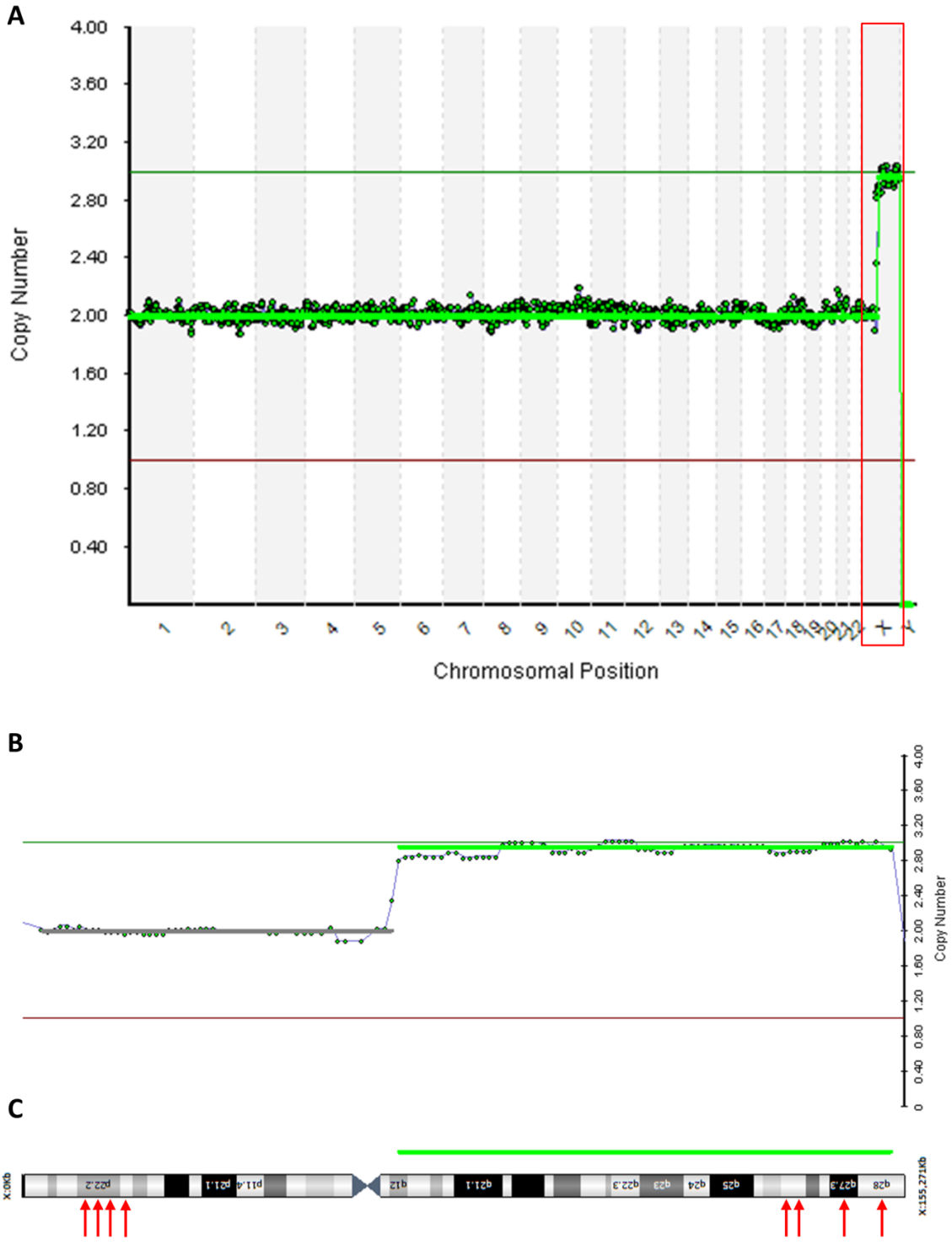


Figure A.7: VeriSeq-NGS result obtained from the 46,XX,+Xq cell line. The tested sample consisted of three cells. **A: 24-CCN profile.** The red rectangle frames the chromosome affected by the structural abnormality **B/C: Chromosome X.** Green lines indicate duplicated chromosome region. Arrows show approximate location of the copy number assays.

Table A.6: Calculation of sensitivity and specificity of results obtained from three- and five-cell samples processed during Phase 3 (~25 µl pre-amplification volume)

Sample diagnosis		Chromosome diagnosis	
Samples	46	Chromosomes	322
True-negatives	13[a]	True-negatives	278[a]
True-positives	31[b]	True-positives	36[b]
False-negatives	2	False-negatives	5
False-positives	0	False-positives	3
Sensitivity	93.94 %(79.77 % - 99.26 %)	**Sensitivity**	87.80 %(73.80 % - 95.92 %)
Specificity	100.00 %(75.29 % - 100.00 %)	**Specificity**	98.93 %(96.91 % - 99.78 %)

a = presence of two copies of chromosome X detected in samples derived from the 46,XX,+Xq cell line (samples 23, 24 and 26) was considered true-negative. b = trisomy X detected in the sample derived from the 46,XX,+Xq cell line (sample 11) was considered true-positive. 95 % CIs are shown in brackets.

Table A.7: Calculation of sensitivity and specificity of results obtained from three- and five-cell samples processed during Phase 3 (~15 µl pre-amplification volume)

Sample diagnosis		Chromosome diagnosis	
Samples	45	Chromosomes	315
True-negatives	13[a]	True-negatives	275[a]
True-positives	32	True-positives	39
False-negatives	0	False-negatives	1
False-positives	0	False-positives	0
Sensitivity	100 %(89.11 % - 100.00 %)	**Sensitivity**	97.50 %(86.84 % - 99.94 %)
Specificity	100 %(75.29 % - 100.00 %)	**Specificity**	100 %(98.67 % - 100.00 %)

a = presence of two copies of chromosome X detected in samples derived from the 46,XX,+Xq cell line (samples 23, 24, 25 and 26) was considered true-negative. 95 % CIs are shown in brackets.

Table A.8: Calculation of sensitivity and specificity of results obtained from single-cell samples processed during Phase 3 (~15 µl pre-amplification volume)

Sample diagnosis		Chromosome diagnosis	
Samples	44	Chromosomes	308
True-negatives	8[a]	True-negatives	248
True-positives	27	True-positives	25
False-negatives	6	False-negatives	14
False-positives	3	False-positives	21
Sensitivity	81.82 %(64.54 % - 93.02 %)	**Sensitivity**	46.10 %(47.18 % - 78.80 %)
Specificity	72.73 %(39.03 % - 93.98 %)	**Specificity**	92.19 %(88.31 % - 95.10 %)

a = presence of two copies of chromosome X detected in samples derived from the 46,XX,+Xq cell line (samples 25 and 26) was considered true-negative. 95 % CIs are shown in brackets.

Table A.9: Copy number and reference assays as well as assays targeting the DiGeorge microdeletion region and the mitochondrial genome utilised during Phase 4 of protocol development

Chromosome	Assay ID	ThermoFisher catalogue ID	Cytoband position
1	1.1	Hs03194153_cn	1p34.1
	1.2	Hs03202460_cn	1p34.3
	1.3	Hs03193256_cn	1p35.3
	1.4	Hs00876448_cn	1p36.13
	1.5	Hs02024837_cn	1q32.1
	1.6	Hs01236436_cn	1q32.1
	1.7	Hs05802141_cn	1q32.2
	1.8	Hs01632078_cn	1q41
	1.9	Hs07226270_cn	1q42.2
2	2.1	Hs03101837_cn	2p16.1
	2.2	Hs04692736_cn	2p23.3
	2.3	Hs03216031_cn	2p24.3
	2.4	Hs04658573_cn	2p25.1
	2.5	Hs04716535_cn	2q24.3
	2.6	Hs02649413_cn	2q24.3
	2.7	Hs04676864_cn	2q24.3
	2.8	Hs01702970_cn	2q31.1
	2.9	Hs03212850_cn	2q32.3
3	3.1	Hs01101888_cn	3p24.2
	3.2	Hs01278165_cn	3p24.2
	3.3	Hs03105052_cn	3p26.1
	3.4	Hs03483197_cn	3p26.1
	3.5	Hs03104058_cn	3p26.1
	3.6	Hs03491014_cn	3q23
	3.7	Hs02815441_cn	3q25.33
	3.8	Hs03226374_cn	3q26.1
	3.9	Hs03102717_cn	3q26.1
4	4.1	Hs03511242_cn	4p11
	4.2	Hs05959876_cn	4p12
	4.3	Hs05953180_cn	4p12
	4.4	Hs05920128_cn	4p14
	4.5	Hs03107722_cn	4p15.33
	4.6	Hs02919098_cn	4q25
	4.7	Hs02075730_cn	4q26
	4.8	Hs06709994_cn	4q26
	4.9	Hs01271024_cn	4q31.21
5	5.1	Hs03549103_cn	5p14.1

	5.2	Hs06126037_cn	5p15.2
	5.3	Hs03109322_cn	5p15.2
	5.4	Hs03089433_cn	5p15.2
	5.5	Hs01044784_cn	5p15.31
	5.6	Hs02178036_cn	5p15.31
	5.7	Hs06063082_cn	5q23.2
	5.8	Hs06001079_cn	5q34
	5.9	Hs06047048_cn	5q35.1
6	6.1	Hs03186028_cn	6p22.1
	6.2	Hs03113069_cn	6q22.1
	6.3	Hs03189620_cn	6p22.2
	6.4	Hs01867208_cn	6p23
	6.5	Hs04902228_cn	6p24.1
	6.6	Hs02988007_cn	6p25.2
	6.7	Hs06798399_cn	6q21
	6.8	Hs03089640_cn	6q22.1
	6.9	Hs02761573_cn	6q22.32
7	7.1	Hs00831737_cn	7p21.1
	7.2	Hs01403568_cn	7p21.1
	7.3	Hs04339214_cn	7p21.3
	7.4	Hs02418225_cn	7p22.1
	7.5	Hs04929461_cn	7q33
	7.6	Hs03113881_cn	7q34
	7.7	Hs03114237_cn	7q34
	7.8	Hs03190951_cn	7q34
	7.9	Hs03179906_cn	7q34
8	8.1	Hs00275884_cn	8p12
	8.2	Hs05034100_cn	8p12
	8.3	Hs06163596_cn	8p23.1
	8.4	Hs02990824_cn	8q22.3
	8.5	Hs00703715_cn	8q23.1
	8.6	Hs00267820_cn	8q23.1
	8.7	Hs02380680_cn	8q24.12
	8.8	Hs00310789_cn	8q24.22
	8.9	Hs01241456_cn	8q24.22
9	9.1	Hs01138416_cn	9p13.2
	9.2	Hs01695071_cn	9p21.1
	9.3	Hs00956247_cn	9p21.1
	9.4	Hs00116749_cn	9p24.3
	9.5	Hs02824874_cn	9q33.2
	9.6	Hs03092434_cn	9q33.3

	9.7	Hs03092506_cn	9q33.3
	9.8	Hs06870576_cn	9q33.3
	9.9	Hs01254139_cn	9q34.3
10	10.1	Hs01210989_cn	10p13
	10.2	Hs05189556_cn	10p15.1
	10.3	Hs03118264_cn	10p15.3
	10.4	Hs03118674_cn	10p15.3
	10.5	Hs03188250_cn	10q26.11
	10.6	Hs03189241_cn	10q26.11
	10.7	Hs01430576_cn	10q26.11
	10.8	Hs07226389_cn	10q26.2
	10.9	Hs07226388_cn	10q26.2
11	11.1	Hs03120100_cn	11p14.1
	11.2	Hs03119349_cn	11p14.1
	11.3	Hs03191801_cn	11p15.1
	11.4	Hs01423651_cn	11p15.4
	11.5	Hs01644358_cn	11p15.4
	11.6	Hs01831183_cn	11q12.3
	11.7	Hs03175547_cn	11q13.4
	11.8	Hs03093481_cn	11q21
	11.9	Hs03194732_cn	11q23.1
12	12.1	Hs02714210_cn	12p13.1
	12.2	Hs00526909_cn	12p13.31
	12.3	Hs02900406_cn	12p13.31
	12.4	Hs01557728_cn	12p13.31
	12.5	Hs01238607_cn	12q22
	12.6	Hs03814263_cn	12q23.2
	12.7	Hs02324507_cn	12q23.3
	12.8	Hs00213327_cn	12q24.33
	12.9	Hs01436960_cn	12q24.33
13	13.1	Hs03189778_cn	13q14.3
	13.2	Hs03186896_cn	13q14.3
	13.3	Hs03122095_cn	13q21.31
	13.4	Hs02596417_cn	13q22.1
	13.5	Hs00854748_cn	13q22.3
	13.6	Hs00275387_cn	13q22.3
	13.7	Hs00614394_cn	13q32.1
	13.8	Hs00201890_cn	13q34
	13.9	Hs00216560_cn	13q34
14	14.1	Hs01881327_cn	14q24.1
	14.2	Hs02603629_cn	14q24.2

	14.3	Hs03308301_cn	14q31.3
	14.4	Hs02295635_cn	14q32.12
	14.5	Hs02294553_cn	14q32.12
	14.6	Hs02968347_cn	14q32.12
	14.7	Hs02269694_cn	14q32.32
	14.8	Hs02330595_cn	14q32.33
	14.9	Hs02277899_cn	14q32.33
15	15.1	Hs01733445_cn	15q25.2
	15.2	Hs03095367_cn	15q25.2
	15.3	Hs03908909_cn	15q26.1
	15.4	Hs05376025_cn	15q26.1
	15.5	Hs05388427_cn	15q26.1
	15.6	Hs05389092_cn	15q26.1
	15.7	Hs05351793_cn	15q26.1
	15.8	Hs03309316_cn	15q26.2
	15.9	Hs02820990_cn	15q26.3
16	16.1	Hs01103036_cn	16p12.3
	16.2	Hs02696945_cn	16p12.3
	16.3	Hs05431908_cn	16p13.3
	16.4	Hs01480069_cn	16p13.3
	16.5	Hs03055169_cn	16p13.3
	16.6	Hs05466164_cn	16q11.2
	16.7	Hs07226330_cn	16q12.1
	16.8	Hs03095894_cn	16q12.2
	16.9	Hs03934353_cn	16q24.1
17	17.1	Hs05474432_cn	17p11.2
	17.2	Hs02280963_cn	17p11.2
	17.3	Hs01959936_cn	17p13.1
	17.4	Hs02194326_cn	17p13.1
	17.5	Hs07226326_cn	17q21.31
	17.6	Hs02862328_cn	17q21.31
	17.7	Hs05512629_cn	17q21.33
	17.8	Hs03192947_cn	17q23.2
	17.9	Hs03184552_cn	17q25.1
18	18.1	Hs06449787_cn	18p11.21
	18.2	Hs00896329_cn	18p11.31
	18.3	Hs02106900_cn	18p11.31
	18.4	Hs00488766_cn	18p11.32
	18.5	Hs03316816_cn	18q22.1
	18.6	Hs03096572_cn	18q23
	18.7	Hs03096428_cn	18q23

	18.8	Hs01306949_cn	18q23
	18.9	Hs06498356_cn	18q23
19	19.1	Hs01486267_cn	19p13.3
	19.2	Hs02117964_cn	19p13.3
	19.3	Hs01413810_cn	19p13.3
	19.4	Hs01339946_cn	19p13.3
	19.5	Hs00566496_cn	19q13.43
	19.6	Hs03181229_cn	19q13.43
	19.7	Hs03187222_cn	19q13.43
	19.8	Hs04025450_cn	19q13.43
	19.9	Hs02995438_cn	19q13.43
20	20.1	Hs03096853_cn	20p12.1
	20.2	Hs03126884_cn	20p12.1
	20.3	Hs07203821_cn	20p12.1
	20.4	Hs00358577_cn	20p12.2
	20.5	Hs04053409_cn	20q13.12
	20.6	Hs07167770_cn	20q13.12
	20.7	Hs03096918_cn	20q13.13
	20.8	Hs03096945_cn	20q13.13
	20.9	Hs00624199_cn	20q13.13
21	21.1	Hs05536051_cn	21q22.11
	21.2	Hs00227140_cn	21q22.13
	21.3	Hs00549243_cn	21q22.13
	21.4	Hs02062007_cn	21q22.13
	21.5	Hs02363779_cn	21q22.2
	21.6	Hs01679653_cn	21q22.3
	21.7	Hs01167169_cn	21q22.3
	21.8	Hs04068763_cn	21q22.3
	21.9	Hs04498861_cn	21q22.3
22	22.1	Hs00826443_cn	22q12.3
	22.2	Hs01112466_cn	22q12.3
	22.3	Hs01179019_cn	22q13.1
	22.4	Hs01010485_cn	22q13.1
	22.5	Hs07226294_cn	22q13.31
	22.6	Hs02311370_cn	22q13.31
	22.7	Hs05561659_cn	22q13.33
	22.8	Hs01941283_cn	22q13.31
	22.9	Hs02065601_cn	22q13.31
X	X.1	Hs03174390_cn	Xp22.33
	X.2	Hs03194350_cn	Xp22.2
	X.3	Hs00982082_cn	Xp22.2

	X.4	Hs02363770_cn	Xp22.2
	X.5	Hs02990337_cn	Xq26.3
	X.6	Hs01936821_cn	Xq26.3
	X.7	Hs01196599_cn	Xq26.3
	X.8	Hs02022459_cn	Xq27.3
	X.9	Hs02497197_cn	Xq28
Y	Y.1	Hs07226066_cn	Yp11.2
	Y.2	Hs01090783_cn	Yp11.31
	Y.3	Hs01075303_cn	Yp11.2
	Y.4	Hs01026488_cn	Yp11.2
	Y.5	Hs01026408_cn	Yp11.31
	Y.6	Hs01075564_cn	Yq11.21
	Y.7	Hs01079454_cn	Yq11.221
	Y.8	Hs05704387_cn	Yq11.221
	Y.9	Hs02560117_cn	Yq11.221
DiGeorge region (22q11)	DGR.1	Hs02374030_cn	22q11.21
	DGR.2	Hs00278664_cn	22q11.21
	DGR.3	Hs01313390_cn	22q11.21
mtDNA	M.1	Hs02596862_g1	NA[a]
	M.2	Hs02596874_g1	NA[b]
	M.3	Hs02596867_s1	NA[c]
5	Reference	TERT	5p15.33
14	Reference	RNase P	14q11.2

Assays shaded in grey are newly added assays. NA = not applicable. a = target sequence located in the MT-ATP6 gene. b = target sequence located in MT-ND2 gene (mitochondrially encoded NADH:ubiquinone oxidoreductase core subunit 2). c = target sequence located in MT-CYB gene (mitochondrially encoded cytochrome b).

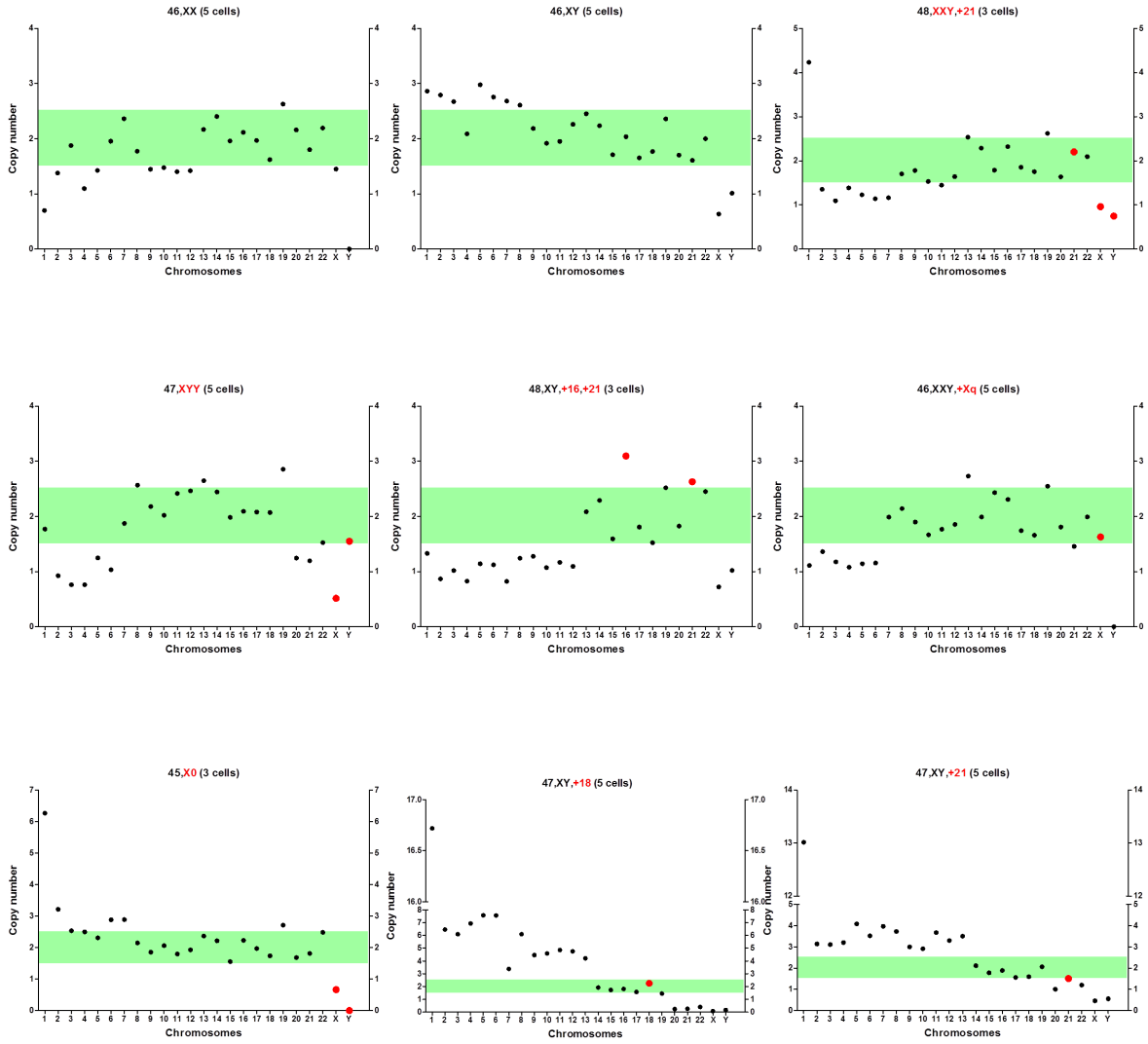


Figure A.8: Examples of real-time qPCR 24-CCN profiles obtained from samples processed during Phase 4 of protocol development. Areas shaded in green indicate CCN of two (ranging from copy number 1.5 - 2.5). Copy number of euploid chromosomes is shown by black dots. Expected aneuploid chromosomes are illustrated by red dots.

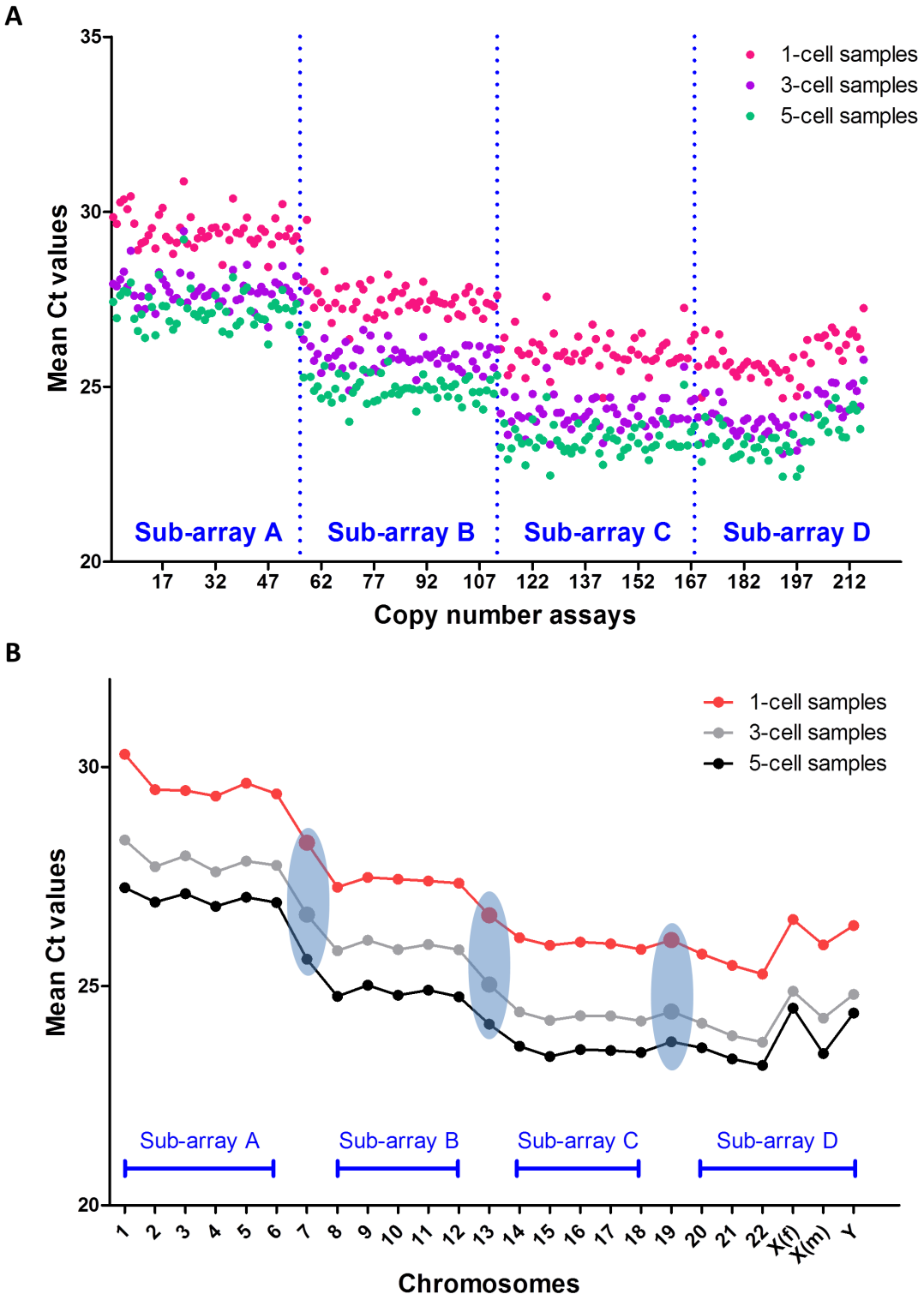


Figure A.9: Distribution of mean Ct values obtained from all samples processed during Phase 4 of protocol development. Results from 24 single-, 24 three- and 24 five-cell samples are shown in pink, purple and green, respectively. **A: Distribution of obtained mean Ct values across sub-arrays A - D.** Each dot represents the mean Ct value of a single assay (total: 216) **B: Distribution of mean chromosome Ct values across sub-arrays A - D.** Ct values of chromosomes targeted by assays located on two different sub-arrays are indicated by blue ovals. Dots represent mean Ct values obtained for each chromosome. X(f) and X(m) refer to chromosome X mean Ct values in female and male samples, respectively.

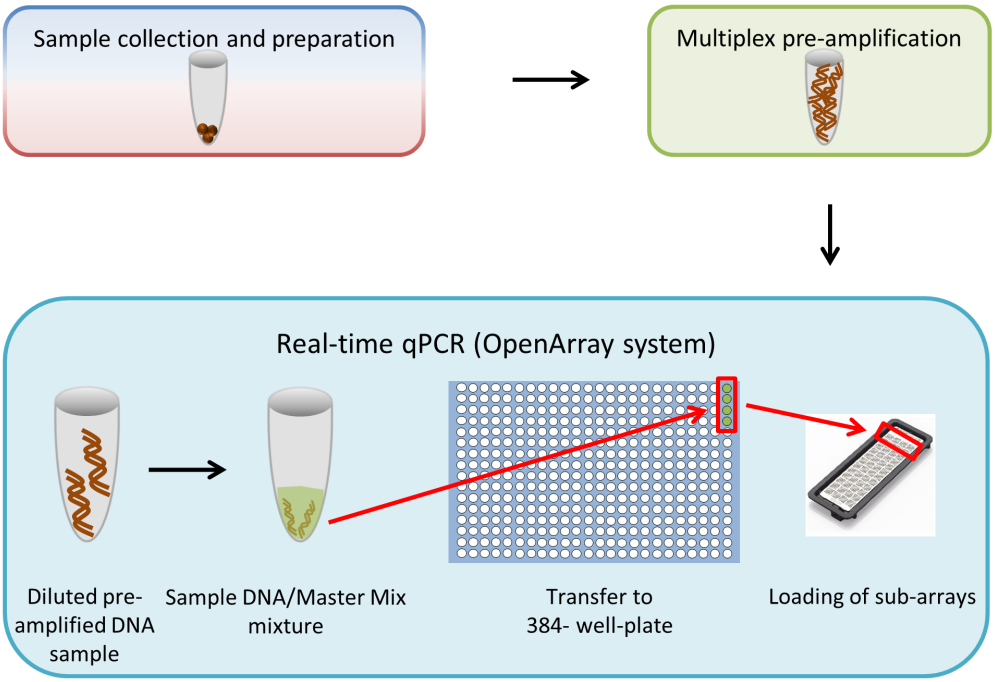


Figure A.10: Flowchart describing sample processing following multiplex pre-amplification. Following sample dilution, amplification products were combined with Master Mix. The mixture was then transferred to a 384-well plate and equally distributed between four wells. Sample mixtures were then loaded into four array sub-arrays using a robotic loading system.

Table A.10: Additional assays targeting the DiGeorge microdeletion region spotted on arrays utilised during Phase 5 of protocol development

Chromosome	Assay ID	ThermoFisher catalogue ID	Cytoband position
DiGeorge region (22q11)	DGR.4	HS01290445_CN	22q11.21
	DGR.5	HS02179842_CN	22q11.21
	DGR.6	Hs01044064_CN	22q11.21
	DGR.7	Hs05574495_CN	22q11.22

Additional assays replaced the reference assays TERT and RNase P as well as assays Hs01936821_cn and Hs01026488_cn from the previous array design outlined in **Table A.9**.

Table A.11: Calculation of sensitivity and specificity of results obtained from three- and five-cell samples processed during Phase 5

Sample diagnosis		Chromosome diagnosis	
Samples	111	Chromosomes	2664
True-negatives	47[a]	True-negatives	2581[a]
True-positives	63[b]	True-positives	79[b]
False-negatives	0	False-negatives	1
False-positives	1	False-positives	3
Sensitivity	100.00 %(94.31 % - 100.00 %)	**Sensitivity**	98.75 %(93.23 % - 99.97 %)
Specificity	97.92 %(88.93 % - 99.95 %)	**Specificity**	99.88 %(99.66 % - 99.98 %)

a = presence of two copies of chromosomes 20 & 22, 5, 22 and 10 detected in samples derived from the 46,XY,+20p,-22q11, 46,XX,-5p, 46,XX,-22q11 and 46,XY,-10p cell lines (samples 88 - 93, 97, 99 - 104 and 105 - 108), respectively, were considered true-negative. b = trisomy X and trisomy 20 as well as monosomy 5 and monosomy 13 detected in the samples derived from the 46,XX,+Xq and 46,XY,+20p,-22q11 as well as 46,XX,-5p and 46,XX,-13p cell lines (samples 84 - 86, 87 & 94 as well as 95 - 96 & 98 and 109 - 114), respectively, were considered true-positive. 95 % CIs are shown in brackets.

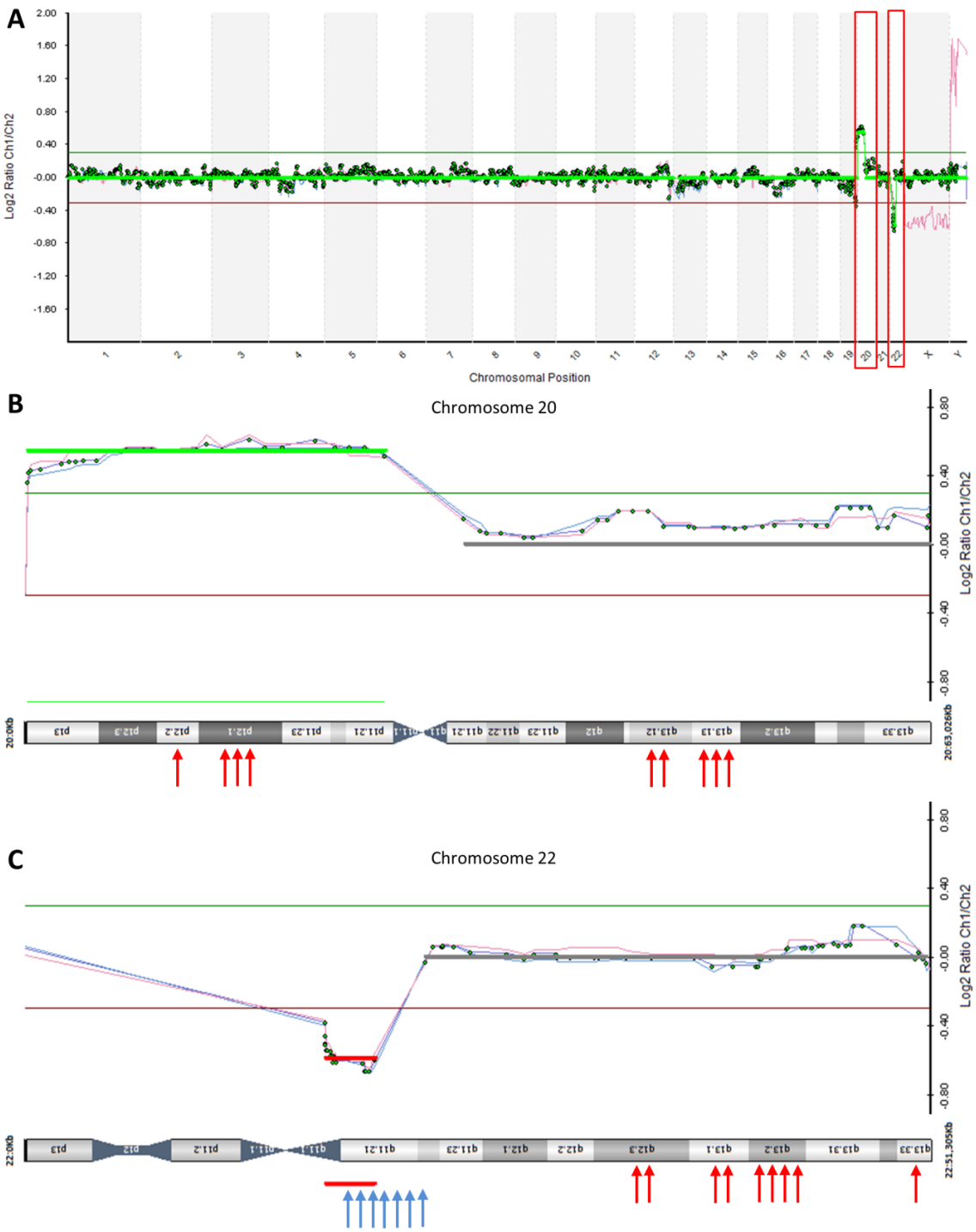


Figure A.11: Array CGH result obtained from the 46,XY,+20p,-22q11 cell line. The tested sample consisted of three cells. **A: 24-CCN profile.** The red rectangles frame the chromosomes involved in the chromosome rearrangement. **B: Chromosome 20.** Green lines indicate duplicated chromosome region. **C: Chromosome 22.** Red lines indicate deleted chromosome region. Red and blue arrows show approximate location of the copy number assays utilised for CCN assessment and assays targeting the DiGeorge microdeletion region, respectively.

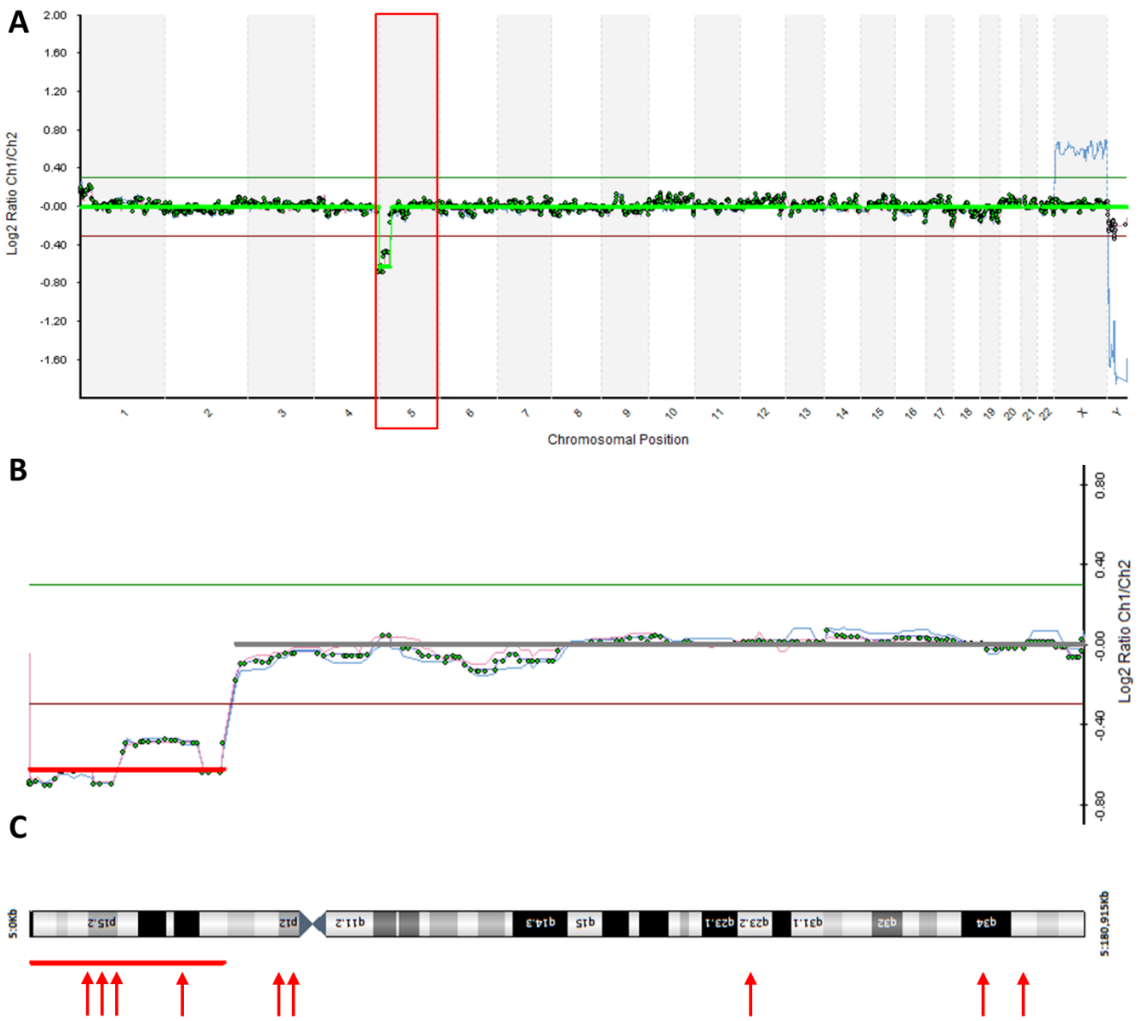


Figure A.12: Array CGH result obtained from the 46,XX,-5p cell line. The tested sample consisted of three cells. **A: 24-CCN profile.** The red rectangle frames the chromosome affected by the structural abnormality. **B/C: Chromosome 5.** Red lines indicate deleted chromosome region. Arrows show approximate location of the copy number assays.

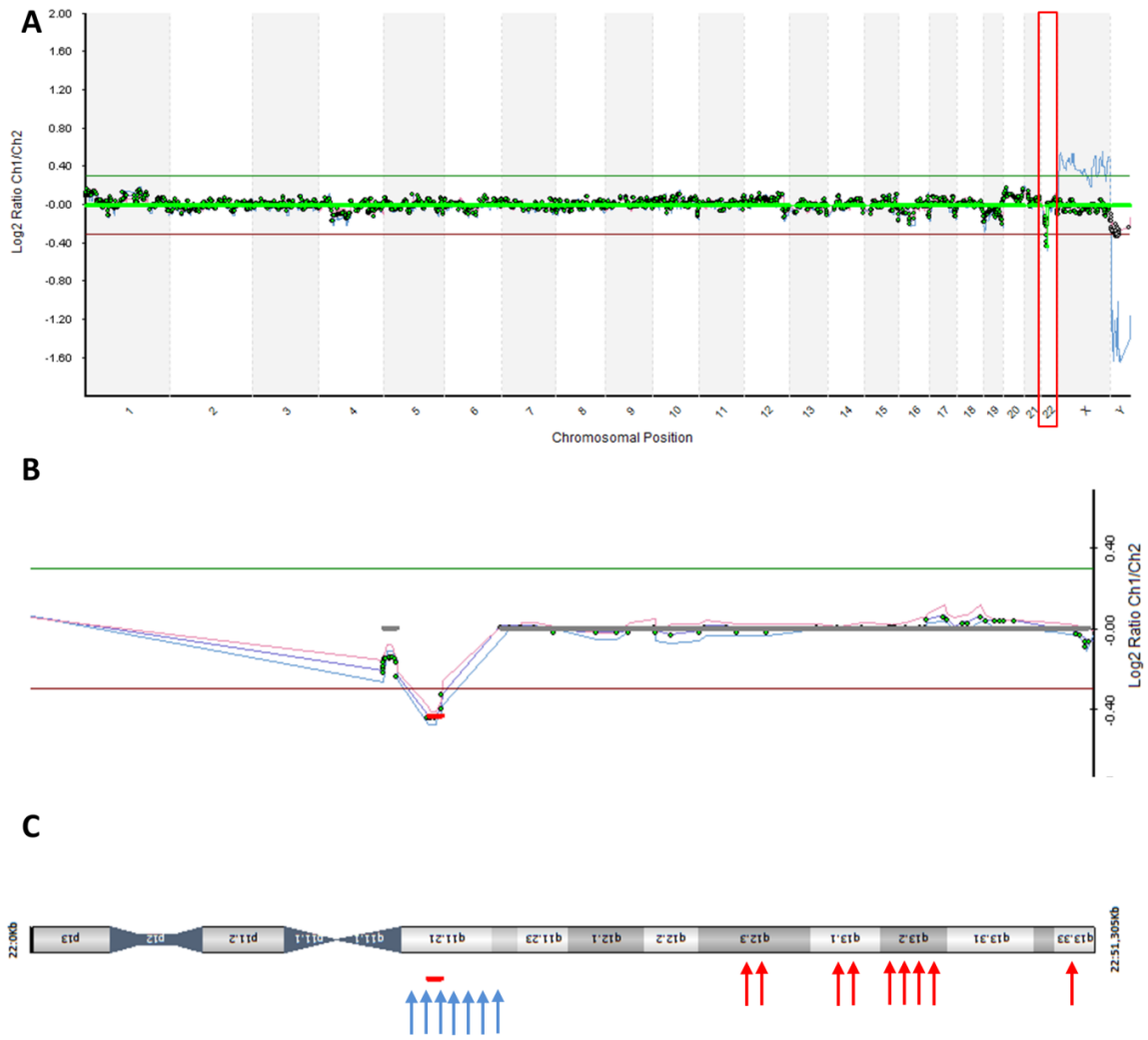


Figure A.13: Array CGH result obtained from the 46,XX,-22q11 cell line. The tested sample consisted of three cells. **A: 24-CCN profile.** The red rectangle frames chromosome 22, affected by the microdeletion. **B/C: Chromosome 22.** Red lines indicate affected chromosome region. Red and blue arrows show approximate location of the copy number assays utilised for CCN assessment and assays targeting the DiGeorge microdeletion region, respectively.

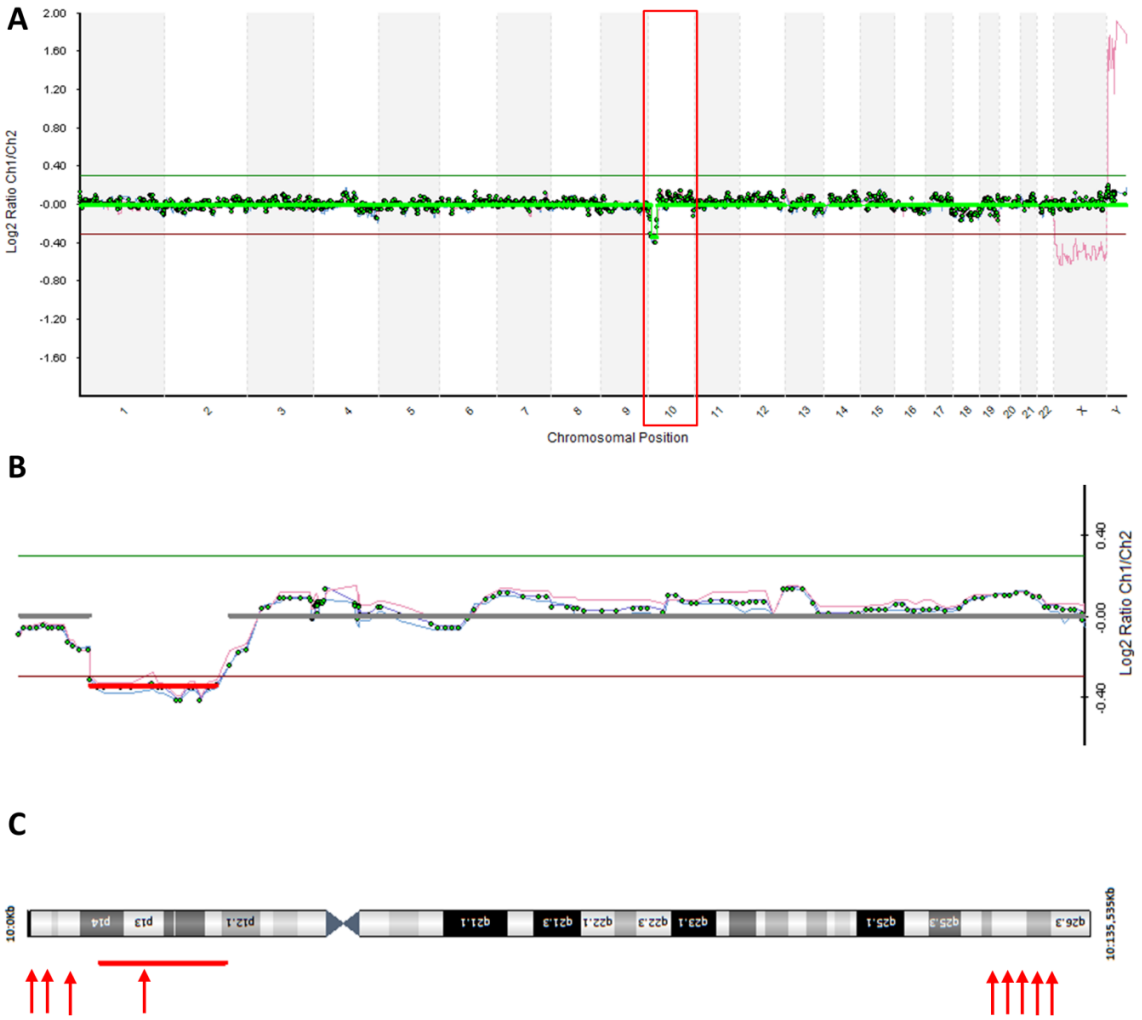


Figure A.14: Array CGH result obtained from the 46,XY,-10p cell line. The tested sample consisted of three cells. **A: 24-CCN profile.** The red rectangle frames the chromosome affected by the structural abnormality. **B/C: Chromosome 10.** Red lines indicate deleted chromosome region. Arrows show approximate location of the copy number assays.

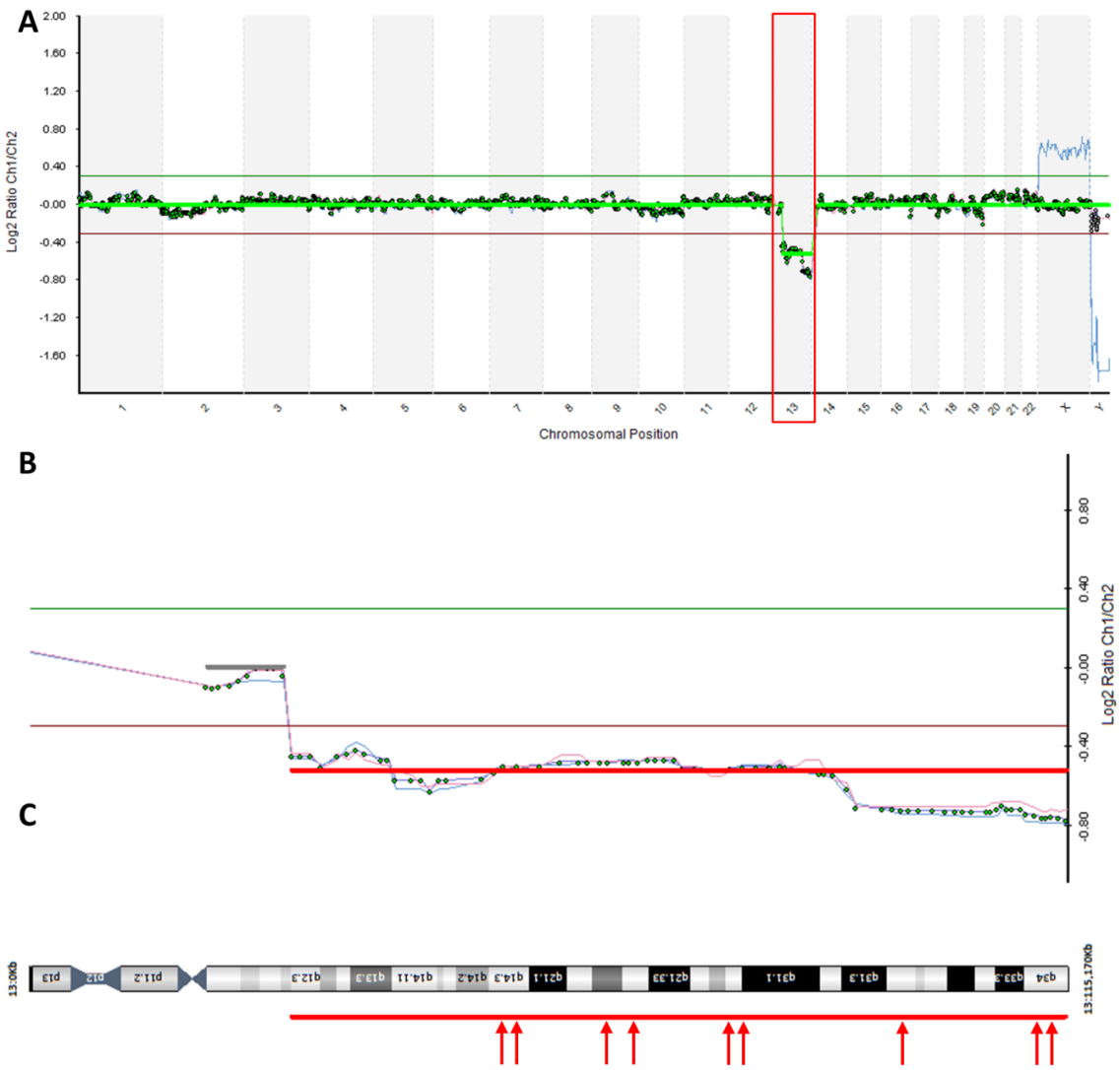


Figure A.15: Array CGH result obtained from the 46,XX,-13p cell line. The tested sample consisted of three cells. **A: 24-CCN profile.** The red rectangle frames the chromosome affected by the structural abnormality. **B/C: Chromosome 13.** Red lines indicate deleted chromosome region. Arrows show approximate location of the copy number assays.

Table A.12: Calculation of sensitivity and specificity of results obtained from frozen single-cell samples processed during Phase 5

Sample diagnosis		Chromosome diagnosis	
Samples	40	Chromosomes	960
True-negatives	10[a]	True-negatives	891[a]
True-positives	20	True-positives	23
False-negatives	0	False-negatives	1
False-positives	10	False-positives	45
Sensitivity	100.00 %(83.16 % - 100.00 %)	**Sensitivity**	95.83 %(78.88 % - 99.89 %)
Specificity	50.00 %(27.2 % - 72.8 %)	**Specificity**	95.19 %(93.62 % - 96.47 %)

a = presence of two copies of chromosomes X, 20 & 22, 5, 22 and 10 detected in samples derived from the 46,XX,+Xq, 46,XY,+20p,-22q11, 46,XX,-5p, 46,XX,-22q11 and 46,XY,-10p cell lines (samples 23 - 25, 28, 32 and 34 - 36), respectively, were considered true-negative. b = trisomy 20 as well as monosomy 5 and monosomy 13 detected in the samples derived from the 46,XY,+20p,-22q11 as well as the 46,XX,-5p and 46,XX,-13p cell lines (sample 26 as well as 29 - 31 and 37 - 41), respectively, were considered true-positive. 95 % CIs are shown in brackets.

Table A.13: Calculation of sensitivity and specificity of results obtained from trophectoderm biopsies processed during Phase 6

Sample diagnosis		Chromosome diagnosis	
Samples	30	Chromosomes	720
True-negatives	25	True-negatives	711[a]
True-positives	4[b]	True-positives	7[b]
False-negative	0	False-negative	0
False-positives	1	False-positives	2
Sensitivity	100.00 %(39.76 % - 100.00 %	**Sensitivity**	100.00 %(59.04 % - 100.00 %
Specificity	96.15 %(80.36 % - 99.90 %)	**Specificity**	99.72 %(98.99 % - 99.97 %)

a = real-time qPCR result of embryo 11 was considered to be in agreement with the NGS-VeriSeq result, because trisomy 21 was mosaic. b = monosomy of chromosome 12 detected in the biopsy of embryo 12 was considered true-positive. 95 % CIs are shown in brackets.

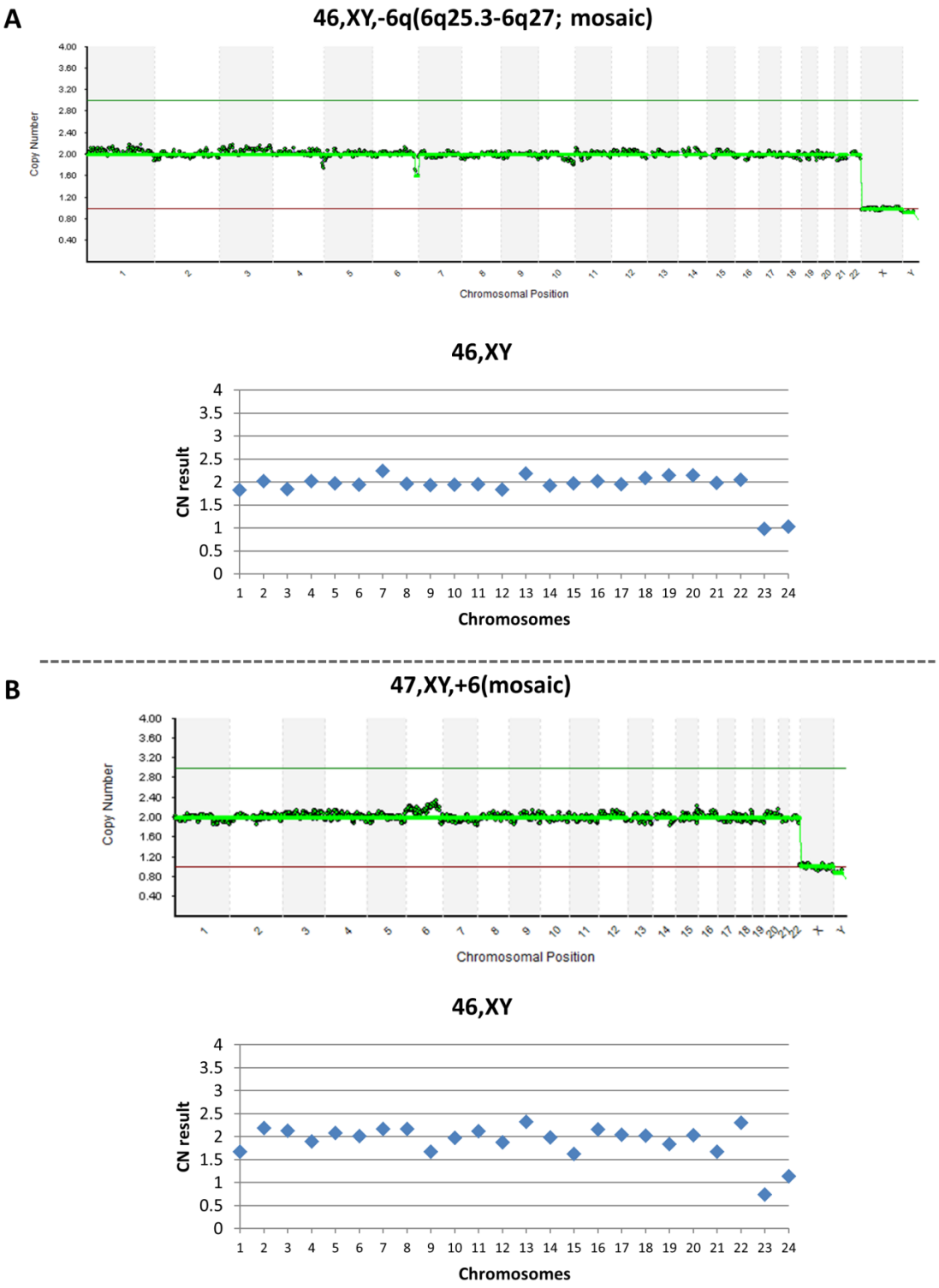


Figure A.16: Comparison of NGS and real-time qPCR 24-CCN profiles of entire embryos M.5 and M.6 and corresponding trophectoderm biopsies. NGS profiles were generated with Bluefuse (for plot descriptions refer to **CHAPTER 2**, **Section 2.5.2**). Real-time qPCR profiles were generated using the PERL programme (for plot descriptions refer to main text). **A: Sample M.5.** NGS identified a mosaic structural loss of chromosome 6 (entire embryo). The abnormality was not identified with real-time qPCR (biopsy). **B: Sample M.6.** NGS identified a mosaic gain of chromosome 6 (entire embryo). The abnormality was not identified with real-time qPCR (biopsy).

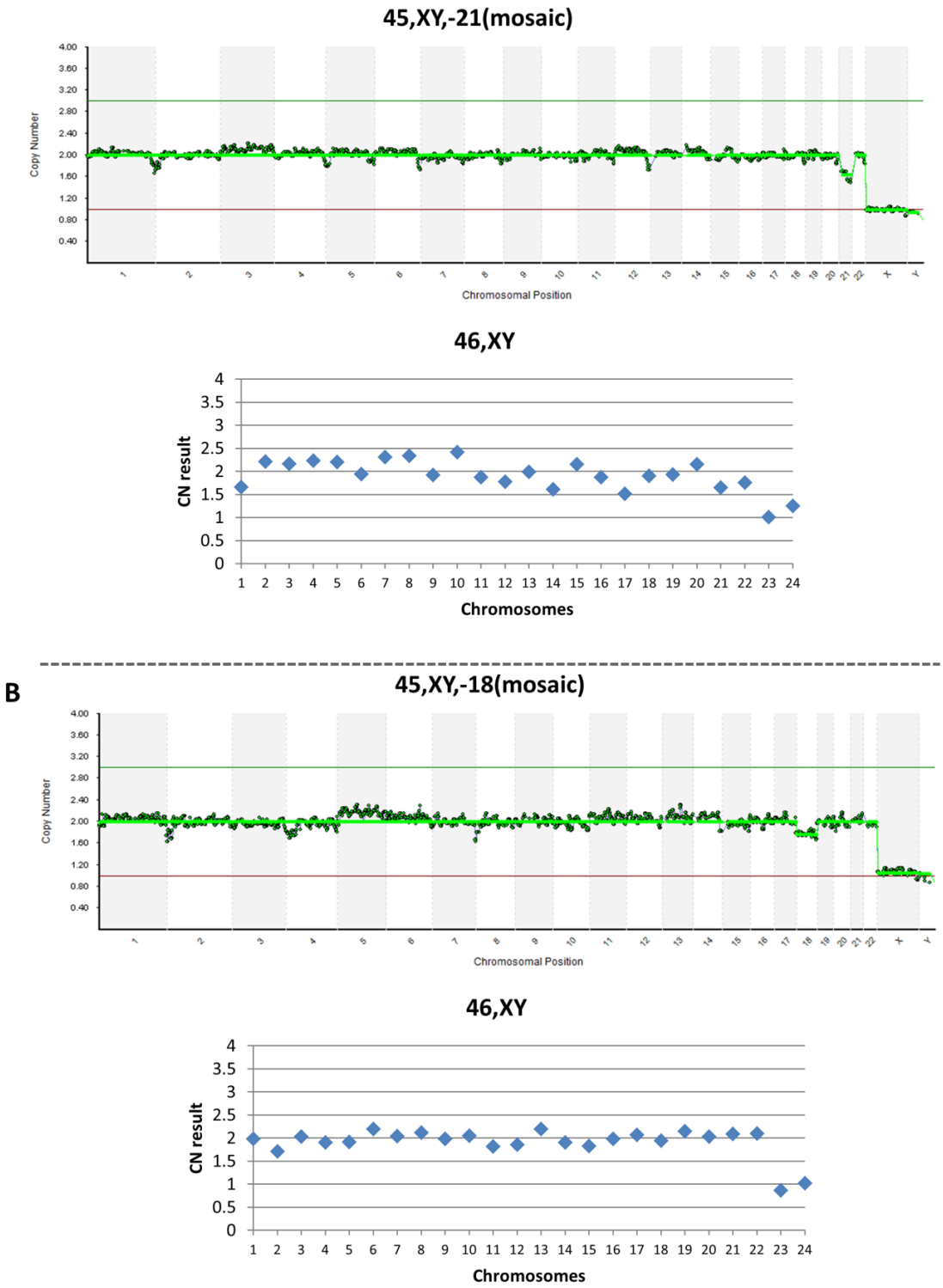


Figure A.17: Comparison of NGS and real-time qPCR 24-CCN profiles of entire embryos M.7 and M.8 and corresponding trophectoderm biopsies. NGS profiles were generated with Bluefuse (for plot descriptions refer to **CHAPTER 2, Section 2.5.2**). Real-time qPCR profiles were generated using the PERL programme (for plot descriptions refer to main text). **A: Sample M.7.** NGS identified a mosaic loss of chromosome 21 (entire embryo). The abnormality was not identified with real-time qPCR (biopsy). **B: Sample M.8.** NGS identified a mosaic loss of chromosome 18 (entire embryo). The abnormality was not identified with real-time qPCR (biopsy).

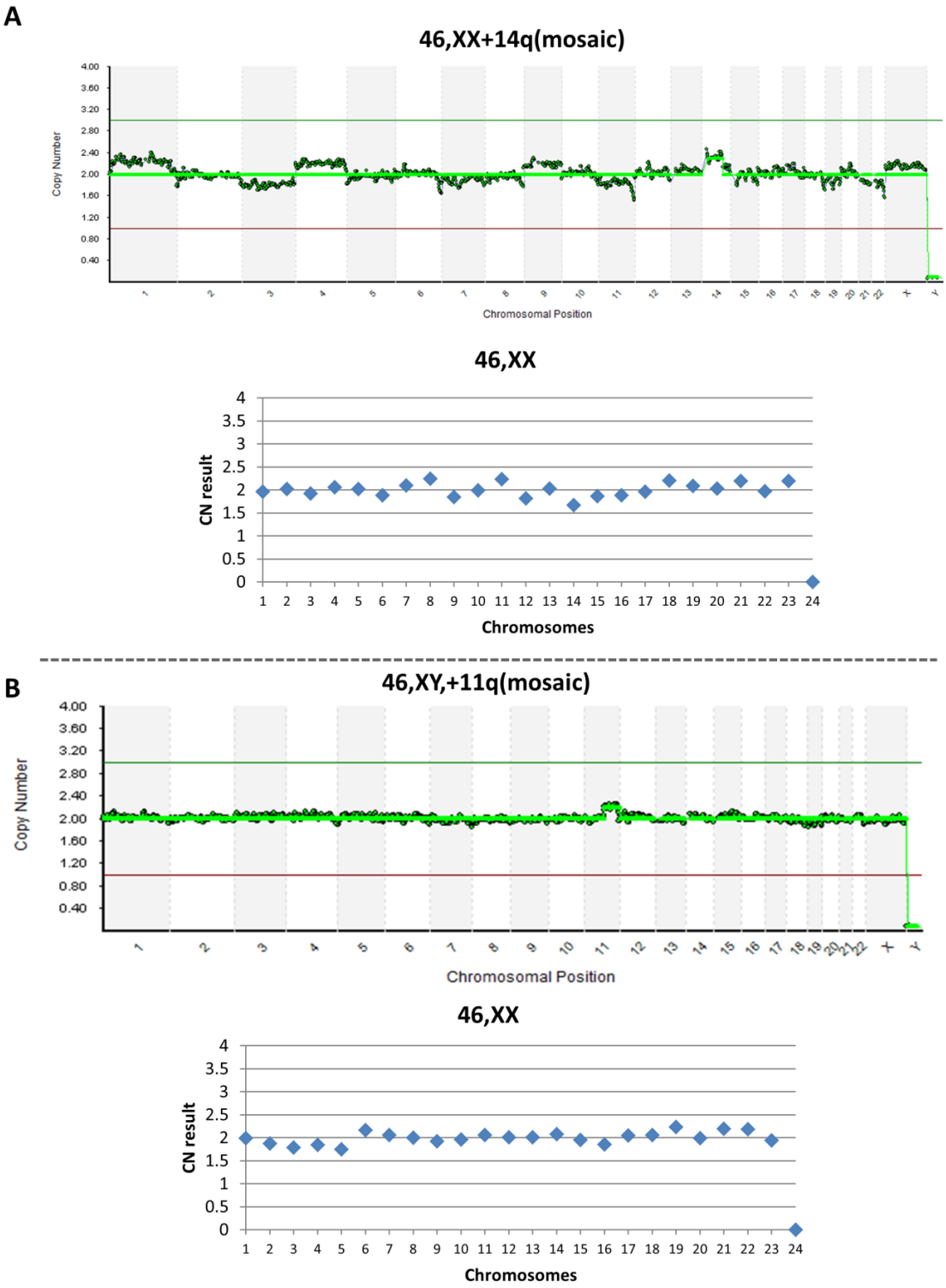


Figure A.18: Comparison of NGS and real-time qPCR 24-CCN profiles of entire embryos M.9 and M.10 and corresponding trophectoderm biopsies. NGS profiles were generated with Bluefuse (for plot descriptions refer to **CHAPTER 2, Section 2.5.2**). Real-time qPCR profiles were generated using the PERL programme (for plot descriptions refer to main text). **A: Sample M.9.** NGS identified a structural mosaic gain of chromosome 14 (entire embryo). The abnormality was not identified with real-time qPCR (biopsy). **B: Sample M.10.** NGS identified a structural mosaic gain of chromosome 11 (entire embryo). The abnormality was not identified with real-time qPCR (biopsy).

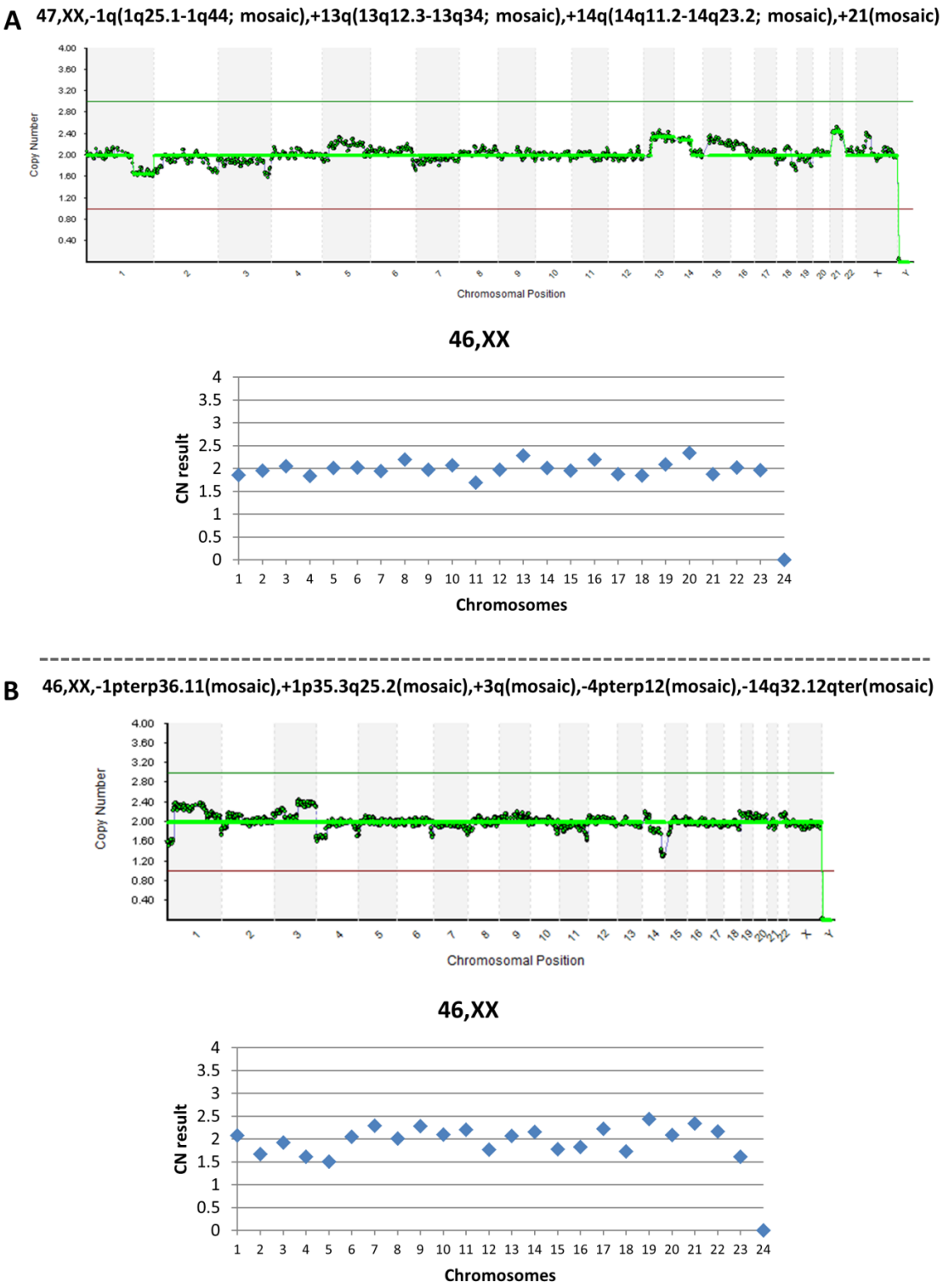


Figure A.19: Comparison of NGS and real-time qPCR 24-CCN profiles of entire embryos M.11 and M.12 and corresponding trophectoderm biopsies. NGS profiles were generated with Bluefuse (for plot descriptions refer to **CHAPTER 2, Section 2.5.2**). Real-time qPCR profiles were generated using the PERL programme (for plot descriptions refer to main text). **A: Sample M.11.** NGS identified several structural and non-structural mosaic errors (entire embryo). These abnormalities were not identified with real-time qPCR (biopsy). **B: Sample M.12.** NGS identified several structural errors (entire embryo). These abnormalities were not identified with real-time qPCR (biopsy).

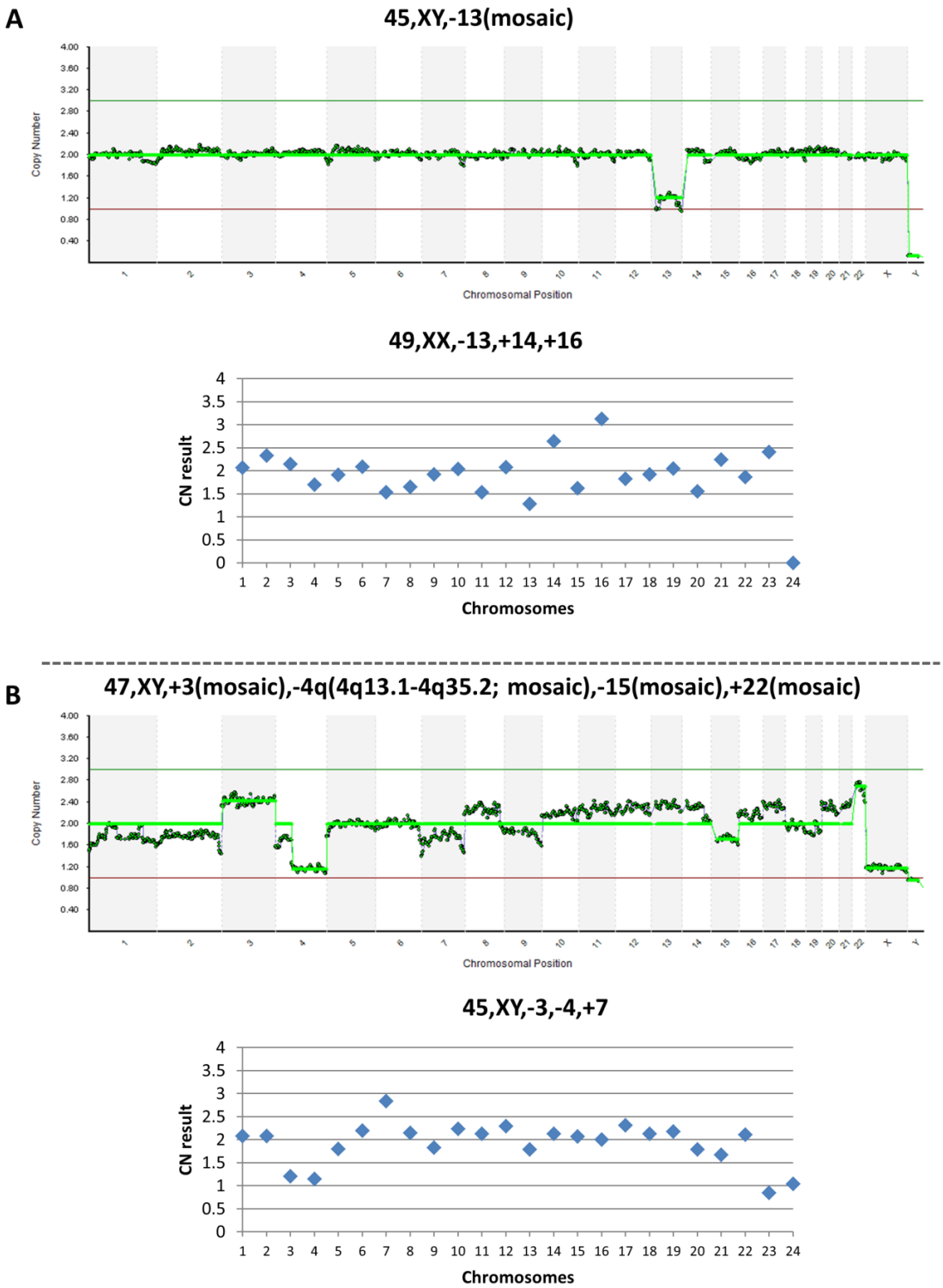


Figure A.20: Comparison of NGS and real-time qPCR 24-CCN profiles of entire embryos M.13 and M.14 and corresponding trophectoderm biopsies. NGS profiles were generated with Bluefuse (for plot descriptions refer to **CHAPTER 2, Section 2.5.2**). Real-time qPCR profiles were generated using the PERL programme (for plot descriptions refer to main text). **A: Sample M.13.** NGS identified a mosaic loss of chromosome 13 (entire embryo). This abnormality was not identified with real-time qPCR (biopsy). **B: Sample M.14.** NGS identified several structural and non-structural errors (entire embryo). The affected chromosomes were partly identified as aneuploid with real-time qPCR (biopsy).

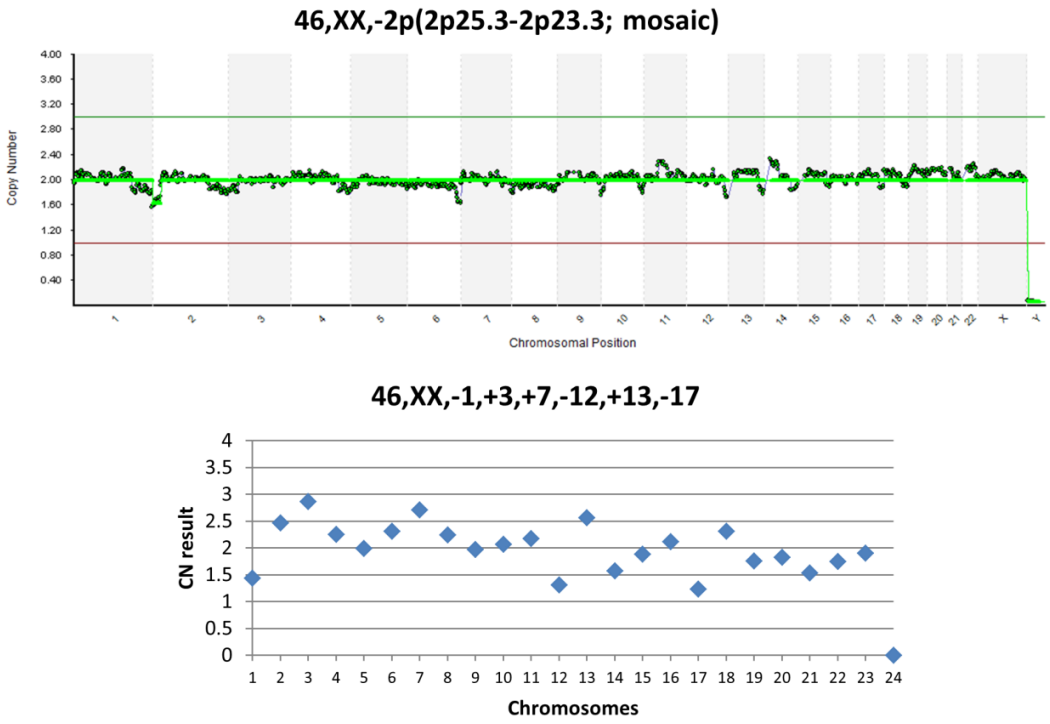


Figure A.21: Comparison of NGS and real-time qPCR 24-CCN profiles of the entire embryo M.15 and its corresponding trophectoderm biopsy. NGS profiles were generated with Bluefuse (for plot descriptions refer to **CHAPTER 2, Section 2.5.2**). Real-time qPCR profiles were generated using the PERL programme (for plot descriptions refer to main text). NGS identified a structural mosaic loss of chromosome 2 (entire embryo). This abnormality was not identified with real-time qPCR. Instead, a wavy profile was obtained with several chromosome abnormalities (biopsy).

Table A.14: Patient/embryo characteristics and PGS outcomes following real-time qPCR

Cycles	Female age	Reason for referral	Embryo ID	Real-time qPCR result	Embryo characterisation	Embryo(s) transferred	Outcome
1	38	PM	1	46, XX	Normal	1	P
2	41	NA	1	44, XX,-16,-18	Abnormal	NA	
3	39	RM	1	47,XY,+19	Abnormal	NA	
			2	45,XX,-1,-6,+22	Abnormal		
4	39	PM	1	46,XX	Normal	1 & 3	P (1 fh)
			2	46,XY	Normal		
			3	46,XY	Normal		
5	35	PAC	1	46,XY	Normal	1	NP
			2	46,XY	Normal		
6	40	AMA	1	44,X0,-14	Abnormal	2	NP
			2	46,XX	Normal		
7	44	AMA & RM	1	48,XY,+19,+21	Abnormal	NA	
			2	47,XY,+2,-13,+16	Abnormal		
			3	47,XX,+10	Abnormal		

8	38	RM	1	46,XY	Normal	1	P
9	32	PM	1	46,XX	Normal	1	P
			2	45,XY,-18	Abnormal		
			3	45,XX,-7	Abnormal		
			4	45,X0	Abnormal		
			5	46,XX	Normal		
			6	46,XY	Normal		
10	40	RM	1	46,XX	Normal	1	P
			2	45,XY,-8,+13,-15	Abnormal		
			3	45,XX,-4	Abnormal		
			4	46,XX	Normal		
11	37	PM & PIF	1	46,XY	Normal	1	M
			2	No amplification	No Result		
			3	46,XX	Normal		
			4	46,XX	Normal		
12	41	AMA	1	No amplification	No Result	NA	
			2	47,XX,+1	Abnormal		
13	43	AMA	1	47,XY,+4,-13,+15	Abnormal	NA	
			2	45,XX,-15	Abnormal		
			3	44,XX,-16,-19	Abnormal		
14	42	PM & AMA	1	45,XY,+9,-16,-21	Abnormal	NA	
15	37	PM	1	47,XY,+22	Abnormal	5	NP
			2	No amplification	No Result		
			3	47,XX,+19	Abnormal		
			4	No amplification	No Result		
			5	46,XY	Normal		
			6	45,XY,-10	Abnormal		
			7	47,XY,+7	Abnormal		
			8	47,XY,+18	Abnormal		
			9	43,X0,-13,-14,-21,+22	Abnormal		
16	39	NA	1	45,XY,-22	Abnormal	NA	
			2	45,XX,-3	Abnormal		
			3	47,XY,+22	Abnormal		
			4	48,XX,+1,+18	Abnormal		
			5	45,XX,-16	Abnormal		
17	41	PR	1	45,XY,-7	Abnormal	2	NP
			2	46,XX	Normal		
			3	47,X0,+1,-5,+6,-16,+17,+22	Abnormal		
18	45	RM & AMA	1	45,X0,-3,+15	Abnormal	NA	

			2	45,XY,-18	Abnormal		
			3	46,XX,-3,-15,+18,+22	Abnormal		
19	35	RM	1	46,XY	Normal	2	NP
			2	46,XX	Normal		
			3	46,XY	Normal		
			4	46,XY	Normal		
			5	47,XX,+1	Abnormal		
			6	46,XY	Normal		
			7	46,XX	Normal		
20	34	PM & RIF	1	46,XY	Normal	1 & 2	P (2 fh)
			2	46,XX	Normal		
			3	46,XY,-3,-4,-6,+9,-10,+13,+16,+17,+18,-22	Abnormal		
21	40	RM	1	46,XY	Normal	1	P
22	39	AMA	1	46,XY	Normal	1	P
			2	46,XY,-21,+22	Abnormal		
			3	46,XX,+13,-22	Abnormal		
			4	47,XY,+21	Abnormal		
			5	45,XX,-6	Abnormal		
23	41	PIF & AMA	1	47,XX,+7	Abnormal	NA	
			2	45,XY,-2	Abnormal		
24	31	PM	1	46,XX	Normal	1	P
			2	46,XX	Normal		
			3	46,XX,-17,+22	Abnormal		
			4	46,XX	Normal		
25	43	AMA	1	45,XX,-7,+9,-16	Abnormal	NA	
			2	46,XY,-4,+5,-6,+7	Abnormal		
26	41	NA	1	45,XX,-16	Abnormal	NA	
27	37	PIF	1	46,XY	Normal	1	P
			2	44,XY,-9,-20	Abnormal		
			3	No amplification	No Result		
28	41	PAC	1	48,XX,+15,+22	Abnormal	NA	
			2	45,XY,-17	Abnormal		
			3	47,XY,+15,-18,+22	Abnormal		
			4	46,XY,+9,+17,-19,-20	Abnormal		
			5	45,XY,+6,-8,-18	Abnormal		
			6	46,XX,+21,-22	Abnormal		
29	33	PM	1	48,XY,+15,+16	Abnormal	2	P
			2	46,XY	Normal		
			3	46,XY	Normal		

			4	No amplification	No Result		
			5	46,XY	Normal		
			6	46,XX	Normal		
			7	No amplification	No Result		
			8	46,XX	Normal		
			9	No amplification	No Result		
30	43	AMA & PAC	1	48,XX,+11,+21	Abnormal	3	P
			2	48,XX,+7,+22	Abnormal		
			3	46,XX	Normal		
31	35	RM	1	46,XX,-7,+20	Abnormal	3	M
			2	46,XX	Normal		
			3	46,XY	Normal		
			4	47,XY,+22	Abnormal		
			5	47,XXX	Abnormal		
32	38	NA	1	47,XY,+22	Abnormal	3	NP
			2	No amplification	No Result		
			3	46,XY	Normal		
			4	47,XX.+16	Abnormal		
33	43	NA	1	46,XY,+18,-19	Abnormal	NA	
			2	47,XX,+21	Abnormal		
			3	45,XX,-16,-20,+22	Abnormal		
			4	48,XX,+7,+22	Abnormal		
			5	48,XX,+19,+21	Abnormal		
			6	48,XXX,-5,+7,+9,-16,+21	Abnormal		
			7	45,XY,+7,-15,-22	Abnormal		
34	39	NA	1	47,XX,+22	Abnormal	2	NP
			2	46,XX	Normal		
35	39	NA	1	45,XX,-22	Abnormal	NA	
			2	47,XX,+13	Abnormal		
			3	48,XY,+19,+21	Abnormal		
			4	No amplification	No Result		

AMA = advanced maternal age. M = miscarriage. NA = not applicable. NP = not pregnant. P = pregnant. PAC = previous aneuploid conception. PIF = previous IVF failure. PM = previous miscarriage. PR = patient request. RIF = recurrent IVF failure. RM = recurrent miscarriage.

Table A.15: Patient/embryo characteristics and PGS outcomes following array CGH

Cycles	Female age	Reason for referral	Embryo ID	Array CGH result	Embryo characterisation	Embryo(s) transferred	Outcome
1	41	AMA	1	46,XY	Normal	1	P
			2	47,XY,-2p,+15	Abnormal		
			3	45,XX,-9	Abnormal		
			4	46,XY,-4p,+4q,+8,-13	Abnormal		
2	43	AMA	1	46,XY	Normal	2	P (2 fh)
			2	46,XX	Normal		
3	42	PAC	1	46,XY	Normal	2	P (2 fh)
			2	46,XX	Normal		
4	42	AMA	1	44,XY,-11,-18,+19,-22	Abnormal	NA	
5	44	AMA	1	47,XX,+15,+16,-21	Abnormal	NA	
			2	47,XX,-6,+13,+15	Abnormal		
6	37	PR	1	47,XX,+22	Abnormal	NA	
			2	46,XX,-13q	Abnormal		
7	42	AMA & PIF	1	45,XY,-15	Abnormal	NA	
			2	47,XY,+21	Abnormal		
			3	48,XY,+15,+22	Abnormal		
			4	49,XX,+3,+11,+19	Abnormal		
8	38	NA	1	47,XX,+10	Abnormal	1	NP
			2	46,XY	Normal		
9	43	AMA & PM	1	45,XY,-13,-19p	Abnormal	NA	
			2	46,XY,+3,-13,+14,+15	Abnormal		
			3	45,X0,+4,-18	Abnormal		
10	30	RM	1	46,XX	Normal	1	M
			2	46,XY	Normal		
			3	45,XX,-19	Abnormal		
			4	46,XY,-18,+22	Abnormal		
			5	47,XY,-2,+3,+4,+5,-6,-7,+9,-10,+11,-12,+13,+15,-17,+19,-20	Abnormal		
			6	46,XY	Normal		
11	32	RM	1	47,XY,+22	Abnormal	1	P
			2	No amplification	No result		
			3	46,XY,-6q	Abnormal		
			4	46,XY	Normal		
			5	46,XY	Normal		
			6	46,XX	Normal		
12	36	NA	1	46,XX	Normal	1	NP
			2	45,XY,-22	Abnormal		
			3	46,XY	Normal		
			4	46,XX	Normal		
			5	46,XX	Normal		

			6	No amplification	No result		
13	38	NA	1	49,XY,+3,+21,+22	Abnormal	NA	
			2	46,XX,-2p,-8q,-10p,-12,+14q,-22q	Abnormal		
			3	47,XX,+6	Abnormal		
14	43	AMA	1	46,XY,+15,-22	Abnormal	NA	
			2	46,XX,-4q	Abnormal		
			3	44,X,-1,-14,-16,+19	Abnormal		
			4	47,XY,-2,+7,-11,+18,+22	Abnormal		
			5	46,XX,-2,+22	Abnormal		
15	40	RM	1	46,XX,+6q	Abnormal	NA	
			2	47,XY,+1,-2,+20	Abnormal		
16	35	NA	1	46,XY	Normal	2	P (2 fh)
			2	46,XY	Normal		
			3	46,XY	Normal		
			4	45,XX,-18	Abnormal		
			5	45,XX,-16	Abnormal		
			6	No amplification	No result		
17	35	RM	1	46,XY	Normal	2	P (1 fh)
			2	46,XY	Normal		
			3	45,XY,-3	Abnormal		
			4	46,XY	Normal		
			5	47,XX,+4q,+14	Abnormal		
			6	46,XX	Normal		
			7	No amplification	No result		
18	38	RM	1	46,XY	Normal	1	M
			2	46,XY	Normal		
			3	49,XX,+3,-4,+6,+8,+21	Abnormal		
			4	No amplification	No result		
19	36	RM	1	46,XX	Normal	2	NP
			2	47,XX,+16	Abnormal		
			3	47,XY+14	Abnormal		
			4	47,XX,+15,-16q	Abnormal		
			5	46,XX	Normal		
20	31	RM	1	No amplification	No result	1	P
			2	46,XX	Normal		
			3	46,XY	Normal		
			4	46,XY	Normal		
			5	46,XY	Normal		
			6	46,XX	Normal		
			7	47,XX,+14	Abnormal		
			8	46,XY	Normal		

			9	46,XY	Normal		
			10	46,XX	Normal		
			11	46,XX	Normal		
			12	47,XX,+16	Abnormal		
			13	45,XX,-16	Abnormal		
			14	45,XX,-5	Abnormal		
21	40	PM	1	47,XY,+11	Abnormal	1	NP
			2	46,XY	Normal		
			3	47,XY,+19	Abnormal		
			4	48,XY,+10,+19	Abnormal		
			5	45,XX,-22	Abnormal		
			6	46,XX	Normal		
			7	45,XY,-16	Abnormal		
22	37	PM	1	46,XX	Normal	1	P
			2	46,XX	Normal		
			3	46,XY	Normal		
			4	46,XX	Normal		
			5	45,XY,-11	Abnormal		
23	39	PM	1	46,XY,+15q	Abnormal	NA	
			2	49,XY,+11,+12,+22	Abnormal		
			3	45,XY,-10	Abnormal		
			4	45,XY,-8	Abnormal		
24	39	PM	1	45,XY,-13	Abnormal	NA	
			2	45,XX,-22	Abnormal		
			3	46,XX,-10q	Abnormal		
			4	52,X0,+1,+4,+7,+8,+10,+11,+12,-16,+17,-19,+20	Abnormal		
			5	50,XX,+5,+14,+19,+21	Abnormal		
25	38	RM	1	51,XX,+3,+8,+9,+15,+17,+20,-21	Abnormal	NA	
26	37	RM & PIF	1	46,XX	Normal	1	P
			2	44,XX,+4q,-15,-21	Abnormal		
			3	46,XX,+3,-4,-5,+12,+13,-17	Abnormal		
27	38	PM	1	46,XX	Normal	1	NP
			2	46,XY	Normal		
			3	47,XX,+20p/q,+21	Abnormal		
			4	47,XX,-5q,+12	Abnormal		
			5	47,XY,+22	Abnormal		
			6	47,XY,+1	Abnormal		
			7	46,XY	Normal		
			8	46,XX	Normal		
			9	46,XY,+4q	Abnormal		
			10	46,XX	Normal		

			11	46,XY	Normal		
			12	46,XX,+4p,-10q,+15q,+16p/q	Abnormal		
28	41	RM	1	45,XX,-4	Abnormal	NA	
			2	No amplification	No result		
29	38	RM	1	46,XX	Normal	1	P
			2	46,XY	Normal		
			3	46,XX	Normal		
30	37	PM	1	47,XY,+13	Abnormal	1	P
			2	No amplification	No result		
			3	46,XX	Normal		
			4	45,XY,-13	Abnormal		
			5	45,XY,-9	Abnormal		
31	43	RM & AMA	1	47,XX,+16	Abnormal	NA	
			2	46,XXY,-22	Abnormal		
			3	45,XY,-14	Abnormal		
32	39	PM & PIF	1	46,XX	Normal	1	P
			2	47,XY,+21	Abnormal		
			3	45,XY,-16	Abnormal		
33	41	AMA & RIF	1	45,XX,-11	Abnormal	1	NP
			2	46,XY	Normal		
			3	No amplification	No result		
			4	48,XX,+13,+15	Abnormal		
			5	46,XX,-6,+16	Abnormal		
			6	45,XX,-22	Abnormal		
34	39	PM & RIF	1	48,XX,+14,+15	Abnormal	NA	
			2	45,XX,-22	Abnormal		
			3	No amplification	No result		
			4	46,XY,+12q	Abnormal		
35	39	PM & RIF	1	47,XX,+16	Abnormal	1	P
			2	46,XX	Normal		
36	31	PR	1	46,XX	Normal	1	NP
			2	46,XX	Normal		
37	34	PIF	1	47,XY,+22	Abnormal	NA	
			2	46,XY,-11q	Abnormal		
			3	45,XX,-2	Abnormal		
			4	45,XX,-13	Abnormal		
38	34	RIF	1	46,XY	Normal	1	NP
			2	46,XY	Normal		
			3	46,XY	Normal		
			4	46,XY	Normal		
39	36	PIF	1	46,XX	Normal	1	NP

			2	46,XX,+2q	Abnormal		
			3	45,XX,+1p,-12	Abnormal		
40	36	RIF	1	47,XX,+21	Abnormal	2	P (2 fh)
			2	46,XY	Normal		
			3	46,XX	Normal		
41	42	RIF & AMA	1	49,XY,+1,+7p,+13,+15	Abnormal	NA	
			2	45,XY,-8	Abnormal		
			3	45,XY,-10	Abnormal		
42	39	RIF	1	46,XX	Normal	1	NP
43	37	RIF	1	46,XY	Normal	1	NP
			2	46,XY	Normal		
			3	46,XY	Normal		
44	42	RIF & AMA	1	47,XX,+14	Abnormal	1	NP
			2	46,XX	Normal		
			3	47,XX,+15	Abnormal		
45	40	RIF & AMA	1	50,XY,+6,+15,+16,+17	Abnormal	NA	
			2	47,XX,+13	Abnormal		
			3	47,XX,+22	Abnormal		

AMA = advanced maternal age. M = miscarriage. NA = not applicable. NP = not pregnant. P = pregnant. PAC = previous aneuploid conception. PIF = previous IVF failure. PM = previous miscarriage. PR = patient request. RIF = recurrent IVF failure. RM = recurrent miscarriage.

Appendix B

Table B.1: Primer sequences and amplicon lengths

m.8993 mutation site	
Forward primer	CCCTAGCCCACTTCTTACCA
Reverse primer	GGTGGCCTGCAGTAATGTTAG
Amplicon length (bp)	135
m.10191 mutation site	
Forward primer	ATCCACCCCTTACGAGTGC
Reverse primer	GGGTAAAAGGAGGGCAATTT
Amplicon length (bp)	124
m.3243 mutation site	
Forward primer	ACCCAAGAACAGGGTTTGT
Reverse primer	TGGCCATGGGTATGTTGTTA
Amplicon length (bp)	108

Table B.2: Expected heteroplasmy levels versus observed heteroplasmy levels at position m.8993 after conventional PCR

Expected heteroplasmy (%)	**Obtained heteroplasmy (%)**	**Difference (%)**
100.0	100.0	0.0
80.0	81.7	1.7
60.0	64.4	4.4
40.0	44.9	4.9
20.0	25.4	5.4
10.0	14.7	4.7
5.0	3.2	1.8
0.0	0.0	0.0

Mean difference: 2.4 % ± 2.8 % SD.

Table B.3: Mapped sequencing reads at position m.8993 after conventional PCR

Samples diluted to:	Reads
100.0 %	37,317
80.0 %	96,205
60.0 %	63,191
40.0 %	72,239
20.0 %	68,389
10.0 %	78,741
5.0 %	54,120
0.0 %	33,986

Mean sequencing reads: 63,024.

Table B.4: Observed heteroplasmy levels after conventional PCR and after WGA combined with conventional PCR at position m.8993

Observed Heteroplasmy (%)		Difference (%)
after conventional PCR	after WGA and conventional PCR	
100.0	100.0	0
81.7	77.7	4
64.4	62.5	1.9
44.9	40.2	4.7
25.4	22.3	3.1
14.7	13.9	0.8
3.2	3.4	0.2
0.0	0.0	0

Observed heteroplasmy levels obtained after conventional PCR are identical to those shown in **Table B.2**. Mean difference: 1.8 % ± 1.9 % SD.

Table B.5: Mapped sequencing reads at position m.8993 after WGA combined with conventional PCR

Samples diluted to:	Reads
100.0 %	34,919
80.0 %	85,173
60.0 %	47,970
40.0 %	67,305
20.0 %	75,508
10.0 %	73,471
5.0 %	86,801
0.0 %	30,023

Mean sequencing reads: 62,646.

Table B.6: Heteroplasmy levels and mapped sequencing reads at position m.8993 after conventional PCR of gDNA samples from Patient A

Genomic DNA (blood sample)		Genomic DNA (buccal sample)	
Heteroplasmy (%)	**Reads**	**Heteroplasmy (%)**	**Reads**
55.0	38,397	56.3	38,479
51.9	69,898	54.4	69,739

Mean heteroplasmy: 54.4 % ± 1.9 % SD. Mean sequencing reads: 54,128.

Table B.7: Heteroplasmy levels and mapped sequencing reads at position m.8993 after WGA and conventional PCR in gDNA samples from Patient A

WGA genomic DNA (blood sample)		WGA genomic DNA (buccal sample)	
Heteroplasmy (%)	**Reads**	**Heteroplasmy (%)**	**Reads**
59.6	31,670	51.9	42,403
60.8	72,273	50.6	42,196
52.8	43,980	56.2	115,901
49.2	34,133	65.8	54,757

Mean heteroplasmy: 55.9 % ± 5.8 % SD. Mean sequencing reads: 54,664.

Table B.8: Heteroplasmy levels and mapped sequencing reads at position m.8993 after conventional PCR in cell samples (lymphocytes) from Patient A

Cell samples	Heteroplasmy (%)	Reads
1 cell	97.3	37,777
	0.0	27,262
3 cells	59.8	37,377
	91.1	34,391
5 cells	74.8	26,309
	19.6	28,764

Calculated mean heteroplasmy: 54.3 % ± 42.9 % SD. Mean sequencing reads: 31,980.

Table B.9: Heteroplasmy levels and mapped sequencing reads at position m.8993 after WGA and conventional PCR in cell samples (lymphocytes) from Patient A

Cell samples	Heteroplasmy (%)	Reads
1 cell	0.0	36,711
	100.0	31,221
3 cells	33.1	48,015
	60.2	42,446
5 cells	72.2	47,640
	95.7	36,579

Calculated mean heteroplasmy: 53.7 % ± 43.0 SD. Mean sequencing reads: 40,435.

Table B.10: Mutant load and mapped sequencing reads at position m.8993 after conventional PCR and after WGA combined with conventional PCR in gDNA from the daughter of Patient A

Cell samples	Heteroplasmy (%)	Reads
Conventional PCR	100.0	33,986
	100.0	35,621
WGA and conventional PCR	100.0	30,023
	100.0	36,081

Mean sequencing reads: 33,928.

Table B.11: Mutant load and mapped sequencing reads at position m.8993 after conventional PCR in the gDNA sample from Patient B

Heteroplasmy (%)	Reads
0.0	39,448

Table B.12: Mutant loads and mapped sequencing reads at position m.8993 after WGA and conventional PCR in the gDNA sample from Patient B

Heteroplasmy (%)	Reads
0.0	62,802
0.0	59,642

Mean sequencing reads: 61,222.

Real incidence of m8993T>G mutation in trophectoderm biopsies of MST embryos generated in the study described by Zhang et al., 2017

Embryo ID	Mutation load (%)[1]
1[2]	~11
2	~7
3	~9
4	~26

1 = analysed in trophectoderm WGA products (used for PGS) using the method described in **CHAPTER 4**. 2 = transferred embryo.

Table B.13: Mutant loads and mapped sequencing reads at position m.8993 after conventional PCR in cell samples (lymphocytes) from Patient B

Heteroplasmy (%)	Reads
0.0	17,233
0.0	359,585
0.0	421,777

Each sample consisted of a single cell. Mean sequencing reads: 266,198.

Table B.14: Heteroplasmy levels and mapped sequencing reads at position m.8993 after WGA and conventional PCR in cell samples (lymphocytes) from Patient B

Heteroplasmy (%)	Reads
0.0	73,206
0.0	41,436
0.0	23,387
0.0	36,202
0.0	40,946
0.0	211,568

Each sample consisted of a single cell. Mean sequencing reads: 71,124.

Table B.15: Heteroplasmy level and mapped sequencing reads at position m.8993 after conventional PCR in the gDNA sample from the son of Patient B

Heteroplasmy (%)	Reads
97.1	38,912

Table B.16: Heteroplasmy levels and mapped sequencing reads at position m8993 after conventional PCR and WGA in gDNA samples from the son of Patient B

Heteroplasmy (%)	Reads
98.4	34,618
91.9	51,436
96.6	102,369

Mean heteroplasmy: 95.6 % ± 3.4 % SD. Mean sequencing reads: 62,808.

Table B.17: Heteroplasmy levels and mapped sequencing reads at position m.8993 after conventional PCR in cell samples (lymphocytes) from the son of Patient B

Heteroplasmy (%)	Reads
93.0	22,139
100.0	171,212
99.9	95,477

Each sample consisted of a single cell. Mean heteroplasmy: 97.6 % ± 4.0 % SD. Mean sequencing reads: 96,276.

Table B.18: Heteroplasmy levels and mapped sequencing reads at position m.8993 after WGA and conventional PCR in cell samples (lymphocytes) from the son of Patient B

Heteroplasmy (%)	Reads
100.0	104,698
100.0	59,734
99.9	20,134
98.8	36,552
100.0	119,747
98.9	154,344
39.5	56,092
100.0	62,625
98.0	77,984

Each sample consisted of a single cell. Mean heteroplasmy: 92.8 % ± 20.0 % SD. Mean sequencing reads: 76,879.

Table B.19: Mutant loads and mapped sequencing reads at position m.10191 after conventional PCR in the gDNA sample from Patient C

Heteroplasmy (%)	Reads
0.0	60,975
0.0	239,241
0.0	19,874

Mean sequencing reads: 106,697.

Table B.20: Mutant loads and mapped sequencing reads at position m.10191 after WGA and conventional PCR in the gDNA sample from Patient C

Heteroplasmy (%)	Reads
0.0	18,923
0.0	13,397

Mean sequencing reads: 16,160.

Table B.21: Mutant load and mapped sequencing reads at position m.10191 after conventional PCR in cell samples from Patient C

Lymphocyte		Buccal cell	
Heteroplasmy (%)	Reads	Heteroplasmy (%)	Reads
0.0	39,316	0.0	96,561

Each sample consisted of a single cell. Mean sequencing reads: 67,561.

Table B.22: Mutant loads and mapped sequencing reads at position m.10191 after WGA and conventional PCR in cell samples from Patient C

Lymphocytes		Buccal cells	
Heteroplasmy (%)	**Reads**	**Heteroplasmy (%)**	**Reads**
0.0	54,146	0.0	40,876
0.0	88,654	0.0	25,814

Each sample consisted of a single cell. Mean sequencing reads: 52,373.

Table B.23: Heteroplasmy levels and mapped sequencing reads at position m.10191 after conventional PCR in the gDNA sample from the daughter of Patient C

Heteroplasmy (%)	Reads
84.2	67,836
85.0	13,482
85.0	16,679

Mean heteroplasmy: 84.7 % ± 0.5 % SD. Mean sequencing reads: 32,666.

Table B.24: Heteroplasmy levels and mapped sequencing reads at position m.10191 after WGA and conventional PCR in the gDNA sample from the daughter of Patient C

Heteroplasmy (%)	Reads
84.5	24,170
85.6	27,408
82.2	15,591
82.1	15,067
84.9	60,098

Mean heteroplasmy: 83.9 % ± 1.6 % SD. Mean sequencing reads: 28,467.

Table B.25: Heteroplasmy levels and mapped sequencing reads at position m.10191 after conventional PCR in cell samples (buccal cells) from the daughter of Patient C

Heteroplasmy (%)	Reads
83.5	113,137
83.9	75,770
93.9	17,187
90.5	12,376

Each sample consisted of a single cell. Mean heteroplasmy: 89.0 % ± 5.1 % SD. Mean sequencing reads: 35,111.

Table B.26: Heteroplasmy levels and mapped sequencing reads at position m.10191 after WGA and conventional PCR in cell samples (buccal cells) from the daughter of Patient C

Heteroplasmy (%)	Reads
77.3	25,853
81.7	58,910
94.3	25,591
75.2	61,891
85.9	69,847
77.3	33,113

Each sample consisted of a single cell. Mean heteroplasmy: 82.0 % ± 7.2 % SD. Mean sequencing reads: 45,868.

Table B.27: Heteroplasmy levels and mapped sequencing reads at position m.3243 after conventional PCR in gDNA samples from Patient D

Genomic DNA (blood sample)		Genomic DNA (buccal sample)	
Heteroplasmy (%)	Reads	Heteroplasmy (%)	Reads
6.0	92,002	13.2	116,376

Mean heteroplasmy: 9.6 % ± 5.1 % SD. Mean sequencing reads: 104,189.

Table B.28: Heteroplasmy levels and mapped sequencing reads at position m.3243 after WGA and conventional PCR in gDNA sample from Patient D

WGA genomic DNA (blood sample)		WGA genomic DNA (buccal sample)	
Heteroplasmy (%)	Reads	Heteroplasmy (%)	Reads
6.7	168,388	14.7	91,714

Mean heteroplasmy: 10.7 % ± 5.7 % SD. Mean sequencing reads: 111,526.

Table B.29: Heteroplasmy levels and mapped sequencing reads at position m.3243 after conventional PCR in cell samples from Patient D

Lymphocyte		Buccal cell	
Heteroplasmy (%)	Reads	Heteroplasmy (%)	Reads
0.0	73,777	0.0	121,546
49.0	71,944	0.0	92,289
0.0	83,533	39.1	179,705
0.0	68,638	0.0	133,806
0.0	112,600	63.8	208,209
0.0	107,603	0.0	118,540

Calculated mean heteroplasmy: 12.7 % ± 23.5 % SD. Mean sequencing reads: 114,349.

Table B.30: Heteroplasmy levels and mapped sequencing reads at position m.3243 after WGA and conventional PCR in cell samples from Patient D

Lymphocyte		Buccal cell	
Heteroplasmy (%)	**Reads**	**Heteroplasmy (%)**	**Reads**
49.7	134,811	0.0	113,173
0.0	197,973	1.2	75,727
0.0	87,703	1.3	206,103
0.0	130,396	0.0	234,067
0.0	212,838	0.0	186,355
0.0	113,587	1.6	131,573

Calculated mean heteroplasmy: 4.5 % ± 14.3 % SD. Mean sequencing reads: 152,026.

Table B.31: Sequencing reads at position m.8993 in clinical samples from Patient A

Sample ID	Number of reads
1	38,574
	46,767
2	39,896
3	39,909
4	35,452

Mean sequencing reads: 40,120. Two libraries were prepared from sample 1.

Table B.32: Sequencing reads at position m.8993 in clinical samples from Patient B

Sample ID		Number of reads
1		49,511
2		72,882
3		83,407
4		33,527
5		84,289
6		96,369
7		82,690
8		91,363
9		52,010
10		76,755
11	a	67,756
	b	43,268
	c	80,879
	d	34,134
	e	38,658
12		105,731
13	a	21,6315
	b	35,413
	c	58,710
	d	70,099
	e	76,422
	f	104,920
	g	71,360
	h	52,826
	i	70,826
	j	525,522
	k	22,200
14		58,134
15		48,974
16		32,612
17		64,309
18		229,798

Mean sequencing reads: 88,490.

Table B.33: Array CGH results of single sister blastomeres derived from the arrested embryo 13

ID	Chromosomes																					
	1	2	3	4	5	6	7	8	9	10	11	12	13	14	15	16	17	18	19	20	21	22	X/Y
a	3	3	1	3	1	1	✓	1	1	✓	1	3	✓	✓	1	3	1	✓	✓	3	3	✓	XXX
b	✓	✓	1	3	✓	✓	3	✓	3	✓	3	3	✓	✓	✓	✓	✓	✓	✓	1	✓	✓	00
c	✓	✓	1	3	✓	✓	3	✓	3	✓	3	3	✓	✓	✓	✓	✓	✓	✓	1	✓	✓	XY
d	1	1	3	1	✓	✓	1	1	✓	✓	1	1	✓	3	✓	✓	3	3	✓	3	✓	✓	XXYY
e	✓	3	3	✓	✓	✓	✓	3	✓	✓	1	✓	✓	✓	1	3	3	1	✓	✓	3	3	XXYY
f	1	1	3	1	✓	✓	✓	✓	✓	✓	1	1	✓	3	✓	✓	3	3	✓	3	✓	✓	XXYY
g	✓	✓	3	1	3	1	3	3	✓	✓	3	✓	✓	✓	3	1	3	✓	1	1	✓	✓	YY
h	3	✓	3	1	3	1	✓	✓	✓	✓	3	✓	✓	✓	3	1	3	✓	✓	1	✓	✓	XY
i	1	3	✓	✓	✓	✓	✓	✓	1	✓	3	✓	✓	1	3	✓	1	✓	3	✓	1	✓	XXY
j	3	3	✓	✓	✓	3	1	1	1	✓	3	3	3	1	3	✓	1	✓	3	3	1	✓	X0
k	1	1	✓	✓	✓	✓	1	1	✓	✓	✓	✓	✓	✓	✓	3	✓	✓	✓	✓	✓	✓	XY

✓ = copy number of two

Table B.34: Sequencing reads at position m.8993 in newborn cord blood and buccal samples

Sample ID	Number of reads
Cord blood	98,807
Buccal swab (2 weeks after birth)	76,485
Buccal swab (3 weeks after birth)	75,560

Mean sequencing reads: 83,617.

Table B.35: Sequencing reads at position m.10191 in clinical samples from Patient C (1st cycle)

Sample ID		Number of reads
1	a	84,426
	b	97,325
	b	92,307
	c	44,587
2		38,828
3		35,268
		36,003

Mean sequencing reads: 61,249. Two libraries were prepared from sample 3.

Table B.36: Sequencing reads at position m.10191 in clinical samples from Patient C (2nd cycle)

Sample ID	Reads
4	13,105
5	17,511
	15,238
6	21,343
	20,238
7	12,176
8	29,324
9	19,199
	20,288
10	25,656
11	13,186

Mean sequencing reads: 18,842. Two libraries were prepared from samples 5, 6 and 9.

Table B.37: NGS-based CCS result of the blastomere biopsy derived from embryo 9

Chromosomes																					
1	**2**	**3**	**4**	**5**	**6**	**7**	**8**	**9**	**10**	**11**	**12**	**13**	**14**	**15**	**16**	**17**	**18**	**19**	**20**	**21**	**22**	**X/Y**
✓	1	1	3	3	3	3	✓	✓	✓	✓	1	✓	3	✓	✓	✓	✓	✓	✓	✓	✓	XXY

✓ = copy number of two.

Table B.38: Sequencing reads at position m.3243 in clinical samples from Patient D

Sample ID		Number of reads
2		99,520
3	a	110,695
	b	111,073
4		151,455
5	a	95,923
	b	113,857
8		96,388
9		156,942
10		112,270
11	a	300,316
	b	205,860
12		89,303
13	a	322,811
	b	149,616
14		123,378
15		140,084
17		100,448
18		205,767
19a		113,528
20		102,528
21	a	258,732
	b	224,156
23	a	126,269
	b	99,059
24	a	169,680
	b	112,433
26	a	111,466
	b	151,156

Mean sequencing reads: 148,383.

Table B.39: Array CGH-based CCS result of the trophectoderm biopsy derived from embryo 3

Chromosomes																					
1	**2**	**3**	**4**	**5**	**6**	**7**	**8**	**9**	**10**	**11**	**12**	**13**	**14**	**15**	**16**	**17**	**18**	**19**	**20**	**21**	**22**	**X/Y**
Part loss	✓	✓	✓	3	✓	3	3	3	✓	✓	3	3	Part loss	✓	3	3	✓	✓	✓	3	3	XYY

✓ = copy number of two.

Appendix C

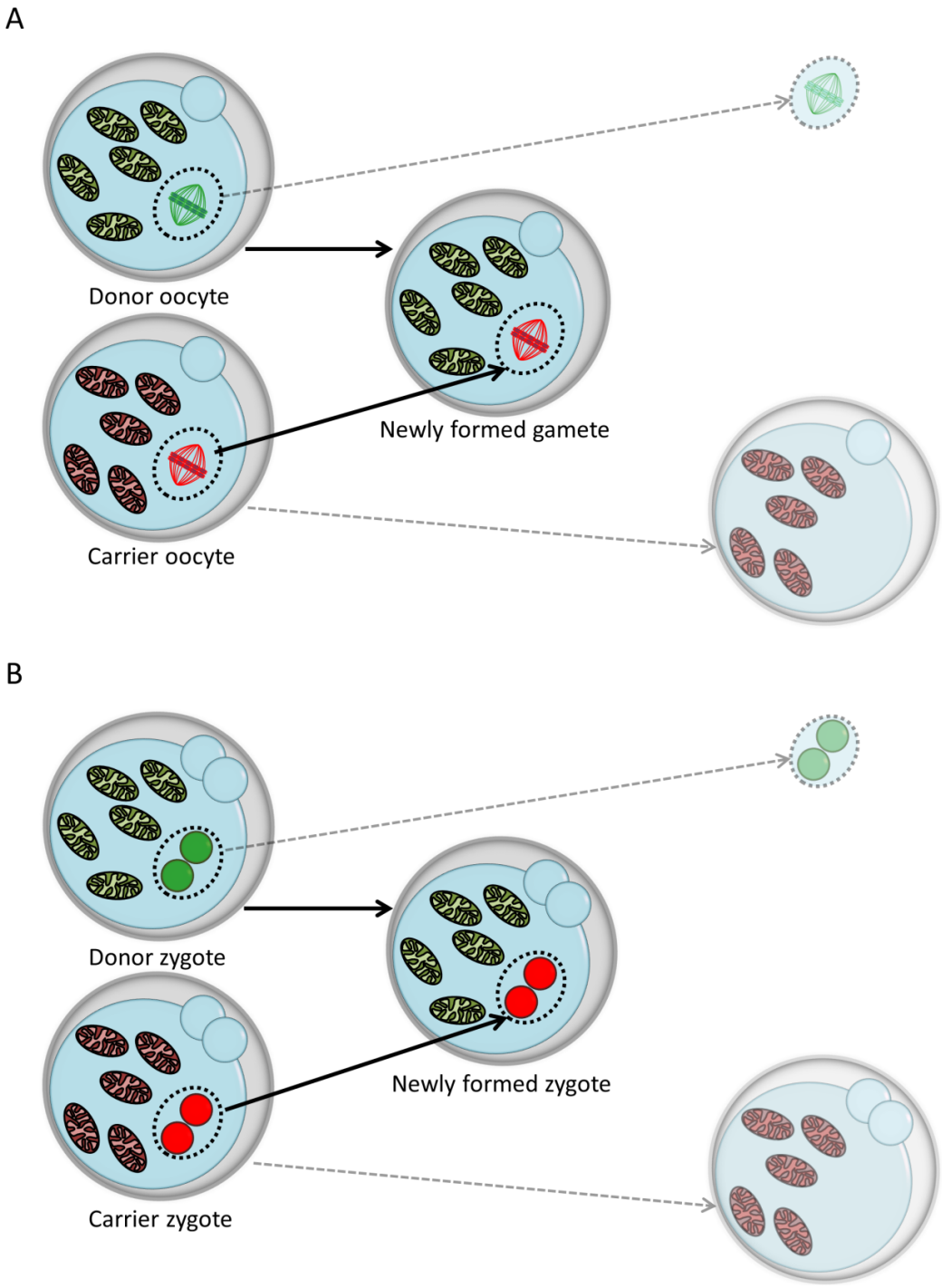


Figure C.1: Schematic representation of common MRTs. A: MST. Following oocyte retrieval, spindle-chromosome complexes of the mtDNA mutation carrier's and the donor's oocytes are removed. The carrier's oocyte spindle-chromosome complex is inserted in the donor's oocyte to generate a mutation-free gamete. The carrier's oocyte and the donor's spindle-chromosome complex are discarded. **B: PNT.** Following fertilisation, pronuclei of the mtDNA mutation carrier's and the donor's zygotes are removed. The carrier's zygote pronuclei are inserted in the donor's zygote to generate a mutation-free zygote. The carrier's zygote and the donor's pronuclei are discarded.

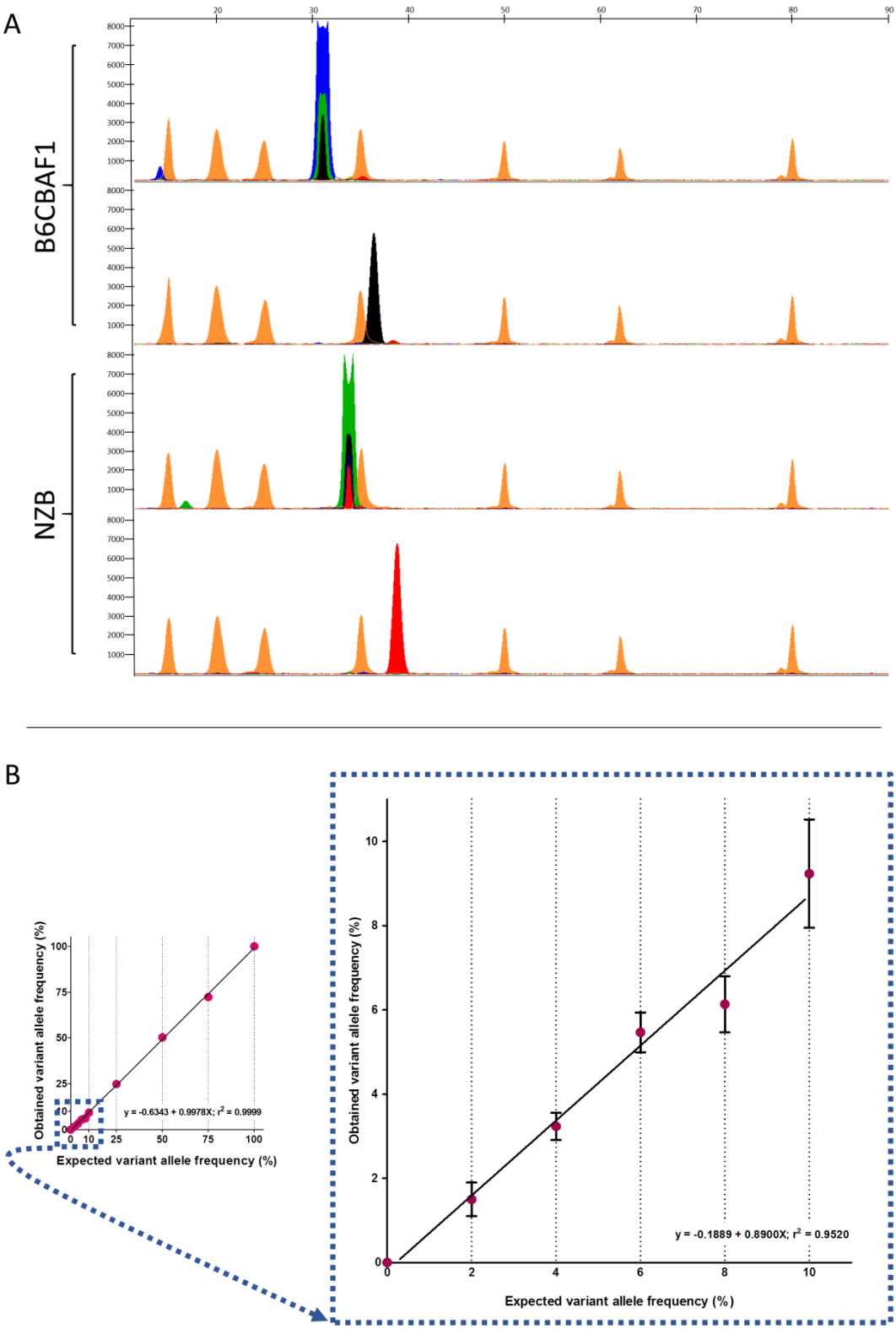


Figure C.2: Validation experiments for mtDNA carry-over rate analysis in mouse samples. A: Minisequencing results at position m.3932. Results from gDNA isolated from tail tips of the B6CBAF1 (upper two panels) and the NZB (lower two panels) strains. Guanine (blue) and cytosine (black) was detected on the forward and reverse mtDNA strand in B6CBAF1 gDNA. Adenine (green) and thymine (red) was detected on the forward and reverse mtDNA strand in NZB gDNA. **B: Expected and obtained allele frequencies at position m.3932 in homoplasmic samples and artificial heteroplasmic sample mixtures.** Error bars show SD. The lines connecting the dots are lines of best fit.

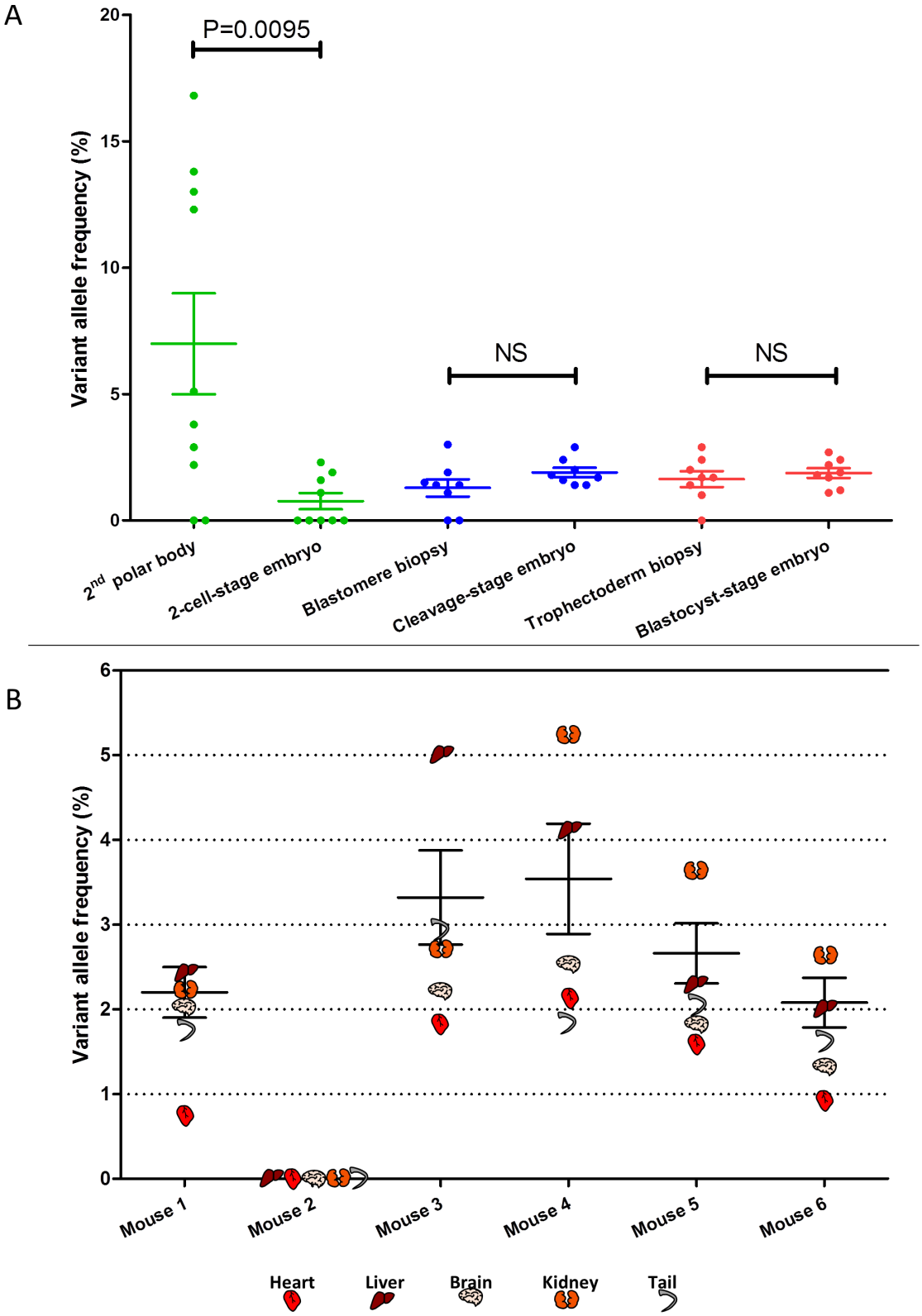


Figure C.3: Variant allele frequencies detected in embryo specimens and adult mouse tissue samples following MST. A: Embryo specimens. Illustrated are variant frequencies of biopsies and corresponding entire embryos. Dots represent allele frequencies of single samples. Horizontal lines show mean allele frequencies and the SEMs. Unpaired t-test was used to compare frequencies between biopsies and corresponding embryos. NS = not significant. **B: Adult mouse tissue samples.** Horizontal lines show mean allele frequencies and the SEM.